

A Study of Heat Transfer and Heat Flow Asymmetry through Water in the presence of the Density Maximum

A thesis submitted for the Degree of
Doctor of Philosophy

Presented by
Priscilla A. Mooney B.Sc.

Department of Experimental Physics
National University of Ireland, Maynooth
Maynooth
Kildare

July 2007

Research Supervisor
Michael F. Cawley M.Sc., Ph.D.

Head of Department
J. Anthony Murphy M.Sc., M.S., Ph.D.



NUI MAYNOOTH

Ollscoil na hÉireann Má Nuad

Contents

Abstract	vi
Acknowledgements	viii
1. Introduction.....	1
1.1 Introduction.....	2
1.2 Review of the density of water.....	4
1.2.1 <i>Historical review of the density maximum of water.....</i>	<i>6</i>
1.2.2 <i>The temperature of maximum density of aqueous solutions</i>	<i>8</i>
1.3 Review of the molecular models of water.....	10
1.4 Mathematical description of fluid dynamics.....	12
1.4.1 <i>Dimensionless numbers.....</i>	<i>13</i>
1.5 Review of differentially heated cavities.....	15
1.6 Review of heat transfer	18
1.6.1 <i>Heat transfer in the vicinity of the density maximum.....</i>	<i>19</i>
1.6.2 <i>Heat transfer measurement techniques.....</i>	<i>21</i>
1.7 Review of asymmetrical heat transfer.....	24
1.7.1 <i>Type I rectifiers</i>	<i>27</i>
1.7.2 <i>Type II rectifiers.....</i>	<i>29</i>
1.7.3 <i>Hybrid rectifiers.....</i>	<i>33</i>
1.8 Thesis chapter outline	35
1.8.1 <i>Author's direct contribution in this thesis.....</i>	<i>35</i>
2. Experimental Apparatus and Procedures.....	39
2.1 Introduction.....	40
2.2 General techniques and equipment	42
2.2.1 <i>Flow visualization.....</i>	<i>42</i>
2.2.2 <i>Thermometry</i>	<i>45</i>
2.2.3 <i>Measurement of heat transfer</i>	<i>48</i>
2.2.3.1 <i>Error analysis</i>	<i>50</i>
2.2.4 <i>Computer interfacing hardware.....</i>	<i>51</i>

2.3	Quasi-steady state system	53
2.3.1	<i>Apparatus overview</i>	53
2.3.2	<i>Data acquisition and operating software</i>	57
2.4	Heat transfer system.....	60
2.4.1	<i>Apparatus overview</i>	60
2.4.2	<i>Data acquisition and operating software</i>	63
2.5	Procedures	64
2.5.1	<i>Temperature of maximum density of Aqueous Solutions</i>	65
2.5.2	<i>Asymmetrical Heat Transfer</i>	68
3.	Experimental Results	71
3.1	Introduction	72
3.2	Data acquisition overview	75
3.3	The density maximum of aqueous solutions.....	79
3.3.1	<i>Quasi-steady state cooling of water</i>	80
3.3.2	<i>Heat flow in the vicinity of the density maximum</i>	86
3.3.2.1	<i>The rate of cooling</i>	91
3.3.3	<i>Measurement technique for the temperature of maximum density of aqueous solutions</i>	93
3.3.4	<i>The temperature of maximum density of aqueous solutions</i>	101
3.3.5	<i>The anomaly feature of Na₂CO₃ solutions</i>	112
3.4	Asymmetrical heat transfer	115
3.4.1	<i>The temperature profiles of water under steady state conditions</i>	117
3.4.2	<i>Water-saline diode</i>	119
3.4.3	<i>Water-Perspex diode</i>	126
4.	Computational Fluid Dynamics	131
4.1	Introduction	132
4.2	Theory	133
4.2.1	<i>Governing equations</i>	133
4.2.2	<i>Numerical methods</i>	135
4.2.3	<i>Comsol Multiphysics © and NaSt2D</i>	136
4.2.4	<i>Calculating heat transfer</i>	139
4.3	The density maximum of aqueous solutions.....	140

4.3.1	<i>Quasi-steady state cooling</i>	141
4.3.2	<i>Measurement technique for the temperature of maximum density of aqueous solutions</i>	143
4.4	Asymmetrical heat transfer	144
4.4.1	<i>Water-saline diode</i>	145
4.4.2	<i>Optimization studies</i>	147
4.4.3	<i>Phase change diode</i>	151
4.4.4	<i>Water-Perspex diode</i>	153
5.	Numerical Results	156
5.1	Introduction	157
5.2	The density maximum of aqueous solutions	160
5.2.1	<i>Quasi-steady state cooling and warming of Ethanol</i>	161
5.2.2	<i>Quasi-steady state cooling and warming of Water</i>	167
5.2.3	<i>Heat transfer in the vicinity of the density maximum</i>	174
5.2.4	<i>Heat transfer during the quasi-steady state cooling and warming</i>	177
5.2.5	<i>Measurement technique for the temperature of maximum density of aqueous solutions</i>	186
5.2.6	<i>The shape of the anomaly feature</i>	191
5.2.6.1	<i>The container dimensions</i>	192
5.2.6.2	<i>The vertical position of the temperature points</i>	194
5.2.6.3	<i>The properties of water</i>	199
5.3	Asymmetrical heat transfer	203
5.3.1	<i>Water-saline diode</i>	204
5.3.2	<i>Optimization of the water-saline diode</i>	209
5.3.2.1	<i>Significance of the boundary temperatures</i>	210
5.3.2.2	<i>Significance of the size of the temperature difference</i>	214
5.3.2.3	<i>Significance of the aspect ratio and scale of the container</i>	217
5.3.2.4	<i>Significance of the number of liquid compartments</i>	219
5.3.3	<i>Water-Perspex diode</i>	221
5.3.4	<i>Optimization of the water-Perspex diode</i>	228
5.3.4.1	<i>Significance of the boundary temperatures</i>	229
5.3.4.2	<i>Significance of the width of the Perspex slab</i>	232
5.3.5	<i>Phase change diode</i>	235

5.3.6	<i>Thermal analogy of Ohm's law for the water-saline diode</i>	237
6.	Conclusions	242
6.1	Conclusions	243
6.2	Future work	246
A.	Comsol m-script for the Water-Saline Diode	250
B.	Thermal Analogy Code	257
	Bibliography	260

Abstract

This thesis is concerned with heat flow asymmetry through composites of water and aqueous solutions. Central to this exploration are the behaviour of heat transfer in the vicinity of the density maximum and the behaviour of the temperature of maximum density of aqueous solutions. Both of these topics are investigated by cooling a rectangular enclosure of the test fluid in a quasi-steady state manner. During cooling, the temperature at select points within the liquid is monitored and the flow of heat at both isothermal walls is measured. As the liquid cools through its density maximum the normal single-cell convection that occurs in the presence of a horizontal temperature gradient changes to a double cell configuration in the vicinity of the density maximum. This transition manifests itself in changes in the horizontal temperature profile across the cavity and in the rate of cooling of the fluid. A measurement technique to study the behaviour of the temperature of maximum density of aqueous solutions is described in this thesis that relies on these changes. These changes are investigated experimentally and numerically.

The study of the behaviour of heat transfer and the temperature of maximum density of aqueous solutions revealed that heat transfer is reduced in the vicinity of the density maximum and that the temperature of maximum density of aqueous solutions depends on the nature and concentration of the solute. Both of these results are exploited in the study of heat flow asymmetry through a device that consists of two cubic enclosures side by side; one enclosure contains water with a density maximum at 4°C and the other enclosure contains a saline solution with a density maximum at 2°C. A temperature gradient, which spans both of these temperatures of maximum density, is applied horizontally across the composite system, resulting in different rates of heat transfer through the device depending on the gradient direction. Experiments performed with a 12cm x 6cm x 6cm container yield heat transfer rates of 0.55W and 0.19W depending on the direction of the temperature gradient, resulting in a rectification factor of 65.4%. Asymmetrical heat transfer rates are also found in composite systems of water and solids when the temperature gradient spans the temperature of maximum density of the water. Results from computational fluid

dynamics confirm the experimental results, and are used to investigate the influence of such parameters as temperature gradient and container aspect ratio on the rectification factor.

Acknowledgements

“As we express our gratitude, we must never forget that the highest appreciation is not to utter words, but to live by them.” -- John F. Kennedy

Throughout my PhD, I have often been humbled and overwhelmed by the generosity of a great many people. I appreciate that there are no words that can do their kindness justice, but I take this opportunity to acknowledge their generous and valuable contributions to this project.

I am much indebted to my supervisor and friend, Dr. Michael Cawley, for his articulate and infallible guidance over the past three years. It has been a privilege to learn from someone with an abundance of knowledge and a flair for scientific research. His unparalleled expertise and insight into experimental fluid dynamics have been a constant source of inspiration for me throughout this project. Michael’s enthusiasm, energy and optimism have helped me through some difficult times and I am deeply grateful for his friendship.

I thank the head of the Department of Experimental Physics, Prof. J. Anthony Murphy, for his advice and support, and for placing the facilities of the department at my disposal during the course of this work.

I thank my fellow postgraduates Daniel McGlynn and Paul O’Connor. I also thank my fellow laboratory demonstrators, Karen Foley, Mark Whale and Ian McCauley for making my time as a laboratory demonstrator enjoyable and for exposing me to new cultural ideas and ways of thinking.

I thank all the staff and postgraduates (past and present) of the Department of Experimental Physics who have made me feel welcome in the department and who have helped me in some form or other over the past few years, in particular, I thank Marie Galligan, John Kelly, Dr. Bill Lanigan, Ian McCauley, Dr. Niall McKeith, Dr. Cr  idhe O’ Sullivan, Gr  inne Roche and David Watson. I take this opportunity

to extend a special thanks to John Kelly for his generous support with my computer problems and to Gráinne Roche for her kind assistance.

I am eternally indebted to my mentor Paul Buffini for his never-ending support, advice, and encouragement over the past seven years. I am also sincerely grateful to Paul for completing the very tedious and monotonous task of proof reading this thesis.

I have always been humbled and inspired by the generosity and compassion of my teacher and friend David Fahey. I am sincerely grateful for his encouragement, his friendship, and his constant belief in my abilities. I also thank Paul Curry for encouraging my curious thinking and for instilling me with a passion and appreciation for science.

I take this opportunity to acknowledge financial support from the Irish Research Council for Science, Engineering and Technology in the form of a Postgraduate Scholarship under the Embark Initiative. I also thank the National University of Ireland, Maynooth for the Postgraduate Scholarship in Science and Engineering.

I am grateful for all the support and the much needed distractions from my housemates and friends over the past few years. Many thanks to Bernie and Liam Maloney, Claire Barrett, Ian Harris, Jeffrey Godsell, Linda Mullens, Chris Duignan, Collette Bourke, Brendan Donohue, Megan Gregory, Kate Gregory, Linda Lyons, Maurice Kennedy, and Karen Foley. A special thanks is extended to Collette Bourke for all the laughs, the chocolates and the many cups of tea and vanilla coffee.

And last but certainly not least, I thank my family, my mother Mary for being a pillar of strength for me and for always being there, my sisters Loretta and Grainne for their generous support and patience with me, and my brother Eamonn for always listening to my ridiculously long rants in the early hours of the morning. I am eternally grateful to my family for their infinite love, support, advice, encouragement and belief in me, without them I could not have completed this work.

I dedicate this thesis to my dearest father, who always unconditionally loved, supported, advised and encouraged me.

*To my loving father,
Eamon Mooney*

Chapter 1

Introduction

1.1 Introduction

Water is an intriguing substance that plays a vital role in sustaining life on Earth. Water participates in virtually every biological process that occurs in both animals and plants. The human body consists of over sixty-five percent water, and almost eighty percent of the adult brain contains water. The role of water in life on our planet is so great that it is often seen as a possible precursor to the existence of life in some basic form on other planets. Over two-thirds of our planet is covered in liquid water and one-twentieth is covered in ice, in fact, one whole continent is almost completely covered in ice. Water also exists in the atmosphere with the composition of air varying between 0% and 4% water vapour. That water can exist in all three states (solid, liquid and gaseous form) on Earth at any one time shows that it is an unusual and fascinating substance.

Despite being the most abundant liquid on Earth, it is also the most anomalous. Several of its properties differ considerably from those of other liquids which, on the basis of their molecular composition, might otherwise be expected to have similar properties. The water molecule is comprised of two hydrogen atoms and one oxygen atom. In a typical water molecule, two hydrogen atoms are covalently bonded to a single oxygen atom; a link is formed between the atoms by the sharing of an electron. Each water molecule consists of four electron pairs; two of which are associated with the hydrogen atom and two are lone pairs. All four of these electron pairs participate in hydrogen bonding with successive water molecules when the substance is in its solid state. The resulting three-dimensional arrays of water molecules are highly cohesive. The conversion of solid water to its liquid form requires that some of the weaker bonds be broken allowing for movement. The breaking of these bonds requires large amounts of energy. Similarly, the alteration of liquid water to its gaseous state requires that all the hydrogen bonds in the liquid state be broken. In comparison to other substances of similar molecular structure, water possesses a high specific heat capacity, a high boiling point, a high freezing point, an unusual solid-liquid phase change, and a density maximum in its liquid state. In fact, water exhibits no fewer than thirty-seven anomalous properties. Some of these anomalous properties make water particularly well adapted for its various roles in sustaining life on the planet.

The specific heat capacity of water at 25°C for one atmosphere of pressure is 4179 J.Kg⁻¹.K⁻¹ [1], which compares to a value of 2453 J.Kg⁻¹.K⁻¹ [2] for ethanol (a substance with a similar mass) under the same conditions. The higher heat capacity value for water is a consequence of the strong hydrogen bonds between the successive molecules. Larger amounts of energy are required to break these bonds and therefore a larger amount of heat energy is required to raise the temperature of water. This property of water allows the oceans to act as huge thermal reservoirs regulating the planet's climate. In fact, the North Atlantic Drift, which brings warm water from the Gulf of Mexico to the British Isles, carries a phenomenal amount of heat; it bears with it every day twice as much heat as would be produced by burning all the coal mined globally in a year [3].

Other anomalous properties of water include a high boiling point (100°C) and a high freezing point (0°C). Hydrogen sulphide, a molecule of similar structure has a boiling point at -61.2°C and a freezing point at -85.6°C. The behaviour of these two similar molecules is notably different; the reason for this is that hydrogen bonding that occurs between neighbouring water molecules is greater than the hydrogen bonds that form between neighbouring hydrogen sulphide molecules. The high polarity of the water molecule is primarily responsible for this difference in the hydrogen bonding of neighbouring molecules for water and hydrogen sulphide. High boiling and freezing points are not the only unusual behaviours of the phase changes. When liquid water freezes, it becomes less dense. Contrary to the behaviour of most other solids, water expands on freezing and the solid state is less dense than the liquid state. This behaviour has a significant impact on aquatic life, as it is responsible for keeping ice at the top of ponds and lakes during cold winters; thus, allowing aquatic life to survive at the bottom where food is more readily found and warm water circulates. The ease at which water can be supercooled is an anomalous property of water also associated with the phase change. Water is easily supercooled to -25°C and with more difficulty down to -38°C.

Another property of water that is exploited by aquatic life to survive under such cold conditions is the colligative nature of the freezing point. When a solute such as sodium chloride or sucrose is added to water the temperature at which it freezes is

lowered. The temperature at which the freezing point occurs when a solute is added to water only depends on the number of solute particles present; it is independent of the identity of the solute. The manner in which the freezing point is depressed can be found in references [1] and [2]. Many insects and fish exploit this property to avoid freezing in cold conditions [3]. They manufacture compounds called cryoprotectants. Natural cryoprotectants include sugars such as fructose and polyalcohols such as ethylene glycol. During the cold winter months, these creatures release these compounds into their blood thus lowering the freezing point of their blood and permitting their survival in cold conditions.

The anomalous property of water that is central to this thesis is the occurrence of a maximum in the density profile at 3.98°C for one atmosphere of pressure. The magnitude of this anomalous behaviour is small compared with the anomaly of water's expansion upon freezing – the latter corresponds to an 8.3% change in volume, compared with a 0.013% volume contraction between 0 and 4°C. The main body of work presented in this thesis is concerned with the influence of the density maximum on free convective flow. The influence of the density maximum on free convective flow has considerable implications globally. Aquatic life living in fresh water lakes, rivers and some low salinity seas are kept alive during the cold winter months as a consequence of the density maximum. For temperatures above the density maximum, fresh water behaves in a manner similar to typical liquids. Warm liquid ascends and cold liquid descends. Consequently, during the summer months, the warm water in ponds, rivers, lakes and low salinity seas is at the top and the cooler liquid is at the bottom. At temperatures below the temperature of maximum density, this trend reverses. Consequently, during the cold winter months, cold liquid is at the top and warmer liquid is at the bottom. As a result, ponds and lakes freeze at the top; thus allowing aquatic life to survive during the cold winter months.

1.2 Review of the density of water

The presence of a density maximum in water has profound effects on the planetary environment and has led to many detailed studies on the density profile of water, [4], [5], [6], [7] and sea water, [8], [9], [10]. Thiesen *et al.* [6] carried out one of the earliest detailed studies on the density of water in 1896. These researchers used a method of balancing water columns of different temperatures to obtain density data

in the range of 0°C to 40°C. Chappius [4] in 1907 also conducted a detailed study on the density of water as a function of temperature. That researcher obtained data, which covered the temperature range 0-42°C, using a dilatometer. The accuracy of both of these studies is such that they are still quoted in the literature. Recent studies either quote one of these two data sets or a mean of the two.

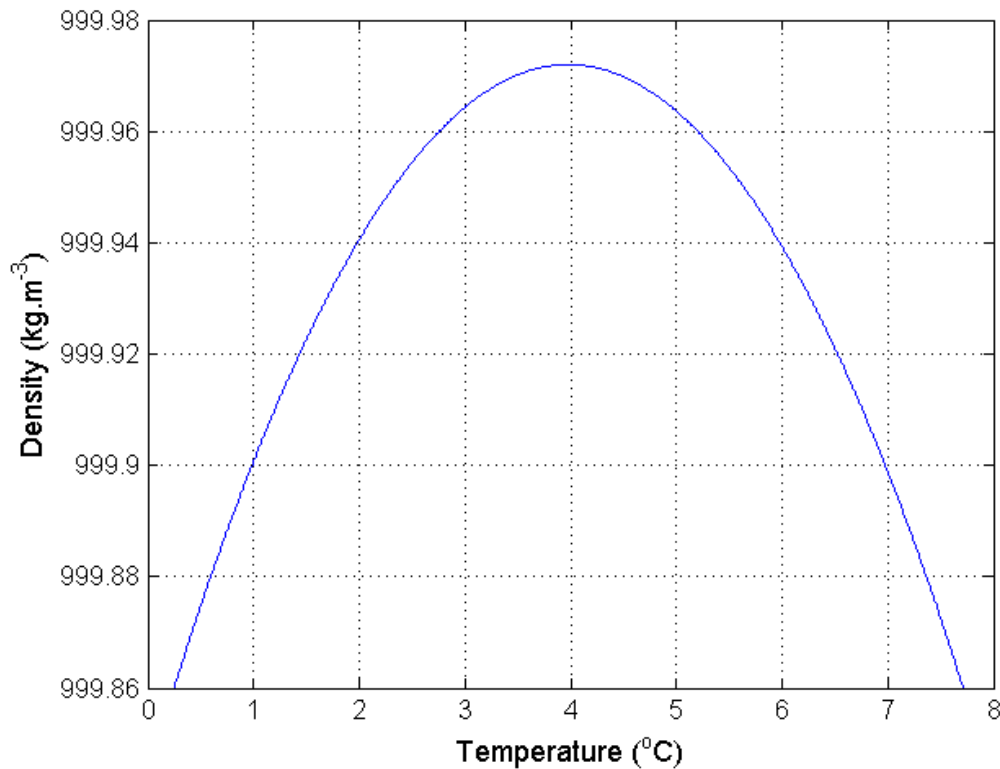


Figure 1.2-1 A third order polynomial fit to the density data in the CRC handbook of chemistry and physics [1] in the range of 0°C to 8°C.

The International Critical Tables of Numerical Data, Physics, Chemistry and Technology [11] published in 1928 compiled a table of the mean of these two datasets in the range 0-40°C. These tables also include density data in the range of 40-100°C taken from Thiesen [7]. The density data for a variety of aqueous solutions including seawater is also presented in the International Critical Tables [11].

In 1975, Kell [5] published a table of density data over the range -30 to 150°C along with a fifth order polynomial equation for the density of water. The 65th edition of the CRC handbook of Chemistry and Physics [1] contains this equation and table of

data. The numerical studies described in this thesis use a third order polynomial which is a best fit to this data in the range of -5°C to 10°C . Figure 1.2-1 shows a plot of this polynomial.

1.2.1 Historical review of the density maximum of water

One of the earliest documented observations of the density maximum of water was carried out at the Academia del Cimento, between 1640 and 1667 [12]. The academy conducted a variety of experiments during this time and published them in the *Saggi di Naturali Esperienze* (translates to *Examples of Natural Experiments*) written by the academy's secretary Lorenzo Magalotti. The experiment involving the maximum density of water was designed to investigate the freezing of water. Water in a glass bulb with a long thin tube was cooled by immersing the bulb in crushed ice. The experimenters reported that the water level in the tube began to decrease but at some point began to rise very slowly and upon freezing the water level in the tube unexpectedly jumped. The point at which the water level stopped falling was labelled the 'point of rest' and is in fact the point of maximum density.

This technique for observing the density maximum relied on the changes in the volume of water due to temperature changes. However, the volume of the container also changes with temperature giving rise to some ambiguity in the matter. Is the slow rise in the water level due to the volume changes in the water or is it due to the contraction of the vessel?

In 1805, Thomas Charles Hope [13] devised an experiment to observe the density maximum which relied on changes in the convection pattern detected by thermometers. Hope's apparatus is shown schematically in Figure 1.2-2 and pictorially in Figure 1.2-3. Water at 0°C is placed in a vertical cylindrical container. A small metallic basin surrounds the centre of the glass cylinder and it contains water at 20°C . In the absence of a density maximum, the liquid at the centre of the container should rise, so that warm water is at the top of the cylinder and cold water is at the bottom. If the liquid has a density maximum then at temperatures below the temperature of maximum density this trend should be reversed. Thermometers were inserted into the top and bottom of the glass cylinder.

Thomas Charles Hope's investigations revealed that water at the top was colder than the water at the bottom as it warmed, but at some point the temperature of the water at the top began to increase, and the temperature of the water at the bottom began to decrease until eventually the water at the top was warmer than the water at the bottom. In Hope's paper [13], he conducts three such experiments and from these experiments he concluded that water had a density maximum at a temperature between 39.5 and 40°F (4.2°C and 4.4°C). This is close to today's accepted value for the temperature of maximum density of pure water of 3.98°C (at one standard atmosphere of pressure).

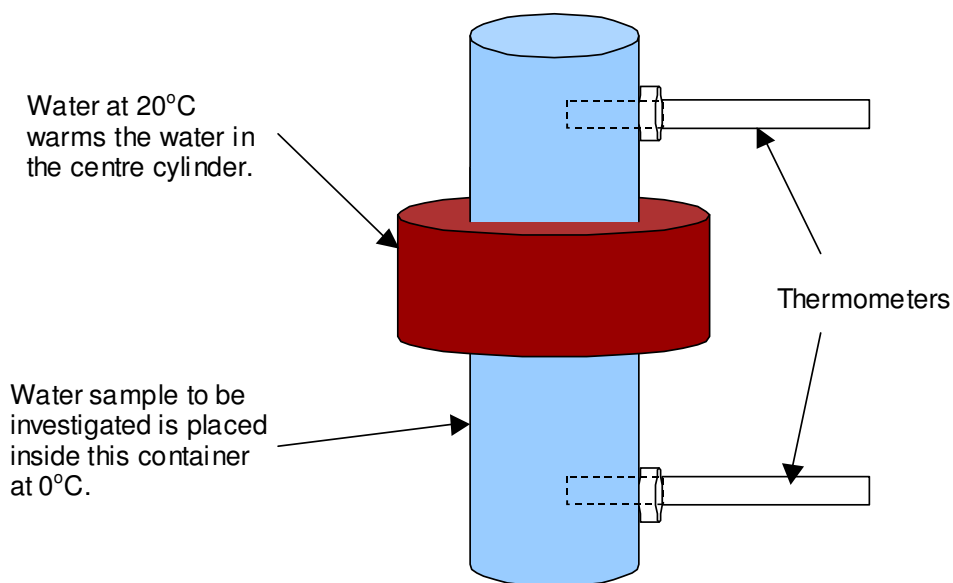


Figure 1.2-2 Schematic diagram of the apparatus used by Thomas Charles Hope in 1805.



Figure 1.2-3 A replica of the apparatus used by Thomas Charles Hope displayed in the National Science Museum of Ireland, St. Patrick's College, Maynooth. The metal basin is situated half way along the glass container and the cork bungs show the holes through which the thermometers are placed.

1.2.2 The temperature of maximum density of aqueous solutions

The addition of solutes to water alters the temperature of maximum density of water. Unlike the depression of the freezing point, the manner in which the temperature of maximum density changes is not colligative (a colligative property depends only on the number of solute particles present). The temperature of maximum density of aqueous solutions depends on both the nature and the concentration of the solute. The temperatures of maximum density for a variety of water solutions has been summarized in the International Critical Tables of Numerical Data, Physics, Chemistry and Technology [11], these data were obtained by a number of researchers (Despretz [14], [15], Rosetti [16], [17], Wright [18]) using standard density measurement techniques. Despretz [14], [15] carried out a considerable amount of work to determine the temperature of maximum density of salt solutions. The main conclusion drawn by Despretz from his work is the law that is named after him: “the lowering of the temperature of the point of maximum density of water caused by the addition of a solute is directly proportional to the concentration of the latter” [18]. Later work by other researchers found solutes that deviate from this law (e.g. the

monohydric alcohols), which renders Despretz's Law invalid. Rosetti [16], [17] attempted to link Despretz's Law with the behaviour of the depression of the freezing point of water solutions. The latter, however, is a colligative property of solutions whereas the temperature of maximum density was found to depend on the nature of the solute as well as the concentration. Mitchell and Wynne-Jones [19] investigated the partial molar volume (the partial molar volume is a measure of the apparent volume occupied by the solute when in solution) and the temperature of maximum density for aqueous solutions of hydrogen peroxide and aqueous solutions of ethanol. The hydrogen peroxide solutions showed a steep linear depression of the temperature of maximum density and the ethanol solutions showed that at low concentrations, the temperature of maximum density was elevated and thereafter it decreased non-linearly. The authors observed a minimum in the partial molar volume of the ethanol solutions but no minimum was observed in the hydrogen peroxide solutions. The authors claim that this minimum is related to the elevation of the temperature of maximum density for low ethanol concentrations. However, the minimum in the partial molar volume occurs at a mole fraction of approximately 0.1 and the elevation of the temperature of maximum density occurs at mole fractions less than 0.015. Furthermore, the minimum in the partial molar volume is observed over wide ranges of temperature and it is not confined to temperatures in the vicinity of the density extremum.

The majority of measurements of the temperature of maximum density for the various solutes quoted in the International Critical Tables [11] used dilatometers (devices similar to mercury thermometers) in which the test liquid revealed its expansion or contraction via changes in length of a liquid column in a thin-bore glass tube. Compensating techniques were used to allow for changes in the volume of the dilatometer bulb (e.g. Wright [18]). Few direct methods of determining the temperature of the density maximum have been reported.

A novel approach to direct detection and measurement of the temperature of the density maximum was reported by Caldwell [20]. The method relies on detecting a reversal in the temperature change when the water sample is subjected to a sudden (adiabatic) reduction in pressure. It is potentially an accurate approach as it involves detection of a zero crossing rather than an extremum in the density curve. However,

it is difficult to implement, and it seems that it has only been used to directly measure the temperatures of maximum density of the saline solutions reported in the original paper.

A novel technique which permits direct detection of the temperature of the density maximum and yields an accurate measurement of the change in the temperature of maximum density as a function of solute concentration (at a pressure of one atmosphere) is described in this study. The method relies on the detection of an anomalous feature in a series of temperature sensor profiles as the liquid sample is slowly cooled through the region of maximum density. The anomalous feature will be explained in this thesis using both Particle Image Velocimetry (PIV) and Computational Fluid Dynamics (CFD).

1.3 Review of the molecular models of water

Water, unlike most other substances, possesses many anomalous properties resulting from its complex and intricate molecular structure. The water molecule is comprised of two hydrogen atoms and one oxygen atom. In a typical water molecule, two hydrogen atoms are covalently bonded to a single oxygen atom; a link is formed between the atoms by the sharing of an electron. Each water molecule consists of four electron pairs; two of which are associated with the hydrogen atom and two are lone pairs. All four of these electron pairs participate in hydrogen bonding with successive water molecules when the substance is in its solid state. The electrons of water's hydrogen atoms are strongly attracted to the oxygen atom, and are actually closer to the nucleus of the oxygen atom than to the hydrogen nuclei (due to oxygen's high electronegativity in comparison to hydrogen's low electronegativity); therefore, water is a polar molecule with a relatively strong negative charge at its oxygen atom and a relatively strong positive charge at its hydrogen atoms. This is directly responsible for the strong hydrogen bonds that occur between successive water molecules.

The anomalous property of water that is of interest in this study is the presence of a maximum in the density of liquid water at 3.98°C and one atmosphere [1]. It is generally believed that the density maximum arises as a consequence of a balance between packing efficiency (high density mode) and bonding optimization (low

density mode). Whereas in most substances the packing density is optimized as the temperature is lowered (removal of vibrational kinetic energy permitting molecules to move closer together, thereby lowering the potential energy) it is speculated that in water it becomes energetically more favourable at lower temperatures for molecules to move further apart in order to optimize the energy of hydrogen bonding. In such models, water at low temperatures is made up of a mixture of lower- and higher-density clustering, resulting in an extremum in the state function.

Cho *et al.* [21] developed an analytical model to explain the occurrence of the density maximum. In their model, the authors assume that the nearest neighbour in the hydrogen structure of water can be ignored and consider only the behaviour of the second nearest neighbour. The authors cite experimental evidence to support this assumption. According to Cho *et al.* [21], the experimental data apparently shows that as the temperature increases, more densely packed second neighbours near 3.4Å (packing efficiency) are created at the expense of the ordinary second neighbours of the open tetrahedral network (bonding optimization). Their analytical model is based on this idea and the results are in agreement with the experimental results provided certain parameters are carefully chosen.

Tanaka [22] developed a model of water to account for some of the anomalous thermodynamic properties of water. The model focuses on the effective attractive interaction potential between neighbouring molecules in water. Tanaka [22] introduces two order parameters, ρ and S , where ρ represents density order (packing efficiency) and S represents bond order (bonding optimization). The author shows that any increase in one of these parameters results in a decrease in the other parameter. The author cites experimental results that show a minimum in the melting temperature of ice as a function of pressure at 2kbar. The author labels this pressure as a crossover pressure P_x . The author postulates that below P_x the primary order parameter is S , while above the crossover pressure ρ is the primary order parameter. The author attributes the unusual behaviour of the thermodynamic properties of water to the crossover pressure. The coupling between these two order parameters gives rise to the density maximum. The author also states that the model was used to explain the behaviour of silica in the supercooled state, which also shows a density maximum in this regime.

Jedlovsky *et al.* [23] developed a computational model to explain the occurrence of the density maximum. The model shows that an increasing number of molecules leave the tetrahedral hydrogen-bonded network with increasing temperature. These interstitial molecules are located in the cavities of the tetrahedral network of the other molecules, forming closely packed structural units with their neighbours. The effect of the increasing number of these closely packed patches on the density of the system can compensate the increasing thermal motion of the molecules up to a certain point. Jedlovsky *et al.* [23] show that these two opposite effects are responsible for the density maximum of water.

While the occurrence of the density maximum has been studied extensively on the molecular scale, it is evident from above that there is no consensus in the literature on a molecular model that accurately explains its occurrence. A common feature of the various molecular models ([21], [22], [23], [24]) is the attribution of the nature of the hydrogen bond in water to account for this anomalous property (and other anomalous properties). However, solid-liquid phase change anomalies are found in some other substances, notably Gallium and Bismuth [1]. While it is not clear if any of these substances exhibit a density maximum in their liquid state under normal pressure conditions, a density maximum has been reported for Gallium [25] under conditions of negative pressure (i.e. tension). Hydrogen bonding plays no role in such elemental metals. Evidently, there is still uncertainty regarding the true origin of the density maximum. However, the detailed molecular behaviour of water is beyond the scope of this study. The main focus of this work is on the macroscopic effects of the density maximum on free convection.

1.4 Mathematical description of fluid dynamics

It is considered that the first and most lasting contribution to the study of fluids came from the Greek mathematician Archimedes (287-212 B.C.). Archimedes principle states that a floating or immersed body must be acted upon by an upward force equal in magnitude to the weight of the liquid that it displaces. Despite the very early discovery of this principle, it was not until eighteen centuries later that the study of liquids and gases began to make great progress.

In the 17th and 18th century, the behaviour of liquids and gases received a lot of attention from very noteworthy mathematicians such as Johann Bernoulli (1667-1748), his son Daniel Bernoulli (1700-1782), and Leonhard Euler (1707-1783). Their studies led to Bernoulli's equation for incompressible fluids and Euler's equation of motion for non-viscous fluids.

In 1822, Louis Marie Henri Navier (1785-1836) attempted to extend Euler's equation of motion to include the flow of a viscous fluid, and although he did not fully comprehend the mechanism of viscosity, he did derive the correct mathematical description of the motion of a viscous fluid. In 1845, George Gabriel Stokes (1819-1903) developed the same equations as Navier, but with greater comprehension. These equations, known as the Navier-Stokes equations, are used in this study to mathematically describe the behaviour of a fluid.

The Navier-Stokes equations are non-linear partial differential equations; their complexity is so great that there are only a few known analytical solutions to these equations. Many researchers in heat and mass transfer since the 19th century have used dimensionless numbers to understand and describe fluids. There are many dimensionless numbers but they are not used in this study to analyse the results. However, the Rayleigh number and the Nusselt number are quoted in certain instances to the aid the reader that is familiar with dimensionless numbers and to compare results from this study to results from studies conducted by other researchers. These numbers will be defined in the next section along with the Reynolds Number, the Prandtl Number and the Grasshof Number.

1.4.1 Dimensionless numbers

The Rayleigh Number, named after the British physicist Lord Rayleigh (1842-1919), indicates whether the heat in a fluid is transferred primarily by free convection or conduction

$$Ra = \frac{g|\Delta\rho|VC_p}{\nu k}$$

where g is gravity, ρ is the density, V is the volume, C_p is the specific heat capacity, ν is the coefficient of kinematic viscosity and k is the thermal conductivity.

The Nusselt Number, named after the German engineer Wilhelm Nusselt (1882-1957), is the ratio of convective heat transfer to conductive heat transfer

$$Nu = \frac{\psi L}{k\Delta T}$$

where ψ is the heat flux (W.m^{-2}), L is a measure of length, k is the thermal conductivity and ΔT is the temperature difference across the system.

The Reynolds Number, named after the Irish engineer and physicist Osborne Reynolds (1842-1912), provides a criterion for dynamic similarity and for correct modelling in many fluid flow experiments. It is defined as follows

$$Re = \frac{\rho UL}{\mu}$$

where ρ is the density, U is a characteristic speed, L is a characteristic length and μ is the coefficient of dynamic viscosity.

The Prandtl Number, named after Ludwig Prandtl (1875-1953), is the ratio of momentum diffusivity to thermal diffusivity.

$$Pr = \frac{\mu C_p}{k}$$

where C_p is the specific heat capacity, μ is the coefficient of dynamic viscosity, and k is the thermal conductivity.

The Grashof Number, which is named after Franz Grashof (1826-1893), is the ratio of buoyancy forces to viscous forces

$$Gr = \frac{g\Delta\rho V}{\rho\nu^2}$$

where g is gravity, ρ is the density, V is the volume and ν is the kinematic viscosity.

1.5 Review of differentially heated cavities

With the advent of computers, extensive studies on free convection in water near the density maximum have been conducted in cylindrical and rectangular enclosures using both experimental and numerical techniques. The work described in this thesis is concerned only with rectangular cavities. The rectangular cavity has two opposing walls at different temperatures. The remaining walls are insulated and the cavity is filled with the fluid under investigation. This type of system is generally referred to as a differentially heated cavity. The general purpose of differentially heated cavities is to study free convection. This system mimics many practical situations and it has been the subject of many theoretical considerations. It is reported in the literature that the first formulation of this problem was published by Batchelor [26], who was interested in the thermal insulation such cavities could provide.

A differentially heated cavity may have a vertical temperature gradient placed across it. When the cavity contains a typical liquid and it is heated from above and cooled from below, heat is transferred via conduction and no convection occurs. When the direction is reversed, so that the cavity is heated from below and cooled from above, convection occurs (conditions must be above a critical number). Oosthuizen [27] numerically investigates free convection in the vicinity of the density maximum using a rectangular cavity that is subjected to such a vertical temperature gradient. The main aim of the study was to determine how far above 4°C the hot wall temperature (which is at the bottom) could be before significant convective motion occurs. The enclosure contains water and the upper wall is maintained at a uniform cold temperature that is below the freezing point of water while the temperature of the lower hot wall is maintained at temperatures above the freezing point of water. The upper portion of the enclosure is thus filled with ice and the lower portion with liquid. Oosthuizen [27] showed for a liquid with no density maximum that when the dimensionless hot wall temperature reached a certain value significant motion develops which decreases the thickness of the ice layer and leads to an intensification of the liquid motion. When the liquid did have a temperature of maximum density, convective motion begins to develop in the fluid when the hot temperature is well above the temperature of maximum density. When convective motion commenced the thickness of the liquid layer increased rapidly. It was also found that as the

temperature of maximum density increased so too did the temperature of the hot wall required to start convection.

Seybert and Evans [28] also conducted a study on free convection near the density maximum in the presence of ice using a differentially heated cavity. Unlike Ooesthuizen [27], their study used a differentially heated cavity that was subjected to a horizontal temperature gradient. Seybert and Evans [28] conducted steady state investigations for three different sets of boundary temperatures: 10°C and -5°C , 8°C and -5°C , and 5°C and -5°C . In each case, the portion of water at the left (hot) wall was in its liquid state and the portion at the right (cold) wall was in its solid state. The purpose of their study was to investigate the influence of the density inversion on the solidification front. Their results show that in the first case two convection cells of unequal magnitude are observed in the liquid portion. They conclude that the larger cell impacts the top of the solidification front (causing that front to be less developed at the top). In the second configuration, they observed two counter-rotating cells of equal magnitude in the liquid portion. The shape of the circulation front is different from the previous configuration; the impacting flow is now at the bottom of the ice and it is therefore here that the front is less developed. Their final experimental results show a single convection cell in the liquid portion that rises along the solidification front. The impacting flow is again at the bottom and therefore the solidification front in both the second and last configuration is similar. Seybert and Evans [28] use a differentially heated cavity subjected to a horizontal temperature gradient to show that the density inversion influences the solidification front.

Numerous studies have been conducted on free convection in the vicinity of the density maximum in differentially heated cavities subjected to a horizontal temperature gradient in the absence of ice. The studies were conducted using both numerical [29], [30], [31], [32] and experimental [33], [34], [35] methods. Watson [32], Seki *et al.* [35] and Lin and Nansteel [29] investigate free convection in the vicinity of the density maximum using a cavity containing water that has two opposing vertical walls, which are isothermal, and all remaining walls are insulated. The influence of the density maximum on free convection through the cavity is investigated under steady state conditions for a range of boundary temperatures. In each steady state investigation, the cold boundary temperature is 0°C while the hot

boundary varies from 1°C to 16°C (for Watson [32] and Lin and Nansteel [29], and 12°C for Seki *et al.* [35]). Their studies concluded that two counter-rotating cells exist in the liquid in the vicinity of the density maximum. When the wall temperatures are symmetric about the temperature of maximum density, the two convection cells are of equal magnitude. They also show that when the wall temperatures are not symmetric about the temperature of maximum density, the smallest convection cell occurs at the wall whose temperature is closest to the temperature of maximum density. Seki *et al.* [35] extended the study to include an investigation on the influence of the container aspect ratio (width w divided by height h) on the behaviour of the flow pattern in the vicinity of the density maximum. They show that the aspect ratio does not have a significant impact on the flow pattern.

Tong and Koster [31] investigated the behaviour of fluid flow in the vicinity of the density inversion under transient conditions. Their numerical study investigated heat transfer by initially setting the temperatures of the walls and the liquid to 3.98°C. At time $t=0$ seconds, the cold wall was abruptly cooled to 0°C and the hot wall either remained at 3.98°C or it was abruptly heated to 8°C or 12°C. Their results show that when their investigations reached steady-state the flow patterns were identical to those reported by the aforementioned researchers under the same temperature conditions. The authors show that when the boundary temperatures are 0°C and 3.98°C the flow pattern develops at the cold wall and one convection cell exists in the liquid when steady state is reached. When the boundary temperatures are 0°C and 8°C (these temperatures are symmetric about the temperature of maximum density) the flow pattern develops at both walls at equal rates and when steady state is reached two convection cells of equal magnitude are found in the liquid. When the boundary temperatures are 0°C and 12°C, the flow pattern develops at both walls but at a faster rate at the hot wall. When this system reached steady state, the convection cell that developed at the hot wall was larger than the convection cell that developed at the cold wall. It is evident from all of these studies that the density maximum has a profound effect on the flow pattern in the liquid.

In this thesis, free convection is investigated in the vicinity of the density maximum using a differentially heated cavity that is subjected to a horizontal temperature gradient. The study investigates the influence of the density maximum on free

convection under steady-state conditions and quasi-steady state conditions. Unlike the previously described investigations, the magnitude of the temperature gradient does not change in the quasi-steady state investigations and most of the steady-state investigations described in this thesis. The investigations are carried out using experimental and numerical techniques.

1.6 Review of heat transfer

Heat transfer in a fluid subject to density inversion is important in many engineering and environmental applications, such as crystal growth, ice formation and the melting of ice. Numerous studies, both experimentally and numerically, have been carried out over the past three decades on heat transfer in the vicinity of the density maximum of water in differentially heated cavities ([29], [30], [31], [32], [35], [36], [37]). The behaviour of heat transfer in the vicinity of the density maximum is of fundamental importance to the study described in this thesis, since much of the work is concerned with asymmetrical heat transfer through composites of water and aqueous solutions in the presence of the density maximum.

Section 1.6.1 describes some of the studies conducted by other researchers. The studies are conducted using either experimental or numerical techniques. Despite the different techniques used and in some cases the different approaches used, all of the studies have the same conclusion: heat transfer is a minimum in the vicinity of the density maximum. All of the studies reported in this section conclude that the minimum is reached when two symmetric counter-rotating cells exist in the fluid, but only Lin and Nansteel [29] speculate about the relationship between the dual cell structure in the fluid flow and the reduction in heat transfer.

The work of Seki *et al.* [35] is the only work described in section 1.6.1 that uses experimental techniques to investigate heat transfer in the vicinity of the density maximum. The method used by Seki *et al.* [35] to measure heat transfer through the differentially heated cavity is described in section 1.6.2 along with various other measurement techniques. The requirements for the heat transfer measurement technique used in the study presented in this thesis are:

- i) It must be capable of measuring heat transfer at the hot and cold walls,

- ii) It must be capable of measuring heat transfer under steady state conditions and under transient conditions,
- iii) Implementation of the technique must require minimal modification to the current experimental system, and
- iv) The technique must be non-invasive and relatively inexpensive.

None of the techniques described in section 1.6.2 are used in this study, as they do not satisfy these requirements for the experimental system described in this thesis.

1.6.1 Heat transfer in the vicinity of the density maximum

It is generally considered that one of the earliest studies on the influence of the density maximum of water on free convection in a differentially heated cavity to be published was that of Watson [32] in 1972. In Watson's study, a square cavity containing water has two opposing vertical walls that are isothermal and all remaining walls are insulated. Watson [32] investigates the influence of the density maximum on heat transfer by obtaining the rate of heat flow through the cavity under steady state conditions for a range of boundary temperatures. In each steady state investigation, the cold boundary temperature is 0°C while the hot boundary varies from 1°C to 16°C. Watson [32] concludes from his study that heat transfer is a minimum when the boundary temperatures are 0°C and 8°C, i.e. the temperature difference is centred on the temperature of maximum density.

Watson's study was entirely numerical. A similar study was later conducted by Seki *et al.* [35] using experimental and analytical techniques. In a similar manner to Watson [32], these authors investigated the influence of the density maximum on free convection in a rectangular enclosure with two opposing isothermal walls (all other walls were insulated). The behaviour of heat transfer in the vicinity of the density inversion was investigated by obtaining the rate of heat flow through the cavity under steady state conditions for a range of boundary temperatures. In each steady state investigation, the cold boundary temperature is 0°C while the hot boundary varies from 1°C to 12°C. The experimental results of Seki *et al.* [35] confirm the numerical results of Watson [32]. The authors conclude that heat transfer is a minimum when the boundary temperatures are 0°C and 8°C and they speculate that the reduction is due to the prevention of heat transmission through the fluid by the two counter-rotating cells that exist in the liquid. Seki *et al.* [35] also

investigated the influence of the container's aspect ratio (height h divided by the width w) on heat transfer. They conducted this investigation by varying the aspect ratio for three sets of boundary temperatures (0°C and 4°C , 0°C and 8°C , 0°C and 12°C). Each set of boundary temperatures showed that as the aspect ratio increased the rate of heat flow increased until the aspect ratio values reached values between 0.8 and 1.5. After this range of aspect ratios, each set of boundary temperatures showed that the heat transfer decreased for increasing aspect ratio.

All of the aforementioned studies were conducted under steady-state conditions. Tong and Koster [31] investigated the influence of the density maximum on heat transfer through a differentially heated cavity under transient conditions. The numerical study of Tong and Koster [31] investigates heat transfer by initially setting the temperatures of the walls and the liquid to 3.98°C . At time $t=0$ seconds, the cold wall was abruptly cooled to 0°C and the hot wall either remained at 3.98°C or it was abruptly heated to 8°C or 12°C . Their results show that for each of these three gradients heat transfer initially decreases rapidly before slowing down and reaching a steady value. Their results show that when steady state is reached for each of these three gradients, heat transfer is a minimum when the boundary temperatures are 0°C and 8°C . This is in agreement with all of the previously mentioned studies. These authors also attribute the reduction in heat transfer to the dual cell structure of the fluid flow but they do not specify the role of the flow pattern.

None of the aforementioned studies specify the exact role of the two counter rotating cells in the reduction of heat transmission. A similar study to those of Watson [32] and Seki *et al.* [35] was conducted by Lin and Nansteel [29] to validate their numerical model and these authors do attempt to explain the exact role of the two counter rotating cells. Lin and Nansteel [29] speculate that the dual-cell structure prohibits direct convective heat transfer between the hot and cold walls. According to Lin and Nansteel [29], each cell behaves like an insulator preventing warm fluid from the hot wall coming in direct contact with the cold wall, and vice versa for the cold fluid. The only direct thermal communication between the two walls occurs at the centre of the cavity where the hot and cold cells meet. Lin and Nansteel [29] state that the transfer of heat between the two walls is predominantly by conduction and hence the reduction in heat transfer.

The study presented in this thesis investigates heat transfer in the vicinity of the density maximum using experimental and numerical techniques. The results agree with those of the aforementioned researchers, that heat transfer is a minimum in the vicinity of the density maximum. Lin and Nansteel's [29] speculation that the reduction in heat transfer is entirely due to the dual-cell structure of the fluid flow is examined in this thesis. It will be shown that although the flow pattern is the primary reason for the reduction in heat transfer, it is not the sole contributor. The work presented in this thesis shows that the reduction in buoyancy due to the curvature of the density profile results in a reduction of the convective velocity and hence, heat transfer.

1.6.2 Heat transfer measurement techniques

The measurement of heat transfer is of major importance to the work reported in this thesis and indeed to many other researchers in free convection. There are a variety of techniques described in the literature for measuring heat transfer. The following are some of the main measurement techniques used by other researchers for measuring heat transfer: liquid crystal thermography, the guarded hot plate technique and the monitoring of electrical power input.

Thermochromic Liquid Crystals (TLCs) change colour with temperature due to a change in their molecular structure. The liquid crystals change from transparent at low temperatures, to red, yellow, green and violet. At higher temperatures the liquid crystals return to the transparent state. TLCs reflect at wavelengths that are related to their temperature, and a temperature versus hue calibration may be done. The heat transfer measurements can be obtained from this relationship in a variety of ways, such as the heated coating method, the transient method and the uniform coating method.

It is reported by Ochoa *et al.* [38] that a heated coating method is used by Mayhew *et al.* [39]. This method can be used to measure heat transfer coefficients under steady state conditions. A nearly uniform heat flux is provided by covering an insulated surface with a thin conductive film that is electrically heated. When this film is coated with liquid crystal, lines of constant colour indicate isotherms and the

corresponding heat transfer coefficients. Heat flux is determined by electrical power measurement, with minor corrections for conduction and radiation losses. The thermal mass of the substrate limits the rate at which a changing heat transfer coefficient can be measured.

Another variation of the liquid crystal thermography technique is reported by Ochoa *et al.* [38] and is used by Baughn [40] and Jones [41]. This method is known as the transient method. This process uses a video recording to provide both time and location of the colour play on a surface when it is exposed to a step change in the fluid temperature. The time that a surface takes to reach the temperature of the selected liquid crystal colour play is used to calculate the local heat transfer coefficient. This method generally assumes that the local heat transfer coefficients are constant with time.

The technique used by Ochoa *et al.* [38] embeds thermochromic liquid crystals into a surface with a low thermal mass substrate that is uniformly heated with incident infrared radiation. A temperature-hue calibration is performed prior to using the TLCs. The authors are concerned with measuring heat transfer coefficients under transient conditions. Changes in the fluid flow cause changes in the heat transfer coefficients, which in turn cause the surface temperatures to fluctuate. Video recordings capture these fluctuations providing time-dependent surface flow visualization and the heat transfer coefficient distribution.

The guarded hot plate method is often used for differentially heated cavities. A metering plate, which is simply an electrically heated plate, is embedded in a guarding hot plate as shown in Figure 1.6-1. The power to the metering plate is adjusted for a fixed power input to the hot plate until the temperatures of the guarding hot plate and the metering plate are the same. Under this condition there is no heat flow between the metering plate and the guarding hot plate, and all electrical power dissipated in the metering plate flows through the sample. The heat flow through the sample can then be obtained from the measurement of the power. A heat flux meter is placed between the metering plate and the guarding hot plate to monitor the heat flow between the plates. The guarded hot plate method is a commonly used method for measuring the conductivity of solids, but it has also been implemented

for other purposes. For example Leong *et al.* [42] used it to measure heat transfer through a differentially heated square cavity and Suehrcke *et al* [43] used it to measure heat transfer across corrugated sheets and honeycomb transparent insulation.

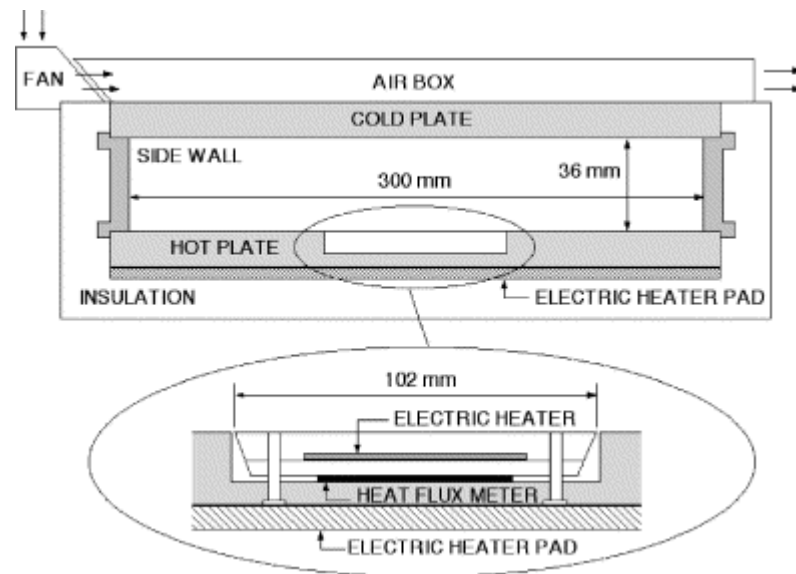


Figure 1.6-1 Schematic diagram of the guarded hot-plate apparatus for measuring the rate of heat transfer (Suehrcke *et al* [43]).

Another popular technique for measuring heat transfer is that used by Seki *et al.* [35]. The technique simply sums up the power consumed by electrical heaters in the experiment. It is assumed that all heat from the heaters enters the experiment and so it is deduced from this that the power consumed by the heaters is equal to the rate of heat flow. For this technique to work effectively all the heat generated by the heating units must flow through the test sample under investigation. The technique used by Seki *et al.* [35] is the only technique described in this section that has been applied to investigations of heat transfer in the vicinity of the density maximum. As discussed in section 1.6.1, the experimental results from their study are in good agreement with the numerical results of Watson [32] and Lin and Nansteel [29], thereby rendering this technique as a viable means of measuring heat transfer.

The technique described in Cawley *et al.* [36] and in the investigations reported in this thesis is a modification of the longitudinal cut-bar method [44]. This method was chosen over the aforementioned methods as it was easier to implement and relatively inexpensive. The technique requires the placement of a solid material of known conductance along the path of heat flow. It is important to choose a position along the path of heat flow that does not interfere with the investigations. The temperature drop across the solid is measured during the experiments and from this the rate of heat flow is inferred. A more detailed description of this technique will be presented in section 2.2.3.

1.7 Review of asymmetrical heat transfer

Asymmetrical heat transfer through a system occurs when different rates of heat transfer are obtained for two opposing directions of heat flow through the system. A simple example of such a system is a composition of a solid and a phase change material. In one direction of heat flow, the phase change material is in one state (e.g. solid); and in the other direction, it would undergo a phase change to a different state (e.g. liquid), with different heat conductance properties. This results in the transfer of heat via conduction in one direction and via convection and conduction in the opposing direction.

It will be shown in this study that composite systems containing water in the vicinity of the density maximum exhibit asymmetrical heat transfer. It has previously been reported [29], [35] that the rate of heat transfer through a rectangular enclosure of water subjected to a horizontal temperature gradient decreases in the vicinity of the density maximum. A simple arrangement will be described in this thesis which exploits this effect in a composite system of pure water and a saline solution to give rise to heat flow asymmetry. Such asymmetry will also be shown to exist in composite systems of water and solids.

Heat flow asymmetry is also a feature of green houses and the so-called green-house effect in planetary systems. In such cases, however, the temperature gradient is not strictly reversed; the effective magnitudes of the hot (T_h) and cold (T_c) temperatures that impose the gradient are not the same between day and night. In this work the following restrictive conditions for heat transfer asymmetry will be assumed:

- i) the values of T_h and T_c must be the same for both directions of the system or of the temperature gradient (excludes green house effects),
- ii) the system has reached steady-state (excludes transient effects).

Asymmetrical heat transfer is often referred to as thermal rectification or a thermal diode effect; systems that exhibit asymmetrical heat transfer are often referred to as heat rectifiers or thermal diodes. In this study, a parameter known as the percentage rectification is used to quantify the degree of asymmetrical heat transfer. The percentage rectification is defined as

$$r = \frac{(H_H - H_L)}{H_H} \quad (1.7-1)$$

where H_H is the high rate of heat transfer and H_L is the low rate of heat transfer. Thus, a rectification of 0% indicates no asymmetry, whereas a rectification value of 100% indicates perfect heat rectification (no heat flow in one direction, i.e. $H_L=0$)

Heat rectification devices offer considerable possibilities in insulation, refrigeration, heat pumps, and control of heat flow in general. A variety of devices exist or have been proposed that offer varying degrees of thermal rectification. A survey of these devices suggests that there are two independent conditions which can give rise to heat flow asymmetry; they shall be classified as Type I and Type II thermal rectifiers in the following discussion. Type I rectifiers require the presence of a body force, such as gravity or an external magnetic field (in the case of fluids with non-zero susceptibility), which gives rise to a preferred direction for heat flow. Type II rectifiers do not require a body force but do require a structural asymmetry in the direction of heat flow. Finally, there is a class of devices that combines both a body force and a structural asymmetry; the devices described in this thesis fall into this hybrid category. Table 1.7-1 shows the performance of the rectifiers described in this thesis along with those investigated by other researchers. Brief descriptions of some of the rectifiers investigated by other researchers in the Type I, Type II and hybrid categories are given in sections 1.7.1, 1.7.2, and 1.7.3, respectively.

Device	Rectification ¹	Reference	Notes
<i>Type I</i>			
Parallelogram enclosure	75% ²	[45]	CFD
Vertical fluid column	88% ²	[36]	CFD
<i>Type II</i>			
Copper oxide rectifier	53%	[46]	Experiment
Metal junction	50%	[47]	Theory ³
Expansion rectifier	65%	[48]	Experiment
Nanotube rectifier	7%	[49]	Experiment
1-D lattice	48%	[50]	Theory
1-D lattice	99%	[51]	Theory ⁴
Molecular junction	34%	[52],[53]	Theory
PCM-solid composite (vertical dT)	35% ²	This study	Theory
Quartz-glass composite	20% ²	[36]	Simulation ⁵
<i>Hybrid (body force and asymmetry)</i>			
Water-saline diode	65%	This study	Experiment/CFD
Water-Perspex diode	38%	This study	Experiment/CFD
PCM-solid composite (horizontal dT)	50% ²	This study	CFD
Heat pump + thermal diode	Not stated	[54]	Experiment/CFD

Table 1.7-1 A summary of the performance of thermal rectifiers investigated by previous researchers and those described in this study.

¹ Rectification factors are not stated in the publications in most cases. Some have been estimated for this work, but could vary over wide ranges depending on the assumed conditions. Most have yet to be verified experimentally.

² Estimated for this work.

³ Metal junctions - some experimental evidence is cited, but it is not compelling (see [47]).

⁴ In [51] the rectification was quantified by the ratio of high heat flow to low heat flow ($J+/J-$). This is related to the rectification factor by: $r = 1 - (J+/J-)^{-1}$.

⁵ Quartz-glass composite; Quartz: $k = -0.1T + 40$ (fit to data in [55]); Glass: $k = 0.003T + 0.4$ (fit to data in [56]), T in degrees Kelvin. Composite of 20cm quartz and 1cm glass was assumed.

1.7.1 Type I rectifiers

Type I rectifiers require the presence of a body force, such as gravity or an external magnetic field (in the case of fluids with non-zero susceptibility), which gives rise to a preferred direction for heat flow. An example of a Type I rectifier is that of a vertical temperature gradient applied across a region of fluid. For simple Newtonian fluids, heat transfer via both conduction and convection will take place if heat flows from the bottom of the enclosure to the top (i.e. warmer fluid below cooler fluid) whereas only conduction will take place if heat flows from the top of the enclosure to the bottom (warmer fluid resting above cooler fluid), thus leading to a decrease in the magnitude of heat transfer (Figure 1.7-1).

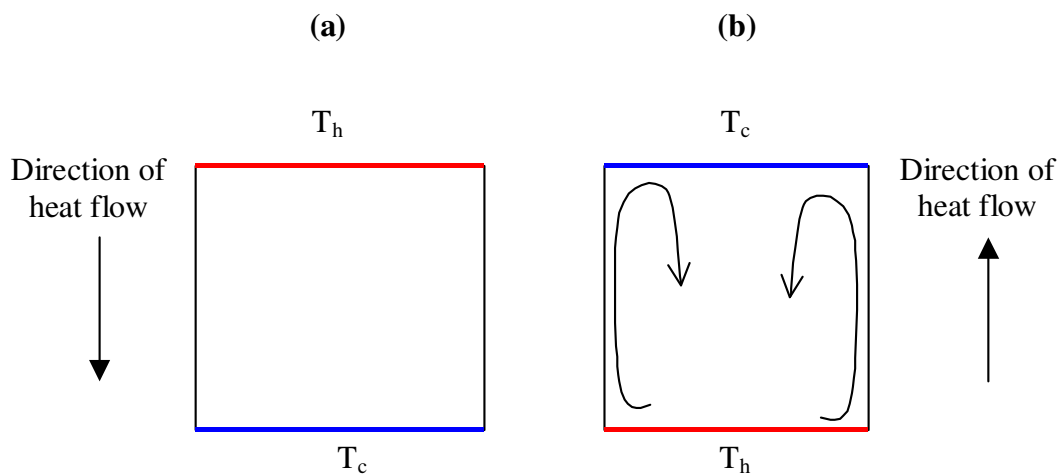


Figure 1.7-1 In the first configuration a rectangular container of a typical liquid cooled from below and heated from above results in heat flow by conduction only. In the second configuration a rectangular container of water heated from below and cooled from above results in heat transfer by conduction and convection. Heat transfer is greater in the second configuration since heat transfer occurs by convection also in this configuration.

Another example of a Type I rectifier is that discussed in Costa *et al.* [45]. They observed a thermal diode effect in a vertical stack of parallelogrammic partial enclosures with variable geometry (Figure 1.7-2). This arrangement of parallelogrammic partial enclosures offered Costa *et al.* [45] the flexibility of

changing the geometry by changing the inclination angle of the partitions. Since each parallelogrammic enclosure is not fully closed, fluid can be exchanged between neighbouring parallelogrammic enclosures, i.e. the enclosures are thermally connected. This feature of the geometry, although potentially useful for optimizing the thermal diode effect, was not necessary for observing the thermal diode effect. The thermal diode effect could be observed in just one parallelogrammic enclosure. The most important feature of the geometry is that the parallelogrammic enclosure has two vertical walls and the top and bottom walls are inclined to the horizontal. The occurrence of asymmetrical heat transfer in this system can be understood by examining an individual parallelogrammic enclosure. When the hot wall is on the left and the cold wall is on the right, the hot wall is below the cold wall. Thus, the hot liquid on the left rises and the cold liquid on the right falls, resulting in vigorous convection. When the direction of heat flow is reversed, the cold wall is below the hot wall. This configuration is not favourable to fluid flow, thus resulting in a reduction of heat transfer by convection.

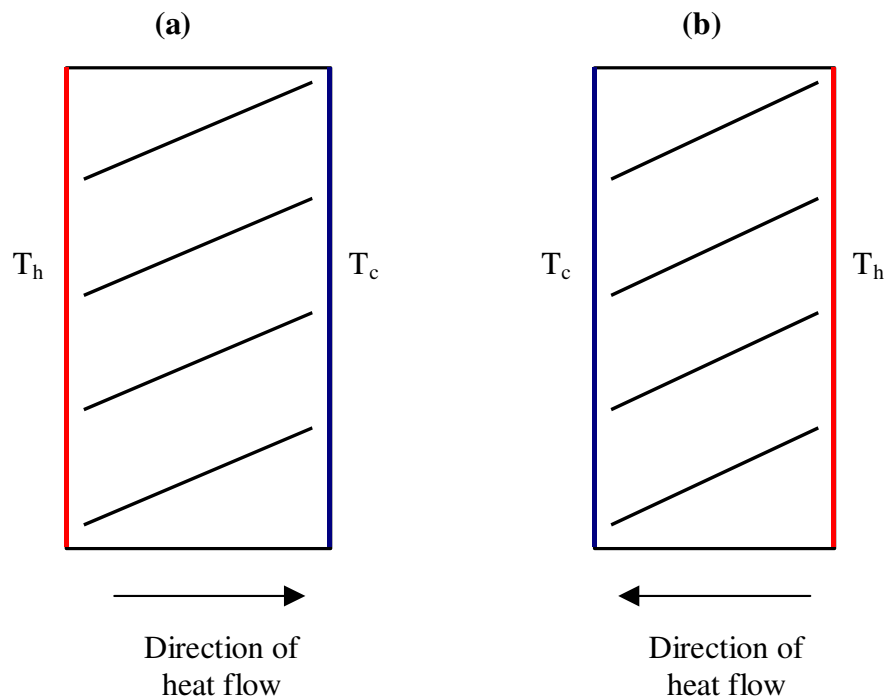


Figure 1.7-2 The thermal diode effect was observed by Costa et al. [45] in the geometry shown in this figure. The configuration in (a) favours fluid flow and hence, convection, more so than the configuration in (b). Thus, configuration (a) has a higher heat transfer value than configuration (b).

1.7.2 Type II rectifiers

Asymmetrical heat transfer may also be present in non-uniform or composite systems which are not invariant to 180° rotation; in such instances, the asymmetry of the heat flow becomes apparent if either the temperature gradient is reversed or if the system is rotated (while holding the temperature gradient fixed). These systems are Type II rectifiers and an example of this sort of system would be a combination of a region of Phase Change Material (PCM) adjacent to a region that does not undergo a phase change within the temperature range in question. For one orientation of the system, the PCM would be in one state (e.g. solid) whereas for the other orientation it would undergo a phase change to a different state (e.g. liquid) as shown in Figure 1.7-3. This system is arranged so that heat transfer occurs via conduction in both configurations (thereby excluding the body force required for Type I rectifiers and hence, this device is exclusively a Type II rectifier). The thermal conductivity of the material decreases when the material changes from a solid to a liquid, thus reducing the transfer of heat via conduction and exhibiting asymmetrical heat transfer.

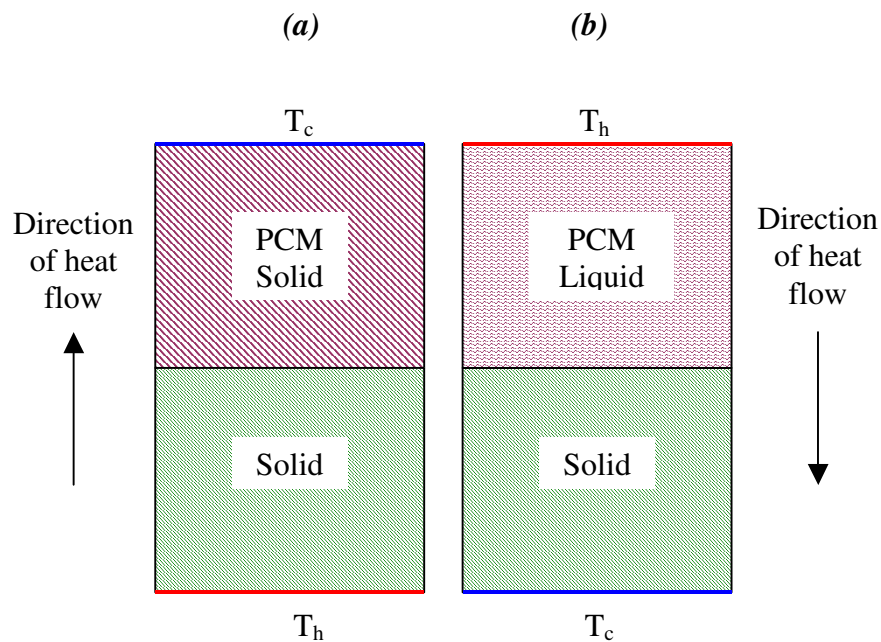


Figure 1.7-3 A composite system of a PCM and a solid with a positive vertical temperature gradient in (a) and a negative vertical temperature gradient in (b). In both directions of heat flow, heat is transferred by conduction; the change in the rate of heat flow is due the change in the thermal conductivity of the PCM when it changes state.

Another example of a Type II rectifier is the expansion rectifier discovered by Jones *et al.* [48]. This device is shown in Figure 1.7-4. The system consists of a stack of thin metallic disks held in series with an aluminium expansion element under constant strain between a heat sink and a heat source. The basis of the thermal diode effect observed in this system is that the thermal conductance of the stack depends on the contact pressure between the individual metallic disks. As the compression of the stack increases, the contact pressure increases and hence the thermal conductance increases. The change in compression of the stack is achieved by the expansion element. The coefficient of expansion for the expansion element increases as the temperature increases. Thus, the mean temperature of the expansion element must change considerably when the direction of heat transfer is reversed. This requirement is fulfilled by selecting a low effective thermal conductivity for the stack by comparison to the expansion element. This results in a large temperature drop across the stack and a very small temperature drop across the expansion element. As a result, when heat flows from left to right the mean temperature of the expansion element is considerably lower than when heat flows in the opposite direction. Hence, the expansion coefficient of the expansion element is less in the upper configuration of Figure 1.7-4 than in the lower configuration. Thus, a larger pressure is exerted on the stack in the lower configuration than in the upper configuration. Hence, the contact pressure changes when the direction of heat flow is reversed. Since the thermal conductance of the stack depends on the contact pressure, heat transfer through this system is altered when the direction of heat flow is reversed.

The rectifiers described above are investigated on the macroscopic scale. However, other examples of Type II rectifiers are found on the microscopic level. A theoretical thermal diode effect using a composition of two dissimilar metals is described by Moon and Keeler [47]. They discuss the directional effect in heat flow at the interface of dissimilar metals due to electronic heat conduction and phonon heat conduction. The authors ascribe the change in heat transfer through the system to the heat transfer across the interface. The authors acknowledge that experimental studies are required to confirm the theoretical study and conclude that the transfer of heat by electronic heat conduction has a direction associated with it. This implies that electronic heat conduction favours a certain direction of heat flow and that when this direction is reversed asymmetrical heat transfer is observed. Another example of a

Type II rectifier on the microscopic level is the rectifier described by Li *et al.* [51]. They present numerical and analytical evidence for the existence of a thermal diode effect when two non-linear one-dimensional lattices are coupled together by a harmonic spring with constant strength k_{int} . The study reports that by increasing the value of k_{int} the efficiency of the thermal diode increases. The study by Li *et al.* [51] shows numerical and analytical evidence for the existence of the thermal diode; however, there is no experimental evidence to confirm their predictions.

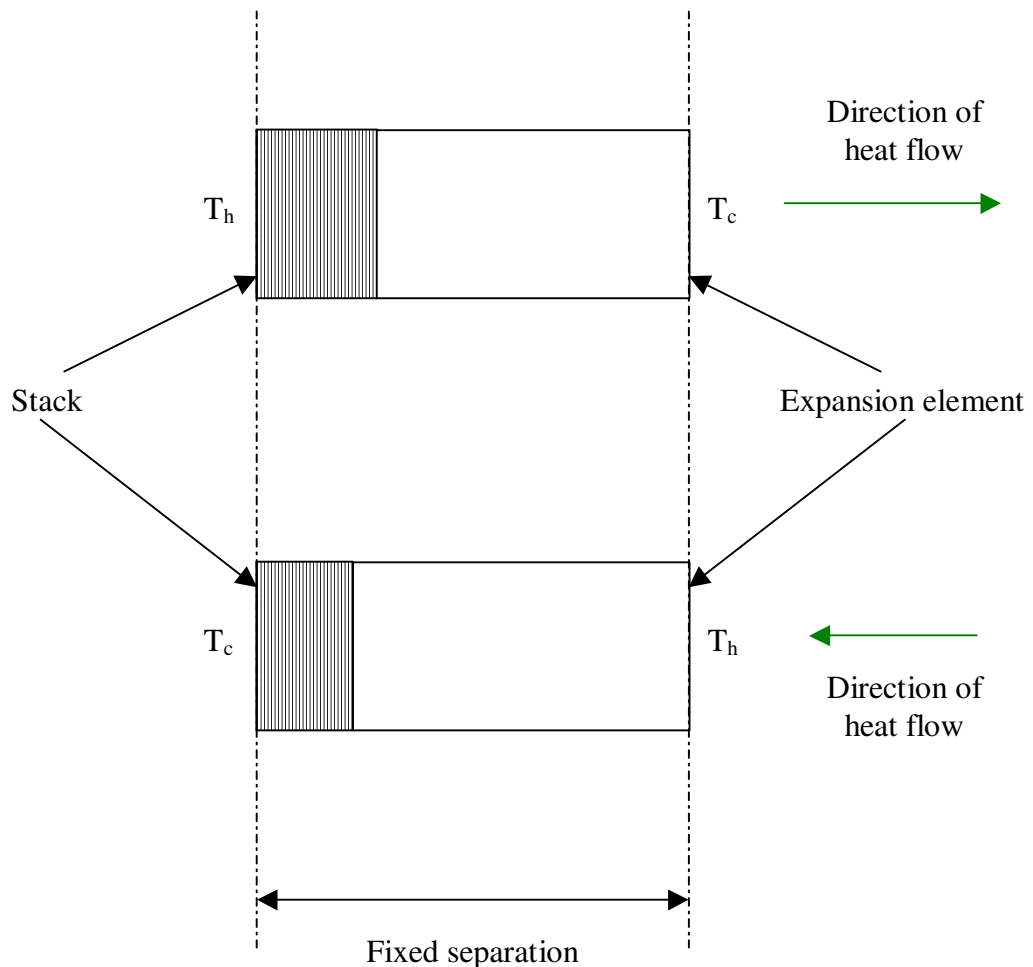


Figure 1.7-4 Thermal rectifier configuration observed by Jones *et al.* [48]. Heat transfer in the upper configuration is less than the heat transfer in the second configuration. The reason for this is that the conductance of the stack increases with increasing compression.

An example of a microscopic type II rectifier that has been investigated experimentally is the nanotube rectifier [49]. This rectifier consists of a nanotube (carbon or boron nitride) with trimethyl-cyclopentadienyl platinum ($C_6H_{16}Pt$) deposited non-uniformly along the length of the nanotube as shown in Figure 1.7-5. The authors investigate the flow of heat through the nanotube prior to the deposition of $C_6H_{16}Pt$ and they found that heat flows symmetrically through this configuration. When the same procedure is applied to the nanotube with the non-uniformly deposited $C_6H_{16}Pt$, they found that heat flows asymmetrically with a rectification of 7%. The authors reject the possibility that the asymmetrical heat transfer is due to the fused $C_6H_{16}Pt$ forming an additional thermal conductance channel on parts of the sample on the basis that the thermal conductivity of $C_6H_{16}Pt$ is less than 1% of that of the nanotube. Instead, they suggest that solitons may be responsible for the different rates of heat flow in the two opposing directions.

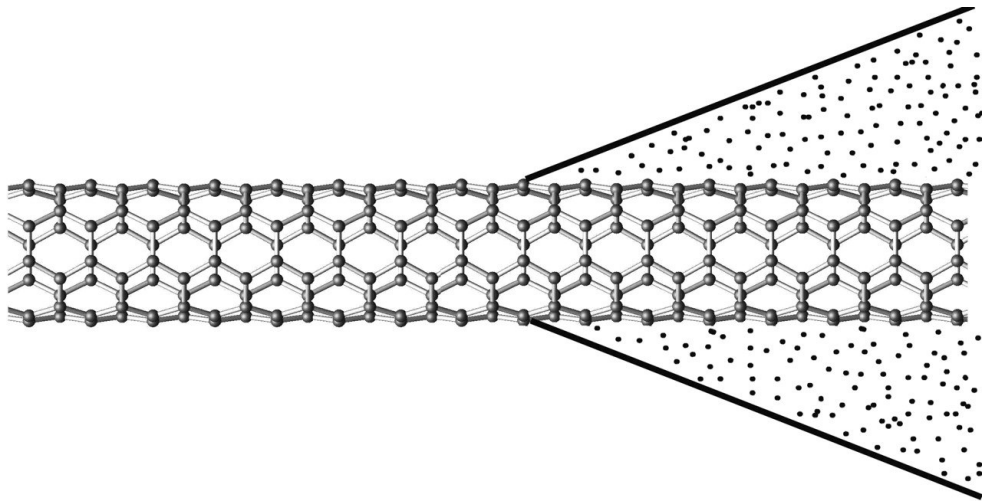


Figure 1.7-5 A schematic description of the nanotube rectifier. The black dots denote the $C_6H_{16}Pt$ deposited on the nanotube which is denoted by the lattice structure (Chang et al [49]).

1.7.3 Hybrid rectifiers

Hybrid rectifiers are the final class of devices described in this study that exhibit asymmetrical heat transfer. Hybrid devices require a body force and a structural asymmetry in order to exhibit asymmetrical heat transfer. An example of a hybrid device is the heat pump reported by Riffat *et al.* [54]. A simplified schematic diagram of the device used by Riffat *et al.* [54] is shown in Figure 1.7-6. In part (a) of Figure 1.7-6 heat at the evaporator causes the working fluid inside the thermal diode to boil and vaporize. As the vapour flows to the condenser, it condenses and releases heat via the heat sink. The vapour flows to the condenser via free convection. In part (b) of Figure 1.7-6, the evaporator is located at the top and the condenser at the bottom, consequently the vapour cannot flow to the condenser via free convection and hence heat transfer is significantly reduced.

The devices described in this study that exhibit asymmetrical heat transfer are hybrid rectifiers. The main device described in this study is the composite system of water and a saline solution (the water-saline diode). The water-saline diode consists of a cubic enclosure of water adjacent to a cubic enclosure of salt water (hence the requirement of a structural asymmetry). The basis of this rectifier is that heat transfer is reduced in the vicinity of the density maximum due to changes in the convection pattern (hence the requirement of a body force). A second hybrid device is described in this study that also relies on the changes in the convection pattern induced by the density maximum (hence the requirement of a body force). This device consists of an enclosure of water adjacent to a slab of Perspex (hence the requirement of a structural asymmetry). Both of these devices are investigated experimentally and numerically and they are described in detail in this thesis.

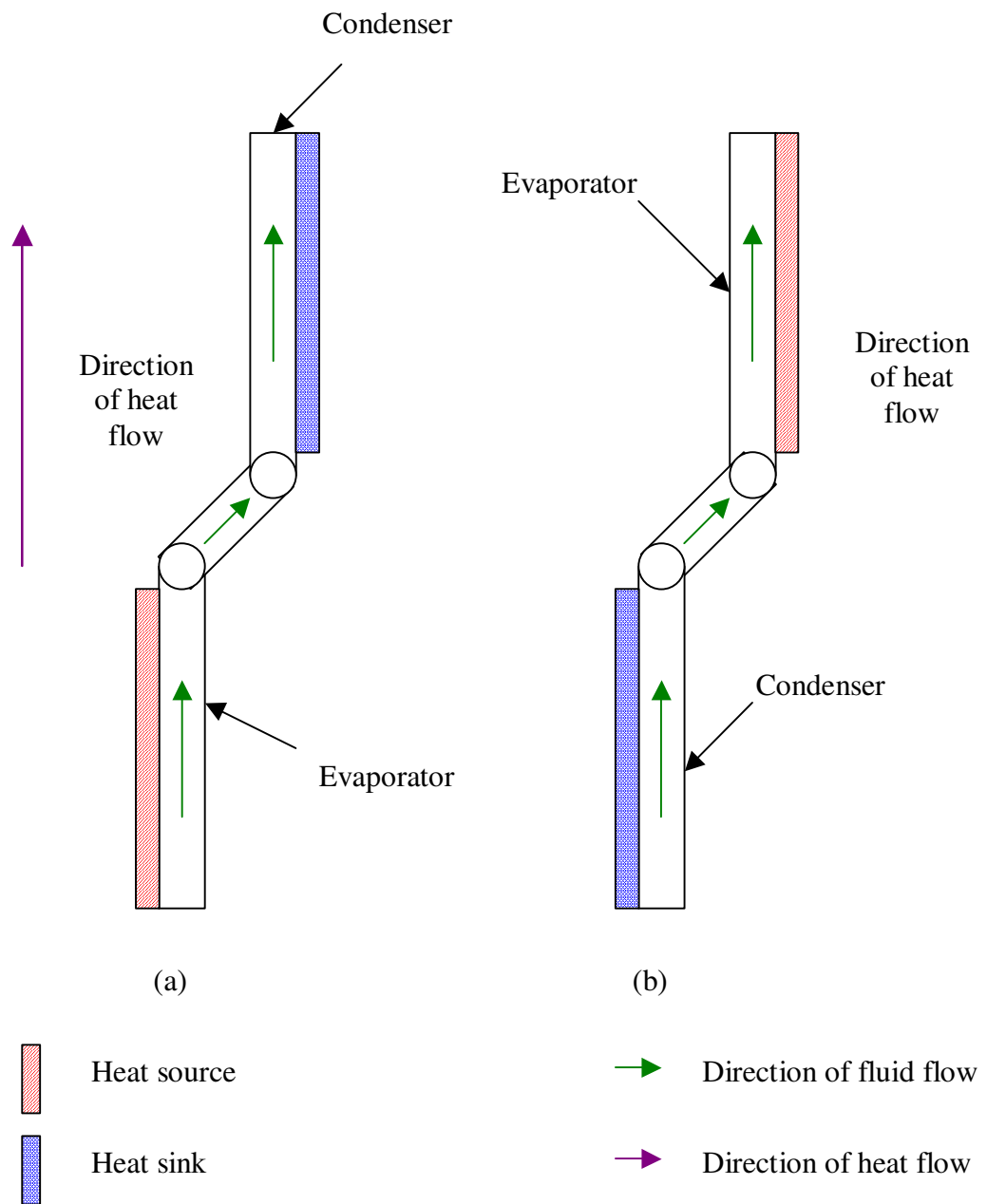


Figure 1.7-6 Simplified schematic diagram of the heat pump described by Riffat et al. [54]. Heat flows faster when travelling upwards than downwards. (a) Heat flows vertically upwards when liquid coolant in the evaporator evaporates and is driven upwards into the condenser by buoyancy forces. (b) Heat transfer is significantly reduced since the vapour cannot flow from the evaporator to the condenser via free convection.

1.8 Thesis chapter outline

This section outlines the overall content of the thesis and summarises the topics covered in each of the chapters.

Chapter 2 describes the experimental systems and the various aspects essential to their operation for investigating asymmetrical heat transfer through composites of water and aqueous solutions in the presence of the density maximum. This chapter also describes the various experimental procedures for investigating asymmetrical heat transfer and the temperature of maximum density of aqueous solutions.

Chapter 3 presents a detailed analysis of all the experimental results obtained for the investigations of the temperature of maximum density of aqueous solutions and asymmetrical heat transfer.

Chapter 4 outlines the theory and procedures used to simulate the experimental results presented in this thesis.

Chapter 5 compares the theoretical predictions to the experimental results. The good agreement permits the use of the numerical models for further detailed investigations and optimization studies.

Chapter 6 Overall conclusions are drawn about the work carried out as part of this thesis. Significant results from the work completed as part of the PhD project and which are relevant to the behaviour of the temperature of maximum density of aqueous solutions and asymmetrical heat transfer in composite systems due to the density maximum are discussed. Possible future work on the behaviour of the temperature of maximum density of aqueous solutions and on the behaviour of heat transfer in the water-saline diode are also discussed.

The work described in this thesis has been achieved with the cooperation of fellow researchers and the direct contribution of this author to the work in each of the above chapters is described in the following section.

1.8.1 Author's direct contribution in this thesis

The accomplishment of this work has been possible thanks to the contribution of fellow researchers working in the fluid dynamics group at NUI Maynooth during the course of the PhD programme. This work represents a summary of the experiences carried out working on different projects built on work by previous group members, therefore resulting in various aspects of involved knowledge. The author's direct

contribution on the work reported in this thesis can be listed for each chapter as follows:

Chapter 2

- Improved the electronics for the thermometry and the computer interfacing.
- Developed and installed the heat transfer measurement technique in the dual fridge/freezer systems (quasi-steady state system and the heat transfer system).
- Improved and tested the quasi-steady state system.
- Designed, implemented and tested the heat transfer system.
- Designed and tested the procedures for investigating asymmetrical heat transfer and the temperature of maximum density of aqueous solutions.

Chapter 3

- Observation and analysis of the occurrence of the anomalous feature in the temperature profiles using Particle Image Velocimetry (PIV).
- Measurement and analysis of heat flow in the vicinity of the density maximum.
- Application and testing of the measurement technique for the temperature of maximum density of aqueous solutions based on the anomaly feature in the temperature profiles.
- Development and testing of the measurement technique for the temperature of maximum density of aqueous solutions based on the anomaly feature in the rate of cooling.
- Analysis of the behaviour of the temperature of maximum density of aqueous solutions.
- Observation and analysis of the anomaly feature of sodium carbonate solutions.
- Measurement and analysis of asymmetrical heat transfer through composites of water and saline solutions in the vicinity of the density maximum.
- Measurement and analysis of asymmetrical heat transfer through composites of water and Perspex.

Chapter 4

- Developed and tested numerical models for analysing the anomaly feature in the experimental temperature profiles.
- Developed and tested numerical models for analysing and obtaining heat transfer values in the vicinity of the density maximum.
- Developed and tested numerical models for investigating the shape of the anomaly feature.
- Developed and tested numerical models for investigating asymmetrical heat transfer through composites of water and saline solutions.
- Developed and tested numerical models for optimising the water-saline diode.
- Developed and tested numerical models for investigating asymmetrical heat transfer through composites of water and Perspex.
- Developed and tested numerical models for optimising the water-Perspex diode.
- Developed and tested numerical models for investigating asymmetrical heat transfer in a composite system of water and a phase change material.

Chapter 5

- Analysis of the quasi-steady state behaviour of the temperature and velocity fields in water and ethanol.
- Analysis of the heat transfer minimum in the vicinity of the density maximum.
- Analysis of the quasi-steady state behaviour of heat transfer in water and ethanol.
- Testing of the measurement technique for the temperature of maximum density of aqueous solutions using the anomaly feature in the rate of cooling profile.
- Analysis of the shape of the anomaly feature.
- Testing of the experimental results for asymmetrical heat transfer.
- Analysis of asymmetrical heat transfer in composites of water and saline solutions and composites of water and Perspex.

- Analysis of the optimisation of the thermal diode effect in the water-saline diode and the water-Perspex diode.
- Developed and tested a thermal analogy to Ohm's Law that represents the water-saline diode.

Chapter 2

Experimental Apparatus and Procedures

2.1 Introduction

This chapter describes the procedures and systems used for the experimental investigations. There are two different experimental systems used; both systems are capable of maintaining steady temperature gradients, monitoring the temperature at select points in the fluid, facilitating flow visualization and measuring the rate of heat flow. The thermometry, flow visualization, the measurement of heat transfer and the computer interfacing hardware are common aspects to both systems and these aspects shall be described in section 2.2. The primary difference between the two systems is that the second apparatus cools the test sample more efficiently and therefore allows the sample to reach colder temperatures than the first system. The first system is primarily used for measuring the temperature of maximum density of aqueous solutions and it will be described in section 2.3 with the operating software associated with that system. The second system is primarily used for investigating the thermal diode effect and it will be described in section 2.4 along with the associated operating software. This chapter concludes in section 2.5 with a description of the various procedures for investigating asymmetrical heat transfer through composites of water and aqueous solutions in the presence of the density maximum.

The measurement and observation of velocity, temperature and heat flow, and the computer interfacing hardware are common aspects of the experimental systems in these investigations. The velocity profile of the liquid is obtained using Particle Image Velocimetry (PIV). Particle image velocimetry infers the motion of the liquid from the motion of tracer particles suspended in the fluid. In this study, the temperature is measured with temperature sensitive resistors (thermistors). A constant current is supplied to the thermistor and the temperature is obtained by measuring the voltage across the thermistor. Heat transfer is measured using a modified version of the longitudinal comparative heat-flow technique. This technique determines the rate of heat flow from the measurement of a temperature difference across a solid reference material of known thermal conductivity. These three techniques along with the computer interfacing hardware are described in detail in section 2.2.

Section 2.3 describes the apparatus and operating software associated with the quasi-steady state system. This system is primarily used for measuring the temperatures of maximum density of aqueous solutions based on the observation of the temperature at select points within the solution. The system is capable of maintaining a constant horizontal temperature gradient across a rectangular enclosure. The temperature difference across the sample can vary from 0°C to 22°C. The highest boundary temperature obtainable is 20°C and the lowest boundary temperature is -2°C. The system facilitates flow visualization and heat transfer measurements. However, the addition of the heat transfer device to the system changes the limit on the coldest boundary temperature of the chamber from -2°C to 0.5°C. This limit presents a difficulty for investigating heat transfer in this study, as the coldest boundary temperature must reach -2°C. This inadequacy necessitated the design of an alternative system for investigating heat transfer.

Section 2.4 describes the experimental system used for investigating heat transfer. This system is capable of performing the same experiments as the system described in section 2.3 with the ability to measure heat transfer through the test region. The system was primarily designed to investigate the rate of heat flow through a sample of water as it is cooled through its density maximum and to investigate asymmetrical heat transfer. This apparatus was later used to investigate an alternative technique for measuring the temperature of maximum density of aqueous solutions as it has a superior cooling ability to the apparatus described in section 2.3.

The procedures for investigating the temperature of maximum density of aqueous solutions and asymmetrical heat transfer are described in section 2.5. The temperature of maximum density of aqueous solutions is measured by applying a constant horizontal temperature gradient to a rectangular container of the sample. The sample is cooled from 8°C to 0°C by varying the bounding temperatures of the gradient. The temperature is monitored at select points inside the fluid. An anomalous feature is observed in the temperature field in the vicinity of the density maximum and this feature indicates the temperature of maximum density. Asymmetrical heat transfer is investigated by applying a constant horizontal temperature gradient to the composition until the system reaches steady state. When the heat transfer is measured, the boundary temperatures are interchanged and the

system is allowed to reach steady state once more. The procedures for each of these investigations are described in section 2.5.

This chapter describes the necessary experimental procedures and systems used in this study to investigate asymmetrical heat transfer through composites of water and aqueous solutions. The chapter begins with a description of the common components of the two systems used and continues with a description of the two experimental systems. A description of the procedures for investigating the temperature of maximum density of aqueous solutions and asymmetrical heat transfer concludes the chapter.

2.2 General techniques and equipment

There are four aspects that are common to each of the experimental systems used in this study and they shall be described here. Flow visualization is the first of these aspects to be described. PIV is used for flow visualization studies and it is described in section 2.2.1. The thermometry used in this study is the thermistor and it is described in section 2.2.2. Section 2.2.3 describes in detail the modified version of the longitudinal comparative heat-flow method that is used for the measurement of the rate of heat flow. The necessary hardware for interfacing the experiment with the computer is described in section 2.2.4. The three techniques and the computer interfacing hardware described in this section are general aspects of each of the systems used in this study.

2.2.1 Flow visualization

Flow visualization studies in this work use particle image velocimetry. Particle image velocimetry determines the motion of the liquid from the motion of tracer particles suspended in the fluid. Polyamid spheres with diameters of 50 μm (Dantec PSP-50) were used in this study. These particles were chosen as they avoid any problems that may arise due to settling, particle lag, camera resolution, and errors due to the influence of gravitational forces.

The polyamid spheres have a density of $1003\text{kg}\cdot\text{m}^{-3}$, which although closely matched to the maximum density of water of $1000\text{kg}\cdot\text{m}^{-3}$ (and hence avoids errors due to the influence of gravity), are more dense than the fluid and are therefore subject to

settling. However, the particles do remain in suspension for tens of minutes, which is adequate time for the observation of the fluid flow in these experiments. A further difficulty associated with settling was the particles tendency to conglomerate when left in a settled state for more than 24 hours. This difficulty was overcome by preparing fresh mixtures when performing PIV experiments.

The diameter of the particles used in this study was 50 μm even though smaller and less massive particles would improve the particles ability to trace the flow, that is, it would reduce effects due to particle lag. Although smaller particles do have this advantage, they scatter less light and create difficulties with imaging. The quality of a PIV measurement depends on a variety of factors such as particle size and particle concentration.

The particle concentration for the mixtures used in this study was 200mg.ltr⁻¹ of PSP-50 particles in pure water. This concentration was determined by McBride [57] through a series of investigations to be the optimal concentration for the measurements made in this study. A series of measurements of laminar flow in a pipe and free convective flow in a differentially heated cavity determined the optimal conditions for PIV measurements. The recommendations from his investigations on window interrogation size for image analysis and particle illumination are also adhered to in this study.

The particle suspension in the test chamber was illuminated with a collimated sheet of white light. The collimated sheet of light was directed through the top wall of the chamber parallel to, but slightly in front of, the row of thermistors. Linear arrays of high intensity LEDs (2000 mcd) mounted behind a simple double slit collimator as shown in Figure 2.2-1 provided the sheet of collimated light. A camera positioned at right angles to the illuminated sheet captures the images for analysis. The camera is located outside the refrigerator environment; this necessitates the insertion of a double glazed window into the door of the refrigerator unit that contains the test chamber as shown in Figure 2.2-2.

Image acquisition was performed with a JAI CV-M50 monochrome CCD camera of 768 x 576 pixels resolution connected to an ImageNation PXC-200 frame grabber

card in the PC. Alessandro Rubini' Linux driver software [58] was used to operate the frame grabber. This package provides a driver which makes image data available from character devices in the /dev directory. A program copies data from one of these devices to individual image files at intervals of one second. Image data was written in Portable GreyMap (PGM) format. Rubini's software also provides a program to display the camera image in real time that was used for aligning and focussing the camera before the experiment.

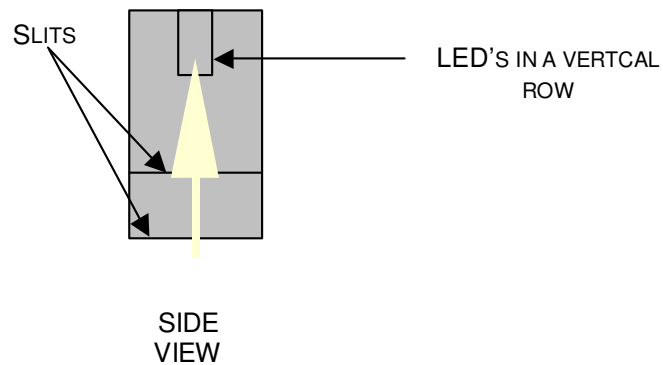


Figure 2.2-1 Side view of the arrangement of the LED array and the collimator.



Figure 2.2-2 The insertion of a double glazed window on the door of the refrigerator that contains the test chamber facilitates flow visualization.

The URAPIV algorithm available on the public domain from [59] was used for image analysis in this study. Imaging analysis divides each of the images, captured by the CCD camera, into interrogation windows of 32 x 32 pixels. The velocity field

is computed by cross-correlating the corresponding windows in a pair of images. Overlapping the 32 x 32 pixel windows on a grid spacing of 16 x 16 pixels enhances the resolution of the final vector plots.

In a typical experiment involving PIV a mixture of 200mg.ltr⁻¹ of PSP-50 particles in pure water is prepared and poured into the test chamber. The linear arrays of LEDs are placed on top of the test chamber illuminating a 2D slice of the 3D chamber in the direction of the fluid flow. A camera placed at right angles to this illuminated sheet captures images of the flow at 1s intervals in JPEG format. The URAPIV algorithm processes these images to produce a series of vector plots such as those shown later in section 3.3.1.

2.2.2 Thermometry

The thermometry used in this study is the thermistor. The temperature sensitive resistors, known as thermistors, used in this investigation have a Negative Temperature Coefficient (NTC) that is the resistance varies inversely with temperature. The advantages of using NTC thermistors is that their change in resistance is predictable and it is relatively large per degree change in temperature, which allows a very accurate measurement of temperature to be taken.

The circuit in Figure 2.2-3 provides a constant current of 200 μ A to the thermistor. It consists of a voltage regulator, a non-inverting amplifier, a voltage follower, and a 25k Ω resistor. The regulator maintains a constant output voltage (+5V) with a changing input or load current. Its purpose in this circuit is to provide a constant current through the thermistor. The 25k Ω resistor is used to limit the current flow from the voltage regulator through the thermistor. The non-inverting amplifier provides a positive voltage gain, and so, in the circuit in Figure 2.2-3 amplifies the voltage from the thermistor by two.

The circuit in Figure 2.2-3 gives a constant current for only one thermistor, but this experiment requires more than one thermistor during any experiment, therefore sixteen of these circuits are available in the apparatus. An electronic circuit board as shown in Figure 2.2-4 is used to house eight of these temperature-to-voltage conversion circuits. Two of these electronic circuit boards were integrated into the

apparatus during the course of this study. The outputs of each circuit are sent to a computer so that the voltages can be recorded and converted into temperature readings.

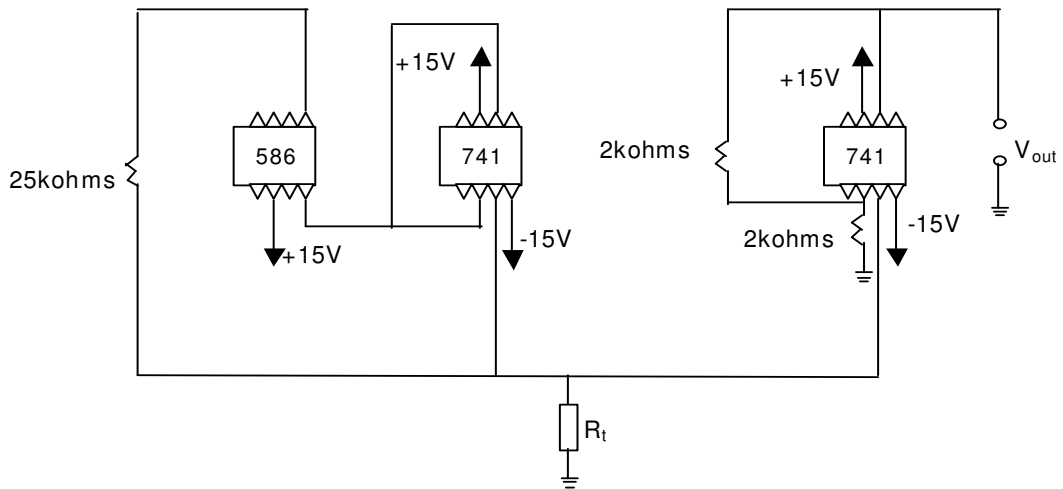


Figure 2.2-3 Temperature to Voltage Conversion circuit (R_T is the Thermistor).

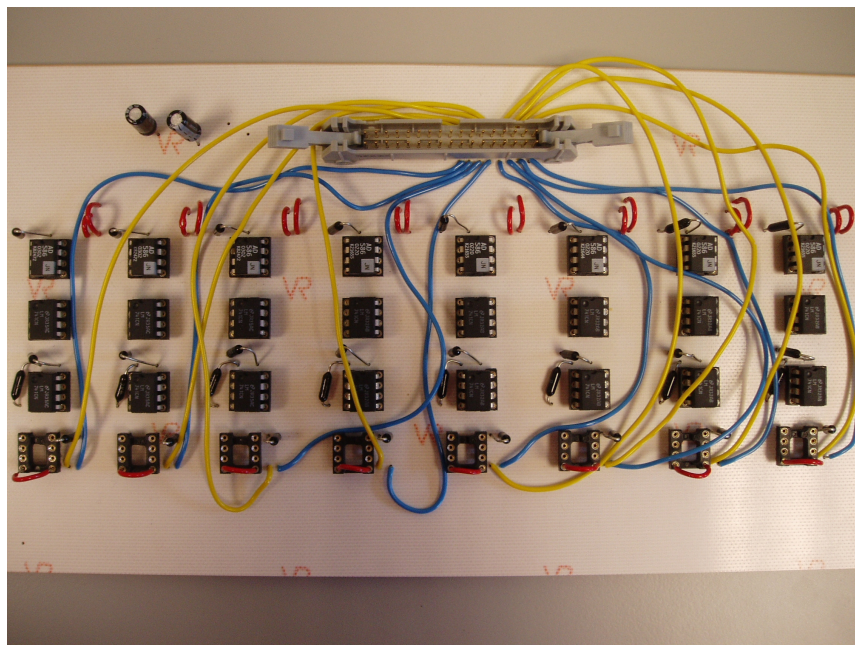


Figure 2.2-4 The eight temperature-to-voltage conversion circuits housed on an electronic board.

The thermistors are calibrated with a mercury thermometer accurate to 0.1°C and traceable to the National Institute of Standards and Technology, USA. The

thermistors and the thermometer are inserted into a beaker of coolant with a magnetic stirrer. The magnetic stirrer ensures that a uniform temperature exists throughout the beaker, so that all the thermistors and the thermometer are reading the same temperature. The temperature of the coolant, read from the thermometer, is recorded along with the ADC number of each thermistor read by the computer. The thermistors were calibrated in the temperature range of 0 - 10°C (the range in which they typically operated). The resistance of the thermistor is directly proportional to the voltage across it, i.e. the ADC number.

The resistance of a semiconductor (such as the thermistor) is given by:

$$R = A \exp\left(\frac{E_g}{2k_B T}\right) \quad (2.2-1)$$

where R is the resistance of the material, k_B is the Boltzmann constant, T is the absolute temperature, E_g is the band gap for the semiconductor and A is a constant depending on the physical composition of the semiconductor material. This equation can be rearranged as shown below by taking the natural logarithms of both sides:

$$\text{Log}_e(R) = \text{Log}_e(A) + \left(\frac{E_g}{2k_B T}\right) \quad (2.2-2)$$

This equation is used for calibrating the thermistors. A plot of $\text{Log}_e(R)$ against $1/T$ gives a straight line with slope of $E_g/2k_B$ and intercept of $\text{Log}_e(A)$. Since R is directly proportional to the ADC number a plot of $\text{Ln}(ADC \text{ number})$ against $1/T$ also produces a straight line. A best-fit line to the data obtained in the calibration procedure yields a slope and an intercept. This equation can then be rearranged as shown below so that the temperature experienced by the thermistor can be interpreted from its ADC number:

$$T = \frac{\text{slope}}{\text{Ln}(ADC \text{ number}) - \text{int ercept}} \quad (2.2-3)$$

Each thermistor has a unique slope and intercept and this equation is integrated into the data acquisition and control software to convert the ADC number from each thermistor into the corresponding temperature.

2.2.3 Measurement of heat transfer

The measurement of heat transfer is of fundamental importance to the study of asymmetrical heat flow and it provides an alternative technique for measuring the temperature of maximum density of aqueous solutions. Heat transfer is measured in this study using a technique based on the longitudinal comparative heat-flow technique [44]. The longitudinal comparative heat-flow technique is normally used to determine the thermal conductivity of solids by sandwiching the solid between two materials of known thermal conductivity. The temperature difference across each reference material is measured and the rate of heat flow is determined using the one-dimensional Fourier conduction equation.

The longitudinal comparative heat-flow technique controls the temperature of the outermost walls of the entire region (the sample and the reference materials) and monitors the temperature of the wall of the sample. This technique is unsuitable for the investigations reported here. The temperature of the walls of the sample must be controlled; this required a modification to the longitudinal comparative heat-flow technique. The technique employed in this study controlled the wall temperatures of the sample and monitored the temperature of the outermost walls of the entire region. The reference material used in this study is Perspex and the arrangement of the system is shown in Figure 2.2-5. Perspex of dimensions 0.125cm x 6cm x 6cm is placed adjacent to each of the isothermal walls of the chamber. An aluminium plate is placed on the other side of each of the Perspex reference materials. Each aluminium plate is embedded with a thermistor for monitoring the temperature difference across the Perspex reference materials. The rate of heat flowing into the chamber and the rate of heat flowing out of the chamber is inferred from the measured temperature differences across the reference material using the following equations:

$$H_{perspex} = \frac{k_p A (T_{m,h} - T_h)}{\Delta x} \quad (2.2-4)$$

$$H_{perspex} = \frac{k_p A (T_c - T_{m,c})}{\Delta x} \quad (2.2-5)$$

where $(T_{m,h}-T_h)$ is the temperature difference across the reference material adjacent to the hottest wall, $(T_c-T_{m,c})$ is the temperature difference across the reference material adjacent to the coldest wall, k_p is $0.19\text{W}\cdot\text{m}^{-1}\cdot\text{K}^{-1}$ (Perspex), A is the cross-sectional area of the test region and the Perspex reference material ($0.06\text{m} \times 0.06\text{m}$), and Δx is the width of the Perspex regions (1.25mm).

This heat transfer device is surrounded by 5cm of expanded polystyrene to reduce the influence of the ambient temperature. To validate the longitudinal comparative heat-flow technique, the test chamber was replaced by a solid of known thermal conductivity (typically 5mm Perspex with the same cross-sectional area as the test chamber), and the temperature drop across the hot-side and cold-side reference materials were checked against predictions for the known rate of heat flow under such circumstances. This procedure does not address the problem of non-isothermal conditions that are expected to prevail at the vertical walls of the test chamber when working with convecting fluids. It is found in practice, however, that there is good agreement between the rates of heat transfer as measured by this technique and those predicted from computational fluid dynamics. Uncertainties in the heat transfer rates were estimated to be of the order of 7%, assuming an uncertainty in temperature measurement of 0.1°C .

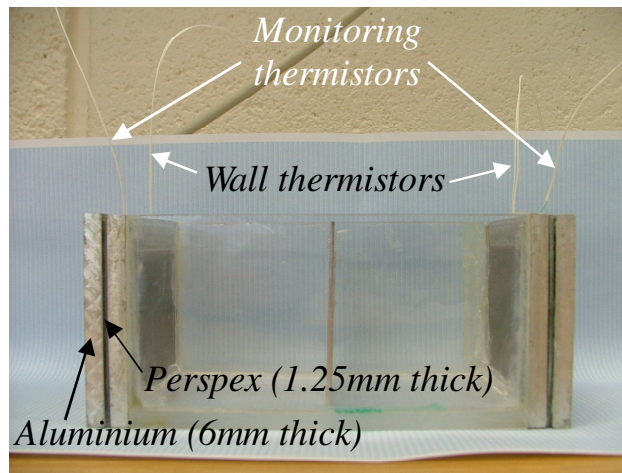


Figure 2.2-5 Test chamber used for heat flow investigations. Water is placed inside this chamber and the temperatures of the two aluminium blocks $T_{m,h}$ and $T_{m,c}$ are monitored while the temperatures of the chamber's sidewalls T_h and T_c are controlled by the computer. The white cables are the thermistors embedded inside the aluminium blocks and the chamber's sidewalls.

2.2.3.1 Error analysis

The rate of heat transfer, H , is obtained by measuring the temperature difference across a reference material of known thermal conductivity and then inserting this measurement into the following equation:

$$H = kA \frac{dT}{dx} \quad (2.2-6)$$

Where k is the thermal conductivity, A is the cross-sectional area, dT is the temperature difference and dx is the width of the reference material. The value for k is taken to be $0.19\text{W}\cdot\text{m}^{-1}\cdot\text{K}^{-1}$ (Perspex) and the error is assumed to be negligible. The uncertainties in the remaining quantities are random and independent, thus the fractional uncertainty of each quantity adds in quadrature to give the fractional uncertainty for the heat transfer measurements, i.e.

$$\frac{\Delta H}{H} = \sqrt{\left(\frac{\Delta A}{A}\right)^2 + \left(\frac{\Delta G}{G}\right)^2} \quad (2.2-7)$$

where G denotes the temperature gradient. The uncertainty in the measurement of the height and depth of the cross-sectional area is 0.001m . Thus the fractional uncertainty on A is

$$\frac{\Delta A}{A} = \sqrt{\left(\frac{\Delta h}{h}\right)^2 + \left(\frac{\Delta d}{d}\right)^2} \quad (2.2-8)$$

$$\frac{\Delta A}{A} = \sqrt{\left(\frac{0.001}{0.06}\right)^2 + \left(\frac{0.001}{0.06}\right)^2} = 0.023$$

The temperature gradient is equal to the temperature difference, dT , divided by the width, dx . The uncertainties associated with each of these measurements are random and independent, therefore, the fractional uncertainties add in quadrature to give the fractional uncertainty in the gradient, i.e.

$$\frac{\Delta G}{G} = \sqrt{\left(\frac{\Delta dT}{dT}\right)^2 + \left(\frac{\Delta dx}{dx}\right)^2} \quad (2.2-9)$$

The temperature difference is obtained by measuring the two temperatures T_1 and T_2 with an uncertainty of 0.1°C and subtracting the two temperatures, so the uncertainty in the temperature difference is the addition of the uncertainties in quadrature, i.e.

$$\Delta dT = \sqrt{\Delta T_1^2 + \Delta T_2^2} \quad (2.2-10)$$

$$\Delta dT = \sqrt{0.1^2 + 0.1^2} = 0.14$$

The typical measurement of dT is 2°C so the fractional uncertainty in dT is

$$\frac{\Delta dT}{dT} = \frac{0.14}{2} = 0.07$$

The measured width of the reference material is 1.25mm with an uncertainty of 0.01mm, so the fractional uncertainty in dx is

$$\frac{\Delta dx}{dx} = \frac{0.01}{1.25} = 0.008$$

Therefore the fractional uncertainty on the temperature gradient is

$$\frac{\Delta G}{G} = \sqrt{0.07^2 + 0.008^2} = 0.07$$

Thus, the fractional uncertainty on the heat transfer measurements is typically

$$\frac{\Delta H}{H} = \sqrt{0.023^2 + 0.07^2} = 0.07$$

So, the typical uncertainty in the heat transfer measurements is 7%.

2.2.4 Computer interfacing hardware

The computer communicates with the experiment via an I/O box that is connected to a CIODIO-48 card. The I/O box consists of two digital to analogue converters (DACs) and two analogue to digital converters (ADCs). The DACs provide control signals to the solid-state relays (SSR1-SSR8 in Figure 2.2-6) and the ADCs digitise the signals from the thermistors (CC1-CC16). The solid-state relays switch AC mains powered devices on/off according to the control signals from the DACs. A source driver (SD) is placed between the DACs and the solid-state relays to increase the driving current from the I/O box to the relays.

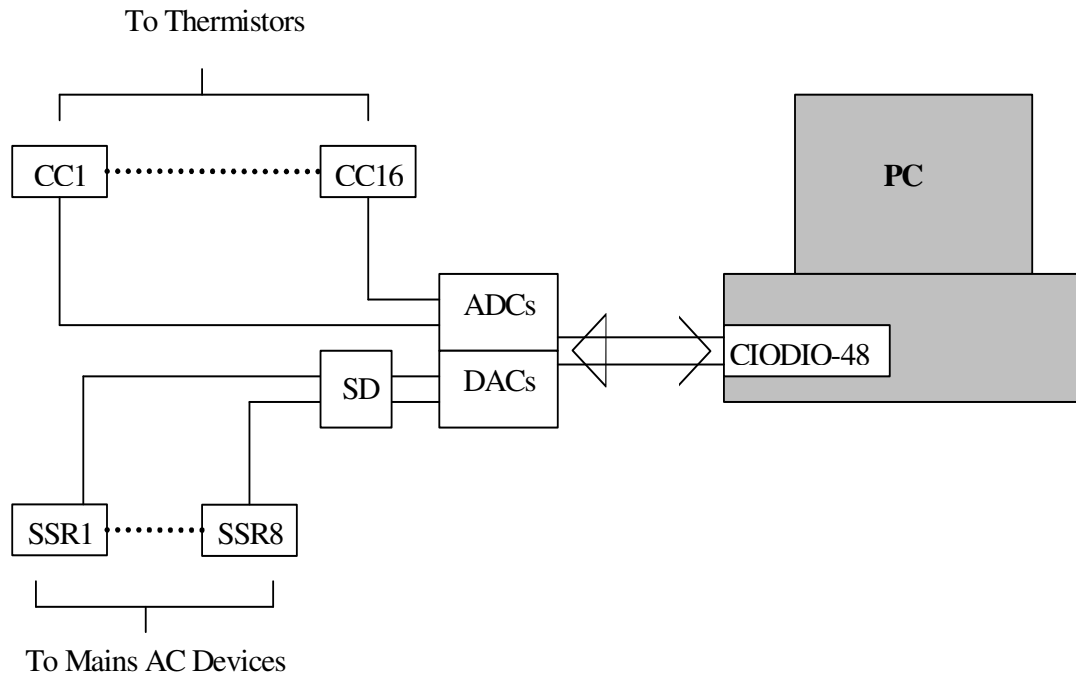


Figure 2.2-6 Block diagram of the electronics used for control and data acquisition.

The ADCs and the DACs in the I/O box are of the tri-state output type and are connected to the CIODIO-48 card in the computer via an 8-bit bus. The I/O box digitises the signals from the temperature sensors via two 12-bit ADCs (MAX197 by Maxim). Since the ADCs are 12-bit devices, results of conversions are obtained by performing an 8-bit read followed by a 4-bit read. Each ADC has eight analogue input channels, providing the experiment with a maximum of sixteen channels for operating the thermistors. The DC control signals, required to operate the solid-state relays, are provided by the two 8-bit DACs (AD7226 by Analog Devices). The digital to analogue converters each contain four digital output channels providing eight control channels to the experiment. The DACs provide a typical input voltage of 5V DC and a current of 2.5 mA to the solid-state relays.

Operation of the solid-state relays typically requires an input current of 3.4mA at 5V DC. The low output voltage provided from the DACs is increased by inserting a source driver (UDN2981A by Allegro Microsystems) between the DACs and the solid-state relays. Although it is not necessary for operation of the apparatus, this

device ensures safer operation of the solid-state relays by reducing the influence of external noise on the system. An additional safety feature associated with the solid-state relays is the ‘float relay’. This relay is connected in series with a float switch inside each reservoir containing coolant and an electric heater. The float relay shuts off power to all the solid-state relays when there is a loss of coolant from the reservoir due to leaks or evaporation (due to malfunction of the heater control). The relay must be manually reset in order to restore power to the devices. In this circumstance, it is necessary to restore the coolant level before resetting the relay. When a power failure occurs, the float relay prevents devices controlled by relays from operating when power resumes. This feature ensures that if the system is unattended after a power failure, it cannot restart in an undesired state.

2.3 Quasi-steady state system

This section describes the apparatus and the associated operating software that is primarily used for investigating the temperature of maximum density of aqueous solutions. This apparatus and its operating software are modified versions of the apparatus and operating software used by McBride [57]. An overview of the original apparatus and its modifications are described in section 2.3.1. A general outline of the code will be described in section 2.3.2 with a detailed description of the modifications necessary for these investigations.

2.3.1 Apparatus overview

In this study, free convection is investigated by applying a horizontal temperature gradient across a rectangular enclosure of the fluid under investigation. The apparatus used for this study is shown schematically in Figure 2.3-1 and pictorially in Figure 2.3-2. A horizontal temperature gradient across the test chamber is achieved by placing isothermal chambers in contact at opposite sides of the test chamber. The side chamber on the left contains coolant at a temperature T_L , while the opposing side chamber on the right contains coolant at a temperature T_R .

The temperature of the coolant in the left side chamber is achieved by constantly circulating the coolant from a reservoir whose temperature is maintained by a cooling coil and a 60W heater that are under computer control. The reservoir for this side chamber is contained in the dual fridge/freezer unit on the left in Figure 2.3-1

and Figure 2.3-2. The cooling coil in the reservoir is connected to a series of coils contained in the freezer compartment that were filled with coolant. Pumping coolant from the coils in the freezer compartment activates the cooling coil in the reservoir. If the temperature of the reservoir is too cold, the electric heater is switched on and if the temperature of the reservoir is too warm, coolant from the freezer compartment is pumped through the cooling coil.

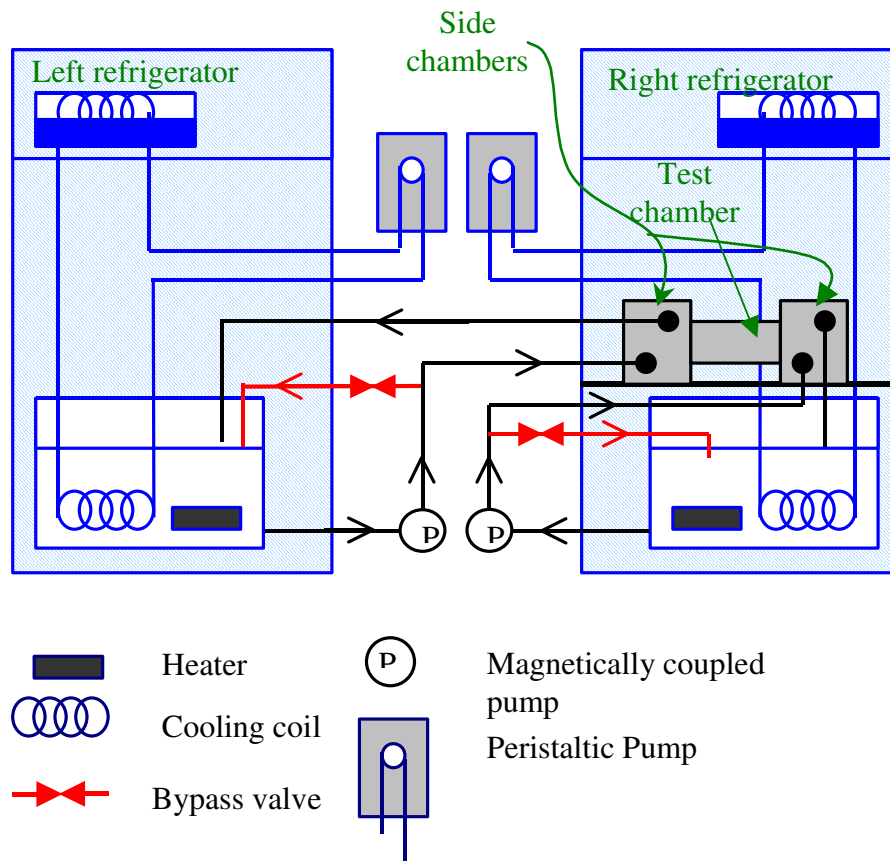


Figure 2.3-1 Schematic overview of the experimental apparatus. P1 and P2 are pumps under computer control.

There are two separate plumbing circuits for each chamber in this system. The main circuit pumps coolant from the reservoir to the side chamber. The secondary circuit pumps coolant from the freezer compartment to the cooling coil in the reservoir. The coolant in the reservoir is a clear mixture of 15% ethylene glycol in water; this concentration prevents the coolant from freezing at the required operating temperatures. When the coolant reaches temperatures below its density maximum the coldest liquid is at the top of the reservoir and the warmest liquid is at the bottom. This presents a difficulty in reaching low temperatures as the outlet to the pumps is

located at the bottom of the reservoir and so the warmest coolant is circulated through the system. An agitator located in the reservoir prevents this problem from arising. Blue dyed ethylene glycol available commercially for automotive purposes is used in the cooling coils. The manufacturer recommends the use of this coolant for temperatures above -36°C . This temperature is well below the typical freezer temperatures of -30°C . The same coolants are used in the plumbing circuits for the side chamber on the right and all external piping is insulated using standard domestic pipe-wrap insulation

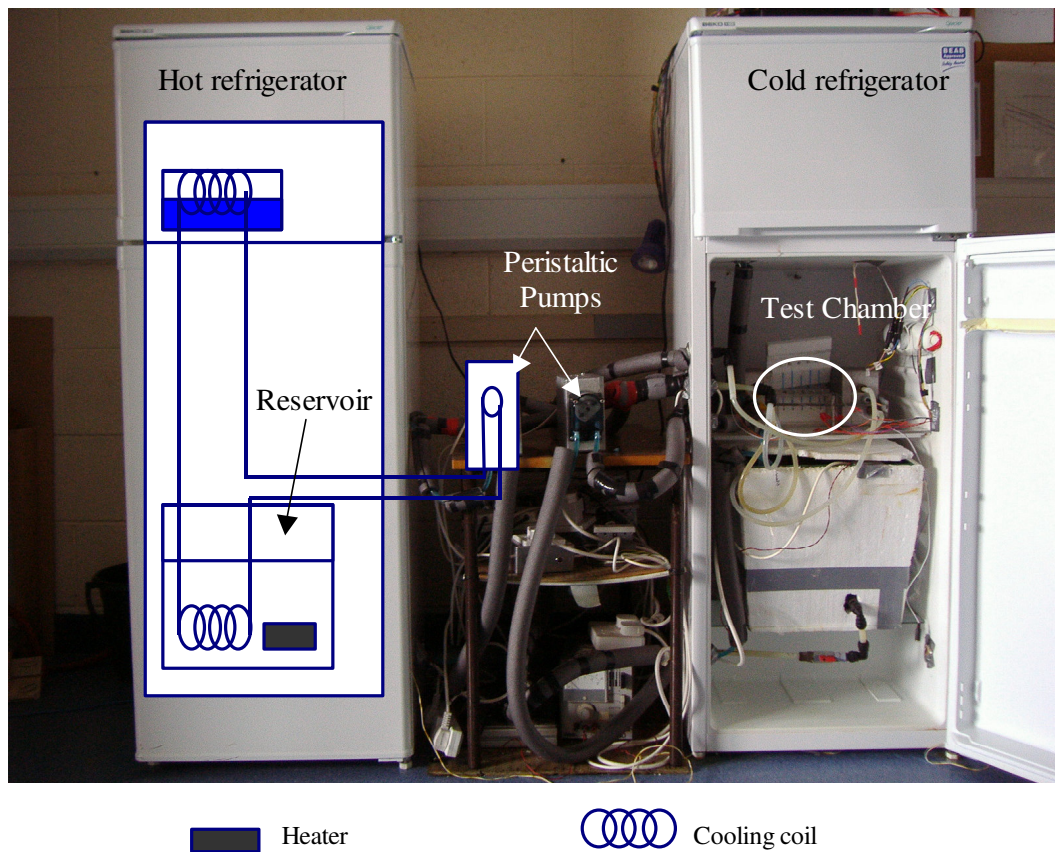


Figure 2.3-2 Graphical overview of the experimental apparatus.

The temperature of the side chamber on the right is achieved in a similar manner to the temperature of the left side chamber. The reservoir for the coolant circulating through this side chamber is contained in the refrigerator/freezer unit on the right in Figure 2.3-1 and Figure 2.3-2. The test chamber along with the two side chambers is

located in this refrigerator/freezer unit since the door of this unit contains a double-glazed window that is necessary for flow visualization. The insertion of a double glazed window into the door of the refrigerator compartment does slightly increase the temperature of the refrigerator ambient.

The refrigerator ambient has the potential to influence the experimental results. This difficulty is overcome in two ways; the computer controls the ambient temperature of the refrigerator and the test chamber is insulated with 5cm of expanded polystyrene. These precautions ensure that the ambient temperature does not have an impact on the experimental results. The ambient temperature of the refrigerator is monitored by a thermistor placed in the vicinity of the test chamber. During preparation for an experiment, the temperature is cycled between 8°C and 10°C. If the ambient temperature is greater than 10°C, the refrigerator's compressor is switched on continuously and the ambient begins to cool until it reaches 8°C. When the ambient reaches this temperature the refrigerator's compressor is switched off and the ambient begins warming until it reaches 10°C, and the cycle begins again. During the experiment, the compressor is switched on continuously. This cools the ambient temperature to lower temperatures than the supplied proprietary thermostat.

The ability to control the refrigerator ambient is just one of the various modifications made to the experimental apparatus of McBride [57]. This study increased the number of thermistor channels in the system, introduced a heater to the reservoir of the right side chamber, introduced the ability to vary the speed of fluid flow through the side chambers and introduced the ability to begin the experiment automatically. The latter modification is mainly a modification to the software and the exact nature of this change will be discussed later in section 2.3.2.

The original system by McBride [57] did not include a heater in the reservoir on the right in Figure 2.3-1 and Figure 2.3-2 since those investigations required that reservoir to reach a maximum temperature of just 6°C. This reservoir relied on the ambient temperature of the refrigerator to increase its temperature and consequently it required more time to reach 6°C than the reservoir that had a heater. The investigations in this study introduced a heater into the T_R reservoir and it was found that this modification increased the capabilities of that reservoir. Both reservoirs in

the system in this study can easily reach a maximum temperature of 20°C and the preparation time for an experiment was significantly decreased.

The rate of the fluid flowing through the side chambers was controlled using a bypass valve as shown in Figure 2.3-1. A bypass valve was introduced to the primary plumbing circuit between the pump output and the side chamber input as shown in Figure 2.3-1. The tap on the valve allows variable amounts of the fluid to flow through the valve thereby allowing control of the flow of fluid into the side chamber. When the valve is completely open, the rate of fluid flowing through the chambers is a minimum and it is a maximum when the valve is completely closed.

2.3.2 Data acquisition and operating software

The data acquisition and operating software used in this study is a modified version of the code used by McBride [57]. The software consists of a main routine followed by a number of functions and it is based on a system of multiple flag variables. Each flag variable corresponds to an operation and the values of the flag variables determine which functions are invoked. The main routine contains a loop synchronised to the system clock that iterates once per second. During this iteration, certain functions are invoked according to the values of the flag variables. The various functions can be categorised into three categories. The first category of functions allows the software to communicate with the hardware. The second category of functions uses the first category of functions to acquire data and to control the experiment. The final category of functions provides user interaction with the experiment and often invokes many of the functions in the second category.

The first category of functions uses the COMEDI interface library obtained from [60]. The COMEDI package provides a loadable kernel and functions for use in C programs that are required for accessing the two Intel 8255 PPI chips that are contained on the CIODIO-48 board. The CIODIO-48 board interfaces the I/O box, which contains the ADCs and DACs, to the Intel Pentium Pro computer that runs Redhat Linux 7.2. The second category of functions operates the solid-state relays and acquires data from the thermistors via the functions in the first category. The third category of functions writes data to the files, presents data to the screen and allows the user to interact with the experiment via a menu system. The menu

consists of a list of letters that change the values of flag variables when entered by the user. The menu options are explained below.

- v View data:** Displays temperature data from all the thermistors and the status of the experiment on the screen in real time. This option must be selected in order to begin logging and temperature control routines.
- b Stop data view:** Stops temperature data and status display.
- l Start logging:** Starts logging data to a new file at every second and starts logging data to a graphing file at every 30 seconds.
- k Stop logging:** Stops logging data and closes both data files.
- r Prepare water for run:** Initiates temperature control of the chamber. This activates the peristaltic pumps and heaters as necessary in order to maintain the coolant in the chambers at the specified temperatures.
- i Maintain idling temperatures:** When an experimental run is not imminent this option is useful for maintaining the reservoirs at intermediate temperatures so that they may quickly be brought to their final temperatures using the **r** option.
- a Start agitators:** Sets the agitators running
- s Stop agitators:** Stops the agitators.
- c Circulate T_c water:** Initiates circulation of the water in the T_R reservoir.
- h Circulate T_h water:** Initiates circulation of the water in the T_L reservoir.
- d Stop circulation:** Stops circulation of coolant from both the T_L and the T_R reservoirs.
- m Stop cooling:** Disables the temperature control of the chambers.
- q Begin temperature stepping:** Decrements the temperature of each chamber by 0.1°C every 540 seconds. When T_R reaches -2°C, the temperature of each chamber is incremented by 0.1°C every 540 seconds.
- w Stop temperature stepping:** Stops decrementing/incrementing the temperature of the side chambers.
- y Acknowledge alarm:** If the two thermistors in either side chamber drift more than 0.1°C apart a warning message appears. The user must acknowledge the warning by selecting this option before selecting another option from the menu.
- f Manual control:** Disables auto control and requires the user to instruct the software when to begin the experiment.

- g Auto control:** Data logging and temperature stepping are initiated automatically when specified conditions are met. The starting conditions used for all experiments were: the average of the five probes in the test chamber must be within 0.5°C of the average temperature of the chosen temperatures for the sidewalls.
- x Exit:** Powers down all devices under solid state relay control and exits from the program.

The above menu system incorporates some of the modifications made to the original code. The original code did not provide the facility of beginning the experiment automatically when certain conditions were fulfilled. This facility was integrated for this study and its availability required the addition of options **f** and **g** into the menu. One advantage of automation is that it allows the system to reproduce conditions at the start of each experiment. This means that all experiments have the same initial conditions; an important feature for investigations depending on comparative experiments, such as those performed for this study. A second modification was made to the code to allow for graphical presentation of data during an experiment. The code was modified so that the software writes the data at 30-second time intervals to a second data file named update.dat. This file is then read by the SCILAB routine update.sci to produce a graph of the most recently acquired data.

Other modifications to the code were required to overcome difficulties with electronic interference. The code clears the first thermistor channel on each of the analogue to digital converters before reading and recording all the thermistor channels. This procedure eliminated electronic interference from the thermistor readings. It was also observed during the course of this study that other experiments in the laboratory interfered electronically with the solid-state relay devices. Consequently, some of the relays could switch on or off without being instructed to do so by the computer. This difficulty did not effect the experiment in any way as the software determines and sets the status of the relays every second during an experiment and hence the computer controls all devices during an experiment. Nonetheless, the issue needed to be addressed since it was potentially unsafe when the system was in standby mode. This problem was overcome by modifying the

code so that when the system is in standby mode the computer switches off the relay devices at set time intervals regardless of their previous state.

2.4 Heat transfer system

It was observed in early investigations of heat transfer in the vicinity of the density maximum that the apparatus described previously in section 2.3 was inadequate. The system for measuring heat transfer required the temperature of the coolant in the side chambers to reach colder temperatures due to the presence of the heat transfer measurement device. The system described in section 2.4.1 applies the available cooling power more efficiently using the same equipment as the apparatus in section 2.3.1. This system required a variety of changes to the data acquisition and control software and these changes shall be described in section 2.4.2. The software also required changes to accommodate the different procedure for measuring asymmetrical heat transfer.

2.4.1 Apparatus overview

Heat transfer through a liquid subjected to a horizontal temperature gradient is investigated in this study using the apparatus shown schematically in Figure 2.4-1 and pictorially in Figure 2.4-2. A heat transfer measurement device is placed in thermal contact at opposite sides of the test chamber. The temperature gradient is achieved by placing isothermal chambers in contact with the heat transfer measurement device. Unlike the previous system, the temperature of the coolants in the side chambers is not the same as the temperature of the sidewalls.

The temperature of the left sidewall is achieved by circulating coolant through coils in the left side chamber. The side chamber contains two copper coils, one of which is responsible for warming the coolant and the other coil is responsible for cooling. The warming coil is linked to a reservoir that is maintained at a temperature of $\sim 16^{\circ}\text{C}$. The reservoir is located within the main refrigerator compartment on the left in Figure 2.4-1 and Figure 2.4-2. A 60W heater in this reservoir maintains the reservoir temperature at $\sim 16^{\circ}\text{C}$. The cooling coil is linked to a bank of coils within the freezer compartment of the refrigerator unit with a temperature of $\sim -30^{\circ}\text{C}$. Circulating coolant from the reservoir in the main refrigerator compartment with a magnetically coupled pump activates the warming coil and circulating coolant from

the freezer compartment with a peristaltic pump activates the cooling coil. If the temperature of the left wall is too cold, the warming coil is activated and if the temperature of the left wall is too warm, the cooling coil is activated.

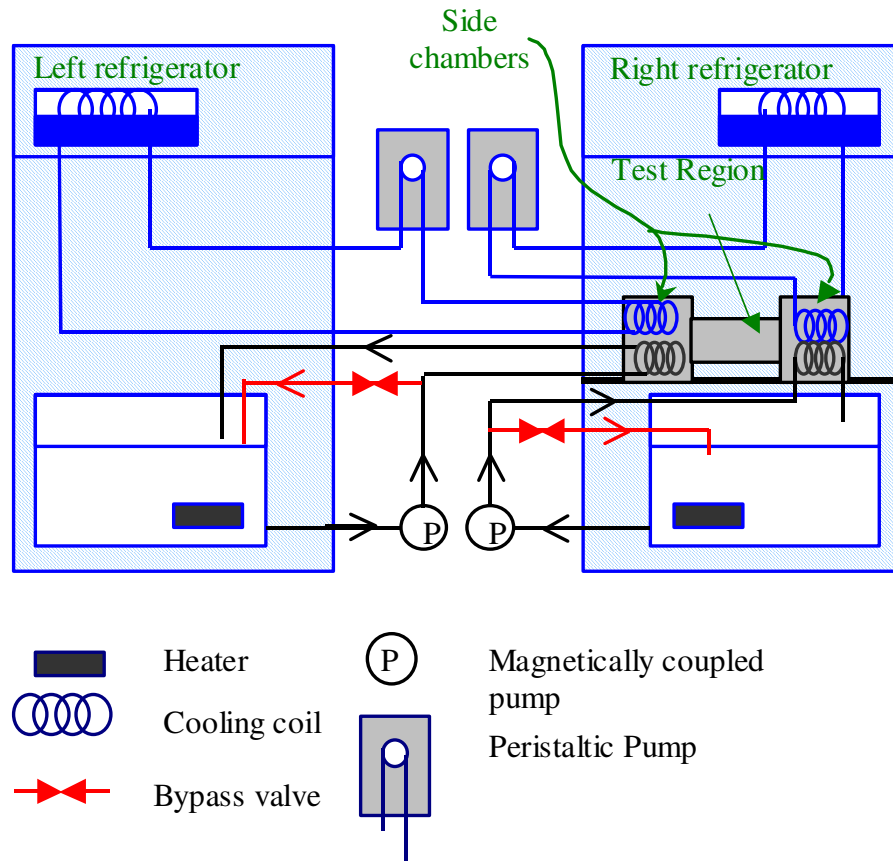


Figure 2.4-1 Schematic overview of the experimental apparatus.

There are two plumbing circuits for each chamber in this system. The warming circuit pumps coolant from the reservoir to the warming coil and the cooling circuit pumps coolant from the freezer compartment to the cooling coil. The coolant in the warming circuit is a clear mixture of 15% ethylene glycol in water. Blue dyed ethylene glycol, available commercially for automotive purposes, is used in the cooling coils. The manufacturer recommends the use of this coolant for temperatures above -36°C . This temperature is well below the typical freezer temperatures of -30°C . The coolant surrounding the coils in the side chambers is a clear mixture of 30% ethylene glycol in water; this concentration prevents the coolant from freezing at the required operating temperatures. Circulating the coolant in the side chamber

using a miniature pump maintains a uniform temperature along the side in contact with the test region. The same coolants are used in the plumbing circuits for the side chamber on the right and all external piping is insulated using standard domestic pipe-wrap insulation.

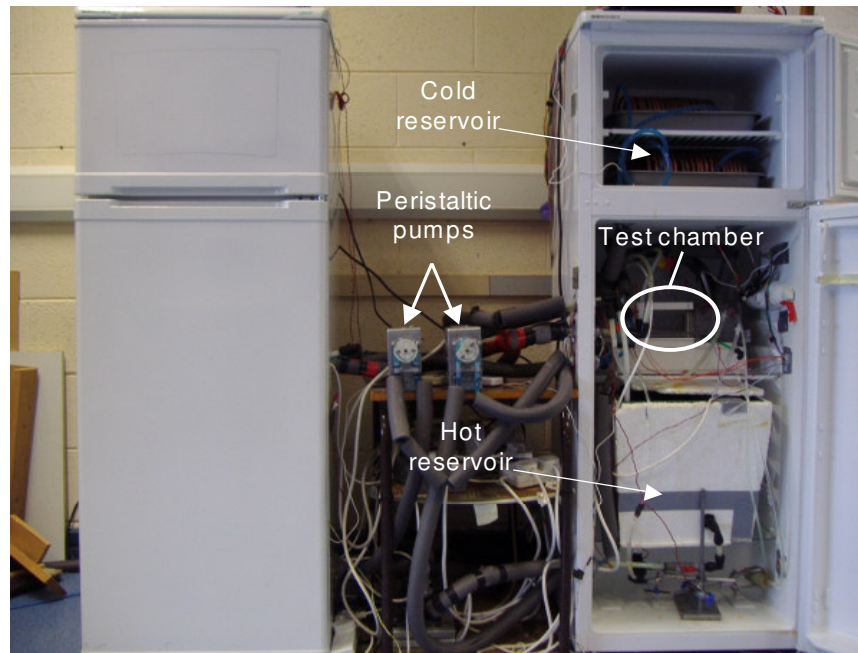


Figure 2.4-2 Graphical overview of the experimental apparatus.

The temperature of the side chamber on the right is achieved in a similar manner to the temperature of the left side chamber. The reservoir for the warming coil in this side chamber is contained in the refrigerator/freezer unit on the right in Figure 2.4-1 and Figure 2.4-2. The test chamber along with the two side chambers is located in this refrigerator/freezer unit since the door of this unit contains a double-glazed window. The insertion of a double glazed window into the door of the refrigerator compartment does slightly increase the temperature of the refrigerator ambient. The refrigerator ambient has potential to influence the experimental results. This difficulty is overcome in two ways; the computer controls the ambient temperature of the refrigerator and the test region (the test chamber and the two heat transfer measurement devices) is insulated with 5cm of expanded polystyrene. These precautions reduce the influence of the ambient temperature on the experimental results. As described previously in section 2.3.1, during an experiment the refrigerator compressor is continuously operating and at all other times it is operated

according to the temperature of the main refrigerator compartment. A clamp consisting of two rods and two crossbars was used to ensure good thermal contact between the aluminium side chambers, the heat transfer measurement devices and the aluminium walls of the test chamber.

2.4.2 Data acquisition and operating software

The apparatus was based on the previous system described in section 2.3.1 and similarly the software for operating this system is based on the software described in section 2.3.2. The code for acquiring data from this system is identical to the code described previously in section 2.3.2; the difference lies in the operation of the system and the intended purpose of the system. There are two distinctively different procedures carried out with this apparatus, thus it was necessary to design separate software for each procedure. The apparatus is primarily used for investigating asymmetrical heat transfer and later it was used for employing a more passive technique of measuring the temperature of maximum density of aqueous solutions. A brief overview of the software that is applicable to both procedures is discussed before describing the different changes associated with the separate codes.

The software consists of a main routine followed by a number of functions and it is based on a system of multiple flag variables. Each flag variable corresponds to an operation and the values of the flag variables determine which functions are invoked. The main routine contains a loop synchronised to the system clock that iterates once per second. During this iteration, certain functions are invoked according to the values of the flag variables. The user interacts with the system via a menu function. The differences between the software for this system and that described in section 2.3.2, due to the difference in operation, is summarised in the changes made to the menu options as explained below.

- c Adjust sump temperatures:** Allows the user to select the desired temperatures of the sumps.
- h Maintain sump temperatures:** Initiates control of the sump temperatures by activating the heaters as necessary.
- d Stop maintain sump temperatures:** Stops control of the sump temperatures and allows the sump to reach thermal equilibrium with its environment.

- r Prepare water for run:** Initiates temperature control of the chambers. This activates the peristaltic pumps (which activates the cooling coil) and the magnetically coupled pumps (which activates the warming coil) as necessary in order to maintain the coolant in the chambers at the specified temperatures.

There are two purposes for this system; the first purpose for this system is to investigate asymmetrical heat transfer and the second purpose is to investigate the temperature of maximum density of aqueous solutions. Since the latter purpose is the same as that of the system described in section 2.3.2, no other changes to the software were required and this software is used for investigating the temperature of maximum density of aqueous solutions. The former purpose requires changes to the operation of the software and those changes are summarised in the changes to the menu options explained below.

- q Begin experiment:** Begins the cycle of maintaining a steady temperature gradient for 30,000 seconds followed by a 48,000 second switching of the desired boundary temperatures completed with a 30,000 second steady temperature gradient. This cycle continues until the user instructs the experiment to stop.
- w Stop experiment:** Allows the user to stop the cycling of the temperature gradient.

The data acquisition and operating software for investigating asymmetrical heat transfer incorporates all six changes in the menu options outlined in this section while the investigations of the temperature of maximum density of aqueous solutions (based on heat transfer measurements) incorporates just the first four menu options. The additional two options outlined above are requirements of the procedure associated with the investigation.

2.5 Procedures

This section describes the procedures required for investigating asymmetrical heat transfer through composites of water and aqueous solutions in the presence of the density maximum. The procedures for investigating the temperature of maximum density of aqueous solutions is distinctively different to the procedure for investigating asymmetrical heat transfer. This requires the two procedures to be

described in separate sections. The procedures associated with investigating the behaviour of the temperature of maximum density of aqueous solutions is described in section 2.5.1 and the procedures associated with the investigation of asymmetrical heat transfer is described in section 2.5.2.

2.5.1 Temperature of maximum density of Aqueous Solutions

This section describes the procedures associated with the investigation of the temperature of maximum density of aqueous solutions. The procedures for investigating the temperature of maximum density of aqueous solutions will be described first, followed by a description of the procedures for investigating the anomalous behaviour observed in the triple cell chamber. Investigations of the temperature of maximum density of aqueous solutions required cooling of a sample of water under the controlled conditions outlined below. An identical procedure is then applied to an aqueous solution. During the cooling, the temperature at select points in the liquid is monitored. The results show an anomalous feature in the temperature profiles centred on the liquid's temperature of maximum density. A comparison between the temperature profiles of the solution with the temperature profiles of pure water shows a shift in the temperature of maximum density. This shift in temperature is measured using a chi-squared comparison and from this the temperature of maximum density of the solution is deduced.

In the cooling experiments, the boundary temperatures are initially set at 10°C (T_L) and 6°C (T_R). These temperatures are decremented simultaneously by 0.1°C at intervals of 540 seconds until T_L reaches 2°C and T_R reaches -2°C . Thus the temperature gradient remains constant throughout the experiment (a 4°C temperature difference across 0.12m) but the mean temperature of the water sample is cooled from 8°C to 0°C over a time span of 43,740 seconds (12.15 hours). The purpose of this slow cooling is to bring the water sample through the region of the density maximum in a quasi-steady-state fashion. The temperature is recorded continuously in the side chambers and at set points along the central horizontal axis through the test chamber. Three investigations are conducted using this procedure, the first of these investigations to be conducted aims to measure the temperatures of maximum density of aqueous solutions based on the occurrence of the anomalous feature in the temperature profiles. The second investigation aims to examine the rate of heat flow

into and out of the liquid in the vicinity of the density maximum and the third investigation aims to exploit any anomalous features in the heat transfer profile to develop an alternative method of measuring the temperature of maximum density that is non-invasive and permits the measurement of the temperature of maximum density of corrosive liquids.

The temperature of maximum density of the solution is obtained by comparing the anomaly feature of the test sample (solution) to the anomaly feature of the control sample (water) using the chi-squared technique. A chi-squared sum is formed by accumulating the squared differences for each of the five temperature probes within the test region. This sum is recalculated as the test profile is shifted relative to the control profile in the direction of the slope of the T_L and T_R cooling curves, i.e. the test anomaly feature is superimposed upon the control feature and the two sets of temperature profiles are shifted relative to each other until an optimal overlap is achieved, as signified by a minimum in the chi-squared sum. The corresponding shift in the temperature of maximum density is then calculated from:

$$T_{\rho_{\max}} = (\text{slope} \times \text{position of chi-squared minimum}) + 4^{\circ} \text{C} \quad (2.5-1)$$

where the slope of the T_h or T_c profile is given by

$$\text{slope} = \frac{2^{\circ} \text{C} - 10^{\circ} \text{C}}{43740} = -1.829 \times 10^{-4} \text{ }^{\circ} \text{C s}^{-1} \quad (2.5-2)$$

The aqueous solutions are prepared using standard laboratory techniques. The desired quantity of solute is weighed using an electronic weighing scale. The solute is dissolved in a beaker that contains distilled water. The volume of distilled water in the beaker was much less than 500ml. When the solute is dissolved, the contents of the beaker are poured into a 500ml volumetric flask. Distilled water is added to the flask until the bottom of the meniscus reaches the 500ml marker on the neck of the flask.

Three different test chambers were used in the investigation of the temperature of maximum density of aqueous solutions. The test chamber used for measuring the temperature of maximum density of aqueous solutions as presented in Cawley *et*

al. [61] was a die-cast aluminium box of dimensions 0.12m x 0.06m x 0.06m (length x height x depth). The thermistors are located along the central horizontal axis at distances of 0.02m, 0.04m, 0.06m, 0.08m, and 0.10m from the T_L wall. The aluminium walls of the test chamber do not provide good resistance to heat flow for the non-isothermal walls. However, the influence of the refrigerator ambient temperature is negligible in these circumstances as the measurements are based on a comparative technique. A second chamber was constructed for PIV investigations. The chamber has dimensions of 0.10m x 0.10m x 0.10m. The thermistors are located along the central horizontal axis at distances of 0.01m, 0.03m, 0.05m, 0.07m, and 0.09m from the T_L wall. The two isothermal walls in contact with the side chambers are made from aluminium and the remaining four walls are constructed from Perspex. The clear Perspex permits flow visualization and provides good resistance to the flow of heat from external sources. A third chamber was constructed for the purpose of observing the thermal diode effect and measuring the temperature of maximum density of aqueous solutions using a similar technique to the technique presented in Cawley *et al.* [61] but which is based on heat transfer measurements. This test chamber has the same dimensions as the die-cast aluminium box and the same thermistor positions but it is constructed in the same way as the PIV test chamber. As this chamber is used for heat flow measurements, it was necessary to construct the non-isothermal walls from an insulating material.

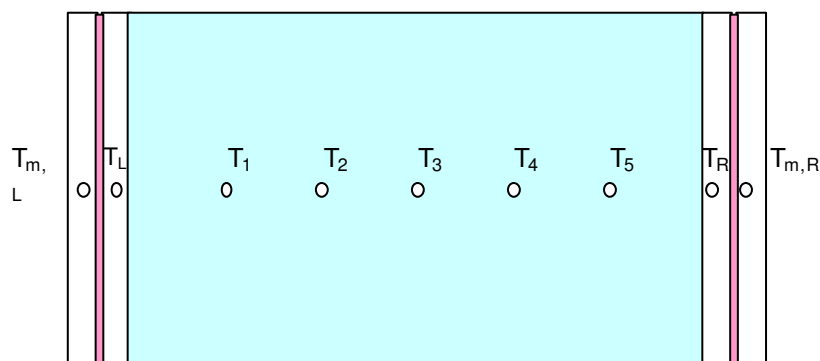


Figure 2.5-1 Typical chamber used in this experiment with the thermistor positions indicated by the letter T . The heat transfer device is also included on the left and right boundaries with relevant thermistors also shown.

2.5.2 Asymmetrical Heat Transfer

This section will describe the procedure associated with investigating asymmetrical heat transfer. In this procedure, the temperatures on the left wall (T_L) and right wall (T_R) of the test chamber are held fixed for long time spans, and the rate of heat transfer is extracted after steady-state conditions have been established. Then the gradient is reversed and when the system reaches steady state conditions, the rate of heat flow is measured again. The rate of heat flow for the two different directions could be measured using two different procedures; in the first procedure, the flow of heat is fixed in space but the cavity is rotated through 180° about a vertical axis. The alternative approach, which is used here, is to fix the cavity in space and reverse the direction of the flow of heat. This approach was selected as it avoids the need for human intervention and hence the system remains undisturbed by the external environment during the entire investigation. The degree of asymmetry is quantified by the relative change in the rate of heat flow:

$$\text{Heat flow rectification, } r = \frac{(H_H - H_L)}{H_H} \quad (2.5-3)$$

where H_h is the highest rate of heat transfer and H_L is the lowest rate of heat transfer. Thus, a rectification of 0% would indicate no asymmetry, whereas a value of 'r' of 100% would indicate perfect heat rectification (no heat flow for one orientation of the temperature gradient).

In typical asymmetrical heat transfer experiments, the values of T_L and T_R are chosen to be T_h and T_c , respectively. The test region is then held under this gradient for 30,000 seconds. When this time has elapsed the value of T_L is decremented by 0.1°C every 1,800 seconds until it reaches T_c . When T_L is decremented by 0.1°C , the value of T_R is simultaneously incremented by 0.1°C . This decrementing and incrementing of the temperatures interchanges the temperatures of T_L and T_R to T_c and T_h , respectively. When this interchanging has completed the temperature gradient is maintained for a further 30,000 seconds. This cycle is repeated several times. During this procedure the rate of heat flowing into and out of the chamber is measured using the technique described in section 2.2.3. With uncertainties of 7% on the heat transfer rates, an uncertainty of the order of 14% applies to experimentally determined values of the rectification factor.

This procedure is applied to a composite system of water and a saline solution. The saline solution is a 9.0g.ltr⁻¹ sodium chloride solution. The temperature of maximum density of pure water is 4°C and the temperature of maximum density of the solution is 2°C (the temperature of maximum density was measured using the technique described in section 2.5.1). The observation of asymmetrical heat transfer relies on the occurrence of the density maximum in both liquids. The wall temperatures for this system was chosen to be 5°C and 1°C from the following equation:

$$T_{h/c} = \left(\frac{T_{\rho,max,w} + T_{\rho,max,s}}{2} \right) \pm (T_{\rho,max,w} - T_{\rho,max,s})$$

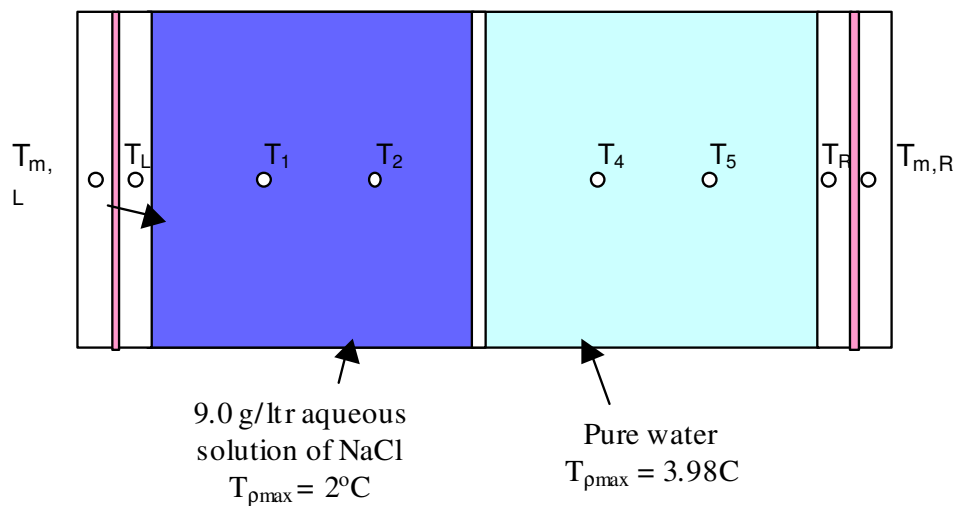
where $T_{h/c}$ is the temperature of the hot/cold wall and the $T_{\rho,max,w}$ is the temperature of maximum density of water and $T_{\rho,max,s}$ is the temperature of maximum density of the sodium chloride solution.

The procedure described in this section was also applied to a composite system of water and Perspex. Computer simulations of the composite system of water and Perspex, which will be discussed later in chapter 5 showed that the optimal wall temperatures for asymmetrical heat transfer for this composition was 6.5°C and 2.5°C. Consequently, these temperatures were used for the experimental investigation of asymmetrical heat transfer through this composition. The composite system consisted of a 0.2cm wide block of Perspex adjacent to a region of water 11.8cm wide. Both the region of water and the Perspex had a cross-sectional area of 6cm x 6cm.

The test chamber used in the investigations of heat flow asymmetry had internal dimensions of 6cm x 6cm (cross-section) and length 12cm, and was constructed from 6mm Perspex with 6mm aluminium end-walls. A removable aluminium partition is inserted into this chamber to divide this chamber equally in two parts for investigating asymmetric heat flow through a composite system of water and a saline solution. The partition is removed for investigations of asymmetrical heat flow through a composite system of water and Perspex. This investigation requires the insertion of a 2mm wide Perspex block into one side of the chamber. The

arrangement of the chamber for each of these investigations is shown in Figure 2.5-2. Five thermistors are arranged in a horizontal line along the centre of the test chamber, at distances of 2cm, 4cm, 6cm, 8cm and 10cm relative to the left wall (during investigations of the water and saline solution composite the middle thermistor T_3 located at the 6cm position is removed to permit insertion of the aluminium partition in the centre of the test chamber).

(a)



(b)

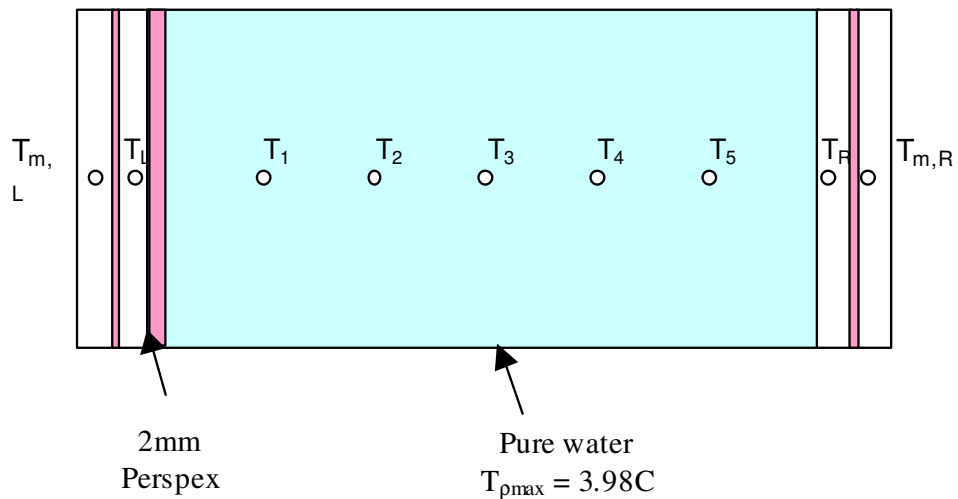


Figure 2.5-2 (a) Test chamber used for investigating asymmetrical heat flow through a composite system of water and a saline solution. (b) Test chamber used for investigating asymmetrical heat flow through a composite system of water and Perspex. The letter T denotes thermistors and their positions are indicated by o .

Chapter 3

Experimental Results

3.1 Introduction

This chapter discusses the experimental results from the investigations of the temperature of maximum density of aqueous solutions and asymmetrical heat transfer. The results from the investigations relating to the temperature of maximum density of aqueous solutions that do not involve heat transfer were obtained using the experimental system described in section 2.3. Investigations involving heat transfer were conducted using the experimental system described in section 2.4. Asymmetrical heat transfer is found in composites of water and aqueous solutions and in composites of water and solids. The study of asymmetrical heat transfer through a composite of water and an aqueous solution requires knowledge of the temperature of maximum density of some aqueous solutions. It is known that when a solute is added to water both the temperature of freezing and the temperature of boiling change linearly as the concentration of the solution increases. This linear relationship between the freezing and boiling temperatures and the concentration is independent of the nature of the solute. This is not the case for the temperature of maximum density of aqueous solutions.

A study of the behaviour of the temperature of maximum density of various solutions was conducted using a novel measurement technique described in section 2.5.1. The technique is based on an anomalous feature that occurs in the temperature profiles of five points equally spaced along the central horizontal axis through a rectangular cavity of the solution as it is cooled through its density maximum. Since the measurement technique relies on this feature, it is important to understand it. The feature is investigated using the flow visualization technique, Particle Image Velocimetry (PIV). The temperature of maximum density of aqueous solutions is investigated using a rectangular metal container, the metal walls of the container renders flow visualization impossible. Flow visualization must be conducted with an alternative container, this requirement of flow visualization resulted in the use of a container of different dimensions for PIV analysis to the container used for measuring the temperature of maximum density of aqueous solutions. This difference in geometries revealed a relationship between the shape of the anomaly feature and the size of the container. This relationship was investigated using computational fluid dynamics and it was found that although the anomaly features

were different, the explanation for the occurrence of the anomaly feature as revealed by the flow visualization studies is valid for both geometries. The container for flow visualization consisted of two opposing metal walls (the isothermal walls) and the remaining four walls were made from clear Perspex. This container was not used for measuring the temperature of maximum density of aqueous solutions as the adhesive between the metal and the Perspex walls was prone to corrosion by some of the solutions. Some aqueous solutions also corroded the protective coating on the thermistors, and consequently they could not be investigated using the measurement technique that exploits the feature in the temperature profiles of five points inside the liquid. These solutions could be investigated using an alternative technique that is also reliant on the convective flow pattern in the vicinity of the density maximum but it is based on the rate of cooling of the liquid.

The rate of cooling of the liquid is obtained from examining the rate of heat flowing into and out of the container. The rate of heat flowing through the walls is measured by monitoring the temperature difference across a material of known conductivity placed outside the container at the two isothermal walls as described in Cawley *et al.* [36] (a similar technique was implemented by O'Connor [62] in an independent experimental system which used Peltier devices to control the cooling of the test region). The rate of heat flow is calculated from this measurement using the one-dimensional Fourier heat equation. During a steady state experiment, the rate of heat flowing into the container equals the rate of heat flowing out of the container, however if a material is being cooled then the rate of heat flowing out of the container must be greater than the rate of heat flowing into the container. Conversely, when a material is warming the rate of heat flowing into the container is greater than the rate of heat flowing out of the container. During cooling, the rate of heat flowing into the container is due to the temperature gradient, while the rate of heat flowing out of the container is due to the temperature gradient and the extraction of heat from the material due to cooling. The influence of the density maximum on the heat transfer measurements is considerable, and during a transient experiment the rate of cooling exhibits an anomaly feature in the vicinity of the density maximum. This feature, like the temperature profiles feature, can be used to measure the temperature of maximum density of aqueous solutions.

The technique used to measure the temperature of maximum density of aqueous solutions compares the anomaly feature that occurs in the temperature profiles of water to the anomaly feature that occurs in the temperature profiles of an aqueous solution. The technique is novel and unlike measurement techniques used by other researchers this technique relies on convective flow. The technique is applied to a variety of aqueous solutions and the application of the technique to a 10g.ltr⁻¹ solution of potassium bromide is shown as an example. This technique is applied to all of the solutions shown in this chapter unless it is stated otherwise. An alternative technique is presented in this chapter that is based on the anomaly feature in the rate of cooling. This technique is applied to solutions of sodium chloride and propan-2-ol in conjunction with the temperature profiles based technique that is described in Cawley *et al.* [61] for the purpose of validation. This technique, unlike the technique described in Cawley *et al.* [61], could be applied to aqueous solutions of acids and bases, which might corrode the protective coatings on the thermistors. It is desirable to investigate the behaviour of the temperature of maximum density of these solutions to further understand the occurrence of the density maximum. However, the technique is not applied to these solutions for this study, as this work is not concerned with the occurrence of the density maximum on a molecular level.

During the investigation of the anomaly feature in the temperature profiles, it was revealed that the addition of solutes to water has a profound effect on the temperature profiles both in the vicinity of the density maximum and in regions away from the temperature of maximum density. It was observed that the temperature profiles for sodium carbonate solutions were consistently distorted. The observed distortions are presented and discussed, but an explanation for such behaviour is not presented and it would require an extensive study.

Asymmetrical heat transfer is observed if the rate of heat transfer changes when the direction of heat flow is reversed. The degree of asymmetry is discussed in terms of heat flow rectification, which quantifies the relative change in the rate of heat flow:

$$\text{Heat flow rectification, } r = \frac{(H_H - H_L)}{H_H} \quad (3.1-1)$$

where H_h is the highest rate of heat transfer and H_L is the lowest rate of heat transfer. Thus, a rectification of 0% would indicate no asymmetry, whereas a value of 'r' of 100% would indicate perfect heat rectification (no heat flow for one orientation of the temperature gradient). The results presented in this chapter show that the density maximum causes a composite system to exhibit asymmetrical heat transfer. Asymmetrical heat transfer is observed in a composite of water and an aqueous solution and in a composite of water and Perspex. The basis of this thermal diode effect is that heat transfer is altered in the vicinity of the density maximum. When heat flows in a given direction through the composite of water and an aqueous solution (the water-saline diode), the two liquids have a mean temperature that is removed from their temperatures of maximum density. When heat flows in the opposite direction, the two liquids have a mean temperature that corresponds to their temperatures of maximum density. Consequently, the rate of heat flow in the opposing direction is different, and asymmetrical heat transfer is observed. Similarly, when heat flows through the composite of water and Perspex, the temperature difference across the water compartment encompasses the density maximum in a certain direction and not in the opposing direction. Consequently, asymmetrical heat transfer is also observed in a composite of water and a solid.

3.2 Data acquisition overview

There are two different experimental systems used to obtain the results presented in this chapter. The first system is the quasi-steady state system that is described in section 2.3. The results presented in sections 3.3.1, 3.3.4, and 3.4.1 were obtained using the quasi-steady state system. The second system is the heat transfer system that is described in section 2.4. The results presented in sections 3.3.2, 3.4.2 and 3.4.3 were obtained using the heat transfer system. The results presented in sections 3.3.3 and 3.3.5 were obtained using either one of these systems, and it is indicated in these sections which system was used to obtain the presented results. It is important to distinguish which system is used for the presented results. The results from the quasi-steady state system are presented without post-processing while the results presented from the heat transfer system require post-processing.

In both experimental systems, the temperatures are measured every second and they are saved to a data file along with the elapsed time since the start of the experiment.

This data file is assigned a title that corresponds to the date of the run and it is stored on the hard drive of the associated personal computer. The file consists of seventeen columns; the first column contains the time and the remaining sixteen columns correspond to the sixteen-thermistor channels. This raw data is presented for the results obtained using the quasi-steady state system. However, the raw data obtained from the heat transfer system must be post-processed before presentation.

An example of the raw data from the quasi-steady state system is presented in Figure 3.2-1. A rectangular enclosure of water is subjected to a constant horizontal temperature gradient with boundary temperatures of 10°C and 6°C. It is evident from this graph that the boundary temperatures are not constantly 10°C and 6°C but vary from these temperatures by less than 0.1°C. This variation in temperature is due to the constant cooling and warming of the sidewalls that is required to prevent the influence of external factors on the temperature of the sidewalls. The variation is less than 0.1°C and it does not obscure the experimental results. Therefore, the results obtained from the quasi-steady state system are presented without post-processing.

This variation in the temperature of the sidewalls occurs in both systems but the variation of the temperature of the sidewalls in the heat transfer system is greater than 0.1°C and it does obscure some of the results. Thus, a moving average of 1500 seconds is applied to the results presented from the heat transfer system. An example of the raw data from the heat transfer system is presented in Figure 3.2-2. The same example is shown in Figure 3.2-3 with the moving average applied to the results. The fluctuations in the sidewall temperatures are larger in this system than in the quasi-steady state system. This is due to the presence of the Perspex reference material between the sidewalls and the side chambers. In both systems, the coolant in the side chambers is warmed/cooled until the sidewalls reach their selected temperature. In the quasi-steady state system, heat flows directly from the side chambers to the sidewalls, so temperature changes in the side chambers are sensed rapidly by the sidewalls. In the heat transfer system, heat flows from the side chambers through the Perspex and to the sidewalls. The addition of the Perspex reduces the response time of the sidewalls to the temperature changes in the side chambers. Consequently, the temperature of the side chambers continue to

increase/decrease for a longer period of time and so the temperature of the sidewalls increase/decrease more in the heat transfer system than in the quasi-steady state system.

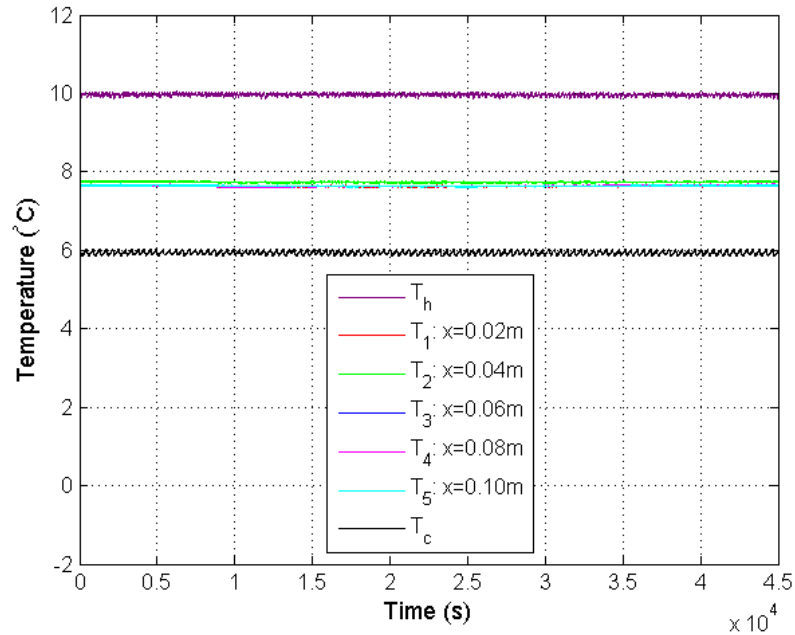


Figure 3.2-1 The raw data of steady state experimental results obtained using the quasi-steady state experimental system described in section 2.3.

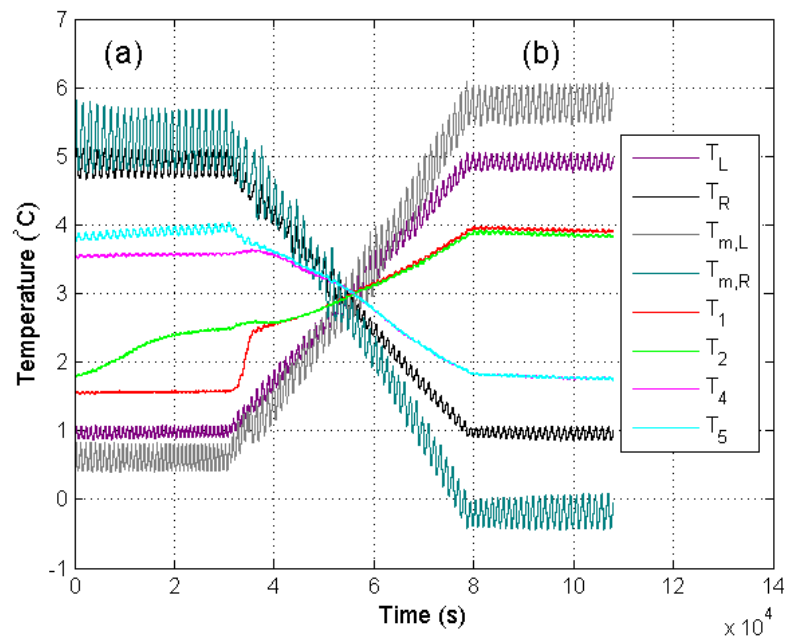


Figure 3.2-2 The raw data for the first cycle of the experimental results of the water-saline diode obtained using the heat transfer experimental apparatus described in section 2.4.

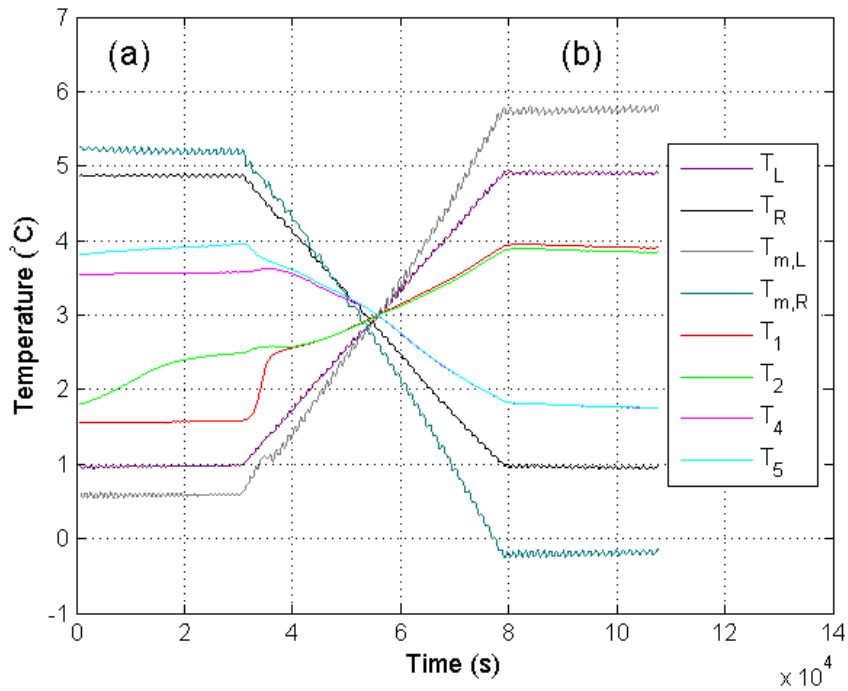


Figure 3.2-3 The smoothed data for the first cycle of the experimental results of the water-saline diode obtained using the heat transfer experimental apparatus described in section 2.4.

An additional factor for the varying sidewall temperatures is the rate of heat flowing through the test sample. The raw data for the first cycle of the investigation of asymmetrical heat transfer through the composite system of water and the saline solution are presented in Figure 3.2-2. The rate of heat transfer in region (a) is much less than the rate of heat transfer in region (b) as indicated by the temperature difference between $T_{m,L}$ and T_L (and $T_{m,R}$ and T_R). The amplitude of the oscillations in T_R is higher in region (a) than in region (b). This is due to the influence on the experimental apparatus of the lower rate of heat transfer in region (a) than in region (b). The time required for the temperature of the sidewall to respond to the changes in the side chamber depends on the rate of heat transfer. Since the rate of heat transfer is lower in region (a) than region (b), the cooling/warming coil remains active for longer and the amplitude of the oscillations in the wall thermistor is larger in region (a) than in region (b).

The amplitude for the oscillations in T_L in region (b) is similar to the amplitude of the oscillations in T_R . However, the amplitude of the oscillations in the profile of T_L in region (a) is not the same as the amplitude of the oscillations in the profile of T_R . This is due to the limited cooling ability of the left side chamber. The associated cooling and heating apparatus for this side chamber is in a separate refrigerator. Consequently, the cold liquid required for cooling this side chamber must pass through the room ambient of 25°C. This reduces the rate of cooling of the left side chamber and it restricts the amplitude of the oscillations of T_L in region (a). Since the temperature of T_L is greater in region (b), this restriction does not impinge on the amplitude of the oscillations in region (b).

3.3 The density maximum of aqueous solutions

This section presents the results of the investigations relating to the temperature of maximum density of aqueous solutions. The first of these investigations examines the occurrence of the anomaly feature in the temperature profiles in the vicinity of the density maximum when a rectangular container of water is subjected to the cooling procedure outlined in section 2.5.1. The controlled cooling procedure is initially applied to a typical liquid and the results are explained before the presentation and discussion of the results of the application of the same cooling procedure to water. The results of this investigation are presented in section 3.3.1.

The second investigation in this section explores the rate of heat transfer in the vicinity of the density maximum and the rate of cooling of the liquid in the vicinity of the density maximum as water is cooled under the controlled conditions outlined in section 2.5.1. As in section 3.3.1, the results of a typical liquid is analysed before presenting and discussing the results of water. The behaviour of heat transfer and the rate of cooling in the vicinity of the density extremum are discussed in section 3.3.2.

The third investigation presented in section 3.3.3 examines the two techniques that are used to measure the temperature of maximum density of aqueous solutions. The first technique presented is based on the temperature profiles at five select points within the liquid and the second technique is based on the anomaly feature that occurs in the profile of the rate of cooling. These two techniques are described in detail, an example of their application is presented and some results obtained using

the technique are compared to measurements obtained by other researchers for the purpose of validation. The second technique is only presented and validated in this study while the first technique is used for the measurement of the temperature of maximum density of the aqueous solutions discussed in this study.

Section 3.3.4 presents the fourth investigation, which examines the temperature of maximum density of a variety of aqueous solutions and discusses the behaviour of the temperature of maximum density as a function of solute concentration. Most of the results presented in this section have been published in Cawley *et al.* [61] and all of the results were obtained using the measurement technique based on the anomaly feature in the temperature profiles within the liquid as described in Cawley *et al.* [61].

The final investigation relating to the temperature of maximum density of aqueous solutions examines the unusual shape of the anomaly feature for aqueous solutions of sodium carbonate. Distorted anomaly features were observed for sodium carbonate solutions. The origins of these distortions are not fully understood at this stage and further work is required in this area.

3.3.1 Quasi-steady state cooling of water

This section discusses the results of applying the quasi-steady state cooling procedure outlined in section 2.5.1 using the apparatus described in section 2.3.1 to a rectangular container of liquid. Since water is an unusual liquid, it was desirable to examine the behaviour of a typical liquid undergoing the same procedure as water before examining the behaviour of water. When a typical liquid (that is, a liquid with no density maximum) was required in this project, pure ethanol was used since it is readily available and many of its properties are similar to those of water. Since both liquids are so similar, except for the presence of the density maximum in water, the differences in experimental results between those for ethanol and water can be attributed mainly to the occurrence of the density maximum in water. A discussion of the results obtained when the cooling procedure is applied to ethanol precedes a discussion of the results of water. The first set of results presented for ethanol and water were conducted with a rectangular container of dimensions 0.06m x 0.06m x 0.12m (width x height x length). The results of the investigations of flow

visualization, which are presented following the results of ethanol and water, were obtained using a square container of dimensions 0.10m x 0.10m x 0.10m.

The results of cooling ethanol from an average temperature of 8°C to 0°C in a quasi-steady state manner are shown in Figure 3.3-1. The undulations in the T_h and T_c profiles are partly due to the feedback required within the system to maintain a constant temperature difference across the test region during the 9 min steps and partly due to the regular stepping of the side-chamber temperatures during the controlled cooling. It is evident from the graph that the temperatures at the five thermistor positions are within 0.1°C of each other. This implies that in the central region of the liquid there is almost no transfer of heat in the horizontal direction. The thermistor profiles may be understood by noting that warmer liquid becomes less dense and rises along the warm wall to the top of the container. Colder more dense liquid descends along the cold wall to the bottom of the container. This behaviour sets up a clockwise convection cell. The movement of the warm ethanol from the left of the container to the top, and the movement of the cold ethanol from the right of the container to the bottom sets up an almost vertical temperature gradient within the fluid. Heat flows from the top of the container, through the central region where the thermistors are located, to the bottom of the container, primarily by conduction. It is this rearrangement of the gradient by the fluid flow in the boundary regions that dominates the temperature distribution in the central region and thus the temperatures at the five points are similar. This analysis of the experimental curves is supported by the flow visualization of water in Figure 3.3-3 and the simulations of the cooling of ethanol in section 5.2.

Water at temperatures above its temperature of maximum density behaves similarly to ethanol, that is, its density decreases with increasing temperature. Therefore, it is expected that at temperatures above 3.98°C free convection in water should be identical to free convection in ethanol. The results of the quasi-steady state cooling of water are shown in Figure 3.3-2. The temperature profiles of the five points at temperatures above 3.98°C are similar to the temperature profiles of ethanol, as expected. The five temperature profiles in this region exhibit temperatures within 0.1°C of each other. This behaviour is not observed in the vicinity of the density extremum.

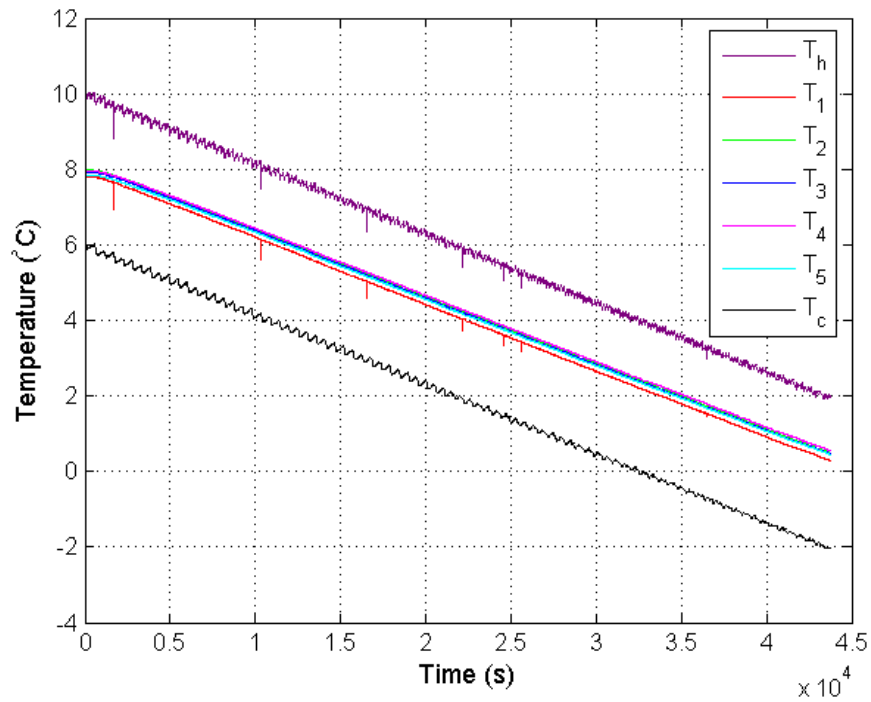


Figure 3.3-1 Temperature against time for pure ethanol in the test chamber. The chamber is 0.06 m x 0.06 m x 0.12 m (width x height x length). ($Ra \approx 6.5 \times 10^8$).

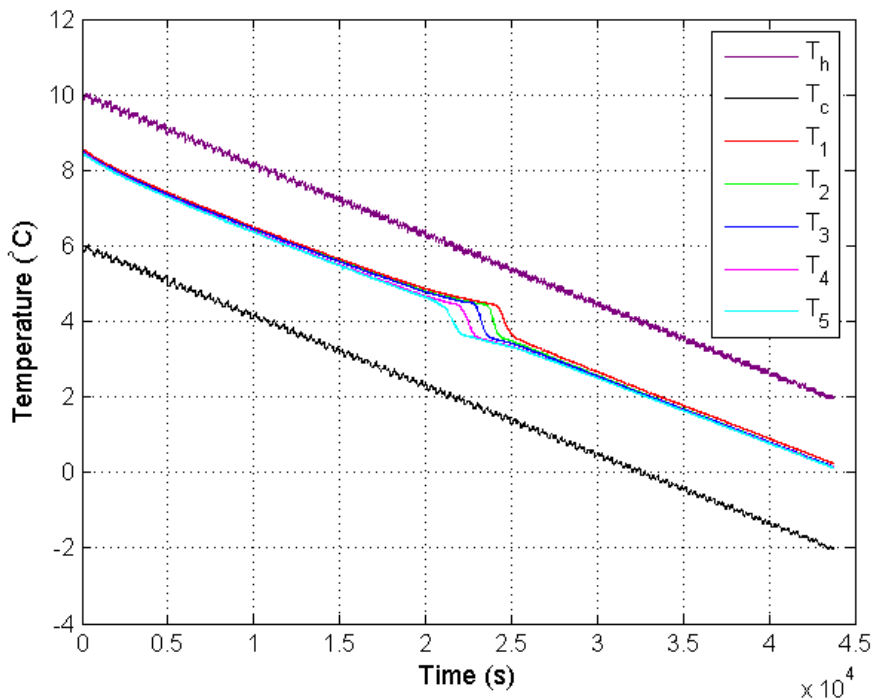
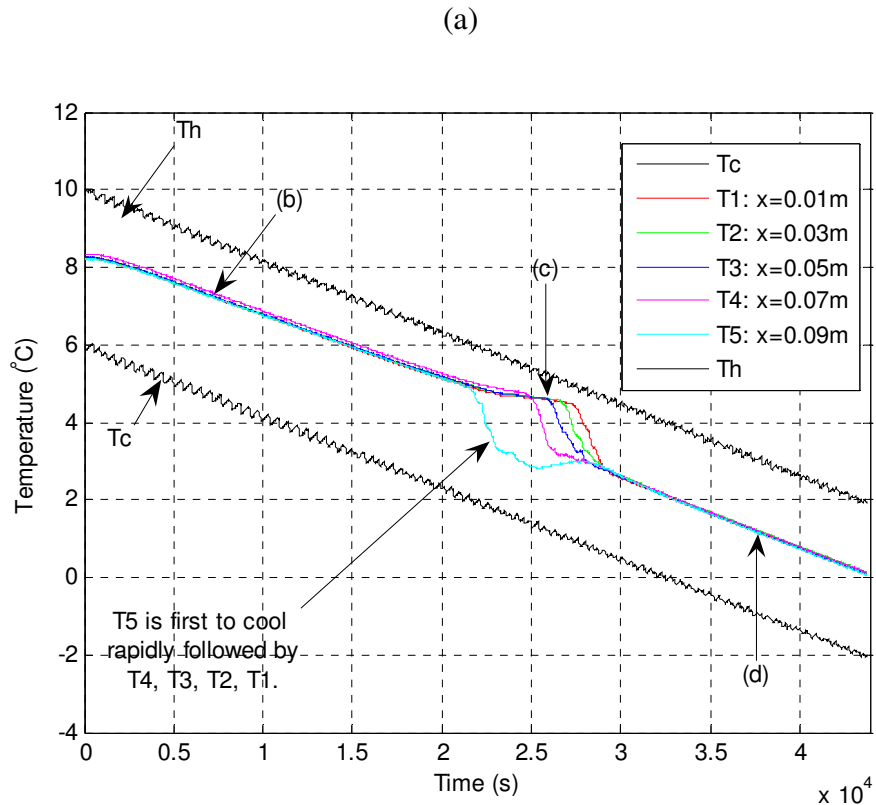


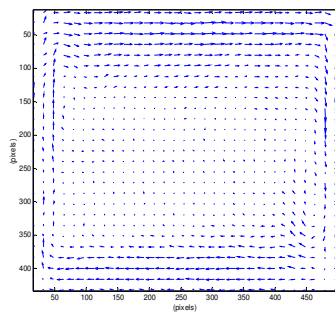
Figure 3.3-2 Temperature against time for pure water in the test chamber. The chamber is 0.06 m x 0.06 m x 0.12 m (width x height x length). The Rayleigh number ranges from 3.0×10^7 at 8°C to 1.5×10^5 at 4°C and back to 3.0×10^7 at 0°C.

As reported in Mooney and Cawley [63], the temperature profiles in the vicinity of the density maximum exhibit a temporary dispersal centred on 4°C. A slight plateau before a rapid descent in temperature near 4°C is observed in the temperature profiles. This plateau indicates a reduction in the rate of cooling and the sudden decrease in temperature implies rapid cooling. The temperatures of the five profiles descend in sequence starting with the profile of the point closest to the cold wall. These features can be understood by examining the behaviour of the convective flow.

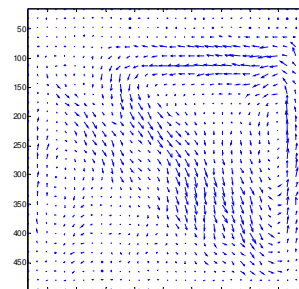
The flow patterns at selected regions of the temperature profiles are shown in Figure 3.3-3 along with the associated temperature profiles plot. The convective flow patterns in these figures reveal the reversal of the single convective cell from a clockwise motion to a counter clockwise motion. As described in Mooney and Cawley [63], the reversal of the fluid density initiates a small counter clockwise convective cell at the cold wall when the temperature of this wall descends below 4°C. This counter clockwise cell grows as the liquid is cooled through its density maximum. Cooling ceases inside the clockwise cell when the counter clockwise cell prevents the clockwise cell from reaching the cold wall. Since the clockwise cell surrounds the five temperature points on the central horizontal axis, the temperatures at these points stop decreasing and the plateau forms in the temperature profiles in the vicinity of the density maximum. The counter clockwise cell now dominates the cooling since it is the only cell in contact with the cold wall. As the counter clockwise cell sweeps across the container, it engulfs each of the temperature points and cools them in turn. The rapid cooling occurs when the counter clockwise cell initially engulfs a point, that is, when the point is located in moving fluid. The cooling slows down when the point is located in stationary fluid inside the counter clockwise convective cell. As the liquid cools below 4°C the clockwise cell ceases to exist and the liquid's convection pattern returns to single cell flow in the counter-clockwise direction. Consequently, the temperature profiles behaviour similar to that in ethanol and at the start of the cooling; they are within 0.1°C of each other again.



(b)



(c)



(d)

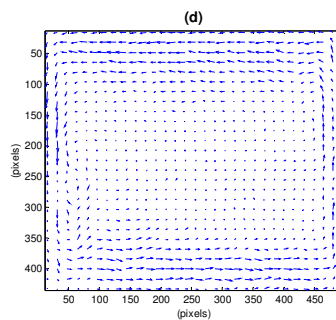


Figure 3.3-3 (a) Temperature against time for pure water in the test chamber (dimension of $0.10\text{ m} \times 0.10\text{ m} \times 0.10\text{ m}$). (b)-(d) are PIV velocity plots for the times indicated by the arrows in (a). (Ra ranges from 1.7×10^7 at 8°C to 8.6×10^4 at 4°C).

The temperature profiles shown in Figure 3.3-3 exhibit a slightly different anomaly shape than the temperature profiles in Figure 3.3-2. The difference in the anomaly features is due to the different container dimensions used. The results shown in Figure 3.3-2 were obtained using a container of dimensions 0.06m x 0.06m x 0.12m (width x height x length) and the results in Figure 3.3-3 were obtained using container of dimensions 0.10m x 0.10m x 0.10m. This explanation for the difference between the two anomaly features is supported by numerical investigations and it is discussed in further detail in section 5.2.6.

A similar anomaly feature also centred on 4°C is observed in the temperature profiles when water is warmed from a mean temperature of 0°C to 8°C in an identical manner as the cooling procedure. The temperature profiles for the warming sequence are shown in Figure 3.3-4. A constant 0.2°C difference is observed between the temperature profile closest to the hot wall and the other four profiles. This difference is due to the drifting out of calibration of the red thermistor and indicates that the thermistors need to be recalibrated. Initially the temperature profiles are closely bunched together but as their temperature approaches the temperature of maximum density, a slight plateau before a rapid increase in temperature near 4°C is observed. The temperatures of the five profiles increase sequentially starting with the profile of the point closest to the hot wall. In contrast to the anomaly feature observed in the cooling curves in Figure 3.3-3, the temperature profile closest to the warm wall is the first profile to diverge in the vicinity of the density maximum. In the cooling sequence, a clockwise convective cell dominates the flow before the liquid enters the vicinity of the density maximum and as the liquid cools, a small counter-clockwise cell starts to grow at the cold wall until the clockwise cell no longer exists. The opposite occurs during a warming sequence. In the warming sequence, a counter-clockwise convective cell dominates the flow before the liquid enters the vicinity of the density maximum and as the liquid warms, a small clockwise cell starts to grow at the hot wall until the counter-clockwise cell no longer exists. Consequently, the temperature profile of the point closest to the hot wall is the first to show a rapid increase in temperature near the density extremum. This analysis of the warming sequence is further supported by the numerical investigations in section 5.2.

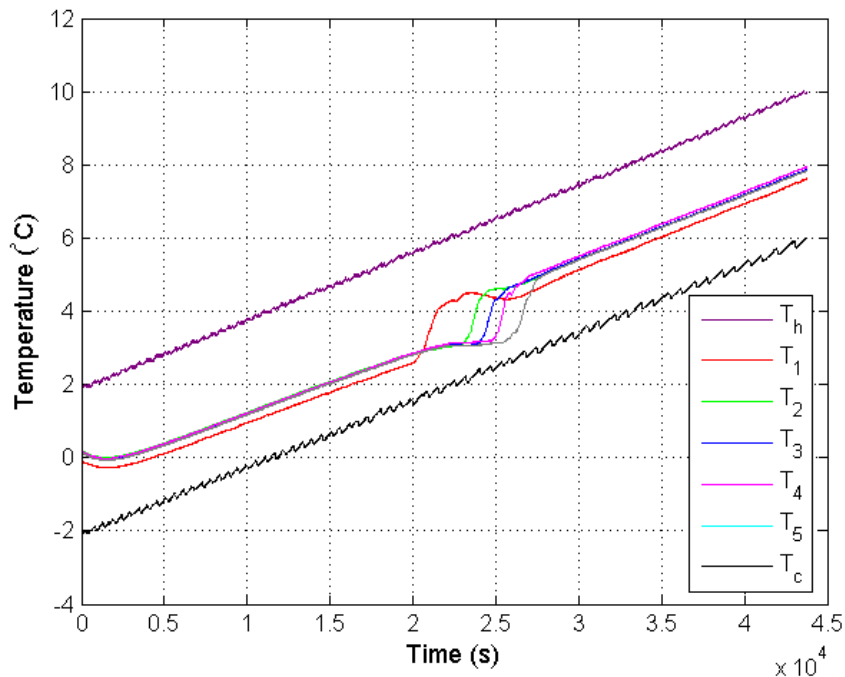


Figure 3.3-4 Temperature against time for pure water in the test chamber (dimension of 0.10 m x 0.10 m x 0.10m) as it is warmed from a mean temperature of 0°C to 8°C. (The Rayleigh number ranges from 1.7×10^7 at 0°C to 8.6×10^4 at 4°C).

3.3.2 Heat flow in the vicinity of the density maximum

Heat is transferred through a fluid primarily by the movement of the fluid. Therefore, it is expected that heat transfer in water at temperatures close to the temperature of maximum density will be affected by the presence of the density extremum since the density maximum influences the fluid flow, as discussed previously in section 3.3.1. Since it is expected that heat transfer will behave unusually in water, it is desirable to examine the behaviour of heat transfer through a typical liquid, such as ethanol, subjected to the procedure outlined in section 2.5.1 before investigating heat transfer through water subjected to the same procedure. The rate of heat transfer is investigated through a rectangular enclosure with dimensions of 0.06m x 0.06m x 0.12m (width x height x length) using the system described in section 2.4 and using the measurement technique described in section 2.2.3. The presence of the heat transfer measurement device between the enclosure's sidewalls and the side chambers causes large variations of the temperatures of the sidewalls (T_h and T_c). These variations have a negligible effect on the central

temperature profiles (T_1 , T_2 , T_3 , T_4 , and T_5) and they are smoothed out of the results presented in all of the figures in this section by applying a moving average of 1,500 seconds to the results.

The graph in Figure 3.3-5 shows the behaviour of the temperature field and an indication of the rate of heat flowing into and out of the chamber as a sample of ethanol is cooled from a mean temperature of 8°C to 0°C over a time span of 12.15 hours under the conditions outlined in the sub-section 2.5.1. The difference between T_h and $T_{m,h}$ indicates the rate of heat flowing into the chamber and the difference between T_c and $T_{m,c}$ indicates the rate of heat flowing out of the enclosure.

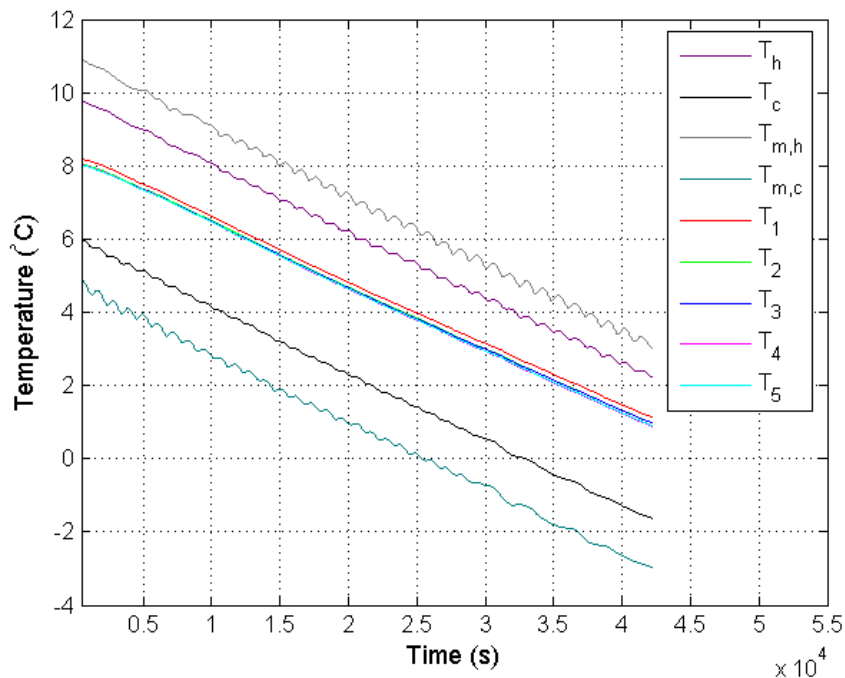


Figure 3.3-5 Temperature against time for pure ethanol in the test chamber. The chamber is 0.06m x 0.06m x 0.12m (width x height x length). The temperature differences between the profiles $T_{m,h}$ and T_h and the profiles T_c and $T_{m,c}$ indicate the rate of heat flowing into and out of the chamber, respectively. ($Nu \approx 11.1$ on the hot side and $Nu \approx 18.0$ on the cold side).

Before the cooling procedure is applied, the wall temperatures are held at 10°C and 6°C until the system has reached steady state. The cooling procedure is initiated when a steady state has been reached. The rate of heat flowing into the chamber is equal to the rate of heat flowing out of the chamber under steady state conditions.

Consequently, when the cooling begins there is a period of time at the start when the rate of heat flowing into and out of the chamber behaves differently to the rest of the experiment. During the rest of the experiment, the rate of heat flowing into the chamber is almost constant and the rate of heat flowing out of the chamber is also almost constant. The rate of heat flowing out of the chamber is greater than the rate of heat flowing into the chamber. This difference is due to the cooling of the volume of ethanol and it is discussed in section 3.3.2.1.

Figure 3.3-6 shows the wall temperatures, the monitoring temperatures and the temperatures at select points along the central horizontal axis of the test chamber containing water. The temperature differences between each wall thermistor and its corresponding monitoring thermistor are converted into heat transfer measurements using equations (2.2-4) and (2.2-5), and the results are plotted in Figure 3.3-7. The difference between these two curves, which is the rate of cooling of the water sample, is discussed in section 3.3.2.1 and it is shown in Figure 3.3-8.

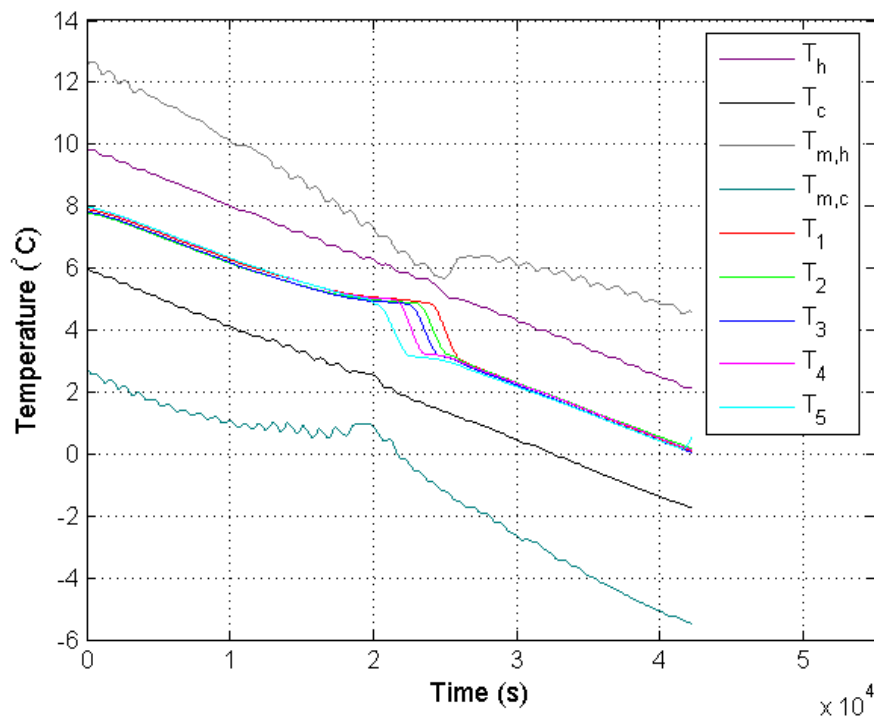


Figure 3.3-6 Temperature against time for pure water in the test chamber. The chamber is 0.06m x 0.06m x 0.12m (width x height x length). The temperature differences between the profiles $T_{m,h}$ and T_h , and the profiles T_c and $T_{m,c}$ indicate the rate of heat flowing into and out of the chamber, respectively.

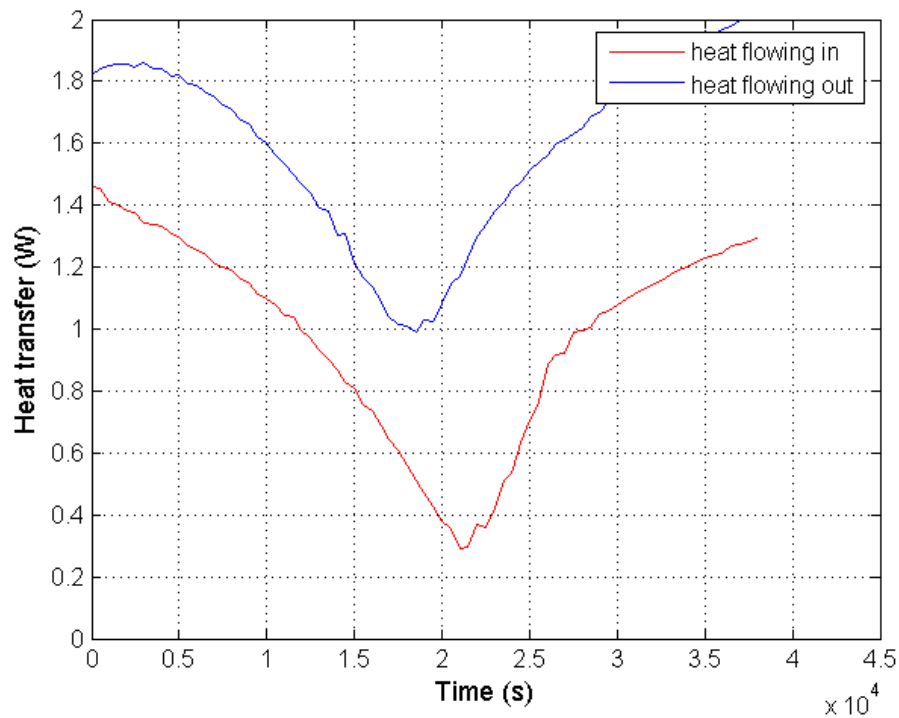


Figure 3.3-7 The rate of heat flowing through the hot wall (red) and the rate of heat flowing through the cold wall (blue) against time. (On the hot side, Nu varies from 19.4 at 8°C to 4.2 at 4°C . On the cold side, Nu varies from 25.0 at 8°C to 14 at 4°C).

It is clear from Figure 3.3-5 and Figure 3.3-6 that the behaviour of heat transfer in the vicinity of the density extremum is unusual compared to the behaviour of heat transfer through ethanol. Figure 3.3-6 shows that the rate of heat flowing out of the enclosure of water reaches a minimum just before the occurrence of the anomaly feature in the temperature profiles of the five points along the central horizontal axis. Similarly, the rate of heat flowing into the enclosure exhibits a minimum just before the anomaly feature finishes. The result that the rate of heat transfer is reduced in the vicinity of the density maximum was also observed in the studies of Lin and Nansteel [29], Watson [32] and Tong [30]. As discussed in Cawley *et al.* [36], the reduction in the rate of heat transfer in the vicinity of the density maximum is attributed to two factors: the formation of a double convective cell and the flattening of the density state function. The formation of the double convective cell reduces direct thermal communication between the hot and cold walls while the flattening of the density state function (density as a function of temperature) of water near the

density extremum results in an overall reduction in the buoyancy as the convective velocity is reduced.

Figure 3.3-7 shows a plot of the rate of heat flowing into the enclosure (red curve) and the rate of heat flowing out of the enclosure (blue curve). Both curves show a minimum in the vicinity of the density maximum but at different times. The rate of heat flowing out of the enclosure reaches a minimum before the rate of heat flowing into the enclosure. This staggering of the minima in the rate of heat transfer through the two sidewalls is a transient effect. The minimum in the rate of heat transfer through the cold wall occurs when the small counter clockwise cell prevents direct thermal communication between the larger clockwise cell and the cold wall. Since the hot wall is the only isothermal wall in contact with the clockwise cell, the clockwise cell contains warm liquid, and similarly the counter-clockwise cell contains cold liquid. Heat is now transferred from the hot wall to the clockwise cell, and from the clockwise cell to the counter clockwise cell and then to the cold wall. This significant change in the path of heat flow between the two walls reduces the rate of heat transfer from the hot wall to the cold wall. The rate of heat transfer through the cold wall increases as the counter clockwise cell grows across the enclosure due to the continuous decreasing of the wall temperatures.

The indirect thermal communication between the clockwise cell and the cold wall slows down the cooling of the clockwise cell. This decrease in cooling of the clockwise cell and the continuous temperature reduction of the hot wall causes the temperature difference between the hot wall and the clockwise cell to decrease, and hence the rate of heat transfer through the hot wall reduces. The rate of heat transfer at the hot wall continues to decrease until the cold counter clockwise cell reaches the hot wall. The large temperature difference between the cold counter clockwise cell and the hot wall causes a sudden increase in the rate of heat transfer at the hot wall. The rate of heat transfer at the hot wall continues to increase as the clockwise cell disappears and the density of the liquid moves away from the flattened region of the density state function.

3.3.2.1 *The rate of cooling*

During the quasi-steady state cooling of ethanol and water, the rate of heat flowing in is less than the rate of heat flowing out. This difference in behaviour is due to the cooling of the volume of liquid. When the temperature of the liquid is reduced from the 8°C to 0°C, heat energy is extracted from the liquid. The amount of energy (Q) that is extracted from the liquid in order to lower the temperature by ΔT is given by

$$Q = \rho V C_p \Delta T \quad (3.3-1)$$

Where ρ is the density in kg.m^{-3} , V is the volume in m^3 and C_p is the specific heat capacity in $\text{J.kg}^{-1}.\text{K}^{-1}$. For ethanol, 6,600J of energy must be extracted over the time span of 43,740 seconds in order to cool it from 8°C to 0°C. Consequently, during cooling the rate of heat extracted is greater than the rate of heat flowing in. During warming the same amount of energy is required to raise the temperature by 8°C so that the rate of heat flowing into the container must be greater than the rate of heat flowing out. The difference between the two rates of heat transfer during cooling yields the rate of cooling. For ethanol, the average rate of cooling is 0.20W and this rate has an error of $\pm 0.07\text{W}$; since the rate of cooling equals the difference in two rates of heat transfer, the error on the rate of cooling is the addition of the error on the individual heat transfer measurements. The amount of energy extracted from the liquid due to cooling can be calculated by multiplying this rate by the duration of the cooling (43,740 seconds) and this value can be compared directly with the value obtained from equation (3.3-1). Alternatively, the amount of energy extracted can be obtained by finding the area under the first 43,740 seconds of the graph in Figure 5.2-14. Both methods yield a value of 8,700J for the amount of energy required to cool ethanol by 8°C. The error on the amount of energy extracted is 3,000J. The value of 6,600J obtained from equation (3.3-1) is within the margin of error for the experimental value of $8,700 \pm 3,000\text{J}$. Although for water, equation (3.3-1) gives a value of 14,200J which is not within the experimental value of $21,800 \pm 7,400\text{J}$. Discrepancies between the expected results and the experimental results are large and can be attributed to the propagation of errors on small values measured every second over a long time span.

The rate of heat transfer out of the enclosure at the cold wall is greater than the rate of heat transfer into the enclosure at the cold wall. The difference between the two rates is due to the cooling of the liquid from a mean temperature of 8°C to 0°C. This rate of cooling of water is presented in Figure 3.3-8. An anomalous feature is observed in the rate of cooling in the vicinity of the density maximum. As the fluid enters the vicinity of the density maximum, the rate of cooling slows down and very rapidly increases, before decreasing back to a constant rate of heat transfer. The minimum is due to the formation of a counter-clockwise cell at the cold wall. This cell stretches from the top to the bottom of the enclosure and prevents the large clockwise cell (which is at this stage responsible for cooling the fluid) from connecting with the cold wall. Since the ‘cooling cell’ cannot reach the cold wall, very little heat can flow out of the enclosure and consequently very little cooling occurs. As the small counter-clockwise cell grows, it becomes responsible for cooling the fluid and the rate of cooling begins to increase rapidly and reaches a maximum, which occurs at the end of the plateau in Figure 3.3-6. This analysis of the rate of heat transfer in water and ethanol subjected to the procedure outlined in section 2.5.1 is supported by the results from the numerical investigations and it is discussed in more detail in section 5.2.

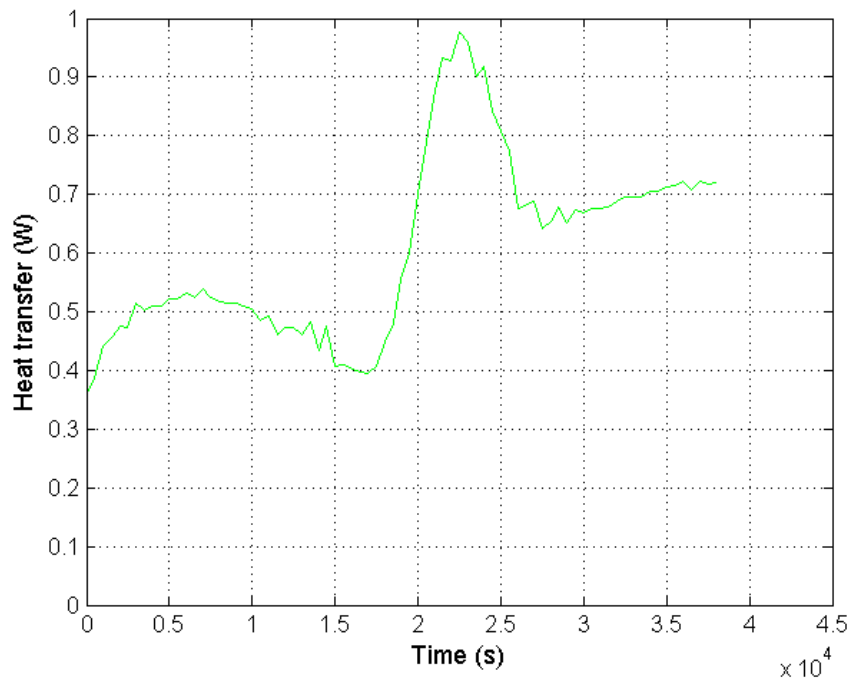


Figure 3.3-8 The rate of cooling against time. The rate of cooling is the difference between the rate of heat flowing through the hot wall and the cold wall.

3.3.3 Measurement technique for the temperature of maximum density of aqueous solutions

This section describes the technique used to measure the temperature of maximum density of aqueous solutions, which is described in Cawley *et al.* [61]. A sample of water is cooled under the controlled conditions outlined in section 2.5.1. An identical procedure is then applied to an aqueous solution. During the cooling, the temperature at select points in the liquid is monitored. The results show an anomalous feature in the temperature profiles centred on the liquid's temperature of maximum density, as discussed for water in section 3.3.1. A comparison between the temperature profiles of the solution with the temperature profiles of pure water shows a shift in the temperature of maximum density. This shift in temperature is measured using a chi-squared comparison and from this the temperature of maximum density of the solution is deduced.

In practice, the temperature of maximum density of a solution could be obtained by printing the temperature profiles of water onto a transparent film. This transparency can then be superimposed on to a graph of the temperature profiles of an aqueous solution. The shift in the temperature of maximum density is determined by sliding the two plots relative to each other until the anomaly feature in one graph covers the anomaly feature in the other one. This procedure is not very precise and contains some uncertainty. An automated approach used by Cawley *et al.* [61] overcomes this problem. The procedure determines the temperature of maximum density of a solution using MATLAB[®] code that slides the two plots relative to each other while keeping the side chamber temperatures collinear. The algorithm isolates the feature associated with the density maximum on the graph of pure water and shifts it along the time axis in one-second increments. The chi-squared sum of the difference between the equivalent cooling curves in the two plots was evaluated for each second of shift along the time axis. A plot of the chi-squared sum for the two plots in Figure 3.3-9 (water) and Figure 3.3-10 (a 10g/ltr aqueous solution of potassium bromide) is shown in Figure 3.3-11. The minimum of the chi-squared sum occurs at a relative shift of 5133 seconds. The temperature of maximum density can be obtained from this information using equation (2.5-1). The temperature of maximum density of the solution in Figure 3.3-10 is 3.0°C. The magnitude of the minimum of the chi-

squared sum indicates the strength of the comparison of the anomaly features. If the two anomaly features were identical, the magnitude of the minimum of the chi-squared sum would be zero.

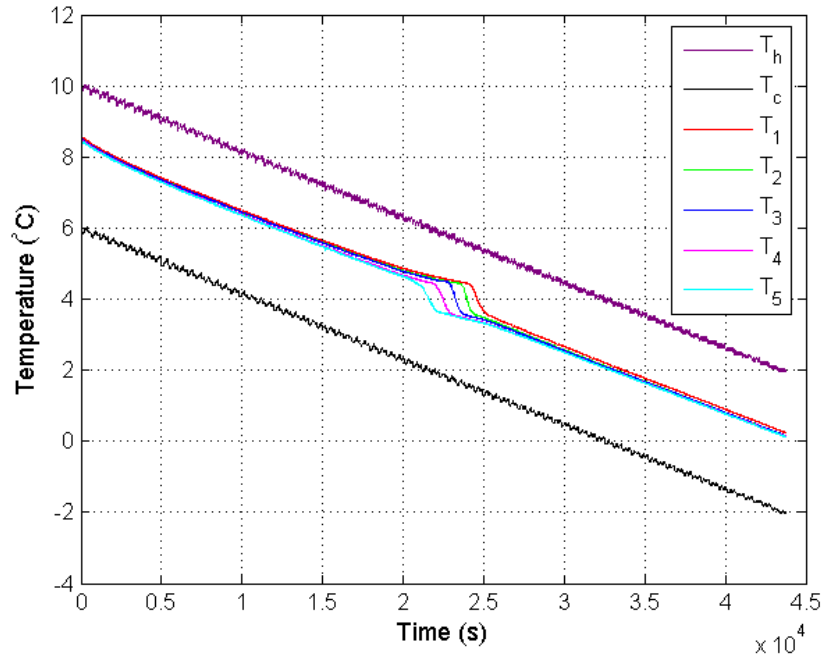


Figure 3.3-9 Temperature against time for pure water in the test chamber. The anomalous feature centred on 4°C is due to the occurrence of the density maximum.

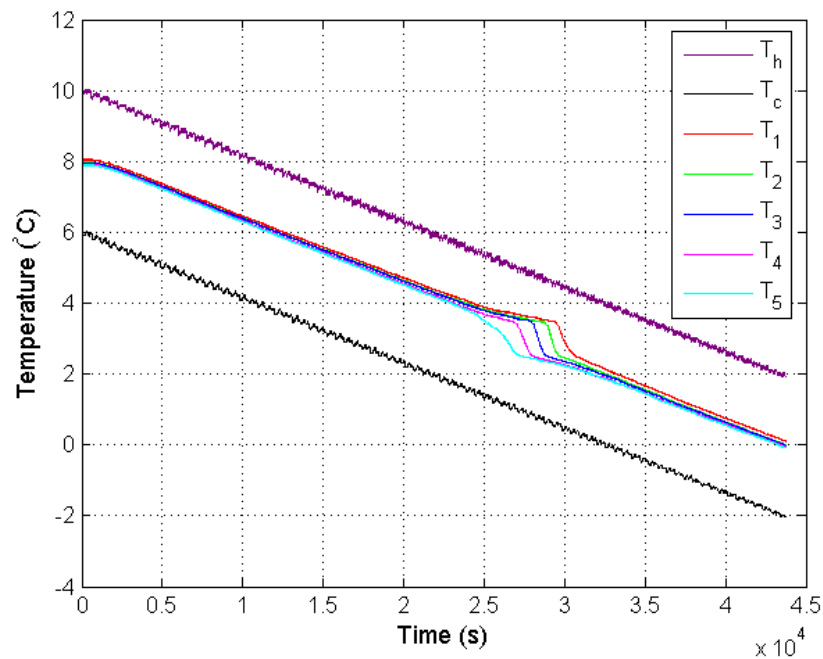


Figure 3.3-10 Temperature against time for a 10g.ltr⁻¹ potassium bromide solution. The anomalous feature is centred on the solutions temperature of maximum density.

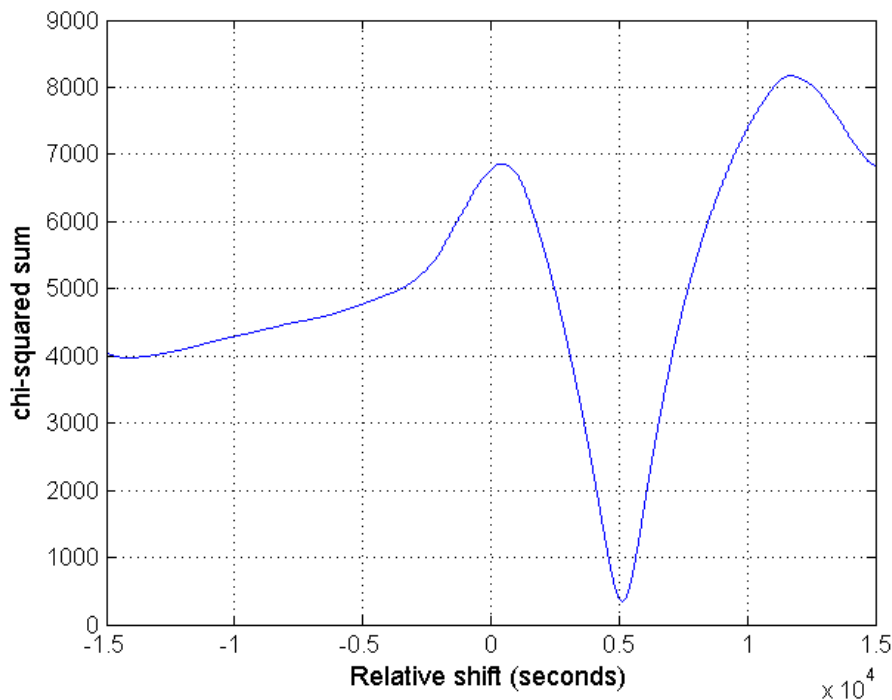


Figure 3.3-11 A chi-squared comparison between the temperature profiles in Figure 3.3-9 and the temperature profiles in Figure 3.3-10.

The accuracy and reliability of the chi-squared procedure was tested by Cawley *et al.* [61] using CFD and it was found that any uncertainty relating to the chi-squared technique was negligible. A larger uncertainty (typically of the order of $\pm 0.1^\circ\text{C}$) is found when the method is applied to repeated experimental runs of the same solute and concentration. This gives rise to an overall error in the determination of $\pm 0.14^\circ\text{C}$ when combined in quadrature with the 0.1°C uncertainty associated with the absolute calibration of the thermistors. A conservative error of $\pm 0.2^\circ\text{C}$ is assumed to apply to all measurements reported here, this error allows for uncertainties in solution preparation, particularly at low concentrations.

A series of measurements of the temperature of maximum density of aqueous solutions always begins with a pure water experiment against which all of the temperature profiles of the solutions were compared. Any significant upward drift of the absolute value of the minimum chi-squared sum during a series of solution measurements implied that some aspect of the experimental system required attention. Recalibration of the thermistors or any other alterations to the system

would always be followed by another pure water experiment before any further solution experiments were performed.

Results for three ionic solutes taken from the International Critical Tables of Numerical Data, Physics, Chemistry and Technology [11] are shown in Figure 3.3-12. These results were obtained using standard density measurement techniques (dilatometers). All of the ionic solutes reported in [11] show linear depressions of the temperature of maximum density with increasing solute concentration. It is evident that there is good agreement in the case of sodium chloride between the results obtained in this work, the results of [11], and the seawater state equation quoted in [10]. For potassium bromide (KBr) and potassium iodide (KI) there are indications that the results obtained in this work fall somewhat higher than the best fit line to the results from [11], but such differences are not statistically significant (the slope for the KBr points from this work is -0.0996 ± 0.008 compared to a slope of -0.110 ± 0.002 for the KBr points from [11]).

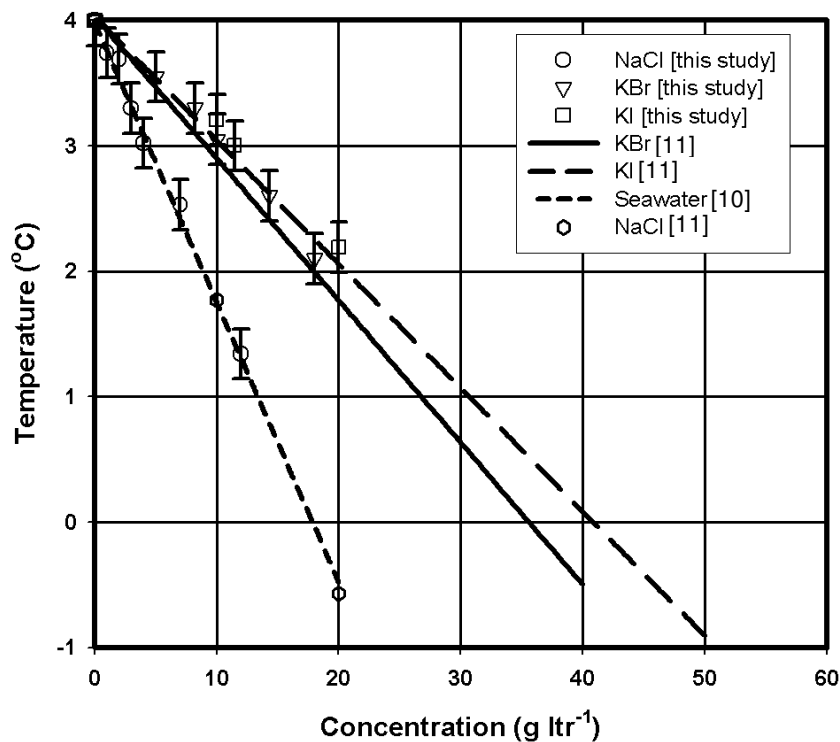


Figure 3.3-12 A selection of results from this work compared with previous studies. Trend lines for KBr and KI are best fits to data taken from the International Critical Tables [11]. The hexagonal points without error bars for NaCl are also from [11]. The trend line for NaCl is derived from the seawater equation of state [10].

It has been shown in section 3.3.2 that when water is cooled in the vicinity of the density maximum, an anomaly feature is also observed in the rate of cooling of the liquid. This feature in the rate of cooling of an aqueous solution can be compared with the feature in the rate of cooling of water to obtain the temperature of maximum density of the aqueous solution. This technique is potentially more useful than the previous technique described in Cawley *et al.* [61] since no thermistors are inserted into the test chamber. The technique is non-invasive and increases the lifetime of the thermistors since their lifetime is reduced when placed in liquids. Unlike the technique based on the temperature profiles, this technique can be used for aqueous solutions that are corrosive for the thermistors.

Figure 3.3-13 shows the temperature profiles and the monitoring profiles for pure water. Figure 3.3-14 shows the temperature profiles and the monitoring profiles for a 50g.ltr⁻¹ aqueous solution of propan-2-ol. The temperature profiles of the aqueous solution are compared to the pure water profiles using the chi-squared technique and the result is plotted in Figure 3.3-15. The minimum of the chi-squared sum for the temperature profiles occurs at a relative shift of 3881 seconds. Comparing the temperature profiles yields a temperature of maximum density of 3.29°C for the propan-2-ol solution. Figure 3.3-16 shows the chi-squared comparison between the monitoring profiles (which indicate the rate of cooling) of pure water and the aqueous solution. The minimum of the chi-squared sum for the monitoring profiles occurs at a relative shift of 3991 seconds. Comparing the monitoring profiles yields a temperature of maximum density of the solution of 3.27°C.

This procedure was carried out for a variety of solutions and it was found that the temperature of maximum density obtained using the two techniques simultaneously varied by approximately 0.05°C and the results are shown in Table 3.3-1 and Table 3.3-2. This error is much less than the margin of error for the measurement technique based on the temperature profiles, which implies that the measurement technique based on the rate of cooling is also a valid measurement technique. Comparing the results of the technique based on heat transfer to independent results from the technique based on the temperature profiles further validates the technique. The independent results were obtained from the technique based on the temperature

profiles using the quasi-steady state system which did not have the capability of measuring heat transfer. The two sets of results are compared in Figure 3.3-17.

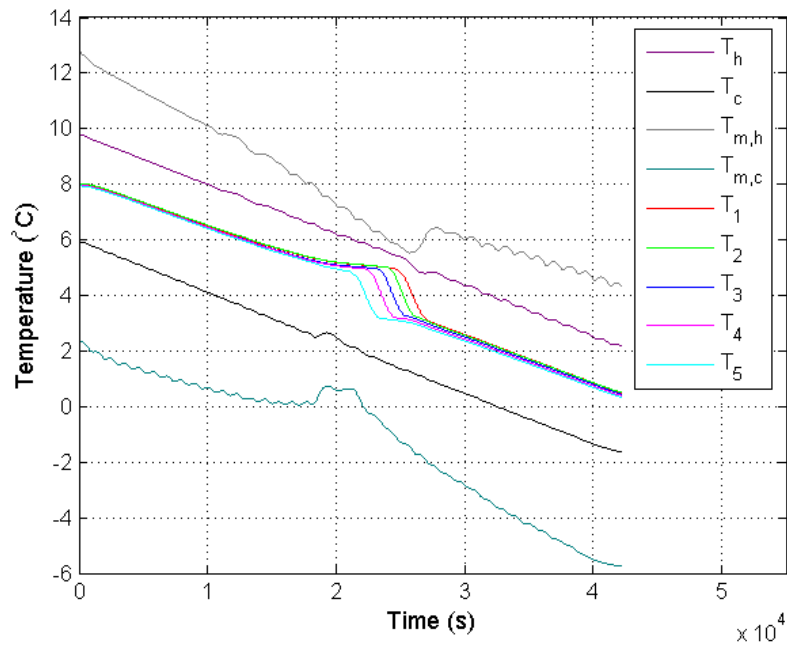


Figure 3.3-13 Temperature against time for pure water in the test chamber. The chamber is 0.06m x 0.06m x 0.12m (width x height x length).

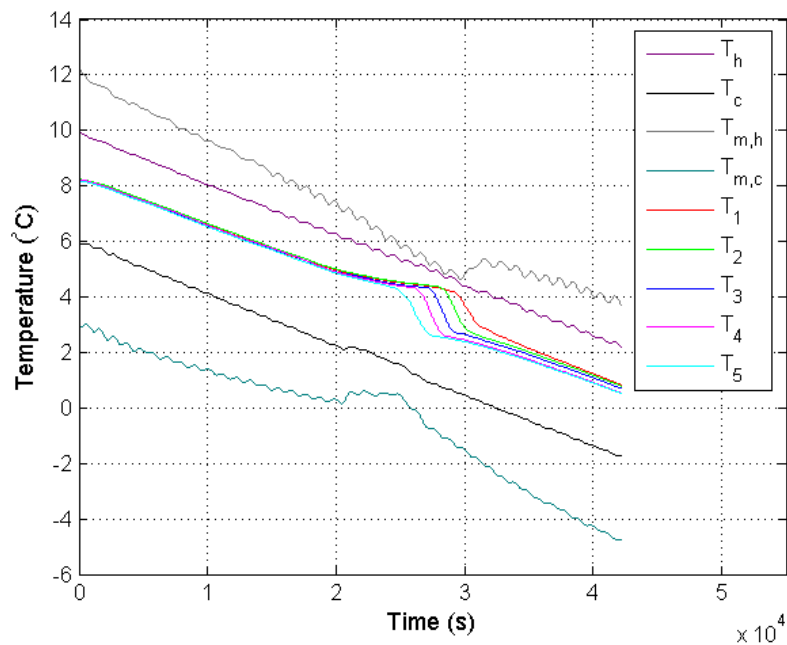


Figure 3.3-14 Temperature against time for a 50 g.ltr⁻¹ solution of propan-2-ol in the test chamber. The chamber is 0.06m x 0.06m x 0.12m (width x height x length).

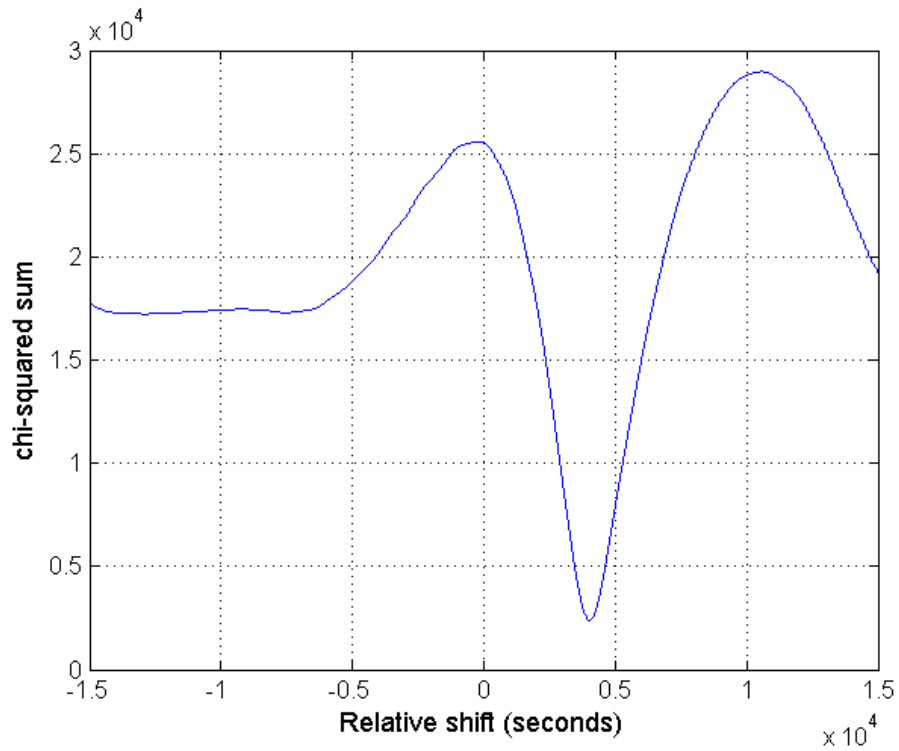


Figure 3.3-15 A chi-squared comparison between the temperature profiles in Figure 3.3-13 and the temperature profiles in Figure 3.3-14.

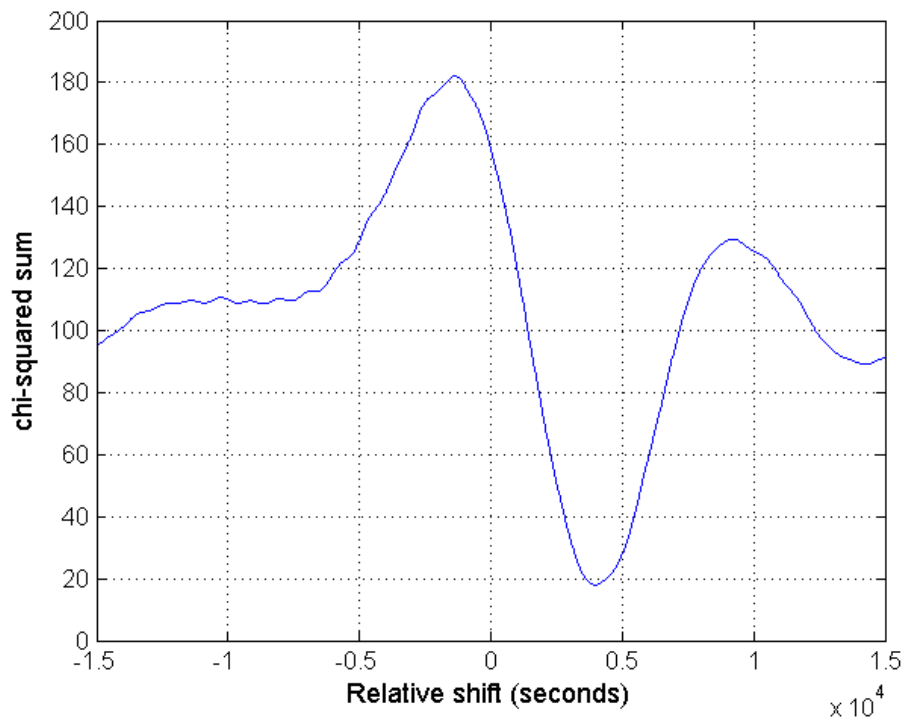


Figure 3.3-16 A chi-squared comparison between the rate of cooling profile in Figure 3.3-13 and the temperature profiles in Figure 3.3-14.

Propan-2-ol (CH ₃ CHOHCH ₃)		
Concentration (g.ltr ⁻¹)	T _{ρ,max} * (°C)	T _{ρ,max} ** (°C)
5	4.06	4.10
10	4.15	4.17
50	3.29	3.27
50	3.29	3.24

Table 3.3-1 The variation of the temperature of maximum density ($T_{\rho,max}$) as a function of concentration for aqueous solutions of propan-2-ol. *obtained using a chi-squared comparison of the temperature profiles. **obtained using a chi-squared comparison of the rate of cooling profile.

Sodium Chloride (NaCl)		
Concentration (g.ltr ⁻¹)	T _{ρ,max} * (°C)	T _{ρ,max} ** (°C)
5	2.79	2.79
10	1.56	1.57

Table 3.3-2 The variation of the temperature of maximum density ($T_{\rho,max}$) as a function of concentration for aqueous solutions of sodium chloride. *obtained using a chi-squared comparison of the temperature profiles. **obtained using a chi-squared comparison of the rate of cooling profile.

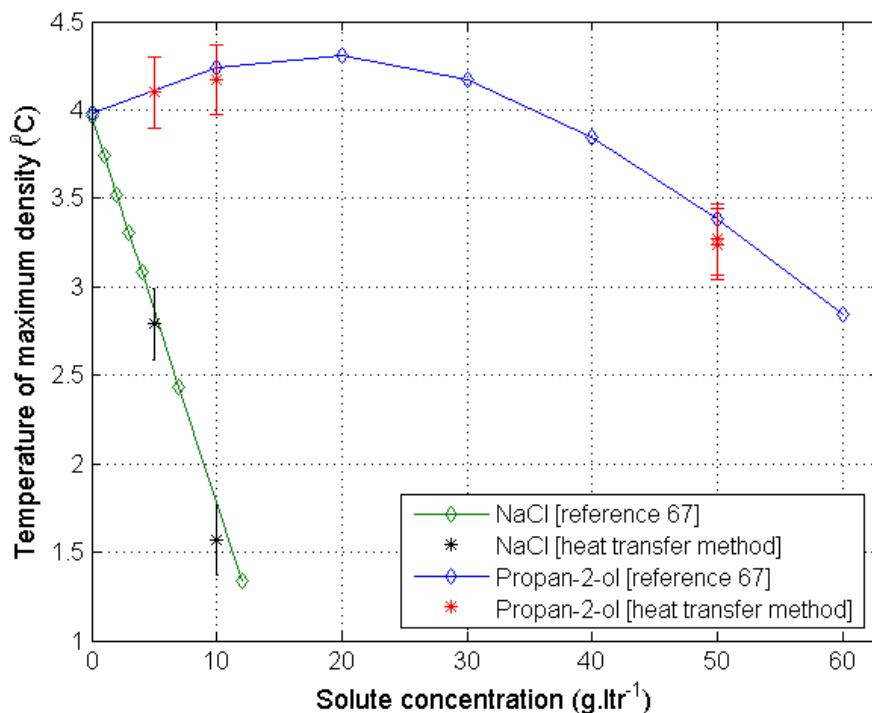


Figure 3.3-17 The results from the measurement technique based on the rate of cooling compared to the results from the measurement technique based on the temperature profiles.

3.3.4 The temperature of maximum density of aqueous solutions

The temperature of maximum density of a variety of aqueous solutions was measured using the novel technique described previously in section 3.3.3 and in Cawley *et al.* [61]. The temperature of maximum density was obtained for a variety of concentrations of the aqueous solutions of sodium chloride (NaCl), potassium bromide (KBr), potassium iodide (KI), glucose (C₆H₁₂O₆), sucrose (C₁₂H₂₂O₁₁), acetone (C₃H₆O), ethylene glycol (C₂H₄(OH)₂), diethylene glycol (C₂H₄C₂H₄(OH)), methanol (CH₃OH), ethanol (C₂H₅OH), propan-1-ol, (CH₃CH₂CH₂OH) and propan-2-ol (CH₃CHOHCH₃). Table 3.3-3 to Table 3.3-13 show the measurements of the temperature of maximum density for these solutions. The solute concentrations are expressed in g.ltr⁻¹ and also in moles.ltr⁻¹ for the purpose of showing the non-colligative nature of the temperature of maximum density and to examine possible relationships between solutes. The results are presented graphically in Figure 3.3-18, Figure 3.3-19, Figure 3.3-20 and Figure 3.3-21. Figure

3.3-18 and Figure 3.3-19 show the variation of the temperature of maximum density of the aqueous solutions as a function of mass concentration while Figure 3.3-20 and Figure 3.3-21 show the variation of the temperature of maximum density as a function of molar concentration. The solutes are divided into two groups; the first group shown in Figure 3.3-18 (in g.ltr⁻¹) and in Figure 3.3-20 (in moles.ltr⁻¹) are the ionic salts and the sugars. The second group of solutes shown in Figure 3.3-19 (in g.ltr⁻¹) and in Figure 3.3-21 (in moles.ltr⁻¹) are the alcohols and a keytone. These solutes all have an OH group that makes the molecule polar.

Sodium Chloride (NaCl)		
Concentration (g.ltr ⁻¹)	Concentration (moles.ltr ⁻¹)	T _{ρ,max} (°C)
1.00	0.0345	3.60
2.00	0.0690	3.36
3.00	0.1035	3.30
4.00	0.1380	3.02
7.00	0.2415	2.53
9.00	0.3105	2.00
12.00	0.4140	1.34

Table 3.3-3 The variation of the temperature of maximum density ($T_{\rho,max}$) as a function of sodium chloride (NaCl) concentration.

Potassium Bromide (KBr)		
Concentration (g.ltr ⁻¹)	Concentration (moles.ltr ⁻¹)	T _{ρ,max} (°C)
5.00	0.084	3.55
8.20	0.138	3.30
10.00	0.168	3.05
14.30	0.240	2.6

Table 3.3-4 The variation of the temperature of maximum density ($T_{\rho,max}$) as a function of potassium bromide (KBr) concentration.

Glucose (C ₆ H ₁₂ O ₆)		
Concentration (g.ltr ⁻¹)	Concentration (moles.ltr ⁻¹)	T _{ρ,max} (°C)
10.00	0.056	3.50
13.66	0.076	3.20
20.00	0.111	2.88
30.00	0.167	2.33

Table 3.3-5 The variation of the temperature of maximum density ($T_{\rho,max}$) as a function of glucose (C₆H₁₂O₆) concentration.

Sucrose (C ₁₂ H ₂₂ O ₁₁)		
Concentration (g.ltr ⁻¹)	Concentration (moles.ltr ⁻¹)	T _{ρ,max} (°C)
10.00	0.029	3.61
23.60	0.069	2.80
35.40	0.103	2.40
47.20	0.138	2.05
60.00	0.175	1.00

Table 3.3-6 The variation of the temperature of maximum density ($T_{\rho,max}$) as a function of sucrose (C₁₂H₂₂O₁₁) concentration.

Acetone (C ₃ H ₆ O)		
Concentration (g.ltr ⁻¹)	Concentration (moles.ltr ⁻¹)	T _{ρ,max} (°C)
4.00	0.069	3.71
8.00	0.138	3.38
17.50	0.302	2.44
20.00	0.345	2.40

Table 3.3-7 The variation of the temperature of maximum density ($T_{\rho,max}$) as a function of acetone (C₃H₆O) concentration.

Ethylene Glycol $C_2H_4(OH)_2$		
Concentration (g.ltr ⁻¹)	Concentration (moles.ltr ⁻¹)	$T_{\rho,max}$ (°C)
5.00	0.081	3.76
10.00	0.161	3.41
20.00	0.323	2.78

Table 3.3-8 The variation of the temperature of maximum density ($T_{\rho,max}$) as a function of ethylene glycol ($C_2H_4(OH)_2$) concentration.

Diethylene glycol $C_2H_4C_2H_4(OH)_2$		
Concentration (g.ltr ⁻¹)	Concentration (moles.ltr ⁻¹)	$T_{\rho,max}$ (°C)
20.00	0.189	3.07
40.00	0.377	2.09

Table 3.3-9 The variation of the temperature of maximum density ($T_{\rho,max}$) as a function of Diethylene glycol ($C_2H_4C_2H_4(OH)_2$) concentration.

Methanol CH_3OH		
Concentration (g.ltr ⁻¹)	Concentration (moles.ltr ⁻¹)	$T_{\rho,max}$ (°C)
10.00	0.312	4.10
15.00	0.468	4.09
20.00	0.624	4.02
35.00	1.093	3.40
50.00	1.561	3.05
70.00	2.185	1.70

Table 3.3-10 The variation of the temperature of maximum density ($T_{\rho,max}$) as a function of methanol (CH_3OH) concentration.

Ethanol C ₂ H ₅ OH		
Concentration (g.ltr ⁻¹)	Concentration (moles.ltr ⁻¹)	T _{ρ,max} (°C)
3.17	0.069	4.00
6.35	0.138	3.95
11.10	0.241	4.15
23.80	0.517	3.95
39.65	0.861	3.80
70.00	1.519	2.50
79.30	1.721	1.90

Table 3.3-11 The variation of the temperature of maximum density ($T_{\rho,max}$) as a function of ethanol (C₂H₅OH) concentration.

Propan-1-ol CH ₃ CH ₂ CH ₂ OH		
Concentration (g.ltr ⁻¹)	Concentration (moles.ltr ⁻¹)	T _{ρ,max} (°C)
10.00	0.166	4.00
18.00	0.300	3.77
35.00	0.583	3.22
55.00	0.915	2.30

Table 3.3-12 The variation of the temperature of maximum density ($T_{\rho,max}$) as a function of propan-1-ol (CH₃CH₂CH₂OH) concentration.

Propan-2-ol CH ₃ CHOHCH ₃		
Concentration (g.ltr ⁻¹)	Concentration (moles.ltr ⁻¹)	T _{ρ,max} (°C)
10.00	0.166	4.22
20.00	0.333	4.30
30.00	0.499	4.16
40.00	0.667	3.80
50.00	0.832	3.49
60.00	0.999	2.80

Table 3.3-13 The variation of the temperature of maximum density ($T_{\rho,max}$) as a function of propan-2-ol (CH₃CHOHCH₃) concentration.

It is apparent from Figure 3.3-20 and Figure 3.3-21 that the shift of the temperature of maximum density with increasing concentration is not a colligative property of the solutions (i.e. a property similar to the depression of the freezing temperature, or the elevation of the boiling temperature, both of which depend on the number of solute particles in solution rather than their nature). If the depression of the temperature of maximum density was a colligative property, it would be expected that all of the experimental points would fall on the same line, such as the dashed line in Figure 3.3-20 which shows a doubling of the temperature of maximum density depression as the molar concentration is doubled. Furthermore, the non-linear dependence of the temperature of maximum density as a function of solute concentration for the monohydric alcohols (methanol, ethanol, propan-1-ol and propan-2-ol) clearly rules out a simple colligative dependence.

All of the salts and sugars measured show a linear depression of the temperature of maximum density with increasing concentration. The primary difference between Figure 3.3-18 and Figure 3.3-20 is the order of the depression of the temperature of maximum density. Figure 3.3-18 shows that sodium chloride gives the steepest depression of the temperature of maximum density, followed by potassium bromide, potassium iodide, glucose and sucrose. In contrast, Figure 3.3-20 shows that sucrose gives the steepest depression followed by glucose, potassium iodide, sodium chloride and potassium bromide. Despite the different ordering that results from the two different plots, each figure shows that the solutes linearly depress the temperature of maximum density. All of the solutes measured show a linear depression of the temperature of maximum density except the monohydric alcohols. A monohydric alcohol has one hydroxyl group (OH) on its molecule. The OH group has a net charge that makes the molecule polar and allows it to form hydrogen bonds with the water molecules. The monohydric alcohols are not only different from the other solutes because of their non-linearity but also because some of them elevate the temperature of maximum density. Methanol, ethanol and propan-2-ol elevate the temperature of maximum density initially but as the concentration increases the elevation decreases and the temperature of maximum density eventually decreases with increasing concentration. Propan-2-ol shows the highest elevation; a 20g.ltr⁻¹ solution of propan-2-ol elevates the temperature of maximum density to 4.33°C.

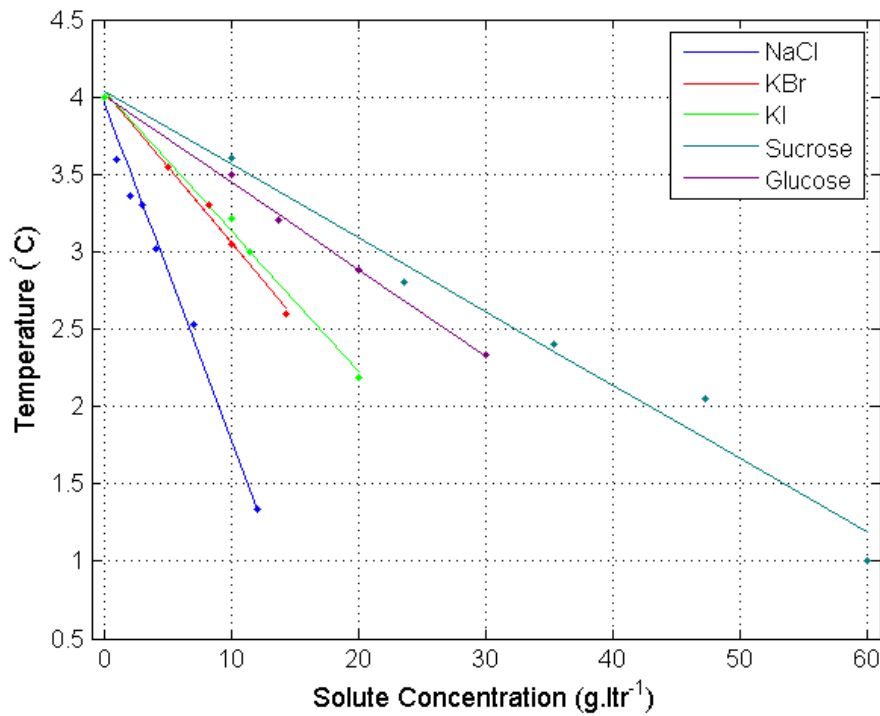


Figure 3.3-18 The behaviour of the temperature of maximum density as a function of mass concentration (expressed in grams per litre) for ionic salts and sugars.

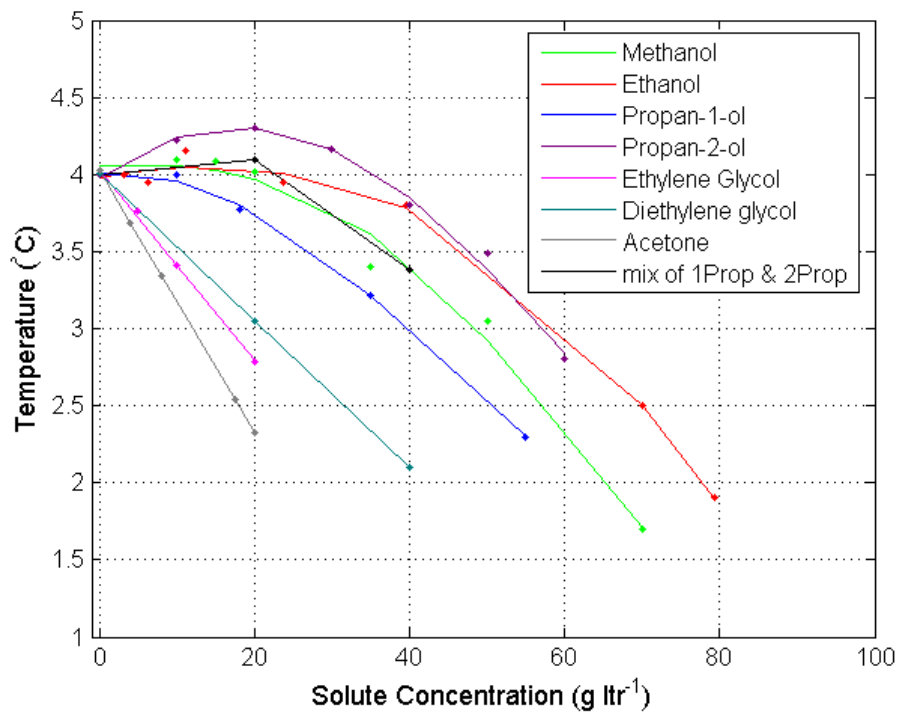


Figure 3.3-19 The behaviour of the temperature of maximum density as a function of mass concentration (grams per litre) for a range of alcohol solutes and a ketone. The mixture of propan-1-ol and propan-2-ol is a 50:50 mixture.

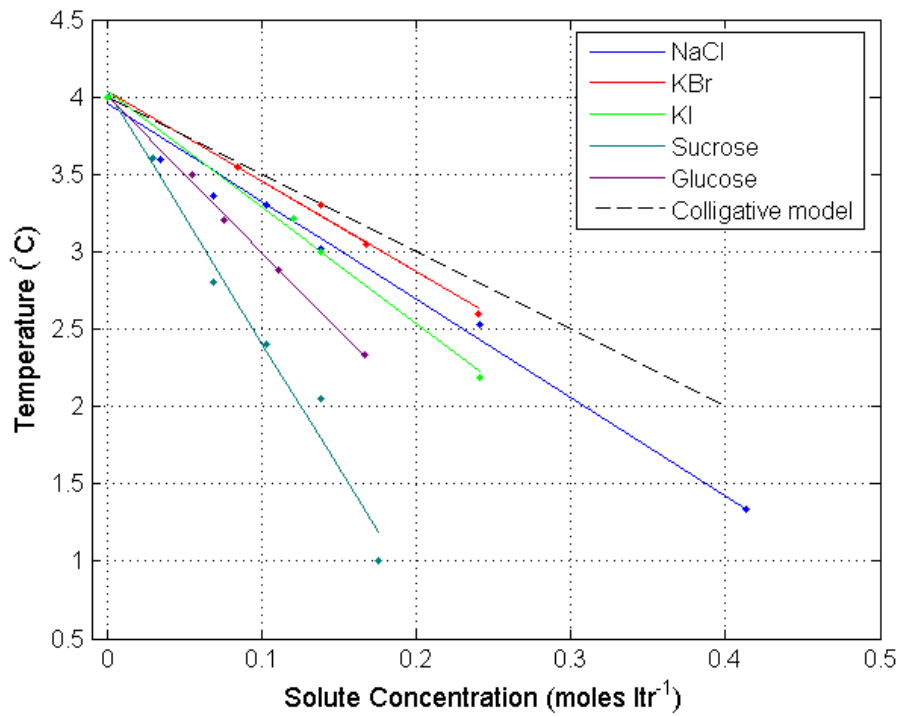


Figure 3.3-20 The behaviour of the temperature of maximum density as a function of mass concentration (expressed in moles per litre) for ionic salts and sugars.

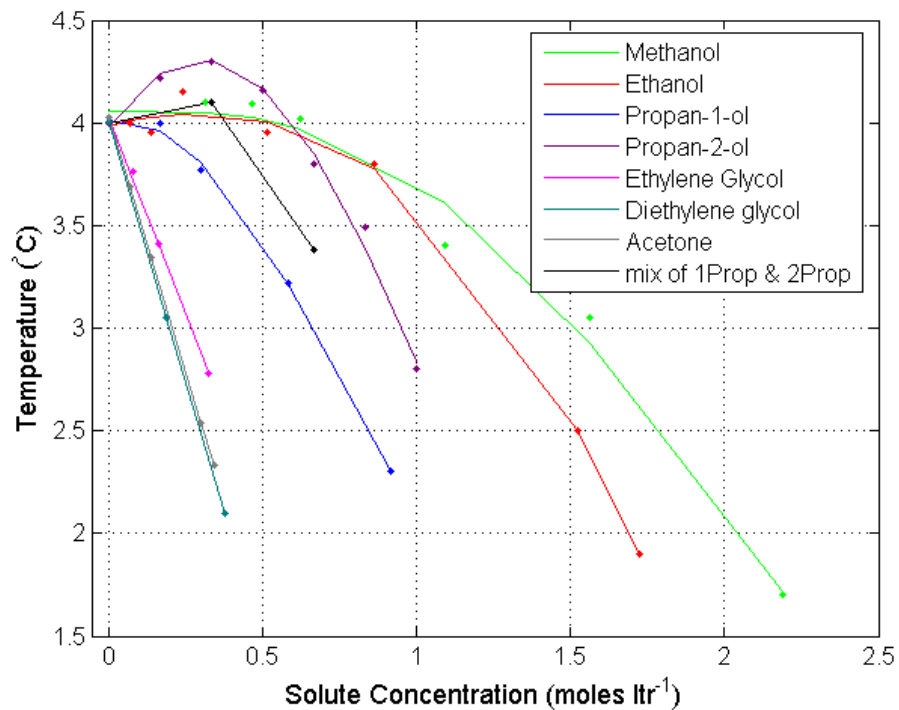


Figure 3.3-21 The behaviour of the temperature of maximum density as a function of mass concentration (moles per litre) for a range of alcohol solutes and a ketone. The mixture of propan-1-ol and propan-2-ol is a 50:50 mixture.

The two isomers of propanol were investigated in this study and the behaviour of the temperature of maximum density of each isomer is different. Propan-1-ol is a primary alcohol with only one carbon atom attached to the C-OH group. Propan-1-ol shows a non-linear depression of the temperature of maximum density but does not elevate the temperature of maximum density. Propan-2-ol, which is a secondary alcohol with two carbon atoms attached to the C-OH group, also shows a non-linear depression of the temperature of maximum density but unlike propan-1-ol, it does elevate the temperature of maximum density. This difference shows that the depression of the temperature of maximum density depends on the molecular arrangement of the molecule. It is also worth noting that methanol and ethanol are primary alcohols and they elevate the temperature of maximum density. On this basis it seems peculiar that it is the secondary alcohol of Propanol that elevates the temperature of maximum density and not the primary alcohol.

Solute	Solute Concentration (moles.ltr ⁻¹)	T _{ρ,max} (°C)
Propan-1-ol (20g.ltr ⁻¹)	0.333	3.75
Propan-2-ol (20g.ltr ⁻¹)	0.333	4.30
Propan-1-ol & Propan-2-ol (each 20g.ltr ⁻¹)	0.333	4.10
Propan-1-ol (40g.ltr ⁻¹)	0.666	3.00
Propan-2-ol (40g.ltr ⁻¹)	0.666	3.80
Propan-1-ol & Propan-2-ol (each 40g.ltr ⁻¹)	0.666	3.38

Table 3.3-14 The variation of the temperature of maximum density ($T_{\rho,max}$) as a function of solutions containing equivalent amounts of propan-1-ol and propan-2-ol.

The difference in the behaviour of the two isomers was further investigated by mixing equal quantities of the two solutes to form one solution. The results are summarised in Table 3.3-14. A 20g.ltr⁻¹ solution of propan-1-ol mixed with a 20g.ltr⁻¹ solution of propan-2-ol gives a 20g.ltr⁻¹ mixed solution of propan-1-ol and propan-2-ol. Similarly, a 40g.ltr⁻¹ solution of propan-1-ol mixed with a 40g.ltr⁻¹

solution of propan-2-ol gives a 40g.ltr^{-1} mixed solution of propan-1-ol and propan-2-ol. The results presented in Table 3.3-14 show that the temperature of maximum density of the 20g.ltr^{-1} mixed solution is approximately the average value of the temperature of maximum density of both the 20g.ltr^{-1} propan-1-ol solution and the 20g.ltr^{-1} propan-2-ol solution. Similarly, the temperature of maximum density of the 40g.ltr^{-1} mixed solution is approximately the average of the 40g.ltr^{-1} solution of propan-1-ol and the 40g.ltr^{-1} solution of propan-2-ol.

Possible correlations were investigated between the variation of the temperature of maximum density and other macroscopic properties of the solution. The macroscopic properties investigated are shown in Table 3.3-15 and the variations of these properties shown in this table were obtained from reference [1]. Each column shows the variation of the macroscopic property with increasing concentrations of the solute in its corresponding row. An arrow pointing upwards indicates that the property increases linearly with increasing concentration and an arrow pointing downwards indicates that the property decreases linearly with increasing concentration. The non-linear behaviour of the temperature of maximum density of the monohydric alcohols is shown with a downward pointing arrow or a combination of an upward and a downward pointing arrow along with the annotation (non-linear).

It is clear that the freezing point depression, which is a colligative property, is not related to the behaviour of the temperature of maximum density. The relative viscosity increases with increasing concentration for all of the solutes except potassium bromide and potassium iodide. Therefore, there is no correlation between the temperature of maximum density and the relative viscosity. Salts dissociate into ions when dissolved in water. The salt solutions are electrolytic containing charged particles, which increase the electrical conductance with increasing concentration. The specific electric conductance was only available for the salt solutions. It is difficult to conclude from such inadequate information that the specific electric conductance is related to the temperature of maximum density. The specific gravity of the salts, the sugars and the dihydric alcohols increases with increasing concentration. All of these solutes linearly depress the temperature of maximum density. The specific gravity of the monohydric alcohols and the ketone decreases with increasing concentration. The temperature of maximum density of the

monohydric alcohols behaves in a non-linear manner while the temperature of maximum density of the keytone behaves linearly. This implies that there is no correlation between the specific gravity and the temperature of maximum density. The index of refraction increases with increasing concentration for all of the solutes and this indicates that there is also no correlation between the refractive index and the temperature of maximum density.

	Freezing point	Relative viscosity	Specific conduction (electrical)	Specific gravity	Index of refraction	Density maximum
NaCl	↓	↑	↑	↑	↑	↓
KBr	↓	↓	↑	↑	↑	↓
KI	↓	↓	↑	↑	↑	↓
Sucrose	↓	↑		↑	↑	↓
Glucose	↓	↑		↑	↑	↓
Acetone	↓	↑		↓	↑	↓
*Eth.Glycol	↓	↑		↑	↑	↓
**Di-eth gl.	↓	↑		↑	↑	↓
Methanol	↓	↑		↓	↑	Non-linear ↑↓
Ethanol	↓	↑		↓	↑	Non-linear ↑↓
Propan-1-ol	↓	↑		↓	↑	Non-linear ↓
Propan-2-ol	↓	↑		↓	↑	Non-linear ↑↓

Table 3.3-15 A summary of the variation of several properties of aqueous solutions as a function of solute nature and concentration. *Ethylene Glycol. **Di-Ethylene Glycol.

3.3.5 The anomaly feature of Na₂CO₃ solutions

During the investigations of the temperature of maximum density of the aqueous solutions of sodium carbonate, it was observed that the anomaly feature was consistently distorted. The distortions in the anomaly feature resulted in unreliable measurements of the temperature of maximum density of the sodium carbonate solutions and so they are excluded from the results presented in section 3.3.4. The cooling procedure outlined in section 2.5.1 was applied to three different concentrations of sodium carbonate. At a low concentration of 1g.ltr⁻¹, a distorted anomaly feature is observed, as shown in Figure 3.3-22. At temperatures above the temperature of maximum density, the temperature profiles are closely bunched together in the usual way. When the temperature profiles enter into the vicinity of the density maximum they begin to diverge as usual, but the temperature profiles begin to undulate and the anomaly feature appears stretched. When the temperature profiles emerge from the anomaly feature, they converge together in the usual way but the undulations that appeared in the vicinity of the density maximum persist.

Different concentrations of sodium carbonate showed a similar behaviour. A plot of the temperature profiles for a 4g.ltr⁻¹ solution is shown in Figure 3.3-23. The 4g.ltr⁻¹ solution shows that the temperature profiles behave in the usual manner before entering the vicinity of the density maximum but in the vicinity of the density maximum, the temperature profiles show undulations that persist as the solution is cooled below 4°C. A third concentration of 5g.ltr⁻¹ was also tested and the results presented in Figure 3.3-24 show the undulations in the temperature profiles after the anomaly feature but not in the anomaly feature. Each of these three results were obtained using the quasi-steady state system described in section 2.3. A 4g.ltr⁻¹ solution of sodium carbonate was tested in the heat transfer system described in section 2.4 to ascertain the dependency of the results on the experimental system. The results of this investigation are presented in Figure 3.3-25 (without the application of a moving average). The results presented in this graph also show undulations in the temperature profiles. It is evident from these graphs that the unusual shape of the anomaly feature and the undulations are a feature of the aqueous solution and not the experimental system. The exact reason for this unusual behaviour merits further investigation but it is not included in this body of work.

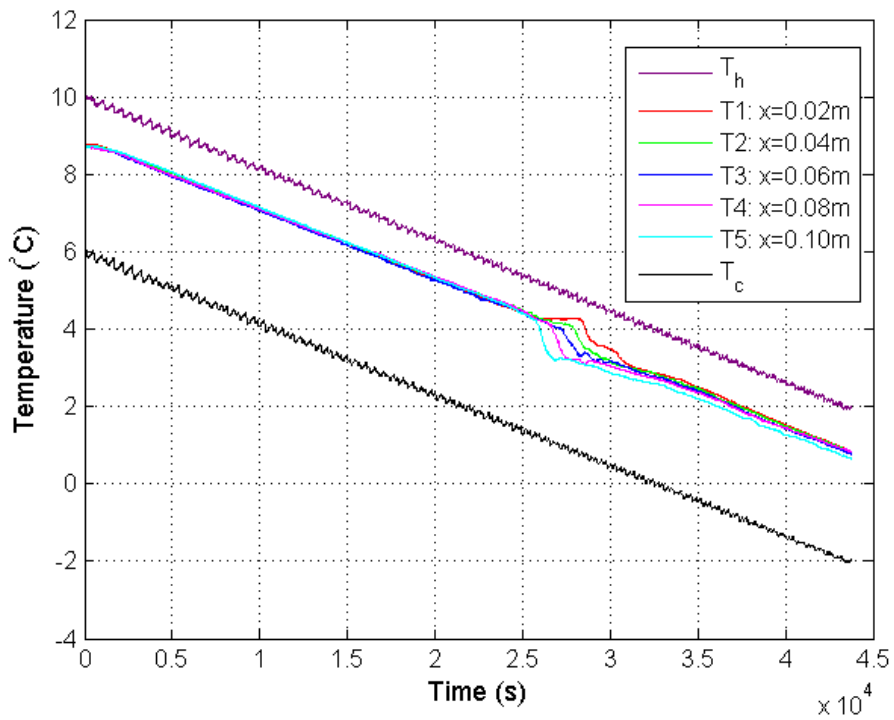


Figure 3.3-22 Temperature against time for a 1g.ltr^{-1} sodium carbonate solution in the test chamber. This result was obtained using the quasi-steady state system.

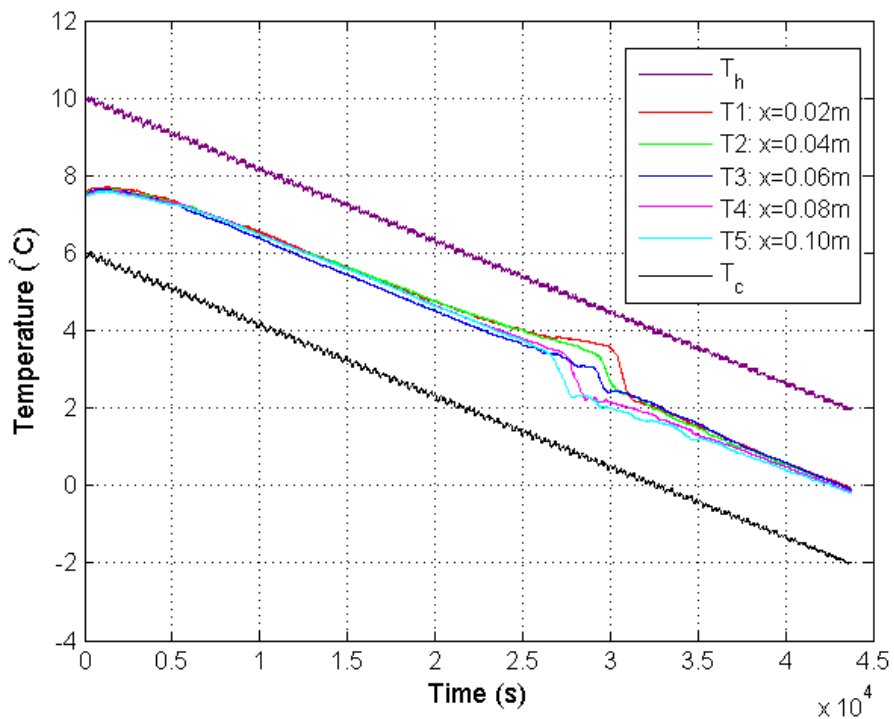


Figure 3.3-23 Temperature against time for a 4g.ltr^{-1} sodium carbonate solution in the test chamber. This result was obtained using the quasi-steady state system.

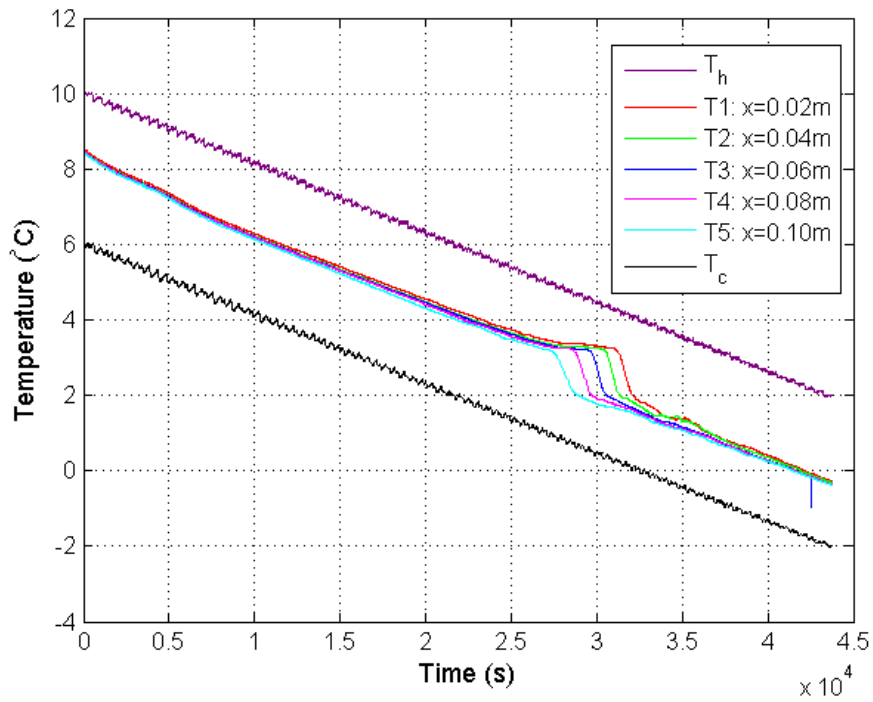


Figure 3.3-24 Temperature against time for a 5g.ltr⁻¹ sodium carbonate solution in the test chamber. This result was obtained using the quasi-steady state system.

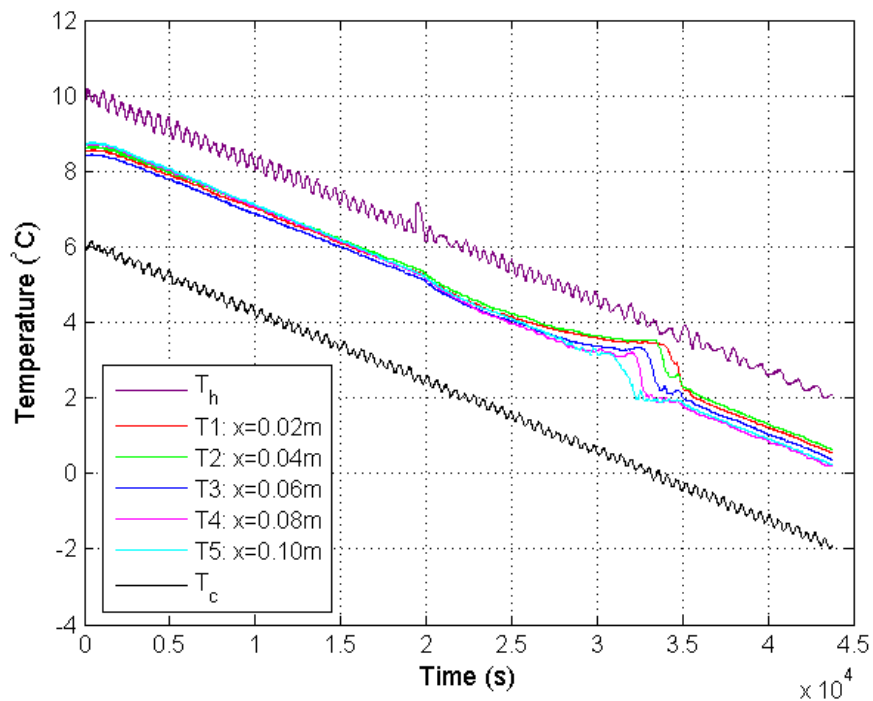


Figure 3.3-25 Temperature against time for a 4g.ltr⁻¹ sodium carbonate solution in the test chamber. This experimental result was obtained using the heat transfer system.

3.4 Asymmetrical heat transfer

Asymmetrical heat transfer is observed if the rate of heat transfer changes when the direction of heat transfer is reversed. The results presented in this section show how the density maximum can cause a system to exhibit asymmetrical heat transfer. Asymmetrical heat transfer is observed in two systems, the water-saline diode and the water-Perspex diode. The first system which is the focus of this study is the composite system of water and saltwater. The water-saline diode as described in Mooney and Cawley [37] consists of two square enclosures with dimensions of 0.06 m x 0.06 m x 0.06 m side by side. The first enclosure consists of an aqueous solution of sodium chloride with a concentration of 9g.ltr⁻¹ and the second enclosure is filled with pure water. Water has a density maximum at 3.98°C and the saline solution has a density maximum at 2°C (obtained using the technique described in Cawley *et al.* [61]). A horizontal temperature gradient is placed across this system and the rate of heat flowing into and out of the system is recorded for two opposing directions.

The basis of this thermal diode is that heat transfer is reduced in the vicinity of the density maximum. When heat flows through the composite in a given direction, the two liquids have a mean temperature that is removed from their temperatures of maximum density. When heat flows in the opposite direction, the two liquids have a mean temperature that corresponds to their temperatures of maximum density. Consequently, the rate of heat flowing in the opposing direction is reduced and asymmetrical heat transfer is observed.

The water-Perspex diode as described in Cawley *et al.* [36], consists of a rectangular container of water adjacent to a thin slab of Perspex. A horizontal temperature gradient is placed across this composite system. When heat flows in a certain direction the mean temperature of the Perspex is high compared to the mean temperature of the container of water. When the direction is reversed the mean temperature of the container of water is high compared to the mean temperature of the Perspex slab. The result of this is that the mean temperature of water is close to the temperature of maximum density in one direction and its mean temperature in the opposing direction is removed from its temperature of maximum density.

Consequently, heat transfer is reduced in one direction and asymmetrical heat transfer is observed.

The experimental procedure for investigating asymmetrical heat transfer is outlined in section 2.5.2. In this procedure, the temperatures of the left wall (T_L) and the right wall (T_R) of the system are held fixed for long time spans (30,000 seconds) and the rate of heat transfer is extracted after steady-state conditions have been reached. The gradient is then reversed over a period of 48,000 seconds, and the system is once again allowed to settle to steady-state conditions (a duration of approximately 30,000 seconds). This cycle is repeated several times. The gradient reversal is achieved by decrementing the wall with the highest temperature by 0.1°C at time intervals of 1,200 seconds until it reaches the original temperature of the opposing wall. Simultaneously the wall with the lowest temperature is incremented by 0.1°C at time intervals of 1,200 seconds. The limited cooling ability of the experimental apparatus demands this slow temperature change that results in an interchanging time of 48,000 seconds.

Each cycle of the results consists of a steady-state region (heat flow in a certain direction), followed by a transient region (gradient reversal) and finishes with another steady-state region (heat flow in the opposing direction). The results of the two steady state regions will be analysed before discussing the transient region of the results. The transient region of the results shows some interesting features; however it is not critical to the occurrence of asymmetrical heat transfer and it shall be discussed after the results of the two steady state regions. This layout of the results applies to both the water-saline diode and the water-Perspex diode.

The experimental results for the two thermal diodes were obtained under steady state conditions unlike the experimental results for the investigation of the maximum density of aqueous solutions. Since the thermal diode results are obtained under steady state conditions, the behaviour of the temperature profiles in a rectangular enclosure of water under steady state conditions is analysed in section 3.4.1 before discussing the results of the water-saline diode and the water-Perspex diode. The water-saline diode is discussed in section 3.4.2 and the water-Perspex diode is discussed in section 3.4.3.

3.4.1 The temperature profiles of water under steady state conditions

The purpose of this section is to establish the behaviour of the temperature profiles along a central horizontal axis through water under steady state conditions. The behaviour of the temperature profiles provides crucial information regarding the convection pattern within the liquid. The behaviour of the temperature profiles in water when the temperature difference across the enclosure is removed from the density maximum is initially examined. This is followed by the analysis of the temperature profiles in water when a temperature difference centred on the temperature of maximum density is placed across the enclosure.

A horizontal temperature difference of 4°C is placed across an enclosure of water so that the mean temperature of the liquid is at temperatures removed from the density maximum. The temperatures of the two opposing walls in Figure 3.4-1 are 10°C and 6°C . These temperatures are held constant and during this time, the temperatures at the five equally spaced points along the central horizontal axis within the liquid are monitored. Figure 3.4-1 shows that when the temperature gradient does not encompass the temperature of maximum density the temperature profiles of the five points remain closely bunched together. This behaviour indicates that a single convection cell exists inside the liquid and this is the typical behaviour of most liquids under the same conditions.

When the wall temperatures are changed to 6°C and 2°C , the temperature profiles along the central horizontal axis exhibit a different temperature pattern to before, as shown in Figure 3.4-2. The temperature profiles of the five thermistors exhibit different temperatures to each other. The temperature difference for the experiment in Figure 3.4-2 is centred on 4°C and this gives rise to two convection cells within the liquid. One of these cells is hot and the other is cold, consequently the two thermistors in the hot cell exhibit temperatures similar to each other but different to the two thermistors in the cold cell. The middle thermistor lies between the two cells and it exhibits a different temperature to the other four thermistors. This analysis of the temperature profiles is supported by the numerical results in section 5.3.1.

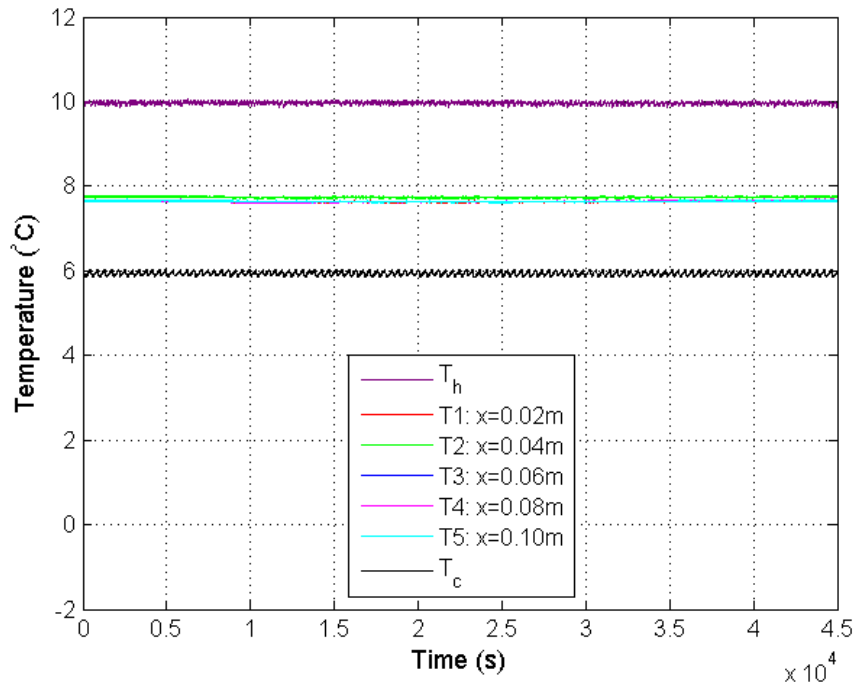


Figure 3.4-1 A plot of temperature against time for a steady state experiment of water. The wall temperatures are held at 10°C and 6°C so that the temperature difference does not encompass the density maximum. ($Ra \approx 2.99 \times 10^7$)

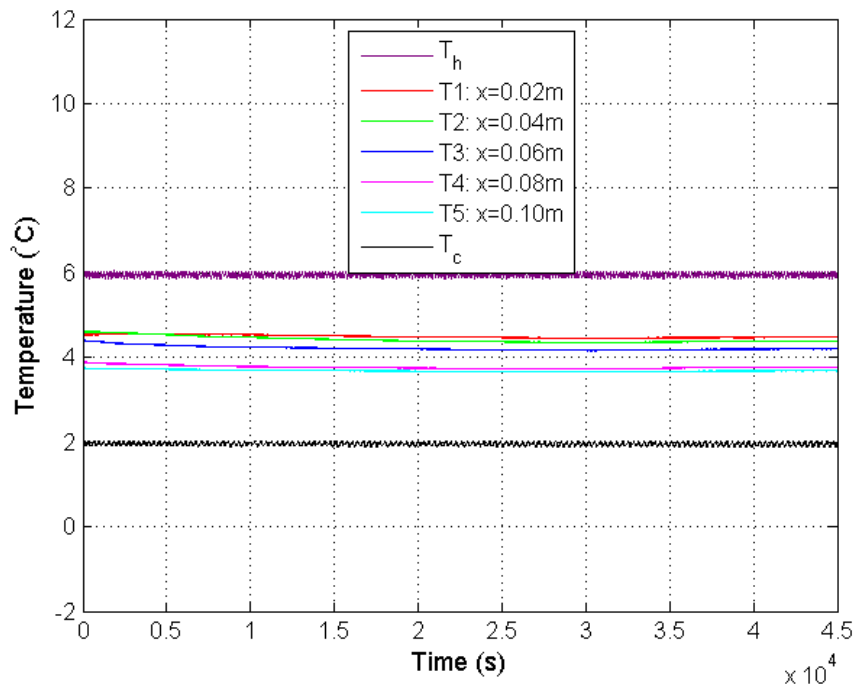


Figure 3.4-2 A plot of temperature against time for a steady state experiment of water. The wall temperatures are held at 6°C and 2°C so that the temperature difference is centred on the temperature of maximum density. ($Ra \approx 1.49 \times 10^5$)

The results show that the temperatures of the five points diverge in the vicinity of the density maximum and converge in regions away from the density maximum. This behaviour of the temperature profiles reveals the convection pattern within the liquid. Consequently, during the investigations of asymmetrical heat transfer, two thermistors are inserted at equally spaced points along the central horizontal axis of each liquid to indicate the nature of the convection within each liquid compartment.

3.4.2 Water-saline diode

The water-saline diode is the main focus of this study and it consists of a cubic enclosure of a saline solution adjacent to a cubic enclosure of water as shown in Figure 3.4-3. The basis of this thermal diode effect is that heat transfer is considerably reduced in the vicinity of the density maximum. The experimental procedure for investigating asymmetrical heat transfer holds a constant temperature gradient across the composition for a set time. When this time has elapsed, the computer instructs the apparatus to reverse the gradient by swapping the wall temperatures. The walls are then held at these temperatures for the same period of time as before. This process is repeated until the user instructs the apparatus to stop.

The results for the entire experiment are shown in Figure 3.4-4. This graph shows several cycles of the water-saline diode investigation. It is evident from this graph that repeated cycles of the investigation produce the same results. Regions (b) and (d) show the results for the high-conductance mode while regions (a), (c) and (e) show the results for the low-conductance mode. The temperature difference between the walls and their corresponding monitoring thermistors are the same in regions (b) and (d). Similarly, the temperature difference between the walls and their corresponding monitoring thermistors are the same in regions (a), (c) and (e). It is also evident from this graph that in the high-conductance mode regions the temperature profiles in each compartment are closely bunched together. In regions (a), (c) and (e) of Figure 3.4-4, the two thermistors in each compartment exhibit different temperatures from each other.

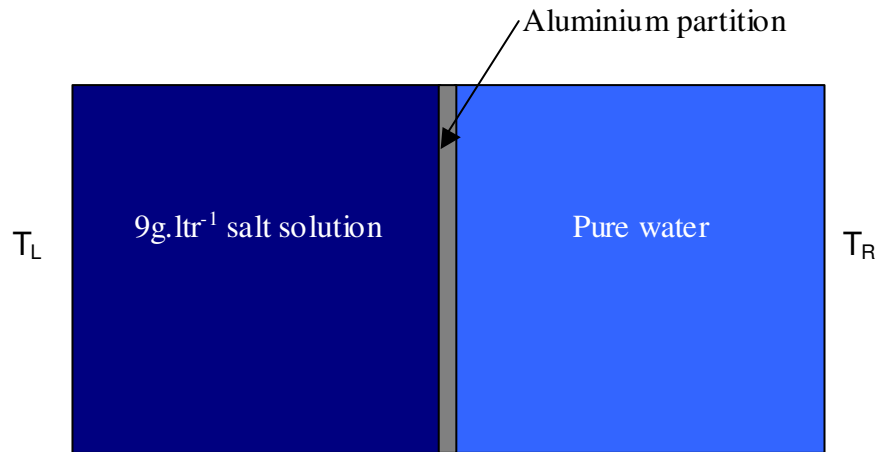


Figure 3.4-3 The water-saline diode consists of a square enclosure of a saline solution adjacent to a square enclosure of water. The square enclosures have dimensions of $0.06\text{m} \times 0.06\text{m} \times 0.06\text{m}$. The saline solution has a density maximum at 2°C and pure water has a density maximum at 4°C .

The results for one cycle are shown in Figure 3.4-5. The results show the wall temperatures and the temperatures at select points within each compartment. Unlike Figure 3.4-4, the monitoring temperatures are not shown in Figure 3.4-5 since they are displayed in a different format in Figure 3.4-7. The behaviour of the temperature within the two liquids for both directions of heat transfer is the focus of the graph in Figure 3.4-5. In the first 30,000 seconds of Figure 3.4-5 the temperature of T_L is 1°C and T_R is 5°C . During this time heat flows from the water compartment to the saltwater compartment. The temperature range across the saltwater compartment is approximately 1°C to 3°C and the temperature range across the water compartment is approximately 3°C to 5°C . Figure 3.4-6 shows the density difference of each liquid encompassed by the temperature gradient when heat flows from the water compartment to the saltwater compartment. The temperature gradient encompasses the density maximum in each compartment when heat flows in this direction. As discussed in Mooney and Cawley [37], this density range causes the formation of two counter rotating convection cells in each compartment. In Figure 3.4-5, the divergence of the temperature profiles of the two thermistors in each compartment indicates that this type of convection occurs when heat flows from the water

compartment to the saline compartment. As discussed in Cawley *et al.* [36] and in accordance with the results of Lin and Nansteel [29], the occurrence of this type of convection inhibits the flow of heat across the compartment.

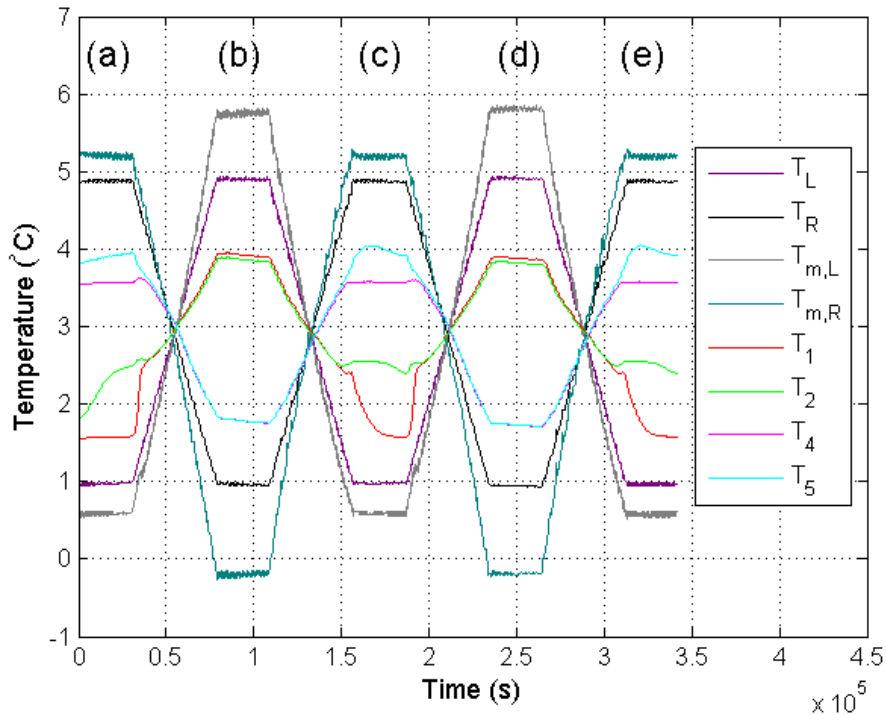


Figure 3.4-4 Experimental results for a long-duration test with the water-saline diode. Regions (a), (c) and (e) are in the low conductance mode; regions (b) and (d) are in the high conductance mode. The temperature gradient was reversed under computer control in the cross-over intervals between the five regions labelled (a) to (e). Thermistors T_1 and T_2 are located in the compartment containing the saline solution (left compartment), and thermistors T_4 and T_5 are located in the compartment containing the pure water (right compartment). ($Ra \approx 9.2 \times 10^5$ in regions (a),(c) and (e) and $Ra \approx 9.3 \times 10^3$ in regions (b) and (d)).

In region (b) of Figure 3.4-5, the temperature of the left wall is 5°C and the temperature of the right wall is 1°C so that heat flows from the saltwater compartment to the water compartment. The temperature range across the saltwater compartment is approximately 3°C to 5°C and the temperature range across the water compartment is approximately 1°C to 3°C. The corresponding density range of each liquid is shown in Figure 3.4-6. The temperature gradient does not encompass the

density maximum of either liquid in this direction of heat flow, thus single cell convection prevails in each compartment as indicated by the bunching together of the temperature profiles of the two thermistors in each compartment.

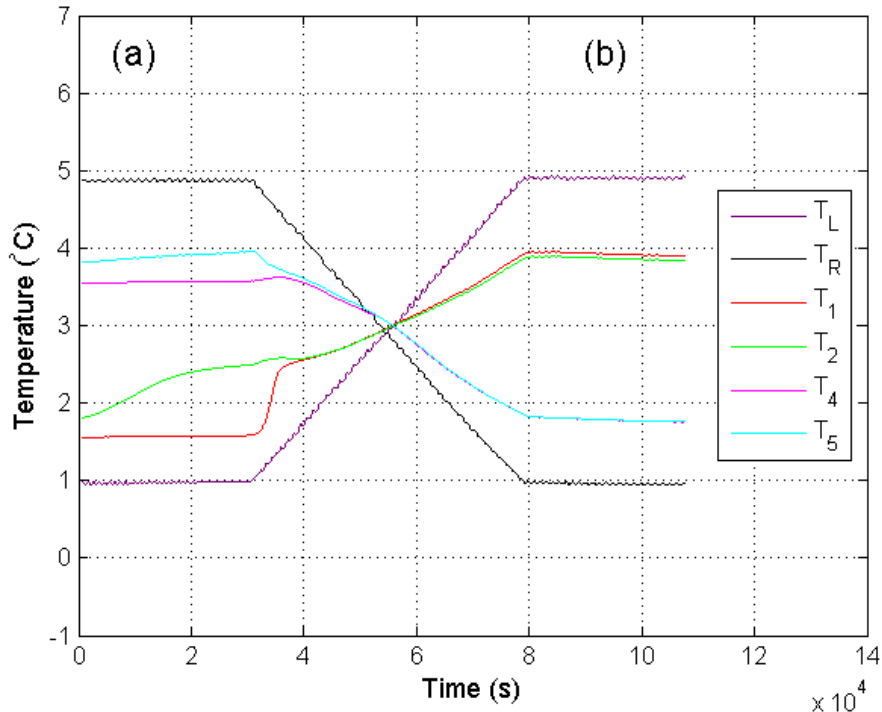


Figure 3.4-5 Smoothed experimental data for the wall thermistors and the thermistors within the liquids for the water-saline diode. Region (a) is the steady state part of the graph for the low-conductance mode and region (b) is the steady state part of the graph for the high-conductance mode.

In the transient region of Figure 3.4-5, the temperature of the right wall is decremented in steps of 0.1°C every 1,200 seconds until it reaches 1°C . Simultaneously, the temperature of the left wall is incremented in steps of 0.1°C every 1,200 seconds. During this time, the temperature difference across the entire composition remains centred on 3°C . The temperature difference is initially decremented to 0°C and then incremented back to 4°C . When the temperature difference begins to decrement, the temperatures at the points inside the liquids begin to converge since the centre of the bounding temperature range of each compartment begins to move away from the temperatures of maximum density. As the temperature difference continues to decrease, the bounding temperatures eventually cease to encompass the temperatures of maximum density. This occurs at

approximately 40,000 seconds. However, the temperatures of the two points in each compartment converge before this happens. This can be explained by considering just one compartment and then extending the explanation to include the second compartment. In one compartment, two convection cells exist and as the temperature difference decreases the size of one cell decreases while the size of the other cell increases. The two points exhibit different temperatures while they are in separate convection cells, but the temperature difference between the two points begins to decrease when one cell becomes larger than the other and the two points eventually show similar temperatures when the both rest in the same convection cell. The two points can be located in the same convection cell when two convection cells of unequal size exist, hence the two temperature points converge in Figure 3.4-5 before the bounding temperatures cease to encompass the temperature of maximum density. This explanation for the behaviour of the temperature field inside one compartment is equally valid for the behaviour of the temperature field in the other compartment and it is supported by the numerical results in section 5.3.1.

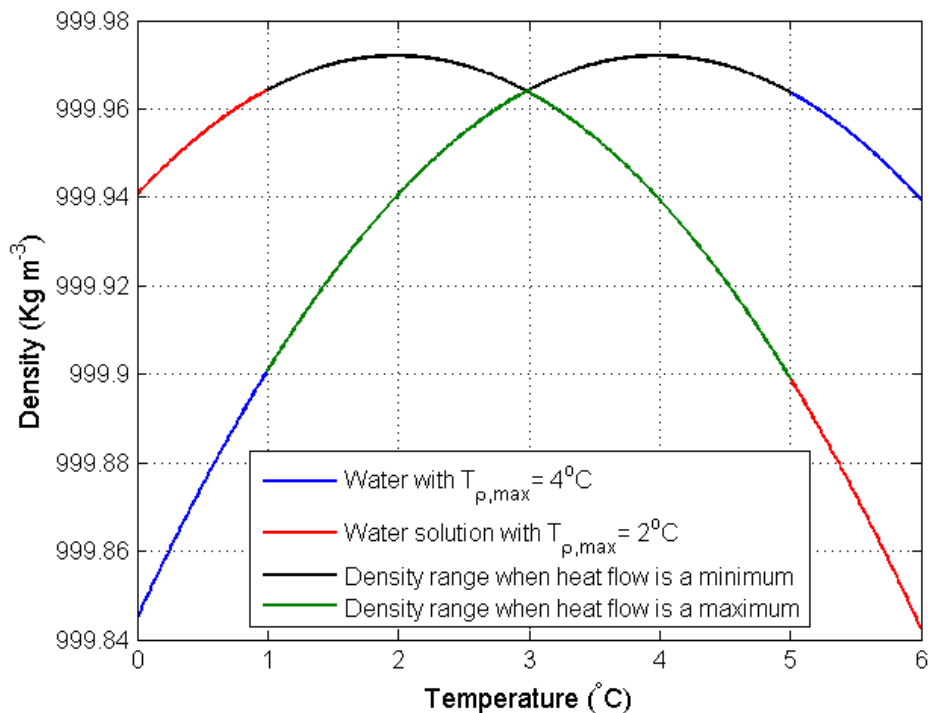


Figure 3.4-6 Density state functions for pure water and a water solution with a temperature of maximum density of 2.0 °C.

When the temperature difference is zero, the temperature of T_L and T_R is 3°C . It is perhaps expected that after 20 minutes, the temperature at the four points inside the cavity should be at 3°C and since there is no gradient, there should be no fluid flow. It is evident from Figure 3.4-5 that this is not the case. This could be due to the imperfect boundary conditions; the temperature of the sidewalls vary from 2.75°C to 3°C due to the servo bounds imposed by the experimental apparatus, so indeed it should not be expected that no convection occurs during this time step. An alternative possibility is that 20 minutes is insufficient time to rearrange the temperature fields of the liquids by 0.1°C and hence stop the movement of the liquids. It is most likely that both of these factors contribute to this feature of the graph in Figure 3.4-5.

The rate of heat flowing through the cavity is shown in Figure 3.4-7. For the purpose of this discussion, the graph will be considered to contain three parts. There are two steady state parts (one between 0 and 30,000 seconds and one between 78,000 seconds and 108,000 seconds) and one transient part (between 30,000 seconds and 78,000 seconds). As in Mooney and Cawley [37], the rate of heat transfer shown in Figure 3.4-7 is obtained by averaging the measured temperature drops across the two solid slabs of Perspex, one located at each wall outside the cavity, i.e. the average of the rate of heat flowing into the cavity and the rate of heat flowing out of the cavity. Under steady state conditions, the rate of heat flowing into any system is equal to the rate of heat flowing out of the system; thus in this experiment the rate of heat transfer has been measured twice and an average of these two measurements yields a more accurate result. Thus, this result is presented in Figure 3.4-7.

Transient conditions generally suggest that the rate of heat flowing into the cavity is not equal to the rate of heat flowing out of the cavity, since transient conditions are often used for cooling or warming a substance. However, the transient conditions imposed on this system require that one compartment heats up while the other compartment cools. Essentially the arrangement of heat within the system changes but heat is neither added nor extracted from the system, therefore the rate of heat flowing into the cavity should equal the rate of heat flowing out of the cavity under the transient conditions imposed here. This implies that it is also valid to assume that

averaging the measured rates of heat flow in the transient part of Figure 3.4-7 adequately describes the behaviour of heat transfer in this part of the graph.

As in Mooney and Cawley [37], the first 30,000 seconds of Figure 3.4-7 correspond to the rate of heat transfer when heat flows from the water compartment to the saltwater compartment. During this time, the rate of heat transfer is $0.19 \pm 0.01 \text{ W}$. The rate of heat transfer in the latter 30,000 seconds of Figure 3.4-7 corresponds to the flow of heat in the opposite direction. The rate of heat transfer in this direction is $0.55 \pm 0.04 \text{ W}$. Inserting these values into equation (3.1-1) gives a heat flow rectification of 65%. Although these two regions of the graph are steady state regions, there are fluctuations in the rate of heat transfer. As discussed previously, these fluctuations in the rate of heat transfer are due to the constant cooling and warming of the sidewalls.

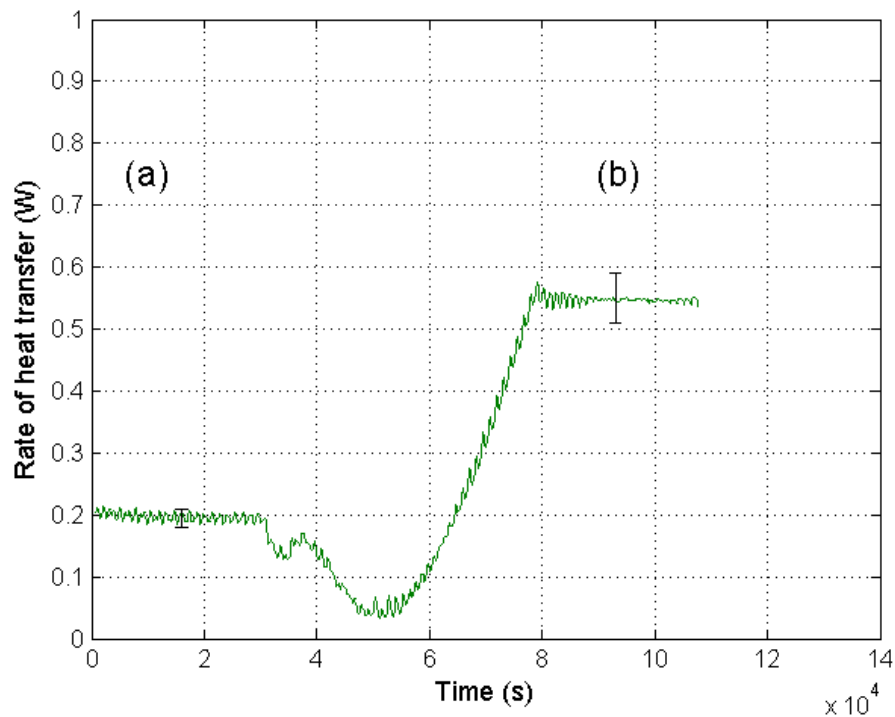


Figure 3.4-7 The rate of heat transfer through the water-saline diode. In the first 30,000 seconds heat flows from the water compartment to the saltwater compartment; in the last 30,000 seconds heat flows in the opposing direction. The direction of heat transfer is reversed under computer control between 30,000 and 78,000 seconds. ($Nu \approx 1.4$ in region (a) and $Nu \approx 3.8$ in region (b))

The transient part of the graph shows that the rate of heat flow decreases as the temperature difference decreases, and that when the temperature gradient begins to increase, the rate of heat flow also increases. A notable feature of the graph is that the rate of heat flow does not reach zero when there is no temperature gradient across the cavity. As explained previously, this feature can be attributed to a number of factors. Firstly, the boundary temperatures would have to be exactly 3°C if no temperature gradient exists. However, the boundary temperatures vary between 2.75°C and 3°C due to the servo bounds imposed by the experimental apparatus, this may account for the nonzero flow of heat through the cavity. Another important factor is that the system is allowed 20 minutes to rearrange its temperature field and this allocated time may be insufficient. These two possibilities most likely combine to cause the nonzero heat transfer value. Another notable feature in Figure 3.4-7 occurs between 30,000 seconds and 40,000 seconds. As the temperature difference decreases the rate of heat transfer decreases, but between 35,000 seconds and 40,000 seconds the rate of heat transfer increases before decreasing again. This feature occurs when the temperature profiles in Figure 3.4-5 converge and it can be explained by considering just one compartment and then extending the explanation to include the second compartment. In one compartment, two convection cells exist and as the temperature difference decreases the size of one cell decreases while the size of the other cell increases. As the rate of heat transfer initially decreases, one of the convection cells shrinks and the other convection cell grows. When the latter convection cell is large enough to make direct contact with the isothermal wall and the partition wall, the rate of heat transfer increases. The same process occurs in the water compartment. However, the temperature difference continues to decrease and so the rate of heat transfer decreases again. This analysis of the rate of heat transfer is supported by the numerical results in section 5.3.1.

3.4.3 Water-Perspex diode

The water-Perspex diode consists of a container of water adjacent to a slab of Perspex as described in Cawley *et al.* [36]. The container of water is of dimensions of 0.06 m x 0.06 m x 0.118 m and the Perspex slab has dimensions of 0.06m x 0.06m x 0.002m. The arrangement of the water-Perspex diode is shown in Figure 3.4-8. The boundary temperatures for the water-Perspex diode are different to those for the

water-saline diode and they were predetermined from the numerical study on the optimisation of the water-Perspex diode. The temperature of the left wall is held at 6.5°C and the temperature of the right wall is held at 2.5°C for 30,000 seconds. These temperatures are then interchanged over a time of 48,000 seconds. Following this interchange the temperature of the left wall is held at 2.5°C and the temperature of the right wall is held at 6.5°C for 30,000 seconds. The basis of the water-Perspex thermal diode is that when heat flows in one direction the mean temperature of the water compartment is in the proximity of the temperature of maximum density; when heat flows in the opposing direction, the mean temperature of the water compartment is at a temperature removed from the temperature of maximum density.

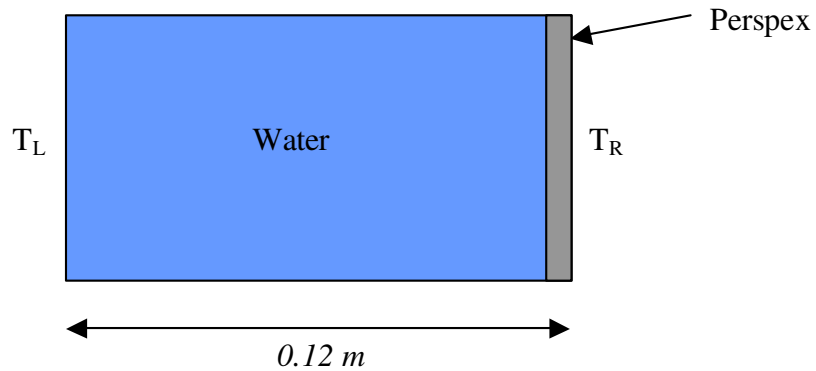


Figure 3.4-8 The water Perspex diode consists of a rectangular enclosure of water (dimensions of $0.06\text{m} \times 0.06\text{m} \times 0.118\text{m}$) adjacent to a slab of Perspex (dimensions of $0.06\text{m} \times 0.06\text{m} \times 0.002\text{m}$).

The results for the experimental investigation of the water-Perspex diode are shown in Figure 3.4-9 and Figure 3.4-10. The temperature profiles at four points along the central horizontal axis (at distances of 0.02m , 0.04m , 0.08m and 0.10m from the left wall) and the temperatures of the two sidewalls are shown in Figure 3.4-9. When heat flows from left to right through this system (region (a) of Figure 3.4-9 and Figure 3.4-10), the temperature profiles inside the liquid are within 0.2°C of each other and the temperatures are removed from the temperature of maximum density. The rate of heat transfer for this entire experiment is shown in Figure 3.4-10. The

rate of heat transfer for region (a) is obtained by averaging the rate of heat transfer over the last 5,000 seconds of this region. When heat flows from left to right through the water-Perspex composite the rate of heat transfer is $0.40 \pm 0.03 \text{ W}$. When heat flows from right to left (region (b) of Figure 3.4-9 and Figure 3.4-10) through the composite system, the temperature profiles are again within 0.2°C of each other but the rate of heat transfer is reduced to $0.28 \pm 0.02 \text{ W}$. This gives a percentage rectification of 30% for the water-Perspex diode.

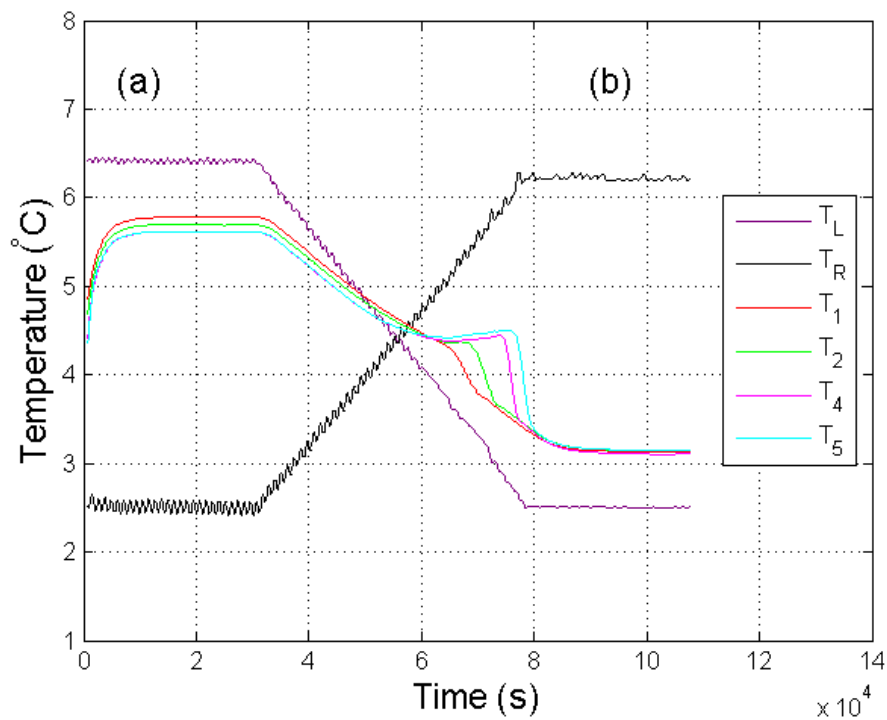


Figure 3.4-9 Smoothed experimental data for the wall thermistors and the thermistors within the liquids for the water-Perspex diode. Region (a) is the steady state part of the graph for the high-conductance mode and region (b) is the steady state part of the graph for the low-conductance mode. ($Ra \approx 5.0 \times 10^6$ in region (a) and $Ra \approx 8.8 \times 10^5$ in region (b)).

The temperature profiles in region (b) are closer to 4°C than the temperature profiles in region (a). In region (a) heat is transferred through the water sample by a single clockwise convection cell as indicated by the behaviour of the temperature profiles. Since the temperature profiles in region (b) are in the proximity of the temperature of maximum density, it is expected that in region (b) heat is transferred through the

liquid via two counter rotating convection cells and that the temperature profiles should not be closely bunched together. However, the experimental results in Figure 3.4-9 show that they are bunched together. This bunching together indicates that the temperature points are in the same cold convection cell that stretches from the cold wall to the partition wall. A small convection cell that does not encompass any of the thermistor points exists at the partition wall and this small cell causes the reduction in the rate of heat transfer. It is evident from Figure 3.4-9 that the temperature of the right wall in region (b) is not 6.5°C , as demanded by the experiment. The temperature of the right wall in Figure 3.3-8 is actually 6.3°C ; this offset of the wall temperature is the cause of the unexpected behaviour of the temperature profiles. This analysis of the temperature profiles is supported by the numerical investigations and the temperature profiles are further analysed in section 5.3.3.

Region (a) of the heat transfer plot in Figure 3.4-10 shows the rate of heat transfer decreasing from approximately 0.95W to 0.40W . This decrease in the rate of heat transfer is due to the warming of the composite system. At the start of region (b), the rate of heat transfer decreases from 0.40W to 0.28W . During the interchanging region, the water sample is cooled through its temperature of maximum density. Between $60,000$ seconds and $70,000$ seconds the rate of heat transfer increases more slowly than before; this is due to the formation of a second convection cell at the left wall as the temperature of the water sample enters the vicinity of the density maximum. The sudden increase in the rate of heat transfer between $70,000$ and $80,000$ seconds is due to the rapid growth of the second convection cell across the enclosure. This rapid growth leaves a high rate of heat transfer through the composite system as the system enters the steady state region. Consequently, the rate of heat transfer decreases from 0.40W to 0.28W at the start of region (b). This feature is also observed in the numerical studies presented in section 5.3.3.

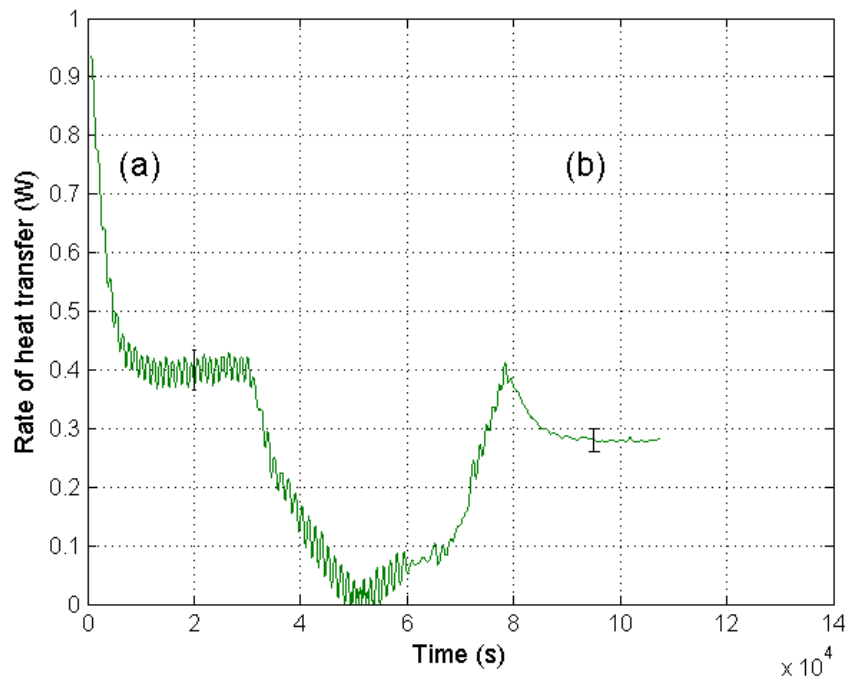


Figure 3.4-10 The rate of heat transfer through the water-Perspex diode. In the first 30,000 seconds heat flows from the water compartment to Perspex slab; in the last 30,000 seconds heat flows in the opposing direction. The direction of heat transfer is reversed under computer control between 30,000 and 78,000 seconds. ($Nu \approx 5.5$ in region (a) and $Nu \approx 3.8$ in region (b))

Chapter 4

Computational Fluid Dynamics

4.1 Introduction

This chapter describes the procedures for investigating the quasi-steady state cooling of a liquid, the technique used for measuring the temperature of maximum density of aqueous solutions, asymmetrical heat transfer through composites of water and aqueous solutions and through composites of water and Perspex using computational fluid dynamics. The aims of the numerical investigations are to confirm the experimental results and to further understand them through the exploration of a variety of conditions.

The governing equations of the fluid flow discussed in this thesis are described in section 4.2 along with the numerical methods used to solve them. In this section two software packages are presented that are capable of simulating the experimental results. The first package, NaSt2D, is an open source code that uses the finite difference method to solve the governing equations. The second package, Comsol Multiphysics ©, is a commercial package that uses the finite element method to solve the governing equations. The latter software package is used for all of the numerical results presented in this thesis unless otherwise specified.

Section 4.3 describes the unique aspects of the numerical model associated with the investigations of the quasi-steady state cooling and the temperature of maximum density of aqueous solutions. This section describes the initial conditions, the boundary conditions, the discretized geometry and the testing of the dependency of the numerical models on the time step size and the mesh density.

Section 4.4 concludes this chapter with a description of the unique features of the models used to investigate asymmetrical heat transfer. The numerical studies investigate asymmetrical heat transfer through composites of water and aqueous solutions (water-saline diode), water and a solid (water-Perspex diode), and water and a phase change material (phase change diode). The focus of these studies is the water-saline diode, and hence a detailed study of the optimal conditions of the water-saline diode is conducted.

4.2 Theory

The governing equations and the numerical method used to solve them are common aspects to all of the models used in this study. The governing equations are the Navier-Stokes equation (the momentum equation), the continuity equation and the heat equation. These equations are used in all models and they will be described in section 4.2.1. Two different codes are described in this chapter; one of these codes uses the finite difference method (NaSt2D) and the other code uses the finite element method (Comsol Multiphysics). Consequently a brief overview of these two numerical methods is given in section 4.2.2. A comparison between numerical results from the Comsol Multiphysics package and the open source code NaSt2D is made in section 4.2.3. A key reason for the use of the commercial software instead of the open source code is the ease at which heat transfer can be studied using the commercial software. The manner in which the heat transfer values are obtained from the commercial software is explained in section 4.2.4.

4.2.1 Governing equations

Mathematically the behaviour of fluids is generally described by the conservation equations, that is the conservation of mass, momentum and energy. Although the Navier-Stokes equation is generally understood to be the equations describing the conservation of momentum and mass, the name is often used for the complete set of equations solved by computational fluid dynamics. However, in this study only the equation describing the conservation of momentum shall be referred to as the Navier-Stokes equation. The conservation of mass equation will be referred to as the continuity equation.

The equation that describes the conservation of momentum is

$$\rho(T) \frac{\partial \mathbf{v}}{\partial t} + \rho(T)(\mathbf{v} \cdot \nabla) \mathbf{v} = -\nabla p + \rho(T) \mathbf{g} + \mu(T) \nabla^2 \mathbf{v} \quad (4.2-1)$$

where ρ is the density of the liquid in units of $\text{kg} \cdot \text{m}^{-3}$, \mathbf{v} is the velocity in units of $\text{m} \cdot \text{s}^{-1}$, p is the pressure in units of Pa, \mathbf{g} is gravity in units of $\text{m} \cdot \text{s}^{-2}$, and μ is the dynamic viscosity in units of Pa.s.

For an incompressible fluid the continuity equation (the conservation of mass) is

$$\nabla \cdot \mathbf{v} = 0 \quad (4.2-2)$$

The heat equation is

$$\frac{\partial T}{\partial t} + \mathbf{v} \cdot \nabla T = \frac{k(T)}{\rho(T)C_p(T)} \nabla^2 T \quad (4.2-3)$$

where T is the temperature in units of Kelvins, C_p is the specific heat capacity in units of $\text{J} \cdot \text{kg}^{-1} \cdot \text{K}^{-1}$ and k is the thermal conductivity in units of $\text{W} \cdot \text{m}^{-1} \cdot \text{K}^{-1}$.

In the numerical investigations presented in chapter 5 the properties of water vary as functions of temperature. For this study the functions for the thermal conductivity, the specific heat capacity, the viscosity and the density are best-fit equations to data taken from reference [1]. Plots of these properties as a function of temperature are shown in Figure 4.2-1. In this study it is assumed that a 2-D slice of the 3-D chamber adequately represents the 3-D chamber, thus all of the above equations are solved in two dimensions.

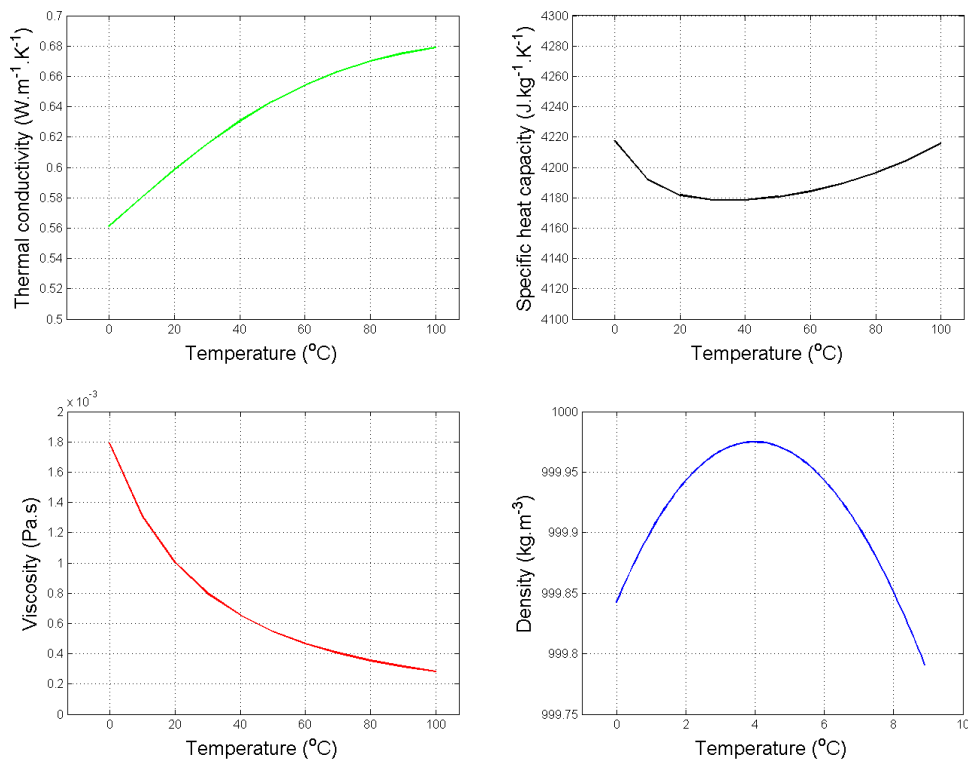


Figure 4.2-1 A plot of the thermal conductivity, the specific heat capacity, the viscosity and the density of water as a function of temperature (data taken from reference [1]).

The variation of the density of a liquid as a function of temperature is of fundamental importance to the study of free convection. In the numerical investigations presented in this thesis the temperature dependency of the density of pure water is described by the following state function based on a second-order polynomial fit to data taken from [1] in the temperature range of -2°C to 10°C :

$$\rho(T) = c_0 + c_1T + c_2T^2 \quad (4.2-4)$$

The values of the coefficients c_0 , c_1 and c_2 are $999.845079\text{kg}\cdot\text{m}^{-3}$, $0.06378\text{kg}\cdot\text{m}^{-3}\cdot^{\circ}\text{C}^{-1}$ and $-0.0080125\text{kg}\cdot\text{m}^{-3}\cdot^{\circ}\text{C}^{-2}$, respectively. According to this equation the temperature of maximum density, $T_{\rho,\text{max}}$, is (setting the first derivative of this equation to zero yields the temperature of maximum density),

$$T_{\rho,\text{max}} = -\frac{c_1}{2c_2} = 3.98^{\circ}\text{C} \quad (4.2-5)$$

4.2.2 Numerical methods

The governing equations in this study are a set of partial differential equations. A partial differential equation involves a function $u(\mathbf{x},t)$ defined for all times t and \mathbf{x} on a specified domain with respect to some given boundary condition. The purpose of the numerical methods is to determine an approximation to the function $u(\mathbf{x},t)$. There are many different numerical methods for obtaining a numerical solution to partial differential equations. These include the finite difference method and the finite element method. Each method has its own advantages and applications for which it is best suited. For example the finite difference method is probably the simplest to apply, but unlike the finite element method it is restricted to simple domains.

The restriction of the finite difference method to simple geometries is due to the manner in which the domain is discretised; the domain is discretised by introducing a grid on it. At each grid point, each term in the partial differential is replaced by a difference formula, which may include the values of u at that point and neighbouring grid points. By substituting the difference formulae into the PDE, a difference equation is obtained.

Unlike the finite difference method, the finite element method requires the discretisation of the domain into subregions or cells. For example, a two-dimensional domain can be divided and approximated by a set of triangles (the cells). On each cell, the function is approximated by a characteristic form. For example, $u(\mathbf{x}, t)$ can be approximated by a linear function on each triangle.

It is essential to appreciate that a numerical solution obtained using any of these numerical methods is only an approximation of the true solution, and it is important to try to estimate the size of the errors in the approximation. This necessitates the study of the solution's sensitivity to the mesh density for all models used in the investigations of the temperature of maximum density of aqueous solutions and asymmetrical heat transfer. The mesh sensitivity studies are unique to each model and they are described along with the associated models in sections 4.3 and 4.4.

4.2.3 Comsol Multiphysics © and NaSt2D

As mentioned earlier, previous numerical work conducted by the fluid dynamics group at NUI Maynooth used the software package NaSt2D. The software package NaSt2D is an open source package available from the public domain. The authors, in addition to making their code available on the Internet [65], have published a book describing the package [66]. NaSt2D applies the finite difference method to the discretisation of the continuous equations of fluid dynamics. With some modifications, this package can be used to reproduce some of the experimental results in this thesis. McBride [57] conducted a detailed study on the validation of the NaSt2D code. The numerical studies described by McBride [57] and McGlynn [67] used this package extensively and some of the early numerical studies conducted during this body of work used this code to confirm the results obtained from the commercial package Comsol Multiphysics [68].

In comparison to Comsol Multiphysics, NaSt2D has no financial cost associated with it and it is relatively inexpensive in terms of computing power. Despite these advantages the numerical results presented in this thesis were obtained using Comsol Multiphysics. Unlike NaSt2D, Comsol Multiphysics easily simulates the heat transfer results obtained experimentally, it is easier to use for complex geometries (such as the water-saline diode) and it has superior post-processing facilities. The

Comsol Multiphysics code is chosen for the numerical investigations in this thesis primarily because of the ease at which the heat transfer values can be obtained.

For the purpose of comparison between NaSt2D and Comsol Multiphysics, some steady state flow patterns and the experimental plot of the quasi-steady state cooling of water are simulated using both packages and the results are shown in Figure 4.2-2 and Figure 4.2-3. There is good agreement between both sets of results, quantitatively and qualitatively.

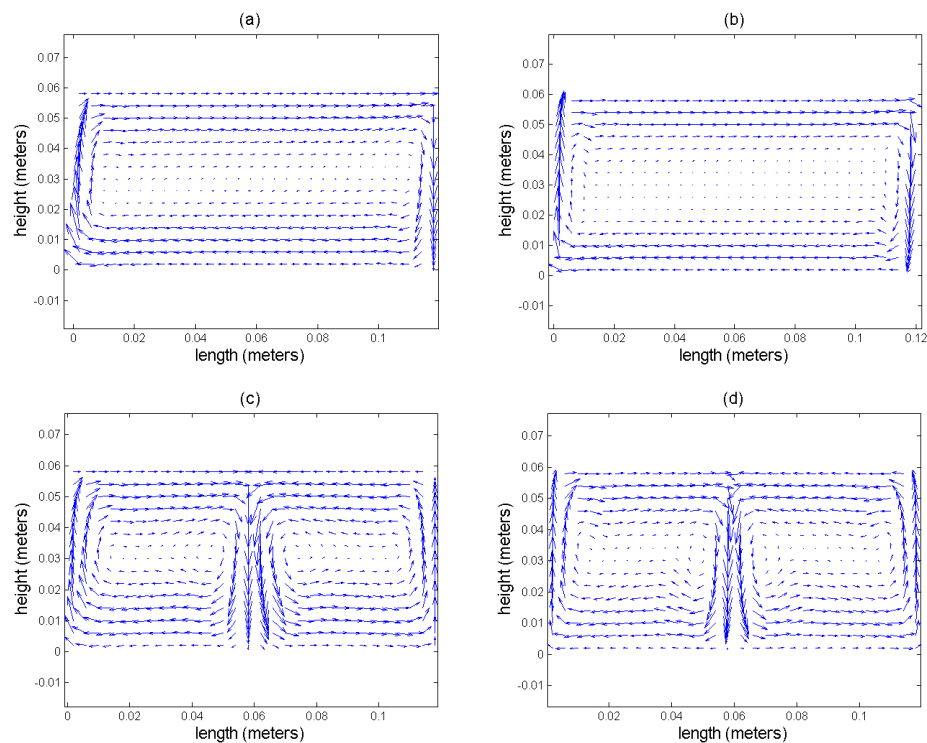


Figure 4.2-2 Numerical simulations of the steady state flow patterns of water (a) NaSt2D for boundary temperatures of 10°C and 6°C , (b) Comsol Multiphysics for boundary temperatures of 10°C and 6°C , (c) NaSt2D for boundary temperatures of 5.98°C and 1.98°C , and (d) Comsol Multiphysics for boundary temperatures of 5.98°C and 1.98°C .

It is important to note that the Boussinesq approximation was assumed in the numerical models that used NaSt2D but it was not used in the Comsol Multiphysics models. The Boussinesq approximation assumes that the density of the liquid is constant except in the body force term of the Navier-Stokes equation. Preliminary

use of the NaSt2D code assumed the Boussinesq approximation and so the NaSt2D results presented in Figure 4.2-2 and Figure 4.2-3 were obtained using this approximation. This assumption is not necessary for the work presented in this thesis and it was decided that this assumption would not be made for this body of work. Consequently, the numerical results obtained from the Comsol Multiphysics package did not use the Boussinesq approximation. The good agreement between the numerical results from the two codes indicates that the Boussinesq approximation would have been an adequate assumption for this body of work.

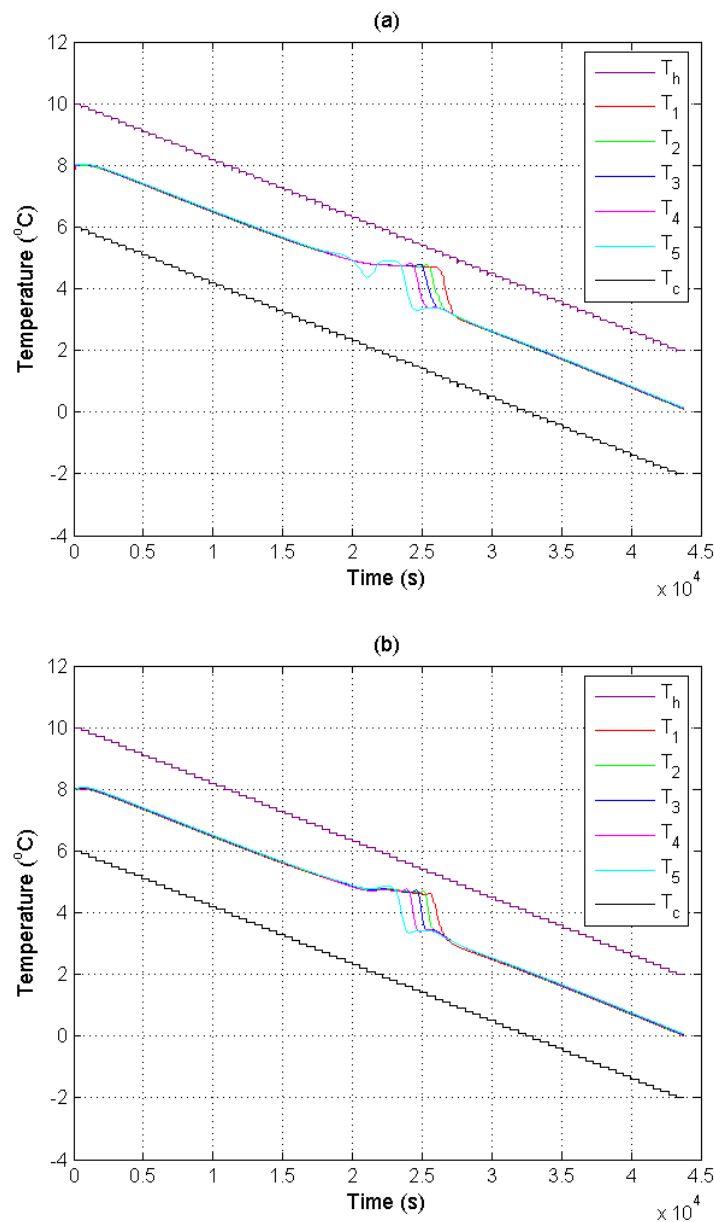


Figure 4.2-3 Numerical simulations of the experimental quasi-steady state cooling of water using (a) Comsol Multiphysics and (b) NaSt2D.

4.2.4 Calculating heat transfer

The behaviour of heat transfer is of primary importance to the main body of work presented in this thesis. Unlike the shareware code NaSt2D, Comsol Multiphysics facilitates the investigation of heat transfer. The Comsol Multiphysics environment permits integration of certain parameters on boundaries. This feature is exploited to obtain the values for heat transfer. Comsol Multiphysics performs the following calculation along a boundary

$$\int (-k\nabla T + \rho C_p T \bar{v}) \cdot \bar{\partial} l \quad (4.2-6)$$

where k is the thermal conductivity in $\text{W}\cdot\text{m}^{-1}\cdot\text{K}^{-1}$, T is the temperature in Kelvin, ρ is the density in $\text{kg}\cdot\text{m}^{-3}$, C_p is the specific heat capacity in $\text{J}\cdot\text{kg}^{-1}\cdot\text{K}^{-1}$, v is the velocity in units of $\text{m}\cdot\text{s}^{-1}$, and ∂l is an infinitesimally length on the boundary under investigation. The expression within the parenthesis in equation (4.2-6) is the heat flux due to conduction ($-k\nabla T$) and convection ($\rho C_p T \bar{v}$). Integrating the expression within the parenthesis in equation (4.2-6) along the hot boundary gives the rate of heat flowing into geometry and integrating along the cold boundary gives the rate of heat flowing out of the geometry. Since the top and bottom boundaries are considered to be adiabatic, that is, no heat flows into or out of the geometry through these walls, integrating the heat flux along each of these boundaries yields $0\text{W}\cdot\text{m}^{-1}$. Integrating the heat flux along the entire boundary yields the net flow of heat into or out of the geometry. Under steady state conditions, integrating along the entire boundary of the container yields a value of $0\text{W}\cdot\text{m}^{-1}$. Under transient conditions, the value of the integral along the entire boundary is equal to the amount of heat required to raise or lower the temperature of the material contained in the geometry. In these models, the rate of cooling of the sample can be obtained from the difference between the values of the integral along the hot and cold boundaries (since the top and bottom boundaries have values of $0\text{W}\cdot\text{m}^{-1}$).

The value of the integral in equation (4.2-6) is in units of $\text{W}\cdot\text{m}^{-1}$. The value of this integral is multiplied by the depth of the experimental chamber to obtain the rate of heat transfer that can be directly compared to the experimental results. The experimental system obtains heat transfer values by monitoring the temperature

difference across a solid reference material and inserting this value into the 1-D Fourier equation,

$$H_h = \frac{k_p A (T_{m,h} - T_h)}{\Delta x} \quad (4.2-7)$$

$$H_c = \frac{k_p A (T_c - T_{m,c})}{\Delta x} \quad (4.2-8)$$

Where H is the heat transfer in units of W, k is the thermal conductivity in $\text{W}\cdot\text{m}^{-1}\cdot\text{K}^{-1}$, A is the cross-sectional area in m^2 , Δx is the width of the reference material in m, T is the temperature of the wall in $^{\circ}\text{C}$, T_m is the monitoring temperature and the subscripts h and c represent the hot and cold walls, respectively. Throughout this thesis, the experimental plots of the temperature profiles often include the monitoring temperature profiles to indicate the behaviour of the rate of heat transfer. For the purpose of consistency and to ease comparison between the experimental and numerical results, the monitoring profiles are included in the numerical plots of the temperature profiles. The monitoring profiles are obtained for the numerical plots by converting the values from the integral in equation (4.2-6) into W and inserting these values into the following equations

$$T_{m,h} = T_h + \frac{\Delta x}{kA} H_h \quad (4.2-9)$$

$$T_{m,c} = T_c - \frac{\Delta x}{kA} H_c \quad (4.2-10)$$

4.3 The density maximum of aqueous solutions

The behaviour of the temperature of maximum density of aqueous solutions is investigated experimentally using a novel measurement technique. The technique is based on the comparison of the temperature profiles of water with the temperature profiles of the solution when both liquids are cooled in a quasi-steady state manner. The purpose of the numerical investigations is to confirm the experimental results relating to the temperature of maximum density of aqueous solutions and to further understand the anomalous feature that occurs in the temperature profiles in the vicinity of the density maximum.

Experimentally a liquid is cooled in a quasi-steady state manner by applying a constant horizontal temperature gradient to a rectangular enclosure of the liquid. At the start of an experiment the temperature of the hot wall is 10°C and the cold wall is 6°C. The cooling of the liquid is achieved by reducing these temperatures in steps of 0.1°C every 540 seconds over a time span of 43740 seconds. The same approach is taken in the numerical investigations. The initial conditions, the boundary conditions, material properties, the geometry and the mesh sensitivity studies required to simulate the quasi-steady state cooling are described in section 4.3.1.

Experimentally the temperature of maximum density of an aqueous solution is measured by comparing the temperature profiles of the solution to the temperature profiles of water. The comparison is carried out using a chi-squared technique. Section 4.3.2 describes the procedures and associated aspects of the models used to verify the experimental technique.

4.3.1 Quasi-steady state cooling

In this study a liquid is cooled in a quasi-steady state manner by applying a constant horizontal temperature gradient with varying boundary temperatures to a rectangular enclosure of the liquid. Initially the boundary temperatures are 10°C and 6°C. When the cooling begins these temperatures are decremented by 0.1°C every 540 seconds until the two boundaries reach 2°C and -2°C. When this procedure is applied to a liquid with a density maximum an anomalous feature occurs in the temperature profiles in the vicinity of the density maximum. The temperature of maximum density of an aqueous solution is obtained by comparing this anomalous feature in the temperature profiles of the solution to that of pure water. It is therefore important to understand the behaviour and occurrence of the anomalous feature.

Experimentally the feature is explored through flow visualization and temperature measurements. The flow visualization required the use of the first geometry shown in Figure 4.3-1. It is necessary that the conditions of the CFD studies and the experimental investigations are identical so that the results of the two studies can be compared, therefore this geometry will also be used in the CFD studies of the

anomalous feature. The second geometry was used for comparing the temperature profiles of water to the temperature profiles of a typical liquid (ethanol).

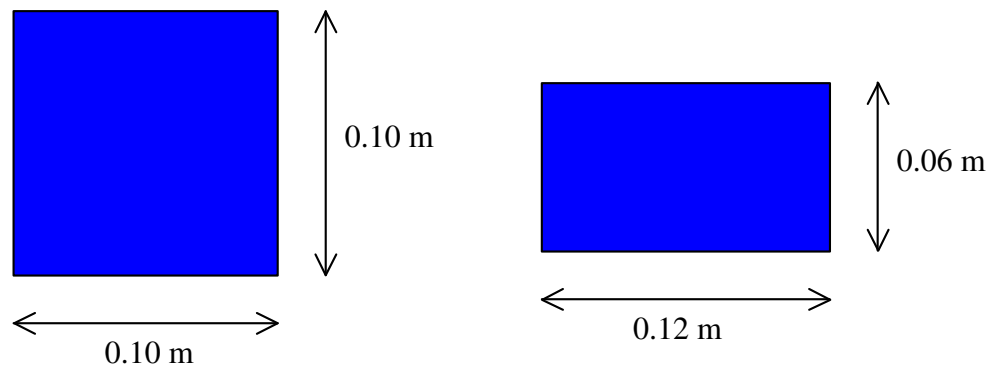


Figure 4.3-1 The two geometries used for understanding and verifying the experimental results of the quasi-steady state cooling.

The boundary condition imposed on the four walls for the Navier-Stokes equation was the no slip boundary condition, that is the velocity at all the boundaries is set to zero. The conservation of energy equation had adiabatic conditions imposed on the two horizontal walls (top and bottom walls), that is heat cannot flow into or out of these boundaries. Isothermal conditions were imposed on the two vertical walls. The temperature of the two vertical walls were set equal to the following equations in order to implement the varying temperature with time condition:

$$T_h = 10 - \text{round}\left(\frac{t}{540} \times 0.1\right) \quad (4.3-1)$$

$$T_c = 6 - \text{round}\left(\frac{t}{540} \times 0.1\right) \quad (4.3-2)$$

where t is the time in seconds. The initial velocity of the liquid was set to zero and the initial temperature was set to 8°C.

The sensitivity of the numerical solution to the grid was analysed using uniform grids in the range of 20 x 10 (width by height) to 60 x 30. The behaviour of a global parameter (the integral of the temperature over the entire grid) was examined for convergence, and it was found that the value of the average temperature was

relatively independent of the grid size for grids in excess of 50 x 20 (less than 1% variation in the average temperature above this mesh size, compared with a 13% variation in this parameter in going from a 10 x 20 to 15 x 30 grid). A range of time steps was also tested, and it was found that the solution was relatively independent of step size for time steps in the range 0.01-1.0s; a time step of 1.0s was used in these numerical investigations.

4.3.2 Measurement technique for the temperature of maximum density of aqueous solutions

The technique for measuring the temperature of maximum density of aqueous solutions is investigated by applying the above numerical model to water with a density maximum at 3.98°C and to water with a density maximum at 3°C. The properties of water varied with temperature according to the data taken from [1]. For the sample of water with a density maximum at 3°C, the density state equation of water is modified as follows

$$\rho(T) = c_o + c_1(T - (T_{\rho_{max}} - T_{\rho_{max,sol}})) + c_2(T - (T_{\rho_{max}} - T_{\rho_{max,sol}}))^2 \quad (4.3-3)$$

where $T_{\rho_{max}}$ is the temperature of maximum density of water in degrees Celsius and $T_{\rho_{max, sol}}$ is the temperature of maximum density of the aqueous solution in degrees Celsius. The numerical model is applied to the geometry shown in Figure 4.3-2 for both of these liquids.

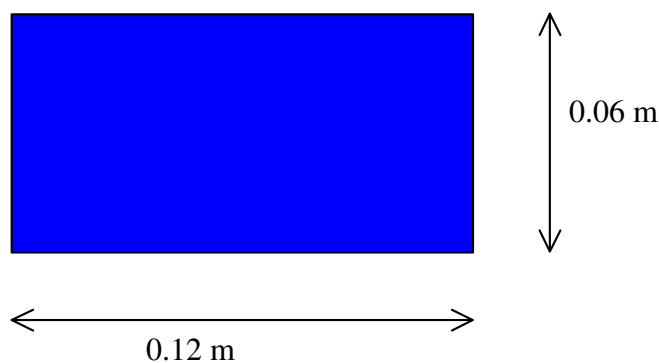


Figure 4.3-2 The geometry used for verifying the technique for measuring the temperature of maximum density of aqueous solutions.

When the sample of liquid is cooled in the vicinity of its density maximum, a unique signature is observed in the temperature profiles and in the rate of cooling. The temperature of maximum density of aqueous solutions is obtained by comparing the signature in the temperature profiles of the aqueous solution to that of pure water. A chi-squared technique, described briefly in Cawley *et al.* [61] and in more detail in section 2.5.1, compares the signature of the solution to the signature of water. The procedure described here will apply the chi-squared technique to the simulated temperature profiles for water with a density maximum at 3.98°C and for water with a density maximum at 3°C.

4.4 Asymmetrical heat transfer

This section describes the unique features of the models used to investigate asymmetrical heat transfer. The aim of these numerical studies is to confirm the experimental results and to explore the possibility of achieving a greater rectification factor. The numerical studies investigate asymmetrical heat transfer through composites of water and aqueous solutions (water-saline diode), water and a phase change material (phase change diode), and water and a solid (water-Perspex diode). The basis of the water-saline diode is that heat transfer is reduced in the vicinity of the density maximum. The operating principle of the phase change diode is that the mechanism of heat transfer is altered by the state of the phase change material. The water-Perspex diode is based on a similar principle to the water-saline diode, that is, the rate of heat transfer changes in the vicinity of the density maximum. The focus of these studies is the water-saline diode and the optimal conditions of the water-saline diode are investigated by varying the boundary conditions and the geometry of the diode.

Section 4.4.1 describes the numerical model used to simulate the experimental results for the water-saline diode. The numerical investigations extend the experimental study by exploring the influence of certain parameters on the rectification factor with the intention of finding the optimal conditions for the water-saline diode. The models used for these investigations are described in section 4.4.2. Asymmetrical heat transfer is also investigated numerically in composite systems containing a phase change material (Phase change diodes). The models used to investigate the

phase change diode are described in section 4.4.3. Experimentally, asymmetrical heat transfer was found in the water-Perspex diode. The numerical model used to simulate the experimental results is described in section 4.4.4 along with the models used for optimizing the water-Perspex diode.

4.4.1 Water-saline diode

The geometry shown in Figure 4.4-1 represents the chamber used in the experimental investigations. The geometry contains three domains; the first domain contains water with a density maximum at 2°C, the second domain contains aluminium and the third domain contains water with a density maximum at 3.98°C. The Navier-Stoke equation, the continuity equation and the heat equation are solved on the liquid domains, but only the heat equation is solved on the aluminium domain (since the aluminium is not a fluid, it is not required to solve the Navier-Stokes equations on the aluminium domain).

The no slip boundary condition is imposed on all boundaries in contact with a liquid. The boundaries not in contact with a liquid are in contact only with the aluminium partition and since the Navier-Stokes equation is not solved on this domain, it is unnecessary to implement boundary conditions for the Navier-Stokes equation on these boundaries. The boundary conditions imposed for the heat equation are shown in Figure 4.4-1, the boundaries on the left and right had isothermal conditions while all the boundaries on the top and bottom of the geometry had adiabatic conditions. The two internal boundaries had the continuity condition imposed on them.

The temperature of the two sidewalls varied with time; the boundary temperatures are held at $T_L=1^\circ\text{C}$ and $T_R=5^\circ\text{C}$ for 30,000 seconds. After 30,000 seconds the boundary temperature, T_L , is incremented by 0.1°C and the boundary temperature, T_R , is decremented by 0.1°C every 1,200 seconds until the T_L and T_R are 5°C and 1°C , respectively. The boundaries are held at these temperatures for 30,000 seconds. These conditions are equivalent to the boundary conditions imposed on the system in the experimental investigations. The initial velocity of the liquids was set to zero and the initial temperature of the first, second and third domains were set to 2°C , 3°C , and 4°C , respectively.

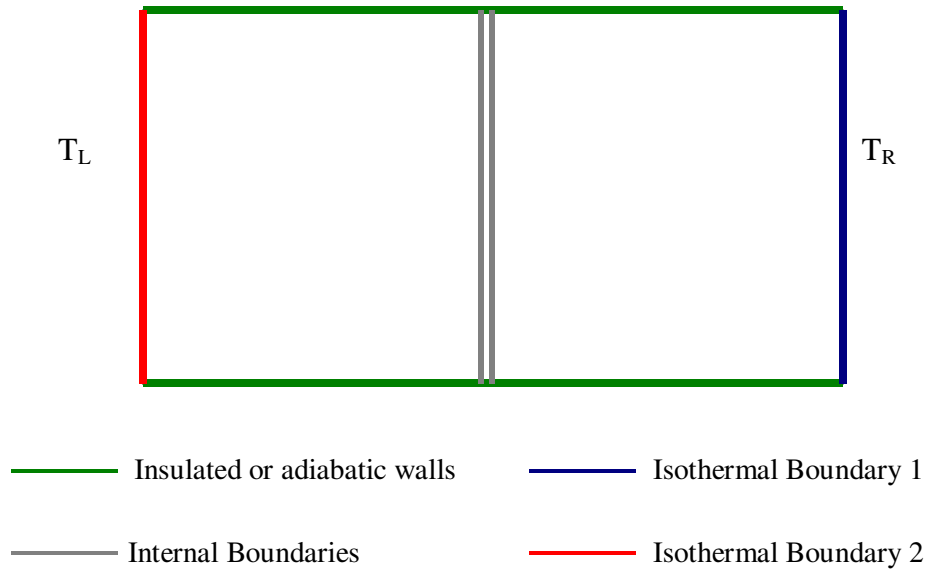


Figure 4.4-1 The thermal boundary conditions imposed on the geometry used for the investigations of the thermal diode effect in the water-saline diode. The geometry contains three domains, the two domains in contact with the isothermal walls are liquid and the centre domain represents the aluminium partition. All the walls in contact with a liquid had the no slip boundary condition imposed on them.

The properties of water varied with temperature according to the data taken from [1] and the properties of aluminium were taken from the Comsol Multiphysics material library. The properties of the saltwater domain were assumed to be similar to water and the density state equation of water is modified in the body force term of the Navier-Stokes equation so that a density maximum occurs at 2°C. The modified density state equation for the saltwater domain is

$$\rho(T) = c_o + c_1(T - (T_{\rho_{max}} - T_{\rho_{max,sol}})) + c_2(T - (T_{\rho_{max}} - T_{\rho_{max,sol}}))^2 \quad (4.4-1)$$

where $T_{\rho_{max}}$ is the temperature of maximum density of water in degrees Celsius and $T_{\rho_{max, sol}}$ is the temperature of maximum density of the aqueous solution in degrees Celsius.

The sensitivity of the numerical solution to the grid was analysed using grids in the range 10 x 21 (height by width) to 40 x 82. The behaviour of the rate of heat flow was examined for convergence, and it was found that the rate of heat flow was relatively independent for grids in excess of 35 x 72 (less than 0.5% variation in the percentage rectification above this mesh size, compared with 2.2% variation in this parameter in going from a 10 x 21 to 15 x 31 grid). A range of time steps was also tested, and it was found that the solution was relatively independent of step size for time steps in the range 1.0-5.0s; a time step of 1.0s was used in these numerical investigations.

4.4.2 Optimization studies

The optimal conditions for the water-saline diode are explored using the models described in this section. There are five explorations; the first exploration changes the boundary temperatures while keeping the gradient constant, the second exploration applies the previous exploration to various gradients, the third exploration increases the length while keeping the temperature difference constant, the fourth exploration keeps the aspect ratio of the diode constant but varies the scale and the final exploration keeps the gradient constant while increasing the number of partitions.

The first four explorations exploited the scripting ability of Comsol Multiphysics, this feature allowed the model to be established and solved several times without user intervention. Configuring the model inside two loops performed the exploration of the changing boundary temperatures and the changing gradients. The internal loop has two increments, the first increment solves the model for heat flowing from left to right and the second increment solves the model for heat flowing in the opposite direction. Each increment of the external loop changed the boundary temperatures, entered the inside loop (hence solving the model for both directions of heat flow), and saved the results to a data file. The investigation of the influence of the length of the cavity on the percentage rectification was performed in a similar manner; each external loop changed the length of the chamber, entered the internal loop (hence solving the model for both directions of heat flow), and saved the results to a data file. The procedure used for these three investigations is presented

graphically by the flow diagram in Figure 4.4-2. Asymmetrical heat transfer through multiple enclosures side by side was investigated using the graphical user interface.

The procedure for exploring the percentage rectification was slightly different to that for verifying the experimental results. Only one model was used to obtain the percentage rectification in the verification procedure while two models were used in the exploration of the maximum obtainable percentage rectification. When verifying the experimental results, the boundary temperatures were interchanged within the model. In contrast, the four explorations obtained the percentage rectification by solving the model once for the boundary temperatures arranged so that heat flows from left to right and once for the boundary temperatures arranged so that heat flows in the opposite direction. This procedure was more convenient and faster than the procedure used in the verification model. However, the approach used in the verification procedure was necessary as it was the same approach used in the experimental procedure, and it was desirable to keep the conditions of the CFD identical to those of the experiment so that the two sets of results could be compared.

The influence of the bounding temperatures on the percentage rectification was investigated by selecting a constant temperature difference of 4°C and changing the mean temperature of the temperature difference from 0°C to 6°C in steps of 0.01°C . This procedure was applied to a selection of temperature differences ranging from 1°C to 8°C .

The influence of the length of the cavity on the percentage rectification was investigated using the scripting feature in Comsol Multiphysics. The temperature difference across the cavity was chosen to be 4°C and the boundary temperatures were chosen to be 5°C and 1°C . The length of the cavity was varied from 0.02 m to 0.22m in steps of 0.002m. In contrast, the influence of the scale of the diode was investigated by varying the size of the diode but keeping the aspect ratio constant.

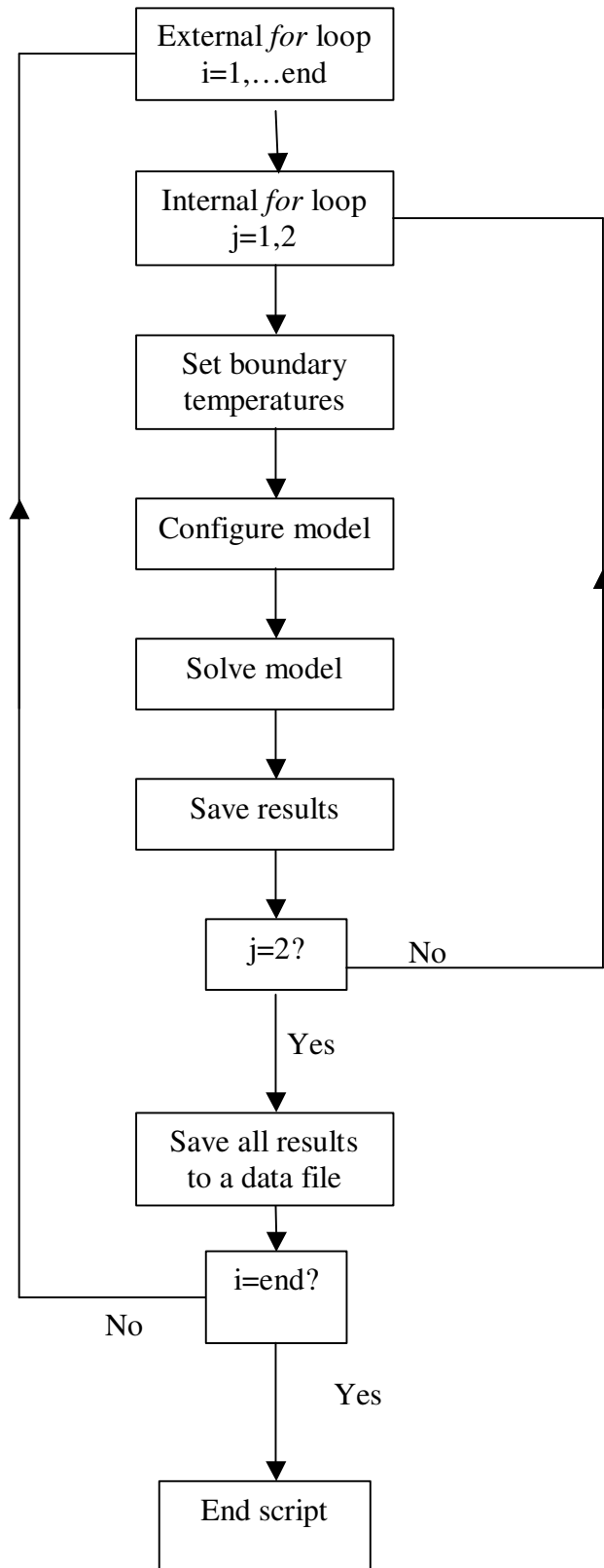


Figure 4.4-2 Flow diagram of the scripting procedure for exploring the maximum obtainable percentage rectification.

The influence of the number of compartments in the cavity was investigated by keeping the temperature gradient constant at $16.667^{\circ}\text{C}\cdot\text{m}^{-1}$ (1°C temperature difference across a compartment of length 0.06m) while changing the length of the cavity as shown in Figure 4.4-3. The addition of a compartment increased the temperature difference across the composite by 1°C . Each compartment contained water with a different temperature of maximum density. The temperature difference between the temperatures of maximum density for consecutive compartments was 1°C . The compartment on the extreme left had a temperature of maximum density at 4°C .

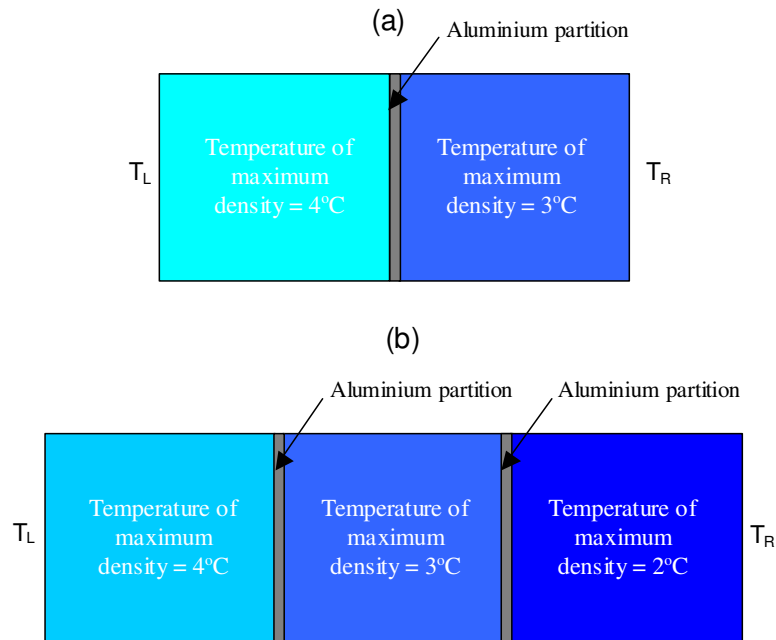


Figure 4.4-3 The influence of the number of liquid compartments in the diode on the percentage rectification is investigated by adding compartments to the rectifier. (a) The typical construction of the water-saline diode. (b) The addition of one compartment to the water-saline diode shown in (a).

The sensitivity of the numerical solution to the grid was analysed using grids in the range 10×21 (height by width) to 40×82 . The behaviour of the rate of heat flow was examined for convergence, and it was found that the rate of heat flow was relatively independent for grids in excess of 35×72 (less than 0.5% variation in the percentage rectification above this mesh size, compared with 2.2% variation in this

parameter in going from a 10 x 21 to 15 x 31 grid and the rate of heat flowing into the enclosure was equal to the rate of heat flowing out of the enclosure for grids in excess of 35 x 72).

4.4.3 Phase change diode

The chamber consisting of two identical square enclosures side by side (used in the previous investigations and shown in Figure 4.4-1) was investigated for asymmetrical heat transfer when it contained a liquid and a phase change material or a solid and a phase change material. When heat flows in a certain direction, the phase change material was in its liquid state and when the direction is reversed, the PCM is in its solid state. Since heat is transferred more efficiently by convection than by conduction the rate of heat flow is considerably reduced when the PCM is in its solid state.

The procedure for investigating asymmetrical heat transfer through this arrangement is similar to the arrangement for the two liquids described in the previous two subsections. Since there are essentially two possible combinations for observing asymmetrical heat transfer in the vicinity of a phase change, they will both be discussed separately. The first combination to be discussed will be the liquid and the PCM. The geometry used and the boundary conditions imposed on this configuration are identical to the geometry used for the two liquids and the boundary conditions imposed on it (Figure 4.4-1). The no slip boundary condition was imposed on all walls in contact with a liquid, the horizontal walls had the adiabatic condition imposed on them, and the vertical walls on the extreme left and right of the geometry had isothermal conditions. The two internal boundaries had the continuity condition imposed on them. The two isothermal walls had temperatures of 2°C and -2°C.

The domain on the left contained water (PCM) that had a freezing point at 0°C and the domain on the right contained water with an artificial freezing point at 3°C. The density of water varies with temperature in the body force term of the Navier-Stokes equation and it assumed constant everywhere else. All other properties of liquid water and ice water are assumed constant. There is a discontinuity in the properties of water when the temperature reaches its freezing point; this discontinuity is

removed by inserting a smooth step function at the freezing point. The properties of the substances are constant when the substances are in their solid state and in their liquid state. The thermal conductivity, the specific heat capacity, the viscosity and the density of water with a freezing point at 0°C are plotted in Figure 4.4-4.

The Navier-Stokes equation and the continuity equation were solved at all times in the liquid domain and in the PCM domain. Since the Navier-Stokes equation and the continuity equation are not required in the PCM domain when it is in its solid state their influence is considerably reduced by setting the viscosity to 2Pa.s when the PCM is in its solid state. It is not necessary to include the latent heat of solidification in this study since this phenomenon is a purely transient effect and these investigations are only concerned with steady state behaviour.

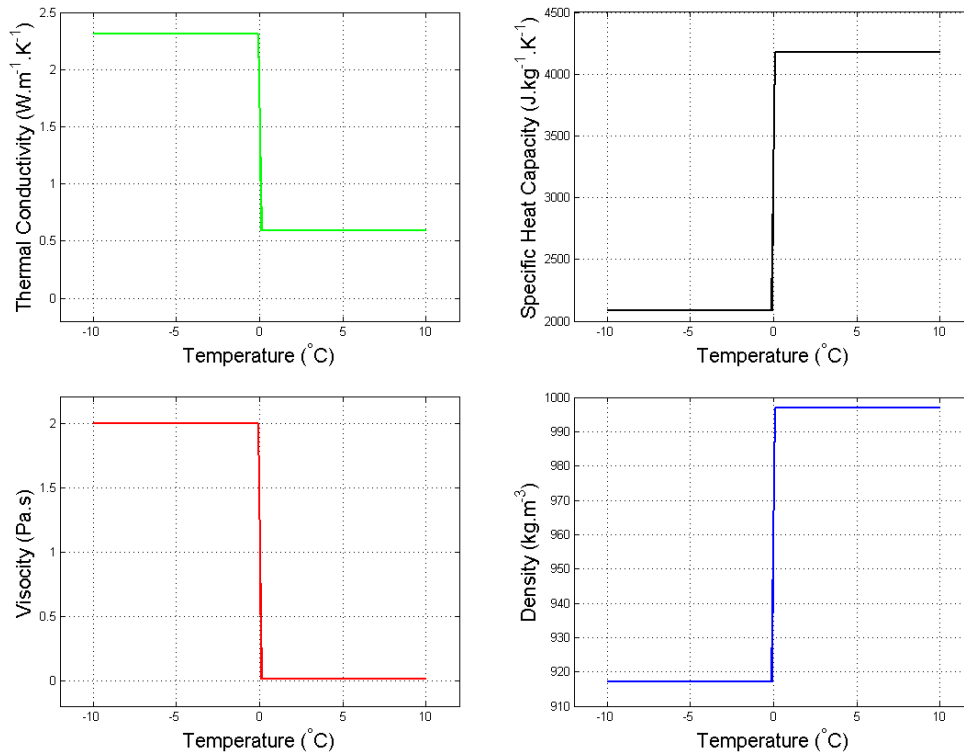


Figure 4.4-4 The properties of water (PCM) used in the investigation of the thermal diode effect in a water-saline diode containing a PCM.

When the temperature of the wall on the left, T_L , and the temperature of the wall on the right, T_R were at -2°C and 2°C, respectively, the initial temperature of the first domain (PCM) was -1°C and the initial temperature of the third domain (liquid) was 1°C. When the wall temperatures were swapped the initial temperature of the PCM

was 1°C and the initial temperature of the liquid was -1°C . The initial velocities were 0m.s^{-1} and the initial temperature of the aluminium partition was 0°C regardless of the wall temperatures. The rate of heat flow was obtained for both variations of the wall temperatures and the percentage rectification was obtained from these values.

The investigation of asymmetrical heat transfer through a solid and a PCM has a procedure almost identical to that just outlined for the composite of a liquid and a PCM. One difference between the two procedures is the initial conditions for the temperature and the boundary conditions for the temperature. The temperature of the wall on the left was -1°C and the temperature of the wall on the right was -5°C . The initial temperatures for the first and third domains were -2°C and -4°C , respectively. When the temperatures of the sidewalls are swapped the initial temperatures for the first and third domain are -4°C and -2°C , respectively. The second domain (aluminium partition) has an initial temperature of -3°C regardless of the boundary temperatures. An additional difference in this configuration is that water with a freezing point at 0°C in the first domain is a solid and the PCM is water with an artificial freezing point at -3°C in the third domain.

The sensitivity of the numerical solution to the grid was analysed using grids in the range 10×21 (height by width) to 40×82 . The behaviour of the rate of heat flow was examined for convergence, and it was found that the rate of heat flow was relatively independent for grids in excess of 35×72 (less than 1.0% variation in the percentage rectification above this mesh size, compared with 2.4% variation in this parameter in going from a 15×31 to 20×41 grid and the rate of heat flowing into the enclosure was equal to the rate of heat flowing out of the enclosure for grids in excess of 35×72).

4.4.4 Water-Perspex diode

The thermal diode effect can be observed in a composite system of a liquid (water) and a solid (Perspex). The purpose of these investigations is to understand the thermal diode effect observed in this system and to obtain the conditions that provide the maximum percentage rectification.

The thermal diode effect is observed in the geometry shown in Figure 4.4-5, the total length of the system is 0.12 m and the height of the system is 0.06 m. The properties of water are taken from reference [1] and the thermal conductivity of Perspex is $0.2\text{W}\cdot\text{m}^{-1}\cdot\text{K}^{-1}$. The Navier-Stokes equation, the continuity equation and the heat equation are solved on the domain containing water and the heat equation is solved on the Perspex domain. The no slip boundary condition is imposed on all boundaries in contact with water. The boundaries on the extreme left and right of the geometry shown in Figure 4.4-5 are isothermal and all the horizontal boundaries are considered to be adiabatic. There is just one internal boundary separating the water from the Perspex, this boundary has the continuity condition imposed on it.

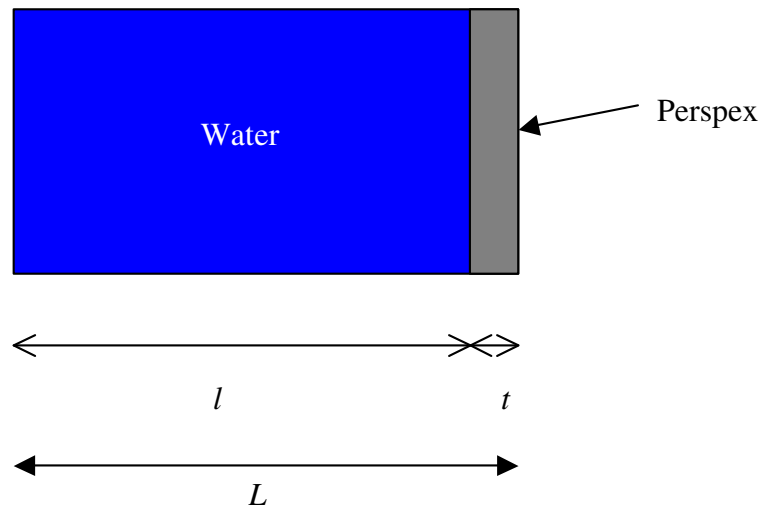


Figure 4.4-5 A composite system that exhibits the thermal diode effect. The length of the entire system (L) does not change during the investigations. The influence of the ratio of the length of the Perspex (t) to the length of the water compartment (l) on the thermal diode effect is investigated.

The experimental results are simulated by varying the temperature of the two sidewalls with time; the boundary temperatures are held at $T_L=6.5^\circ\text{C}$ and $T_R=2.5^\circ\text{C}$ for 30,000 seconds. After 30,000 seconds the boundary temperature, T_L , is incremented by 0.1°C and the boundary temperature, T_R , is decremented by 0.1°C every 1,200 seconds until the T_L and T_R are 2.5°C and 6.5°C , respectively. The

boundaries are held at these temperatures for 30,000 seconds. These conditions are equivalent to the boundary conditions imposed on the system in the experimental investigations. The initial velocity of the liquid was set to zero and the initial temperatures of the water domain and the Perspex domain were set to 5.5°C and 3.5°C, respectively.

The optimal conditions of the water-Perspex diode are investigated by varying the boundary temperatures and the width of the Perspex slab. A constant temperature difference is maintained in all optimization investigations. Each model is solved twice for each set of boundaries, once for $T_L=T_h$ and $T_R=T_c$ and once for $T_L=T_c$ and $T_R=T_h$. In the investigation of the influence of the boundary temperatures on the rectification, the values of T_h and T_c begin at 4°C and 0°C and the model is solved twice for this set of temperatures. The values are incremented by 0.01°C, and the model is solved twice for each increment, until the boundaries have reached the temperatures of 8°C and 4°C. The influence of the width of the Perspex slab on the rectification is investigated by applying this procedure to eight different widths of Perspex. The Perspex thickness has values of 1mm, 2mm, 3mm, 4mm, 5mm, 6mm, 7mm, and 8 mm and the corresponding values for the length of the compartment of water are 119mm, 118mm, 117mm, 116mm, 115mm, 114mm, 113mm, and 112mm.

The sensitivity of the numerical solution to the grid was analysed using grids in the range 15 x 34 (height by width) to 40 x 79. The behaviour of the rate of heat flow was examined for convergence, and it was found that the rate of heat flow was relatively independent for grids in excess of 35 x 74 (less than 0.1% variation in the percentage rectification above this mesh size, compared with 1.5% variation in this parameter in going from a 15 x 34 to 20 x 59 grid and the rate of heat flowing into the enclosure was equal to the rate of heat flowing out of the enclosure for grids in excess of 35 x 74). A range of time steps was also tested, and it was found that the solution was relatively independent of step size for time steps in the range 1.0-5.0s; a time step of 1.0s was used in these numerical investigations.

Chapter 5

Numerical Results

5.1 Introduction

This chapter discusses the numerical results from the investigations of the temperature of maximum density and asymmetrical heat transfer. The aims of the numerical investigations are to confirm the experimental results, to aid understanding of the experimental results and to explore further possibilities that could not be easily achieved experimentally. All of the results presented in this chapter have been obtained using the commercial package Comsol Multiphysics. Comsol Multiphysics solves the Navier-Stokes equations and the heat equation on a specified geometry

Asymmetrical heat transfer is found in composites of water and aqueous solutions and in composites of water and solids. Experimentally, the study of asymmetrical heat transfer through a composite of water and an aqueous solution requires knowledge of the temperature of maximum density of some aqueous solutions. For this purpose an experimental technique was developed to measure the temperature of maximum density of aqueous solutions. The technique relies on the convective flow pattern in the vicinity of the density maximum as a liquid is cooled in a quasi-steady state manner. The convective flow pattern due to the density maximum causes the occurrence of an anomaly feature in the temperature profiles at five equally spaced points along the central horizontal axis. This anomaly feature observed in the experimental results is confirmed by the numerical results and its occurrence is explained by examining the velocity and temperature fields at select times during the cooling procedure. The experimental results present the anomaly feature for a container with dimensions of 0.06m x 0.06m x 0.12m (width x height x length) and a container with dimensions of 0.10m x 0.10m x 0.10m. The anomaly feature for two different containers are presented since the first container is used for the measurement technique presented in Cawley *et al.* [61] and the second container is used for experimental investigations of the fluid flow. Since the first container is used for measuring the temperature of maximum density of aqueous solutions, the numerical studies investigate the occurrence of the anomaly feature for this geometry. Comparisons between the numerical model and the experimental results are conducted for a geometry that matches the dimensions of the second container since this container is used experimentally for flow visualization.

Experimentally it has been shown that the rate of heat transfer is reduced in the vicinity of the density maximum. This behaviour has been observed previously by Lin and Nansteel [29] and Tong [30], and their results are compared to results from this study of heat transfer. It is suggested by Lin and Nansteel [29] that the reduction in the rate of heat transfer is due solely to the insulating nature of the two counter rotating convection cells that occurs within the fluid due to the density maximum. The behaviour of heat transfer in the vicinity of the density maximum is investigated in this chapter using computational fluid dynamics and it is shown that Lin and Nansteel's explanation is incomplete. The reduction in heat transfer is due to two factors: the formation of two counter rotating cells (as reported by Lin and Nansteel) and the flattening of the density state function of water near the density extremum. The formation of two counter rotating cells reduces direct thermal communication between the hot and cold walls and the flattening of the density state function near the extremum results in an overall reduction in buoyancy as the convective velocity is reduced.

The rate of heat transfer and the rate of cooling during the quasi-steady state cooling of water are simulated in this chapter and the results are compared to the experimental results. The numerical results are in good agreement with the experimental results and the numerical model confirms the explanation given in section 3.3.2 for the occurrence of the features in the rate of heat transfer and the rate of cooling. The numerical model permits examination of the velocity field and the temperature field during the quasi-steady state cooling, thereby aiding understanding of the behaviour of the rate of heat transfer and the rate of cooling in the vicinity of the density maximum.

The novel measurement technique presented in section 3.3.3 and described in Cawley *et al.* [61] relies on a chi-squared comparison between the anomaly feature in the temperature profiles of water and the anomaly feature in the temperature profiles of the aqueous solution when they are cooled in the same quasi-steady state manner. This technique is validated numerically in this chapter by comparing the anomaly features in the temperature profiles of water with a density maximum at 4°C and water with a density maximum at 3°C. A second measurement technique is presented experimentally in section 3.3.3. This measurement technique relies on the

chi-squared comparison of the density anomaly feature in the rate of cooling of water to the density anomaly feature in the rate of cooling of the solution. This technique is also validated numerically in this chapter.

Since the novel measurement technique based on the anomalous feature in the temperature profiles as described in Cawley *et al.* [61] is used for the experimental investigation of the behaviour of the temperature of maximum density of aqueous solutions it is important to investigate the behaviour of the anomalous feature under various conditions. These conditions are investigated to a certain extent experimentally, but a more detailed investigation is conducted numerically. Experimentally, it was observed that the dimensions of the container influenced the shape of the anomaly feature. This behaviour is confirmed numerically and it is further investigated by simulating the anomaly feature for various aspect ratios. The addition of solutes to water alters the properties of water and this prompts the numerical investigation of the influence of the properties of water on the shape of the anomaly feature. Experimentally, the temperature probes are inserted into the liquid at a depth of 0.03m for the container with a height of 0.06m. Thus, the influence of the depth of the temperature probes on the anomaly feature is investigated numerically.

Experimentally, asymmetrical heat transfer is observed in a composite system of water and a saline solution and in a composite system of water and Perspex. The numerical investigations confirm the experimental results and they aid understanding of the results through the analysis of the velocity field and the temperature field. The numerical investigations explore the possibility of increasing the percentage rectification of both the water-saline diode and the water-Perspex diode. The optimisation studies of the water-saline diode investigate the influence of the size of the diode, the influence of the bounding temperatures and the influence of the number of liquid compartments on the percentage rectification. The optimisation studies of the water-Perspex diode investigate the influence of the bounding temperatures and the influence of the width of the Perspex slab on the percentage rectification. The numerical studies extend the experimental investigations through the optimisation studies. In thermal engineering, there exists a thermal analogy to Ohm's Law. This analogy is described at the end of this chapter and it provides an

alternative approach to the illustration of the mechanism by which asymmetrical heat transfer arises.

5.2 The density maximum of aqueous solutions

This section presents the CFD investigations relating to the temperature of maximum density of aqueous solutions. The first investigation shows the behaviour of the quasi-steady state cooling of ethanol as described in Cawley *et al.* [61] and the results are presented in section 5.2.1. These results are directly comparable to the experimental results presented in Figure 3.3-1. The numerical results confirm the experimental results and they aid the understanding of the experimental results.

The second investigation is presented in section 5.2.2 and it is concerned with the quasi-steady state cooling of water. The numerical model investigates the behaviour of the temperature profiles in the vicinity of the density maximum and the behaviour of the velocity field and the temperature field in the vicinity of the density maximum. The first model presented in this section uses a geometry with dimensions of 0.06m x 0.12m (height x length). This geometry represents the container used for the measurement of the temperature of maximum density of aqueous solutions and the temperature profiles for this model can be compared directly to the experimental results in Figure 3.3-2. A second model simulates the temperature profiles and the velocity field for a geometry with dimensions of 0.10m x 0.10m. This geometry represents the experimental container that is used for the flow visualization in the experimental results presented in section 3.3.1 and in Mooney and Cawley [63]. The numerical results for this model are compared to the experimental results in section 5.2.2.

The third investigation relating to the temperature of maximum density of aqueous solutions is presented in section 5.2.3. This section discusses the rate of heat transfer in the vicinity of the density maximum. Numerical results from this study are compared to results from other researchers [29], [30] and the behaviour of the rate of heat transfer is explained. The fourth investigation is also related to heat transfer and it examines the behaviour of the rate of heat transfer and the rate of cooling in the vicinity of the density maximum during the quasi-steady state cooling as described in Cawley *et al.* [36]. The results of this investigation are presented in section 5.2.4.

The fifth investigation verifies the chi-squared measurement technique used experimentally for obtaining the temperature of maximum density of aqueous solutions as described in Cawley *et al.* [61]. Experimentally the temperature of maximum density of aqueous solutions is obtained by comparing the anomaly feature in the temperature profiles of the aqueous solution to those of water. An alternative experimental technique is presented that compares the anomaly feature in the rate of cooling of the aqueous solution to the rate of cooling of water. The comparison for both of these techniques is conducted using a chi-squared comparison. Therefore, it is important to investigate the validity of the chi-squared comparison and this is done in section 5.2.5.

Section 5.2.6 presents the results of the investigation of the influence of various parameters on the shape of the anomaly feature. It is important to investigate the shape of the anomaly feature as it has been observed experimentally that the addition of solutes to water alters the shape. Furthermore, the experimental measurements of the temperature of maximum density of aqueous solutions presented in section 3.3.4 rely on the anomaly feature in the temperature profiles.

5.2.1 Quasi-steady state cooling and warming of Ethanol

The experimental results of the quasi-steady state cooling of ethanol are reproduced numerically by modelling a 2-D slice of the 3-D experimental chamber. The 2-D slice has dimensions of 0.12m x 0.06m (width x height). Ethanol is cooled from an average temperature of 8°C to 0°C by varying the temperature of the two opposing vertical boundaries from 10°C and 6°C to -2°C and 2°C, respectively. The temperature of the left wall begins at 10°C and it is decremented by 0.1°C every 540 seconds until it reaches -2°C. Simultaneously, the temperature of the right wall is decremented from 6°C by 0.1°C every 540 seconds. The duration of the entire procedure is 43,740 seconds.

The numerical results of cooling ethanol from an average temperature of 8°C to 0°C in a quasi-steady state manner are shown in Figure 5.2-1. It is evident from the graph that the temperatures at the five points are within 0.1°C of each other. This implies that in the central region of the liquid there is almost no transfer of heat in the

horizontal direction. The thermistor profiles may be understood by noting that warmer liquid becomes less dense and rises along the warm wall to the top of the container. Colder more dense liquid descends along the cold wall to the bottom of the container. As described in Cawley *et al.* [61], this behaviour sets up a clockwise convection cell as shown in Figure 5.2-2. The movement of the warm ethanol from the left of the container to the top, and the movement of the cold ethanol from the right of the container to the bottom sets up an almost vertical temperature gradient within the fluid. Heat flows from the top of the container, through the central region where the thermistors are located, to the bottom of the container, primarily by conduction. It is this rearrangement of the gradient by the fluid flow in the boundary regions that dominates the temperature distribution in the central region and thus the temperatures at the five points are similar. This behaviour of the temperature field and the velocity field persist throughout the entire cooling process and it also occurs during the warming of ethanol, the temperature profiles of which are shown in Figure 5.2-3.

The numerical plot in Figure 5.2-1 is directly comparable to the experimental plot in Figure 3.3-1. Discrepancies between the experimental results and the CFD results can be ascribed to the approximations in the CFD calculations, the departure from the ideal conditions in the experiment, and the assumption that the two-dimensional geometry represents a two-dimensional slice of a three dimensional chamber. The overall trend of the CFD temperature profiles is in good agreement with the experimental results. In both the numerical and the experimental plots, the temperature profiles are closely bunched together as the liquid is cooled from an average temperature of 8°C to 0°C.

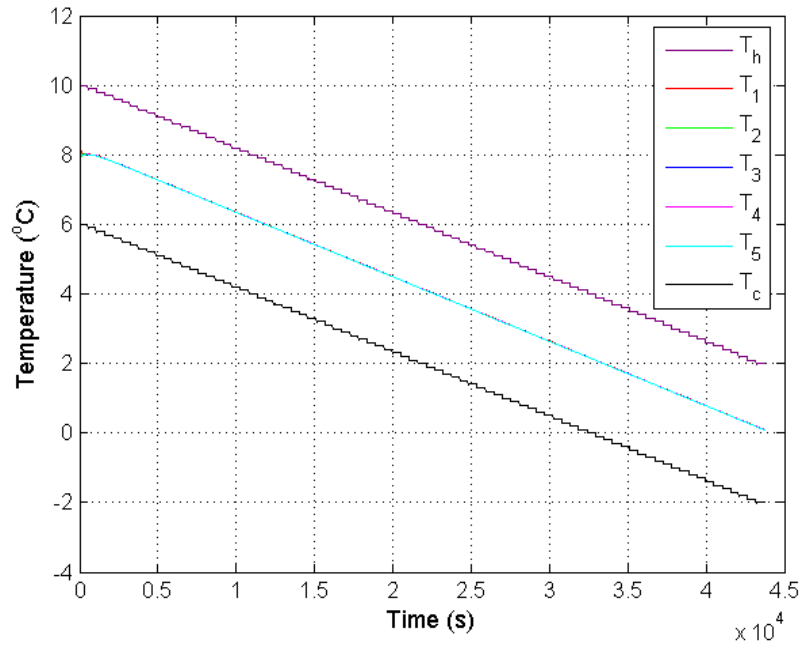


Figure 5.2-1 Numerical results for the temperature against time for the cooling of pure ethanol in a rectangular enclosure. Curves T_1 through T_5 lie on top of each other. ($Ra \approx 6.5 \times 10^8$).

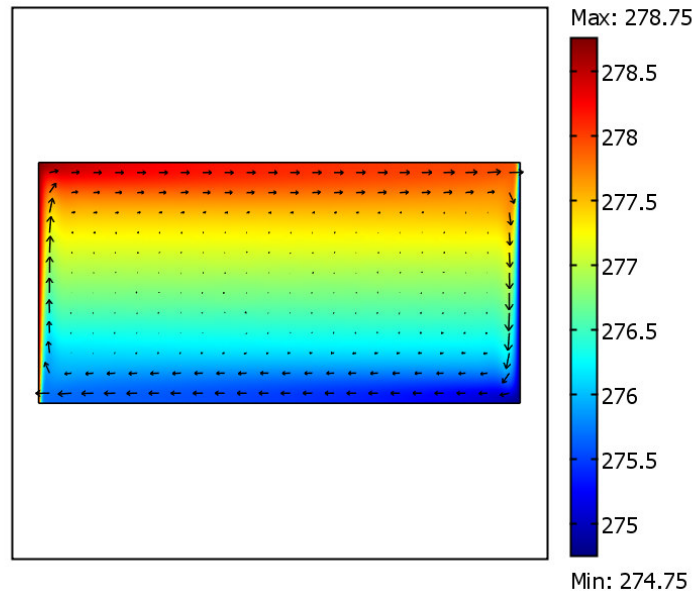


Figure 5.2-2 A plot of the temperature field (surface plot) and the velocity field (arrow plot) in the fluid domain for ethanol corresponding to a time of 25,000 seconds in Figure 5.2-1.

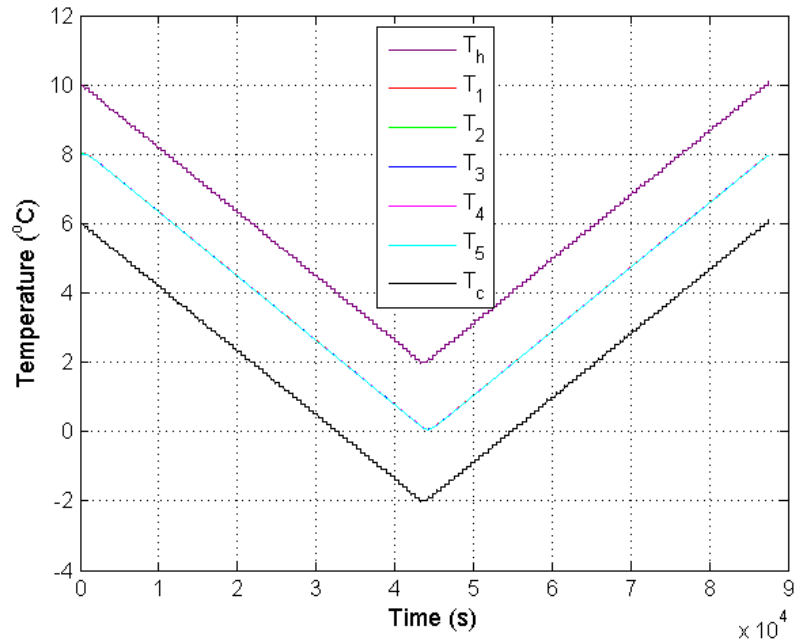


Figure 5.2-3 Numerical results for the temperature against time for the cooling and warming of pure ethanol in a rectangular enclosure. Curves T_1 through T_5 lie on top of each other. ($Ra \approx 6.5 \times 10^8$).

The temperature profiles T_1 to T_5 in Figure 5.2-1 are superimposed on each other as they lie on the same isotherm. If the dimensions of the container changes the behaviour of the isotherms change. Figure 5.2-4(h) shows that the isotherm for a container with the same aspect ratio (width / height) as the container used for the plot in Figure 5.2-1 is horizontal in the central region. The plots in Figure 5.2-4 show the behaviour of the isotherms as a function of aspect ratio. It is evident from each of these plots that the isotherms are almost vertical at the hot and cold walls, regardless of the aspect ratio. As the aspect ratio increases, the separation between the hot and cold walls increases and the behaviour of the isotherms in the central region changes from vertical lines to lines with positive slopes to horizontal lines. The isotherms continue changing as the aspect ratio increases and the horizontal lines become lines with negative slopes to being horizontal again. Increasing the aspect ratio beyond 0.8 yields isotherms that are horizontal in the central region as shown in Figure 5.2-4.

When the aspect ratio is 0.1 the isotherms are vertical throughout the container as shown in part (a) of Figure 5.2-4. Consequently, five equally spaced points along the

central horizontal axis in this container will exhibit different temperatures from each other. The narrow width between the two isothermal walls does not readily permit the movement of warm liquid at the bottom of the hot wall to the top of the container; and similarly it does not permit the movement of cold liquid at the top of the cold wall to the bottom of the container. This constraint on the flow of the liquid results in the transfer of heat primarily by conduction. Consequently, the isotherms shown in part (a) of Figure 5.2-4 are vertical in the central region.

When the aspect ratio increases from 0.1 to 0.2 the isotherms have a positive slope in the central region. This also gives rise to different temperatures at the five equally spaced points as they are still on different isotherms as shown in part (b) of Figure 5.2-4. The change in the slope of the isotherm in the central region is due to the increased space in the centre of the container. The increased space between the hot and cold walls allows more hot liquid to move to the top of the container and more cold liquid to move to the bottom. The downward flow of liquid at the cold wall and the upward flow of liquid at the hot wall are influential on the isotherms in the centre of this geometry as the space between the boundary flows is very narrow. When the aspect ratio is changed from 0.2 to 0.22, the isotherms are almost horizontal in the central region and when the aspect ratio changes from 0.22 to 0.4 the behaviour of the isotherms in the centre of the container is that of a line with a negative slope. The flows at the hot and cold wall are still influential for these aspect ratios but their influence weakens as the aspect ratio increases. When the aspect ratio changes from 0.4 to 0.6 the distance between the flows at the hot wall and the cold wall has increased, to the point where the isotherms are less influenced by the hot and cold wall flows and more influenced by the top and bottom wall flows. This results in the behaviour of the isotherms in the central region changing from lines with negative slopes to horizontal lines as the aspect ratio increases. The distance between the hot and cold walls for an aspect ratio of 0.8 becomes too large for the flows at these walls to influence the isotherms in the central region. Thus, increasing the aspect ratio beyond this point yields isotherms that are horizontal in the central region of the container.

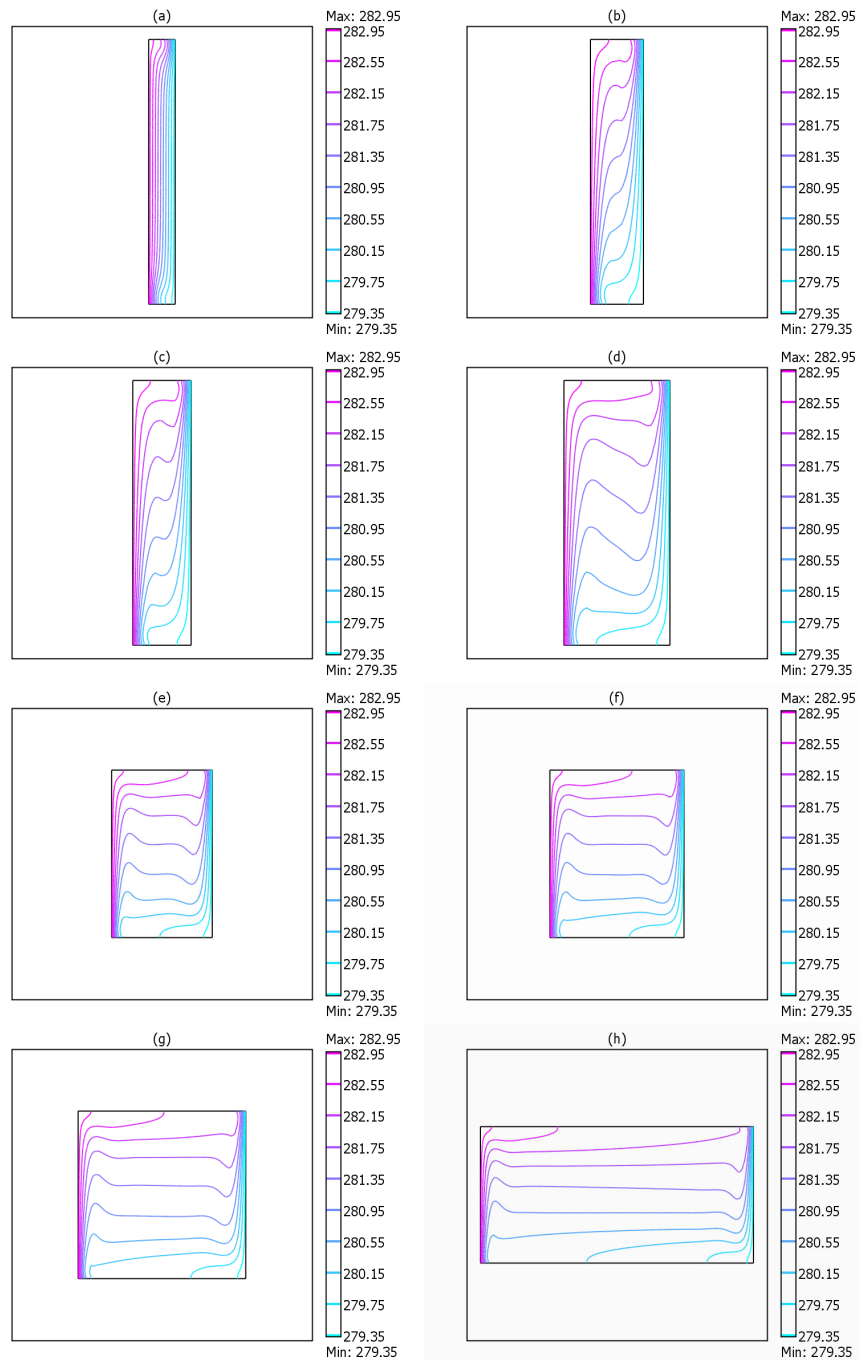
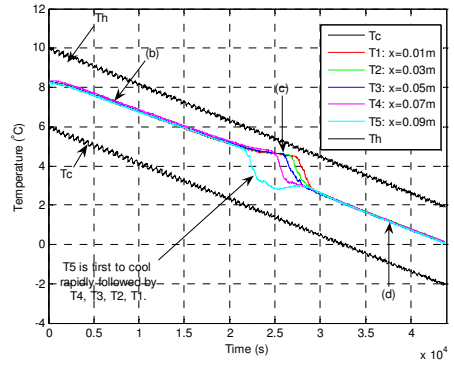
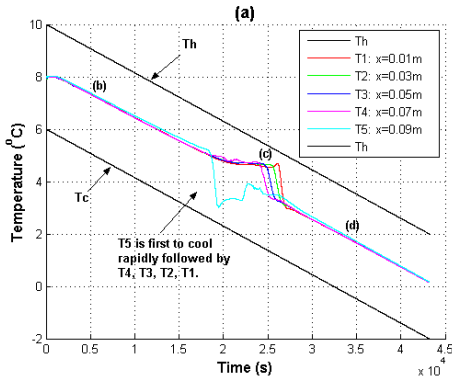


Figure 5.2-4 The isotherms for a rectangular enclosure of water with a constant horizontal temperature gradient across it (the left wall has a temperature of 10°C and the right wall has a temperature of 6°C). In each plot from (a)-(h), the height of the enclosure is 0.05m but the width changes. The aspect ratio (α) and width (w) of the enclosure in each plot is: (a) $\alpha=0.1$, $w=0.005\text{m}$, (b) $\alpha =0.2$, $w=0.01\text{m}$, (c) $\alpha=0.22$, $w=0.011\text{m}$, (d) $\alpha =0.4$, $w=0.02\text{m}$, (e) $\alpha =0.6$, $w=0.03\text{m}$, (f) $\alpha =0.8$, $w=0.04\text{m}$, (g) $\alpha =1.0$, $w=0.05\text{m}$, and (h) $\alpha =2$, $w=0.10\text{m}$.

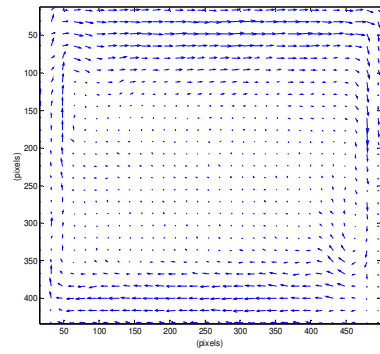
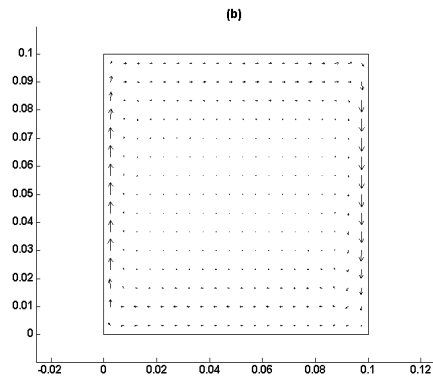
5.2.2 Quasi-steady state cooling and warming of Water

This section aims to simulate the experimental results in section 3.3.1 and to further understand and investigate the anomaly feature in the temperature profiles. Experimentally, a rectangular container of water is cooled from a mean temperature of 8°C to 0°C by changing the temperature of the two opposing vertical walls (all other walls are insulated) from 10°C and 6°C to 2°C and -2°C, respectively. As described in Mooney and Cawley [63], the wall temperatures are simultaneously decremented by 0.1°C every 540 seconds for a time span of 43,740 seconds. This experiment is simulated using the procedure outlined in section 4.3.1. It is assumed that a 2-D slice of the 3-D experimental container adequately describes the experimental conditions. The Navier-Stokes equations and the heat equation are solved on the 2-D domain for water with properties that vary with temperature (taken from reference [1]). The two vertical walls are isothermal and the two horizontal walls are adiabatic. All of the walls have the no slip condition imposed on them.

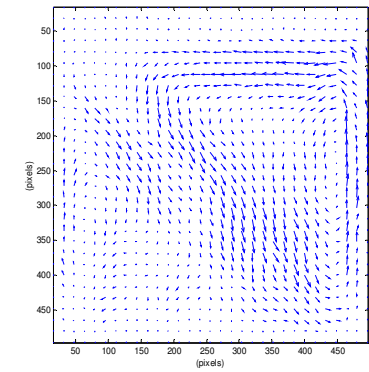
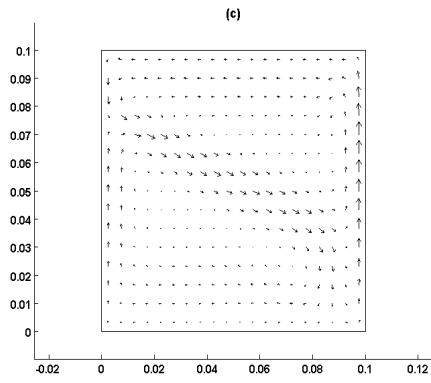
The results of this model for a container of dimension 0.10m x 0.10m are presented in Figure 5.2-5 along with the corresponding experimental results. As described in Mooney and Cawley [63], the overall trends of the CFD temperature profiles and the CFD velocity profiles are in good agreement with the experimental results. The temperature profiles show the expected plateaux followed by the sharp descent in temperature. This feature is centred on 4°C in both the experimental and numerical results. The convective flow pattern generated by the numerical model reveals the single clockwise convective cell at the start of the cooling sequence and the growth of the counter-clockwise cell from the cold boundary across the chamber until it completely dominates the convective flow. This agrees with the experimental results obtained from PIV. Discrepancies between the experimental results and the CFD results can be ascribed to the approximations in the CFD calculations, the departure from the ideal conditions in the experiment, and the assumption that the two-dimensional geometry represents a two-dimensional slice of a three dimensional chamber.



(b)



(c)



(d)

(d)

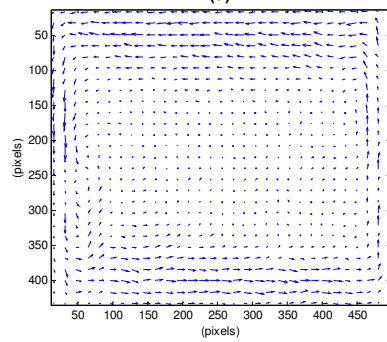
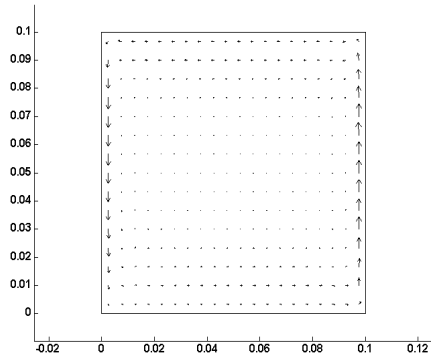


Figure 5.2-5 CFD results (left column) Vs Experimental Results (right column).

This model is applied to a rectangular geometry with dimensions of 0.06m x 0.12m (height x width) and the results are presented in Figure 5.2-6. These results are directly comparable to the experimental results presented in Figure 3.3-2 and they are in good agreement with each other. As described in Cawley *et al.* [61], the temperature profiles are closely bunched together at the start of the cooling and as they enter the vicinity of the density maximum, they diverge. When the liquid emerges from its density maximum the profiles converge. This behaviour can be understood by examining the velocity field and the temperature field. Figure 5.2-7 shows plots of the velocity field (quiver plots) and the temperature fields (surface plots) for a selection of times. At the start and the end of the cooling, the temperature profiles are closely bunched together. This bunching together is similar to the behaviour of the temperature profiles for ethanol. Part (b) of Figure 5.2-7 shows the behaviour of the velocity and temperature fields before the anomaly feature when the temperature profiles are closely bunched together. The velocity and temperature fields are similar to those for ethanol. The five temperature points are located in a region of fluid that is relatively undisturbed and the temperature in this region varies vertically. Consequently, the temperature profiles exhibit similar temperatures as each other before the anomaly feature occurs. Part (g) of Figure 5.2-7 shows the velocity and temperature fields after the anomaly feature when the temperature fields are closely bunched together. Unlike part (b) of Figure 5.2-7, the fluid flows in a counter-clockwise direction and the hot water is at the bottom of the container while the cold water is at the top. Despite these differences in the two plots, the temperature profiles are still closely bunched together since the five points are located in a region of fluid that is relatively undisturbed and the temperature in this region varies vertically.

The temperature profiles in Figure 5.2-7 show a slight plateau before a rapid descent in temperature in the vicinity of 4°C. This plateau indicates a reduction in the rate of cooling and the sudden decrease in temperature implies rapid cooling. These features can be understood by examining the behaviour of the convective flow as shown in Figure 5.2-7(b)-(e). When the cold wall reaches 4°C, a small counter-clockwise convection cell develops at the cold wall as described in Cawley *et al.* [61]. This convection cell develops at the bottom since it is the densest liquid. When the counter clockwise cell prevents the clockwise cell from reaching the cold

boundary, as shown in part (d) of Figure 5.2-7, cooling reduces inside the clockwise cell that surrounds the five selected temperature points. The counter-clockwise cell now dominates the cooling since it makes contact with the cold wall. As the counter-clockwise convective cell sweeps across the chamber, it engulfs each of the temperature points and cools them in turn, starting with the point closest to the cold wall. The rapid cooling occurs when the counter clockwise cell initially engulfs a point, that is, when the point is located in moving fluid. The cooling slows down when the point is located in stationary fluid inside the counter-clockwise convective cell. It is evident from both the experimental results (Figure 3.3-2 and Figure 3.3-3) and the numerical results presented in Figure 5.2-3 and Figure 5.2-5, that the shape of the anomaly feature is dependent on the dimensions of the container. This dependency is explored numerically and the results are presented later in section 5.2.6.

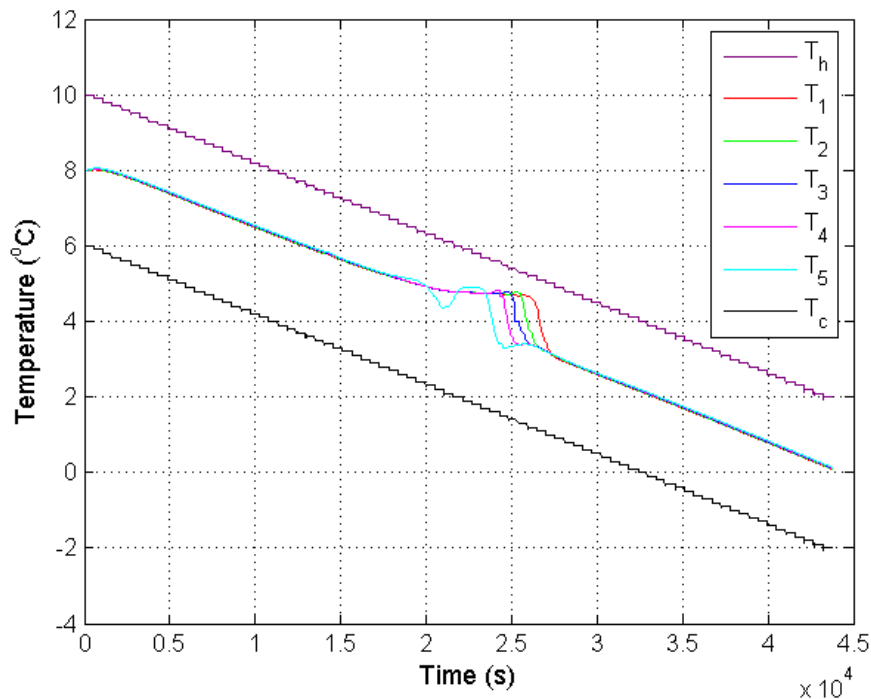


Figure 5.2-6 Numerical results for the temperature against time for the cooling of pure water in a rectangular enclosure. The Rayleigh number ranges from 3.0×10^7 at 8°C to 1.5×10^5 at 4°C and back to 3.0×10^7 at 0°C .

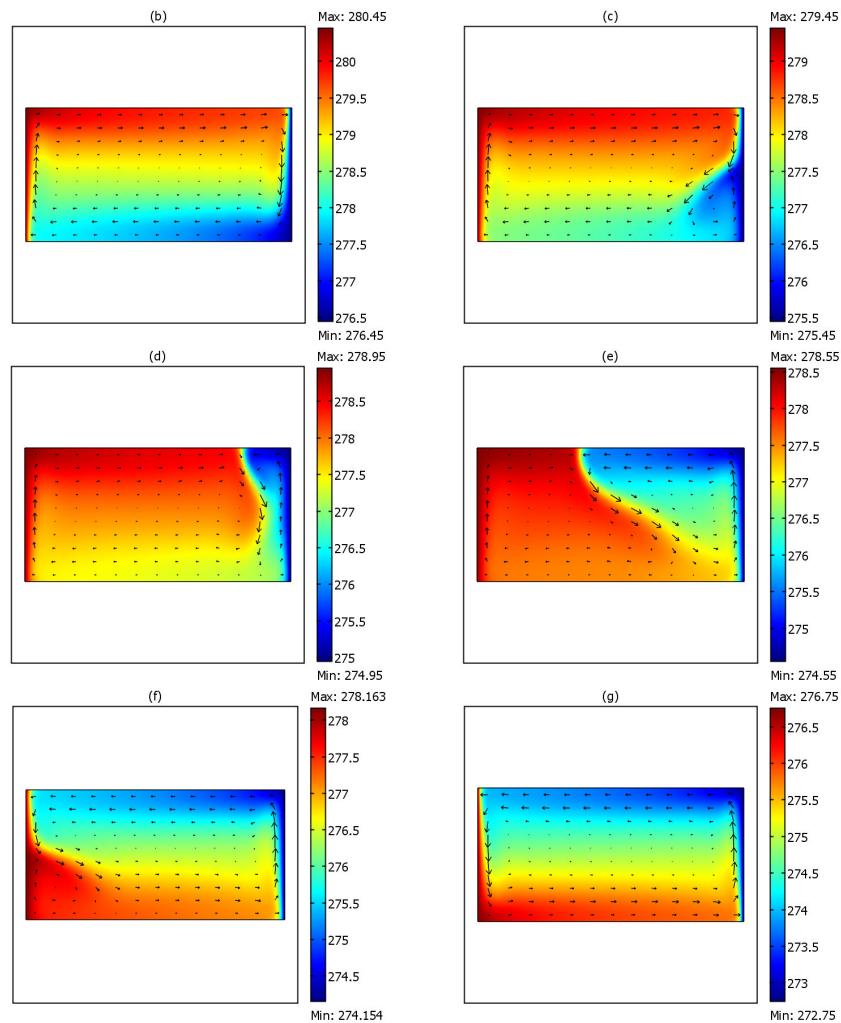
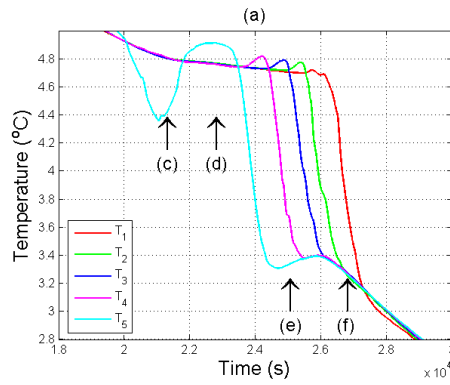


Figure 5.2-7 Detail of Figure 5.2-6. Plots (b)-(g) are the temperature fields (surface plot) and the velocity fields (quiver plot) in the fluid domain corresponding to the following times: (b) 15,000 seconds, (c) 20,050 seconds (d) 23,000 seconds, (e) 25,000 seconds, (f) 27,000, and (g) 35,000 seconds. Arrows in (a) indicate the positions corresponding to plots (c), (d), (e), and (f). (note: the temperature scales change in each of the surface plots).

This model is extended to include the warming of water immediately after it has been cooled and in the same manner that it was cooled. The wall temperatures are simultaneously incremented from 2°C and -2°C by 0.1°C every 540 seconds until they have reached 10°C and 6°C , respectively. The results are shown in Figure 5.2-8. As previously discussed, there is an anomaly feature centred on 4°C in the temperature profiles as water is cooled. A similar feature occurs in the profiles as water is warmed, but there are differences. Firstly, the profiles show a rapid increase in temperature as opposed to the decrease that occurs during cooling. Secondly, the point closest to the hot wall is the first to show this change. This contrasts to the cooling feature where the point closest to the cold wall is the first to deviate from the other points. These differences can be understood by examining the behaviour of the velocity field (quiver plot) and the temperature field (surface plot) as shown in Figure 5.2-9(b)-(g).

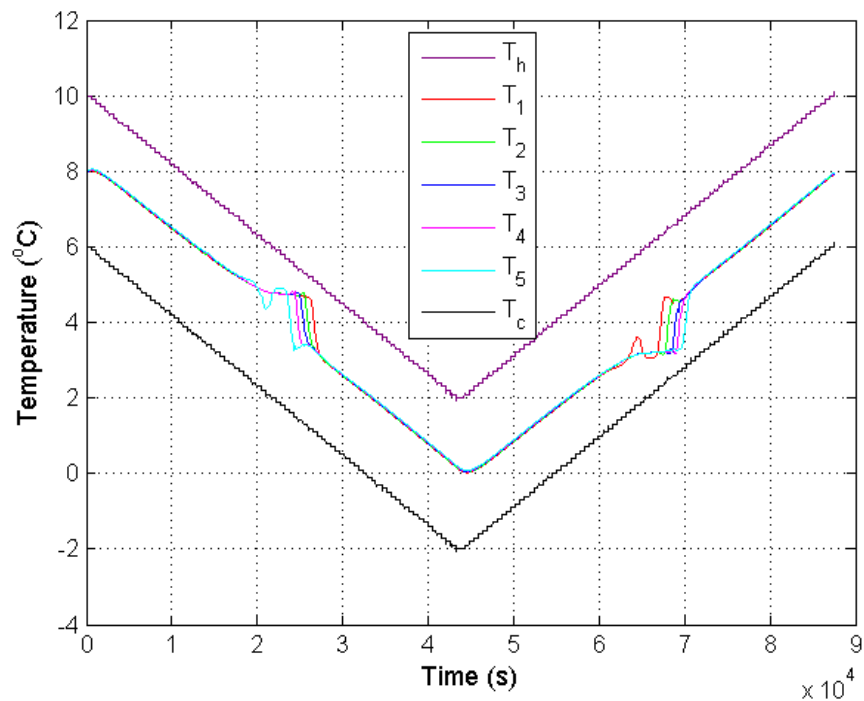


Figure 5.2-8 Numerical results for the temperature against time for the cooling and warming of pure water in a rectangular enclosure. The Rayleigh number ranges from 3.0×10^7 at 8°C to 1.5×10^5 at 4°C and back to 2.9×10^7 at 0°C .

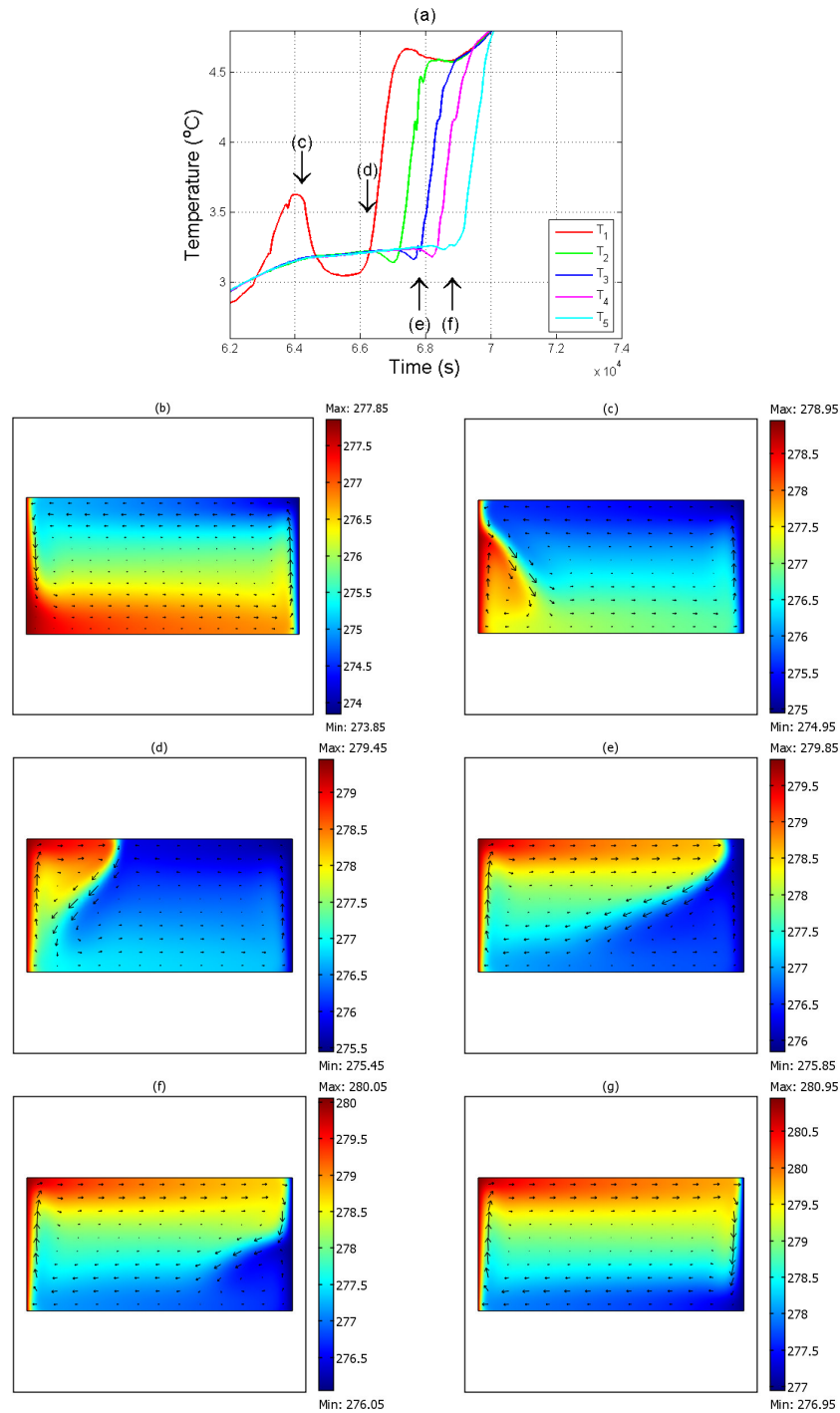


Figure 5.2-9 Detail of the anomaly feature in the warming profiles in Figure 5.2-8. Plots (b)-(g) are the temperature fields (surface plot) and the velocity fields (quiver plot) in the fluid domain corresponding to the following times: (b) 58,740 seconds, (c) 64,050 seconds (d) 66,740 seconds, (e) 68,740 seconds, (f) 69,740, and (g) 75,000 seconds. Arrows in (a) indicate the positions corresponding to plots (c), (d), (e), and (f). (note: the temperature scales change in each of the surface plots).

As water warms from an average temperature of 0°C to 8°C , its convective flow pattern is initially in the counter-clockwise direction. As the temperature increases, the hot wall is the first to reach 4°C so a clockwise convection cell forms at the bottom of the hot wall as shown in part (c) of Figure 5.2-9. When the clockwise cell prevents the counter clockwise cell from reaching the cold boundary, as shown in part (d) of Figure 5.2-7, warming is rapidly reduced inside the counter-clockwise cell that surrounds the temperature points. The clockwise cell now dominates the warming since it makes contact with the hot wall. As the clockwise convective cell sweeps across the chamber from the hot wall to the cold wall, it engulfs each of the temperature points and warms them in turn, starting with the point closest to the hot wall. The rapid warming occurs when the clockwise cell initially engulfs a point, that is, when the point is located in moving fluid. The warming slows down when the point is located in stationary fluid inside the clockwise convective cell.

5.2.3 Heat transfer in the vicinity of the density maximum

Heat flows through a differentially heated cavity containing a fluid via free convection and conduction, consequently the behaviour of the velocity field inside the cavity is of critical importance to heat transfer through the cavity. The rate of heat flow is influenced by the velocity of the fluid and by the fluid flow pattern. Free convection relies on density differences due to temperature differences. As the density difference in a liquid increases, the velocity of the liquid increases and hence heat is transferred more quickly from the hot wall to the cold wall. Typical liquids have a density that depends linearly on temperature, consequently if the temperature difference in the liquid increases, the density difference increases and the rate of heat flow increases. If the temperature difference is constant, the rate of heat flow is unchanged regardless of the bounding temperatures of the temperature gradient. This contrasts with the behaviour of water.

Water has a density maximum at a temperature of 4°C . If the temperature difference remains constant and the bounding temperatures change, the density difference changes. The changes are most pronounced in the vicinity of the density maximum where the density profile has its greatest curvature. As the bounding temperatures approach the density extremum, the density difference decreases. This relationship between density and temperature causes the rate of heat flow to decrease as the

bounding temperatures approach the density maximum, despite having a constant temperature difference. The rate of heat flow through a cavity (0.06m x 0.12m) containing water with a constant temperature difference of 2°C with varying bounding temperatures is shown in Figure 5.2-10, the graph includes the corresponding density differences.

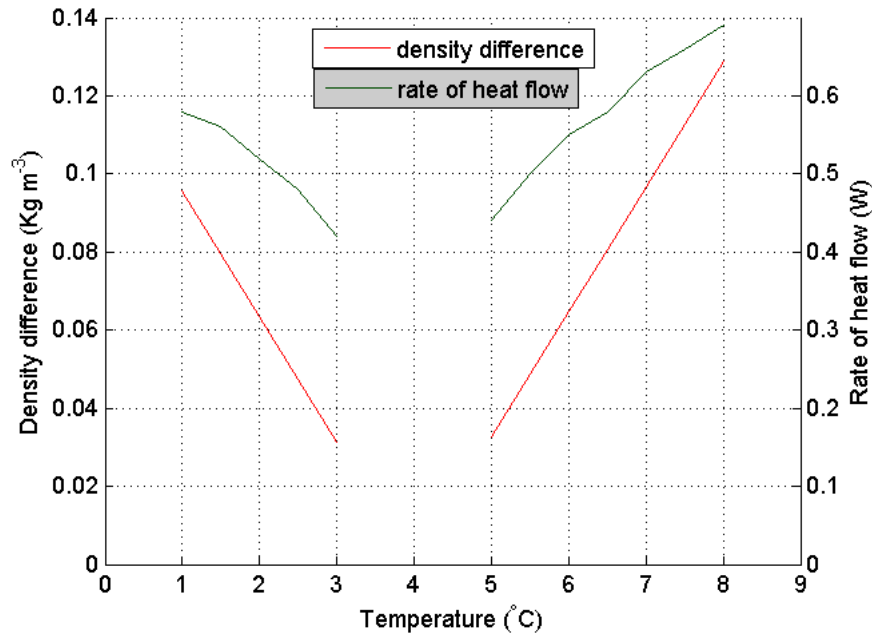


Figure 5.2-10 The rate of heat flow and the corresponding density difference as a function of the mean temperature of the bounding temperatures.

It is evident from Figure 5.2-10 that both the rate of heat flow and the density difference decrease in the vicinity of the density maximum. The results presented in Figure 5.2-10 do not show the rate of heat flow when the bounding temperatures encompass the density maximum since those boundary temperatures result in changes in the convective flow pattern which also causes changes in the rate of heat flow and this figure is only concerned with the behaviour of the rate of heat flow in relation to density differences.

When the bounding temperatures of the cavity containing water change from 10°C and 6°C to 6°C and 2°C the rate of heat flow is reduced by 67%. Experimental investigations in section 3.4.2 showed that the Nusselt number decreases from 3.8 to 1.4 in the vicinity of the density maximum; this yields a reduction of 64%. For Rayleigh numbers of the same of order of magnitude as those in the experiments, the

numerical study of Lin and Nansteel [29] found that the Nusselt number decreases from 4.7 to 1.0 in the vicinity of the density maximum; this yields a reduction of 78%. A similar numerical study by Tong [30] also showed that the Nusselt number decreased from 4.7 to 1.0 in the vicinity of the density maximum. According to Lin and Nansteel [29], the reduction in the rate of heat flow is due to the formation of the two convection cells since heat transfer between the two cells occurs via conduction.

The proposal of Lin and Nansteel is examined by obtaining the rate of heat flow through a cavity containing water with boundary temperatures of 10°C and 6°C. A second cavity of equal dimensions containing water is divided by inserting a solid partition of water into the centre of the cavity as shown in Figure 5.2-11. This configuration forces the flow pattern to exhibit two convection cells in the cavity, and heat is transferred from one cell to the other via conduction through the solid water partition. The pattern of the velocity field changes but the temperature difference across the entire enclosure remains the same as before and while there is a slight reduction in the maximum speed of the liquid it is not comparable to the reduction in heat transfer. The rate of heat flow decreases by 50% when single cell convection changes to two-cell convection. This compares to a 67% reduction when the boundary temperatures change from 10°C and 6°C to 6°C and 2°C. Thus, the reduction of heat transfer in the vicinity of the density maximum cannot be entirely due to the flow pattern, but it is also due to the reduced density differences.

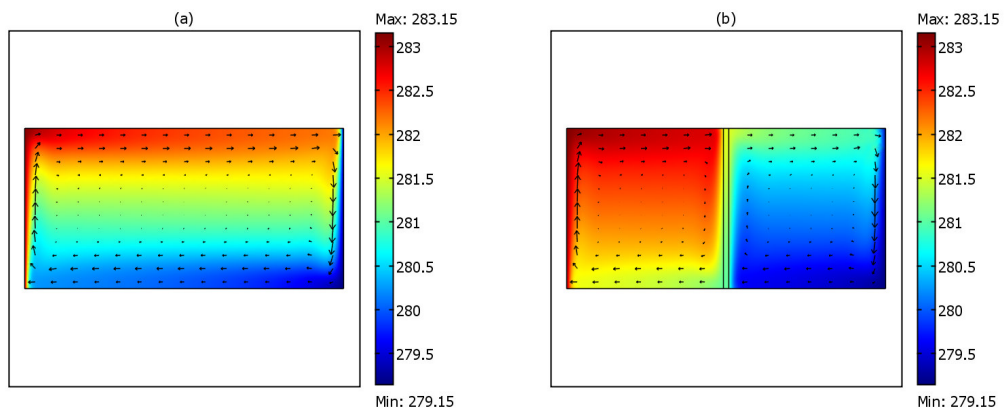


Figure 5.2-11 (a) A rectangular enclosure of water subjected to a horizontal temperature gradient with boundary temperatures of 10°C and 6°C. (b) The same configuration as (a) but with a solid partition in the centre of the enclosure that has the same properties as water. (Note: the temperature scales do not change in each of the surface plots).

5.2.4 Heat transfer during the quasi-steady state cooling and warming

This section aims to simulate the experimental results in 3.3.2 and to further understand and investigate heat transfer in the vicinity of the density maximum during the quasi-steady state procedure. The rate of heat transfer for the quasi-steady state models is obtained by applying the procedure outlined in section 4.2.4 to the models used in section 5.2.1 and in section 5.2.2. The results for the rate of heat transfer through ethanol are discussed and verified preceding a discussion on the rate of heat transfer through water.

Figure 5.2-12 shows the temperature profiles, the boundary temperatures and the monitoring temperatures for cooling ethanol from a mean temperature of 8°C to 0°C followed immediately by warming to 8°C. The temperature difference between $T_{m,h}$ and T_h indicates the rate of heat flowing into the geometry and the difference between T_c and $T_{m,c}$ indicates the rate of heat flowing out of the container. These temperature differences are converted into heat transfer values and they are plotted in Figure 5.2-13. During cooling the temperature differences are approximately constant and this implies that the rate of heat transfer is unchanged during the cooling. This is as expected, since neither the convective flow pattern nor the density difference change as ethanol cools. This behaviour also occurs when ethanol is warmed from 0°C to 8°C. The monitoring curves exhibit periodic spikes; these spikes are due to the discontinuous temperature steps of 0.1°C every 540 seconds. As outlined in Cawley *et al.* [36], there is a difference between the rates of heat transfer during cooling and warming. This difference indicates the energy required to change the temperature of the liquid by 8°C. The rate of cooling for ethanol has a value of 0.16 ± 0.01 W (the error is due to the change in heat transfer values when the mesh density is varied) and this yields a value for energy extracted of $6,900 \pm 400$ J. This value compares favourably to the value of 6600J obtained in section 3.3.2.1.

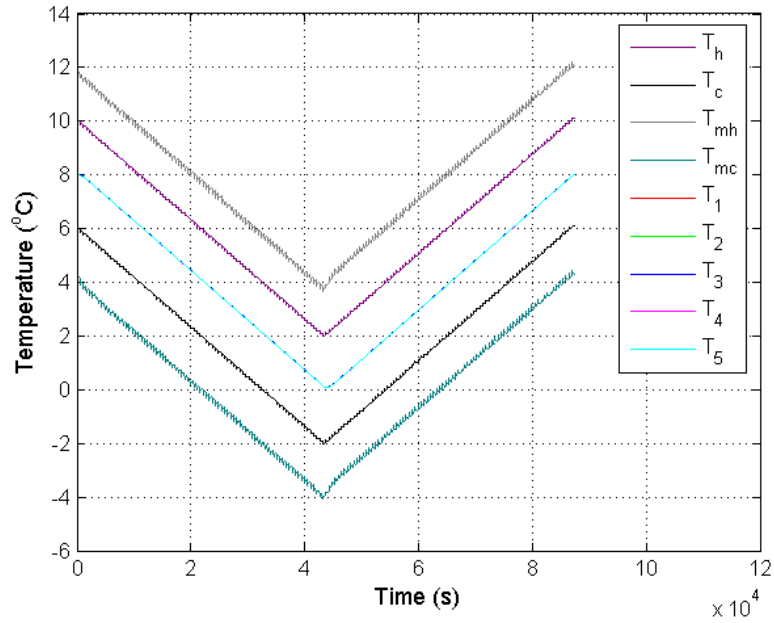


Figure 5.2-12 An enclosure of Ethanol is cooled from 8°C to 0°C and immediately warmed back from 0°C to 8°C . The temperature difference between T_h and $T_{m,h}$, and between T_c and $T_{m,c}$, indicate the behaviour of the rate of heat flowing into and out of the enclosure, respectively. (During cooling $Nu_H \sim 15.5$, and $Nu_C \sim 17.4$.)

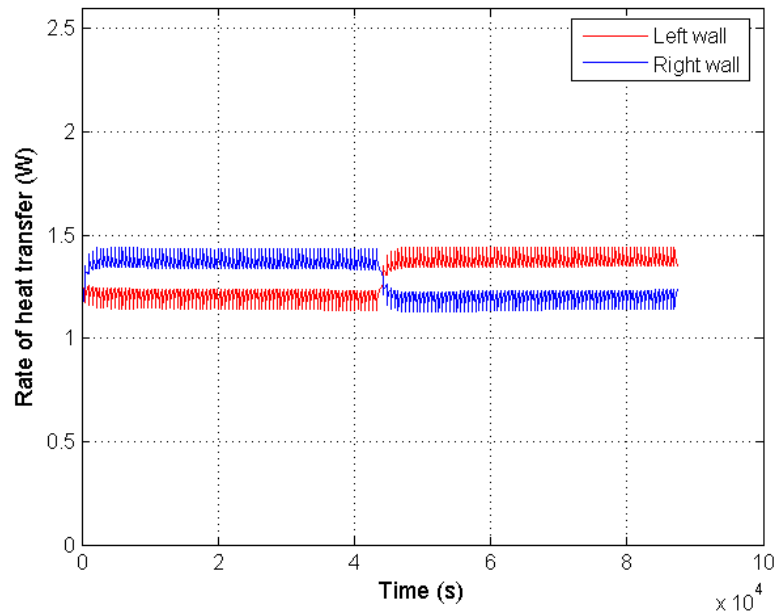


Figure 5.2-13 Rate of heat leaving and entering a rectangular enclosure of ethanol with dimensions of $0.12\text{ m} \times 0.06\text{ m} \times 0.06\text{ m}$ as it is cooled from 8°C to 0°C (first 43,740 seconds) and immediately warmed back from 0°C to 8°C (last 43,740 seconds). (During cooling $Nu_H \sim 15.5$, and $Nu_C \sim 17.4$.)

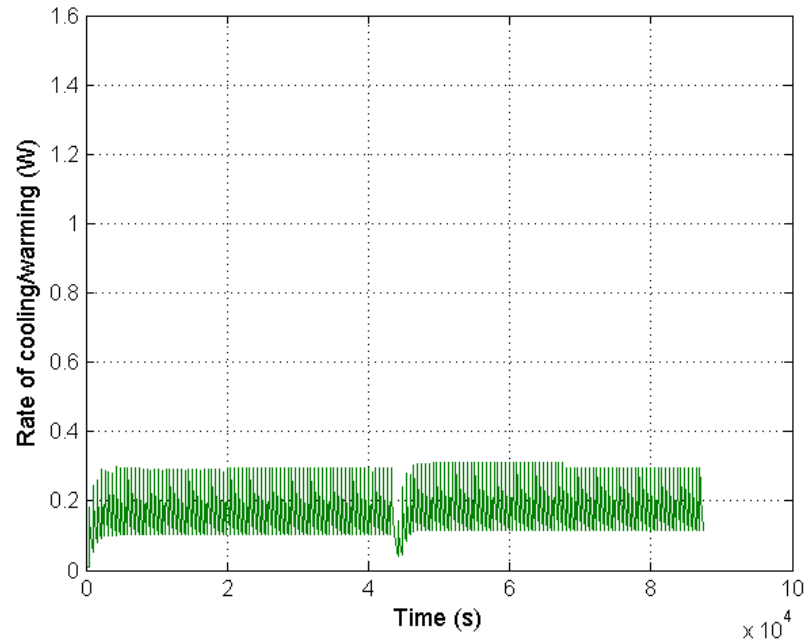


Figure 5.2-14 Rate of cooling of a rectangular enclosure of ethanol with dimensions of 0.12 m x 0.06 m x 0.06 m as it is cooled from 8°C to 0°C (first 43,740 seconds) and the rate of warming as it is warmed back from 0°C to 8°C (last 43,740 seconds).

Ethanol is a typical liquid and the behaviour of the rate of heat transfer for ethanol is as expected. Water is an unusual liquid that has a density maximum at 4°C and so the rate of heat transfer deviates from the typical behaviour. The graph in Figure 5.2-15 shows the variation with time of the temperature at the five points inside the test chamber, the temperature of the sidewalls and the monitoring temperatures. As discussed in Cawley *et al.* [61], the five points in the test chamber diverge as the sample enters the vicinity of the density maximum and converge when exiting the vicinity of the density maximum. This divergence occurs, as outlined in section 5.2.2, when a counter clockwise convective cell begins to grow at the cold wall. The convergence occurs when this cell has grown across the container and a small clockwise cell exists at the bottom corner of the hot wall. As outlined in Cawley *et al.* [36], the difference between the temperatures T_h and $T_{m,h}$ indicates the rate of heat flowing into the test chamber and the difference between the temperatures T_c and $T_{m,c}$ indicates the rate of heat flowing out of the chamber. In Figure 5.2-15 the difference between T_c and $T_{m,c}$ reaches a minimum as the five temperature points in the centre

of the chamber begin to diverge and the difference between T_h and $T_{m,h}$ reaches a minimum when the five points have converged.

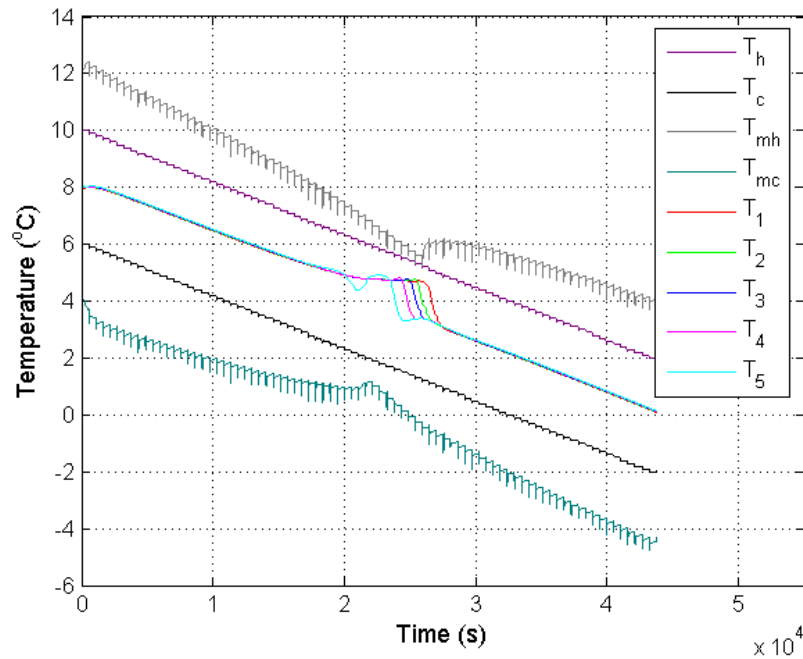


Figure 5.2-15 An enclosure of water is cooled from 8°C to 0°C . The temperature difference between T_h and $T_{m,h}$, and between T_c and $T_{m,c}$, indicate the behaviour of the rate of heat flow into and out of the enclosure, respectively.

The rate of heat flowing into and out of the cavity is shown in Figure 5.2-16. The rate of heat transfer at the cold wall decreases in the vicinity of the density maximum as the cold cell grows at the cold wall. The rate of heat flowing out of the cavity reaches a minimum when the cold cell straddles the cold wall as shown in part (a) of Figure 5.2-17. The hot cell and the cold wall possess a higher temperature difference than the cold cell and the cold wall, consequently when the cold cell prevents the hot cell from reaching the cold wall the rate of heat flowing out of the chamber rapidly decreases. The rate of heat transfer at the cold wall increases as the cold cell grows across the chamber.

The rate of heat flowing into the cavity reaches a minimum when the counter clockwise convection cell reaches the hot wall as shown in part (b) of Figure 5.2-17. It has been shown in section 5.2.3 that the occurrence of two convection cells inhibits the flow of heat. The mean temperature of the counter clockwise cell (cold cell) is

colder than the mean temperature of the clockwise cell (hot cell). Before this cell straddles the cold wall, heat is transferred from the hot wall to the hot cell and from the hot cell to the cold wall. As the cell grows, the surface area of the cold wall in contact with the hot cell lessens. Consequently, the rate of heat flowing from the hot wall to the cold wall via the hot cell is reduced. This also means that the temperature of the hot cell reduces more slowly. Since the temperature of the hot cell reduces more slowly and the temperature of the hot wall continues to be reduced (according to the applied procedure) the temperature difference between the hot cell and the hot wall reduces and consequently the rate of heat flowing into the cavity decreases until the cold cell reaches the hot wall. The large temperature difference between the cold cell and the hot wall causes a rapid increase in the rate of heat flowing into the cavity when the cold cell reaches the hot wall.

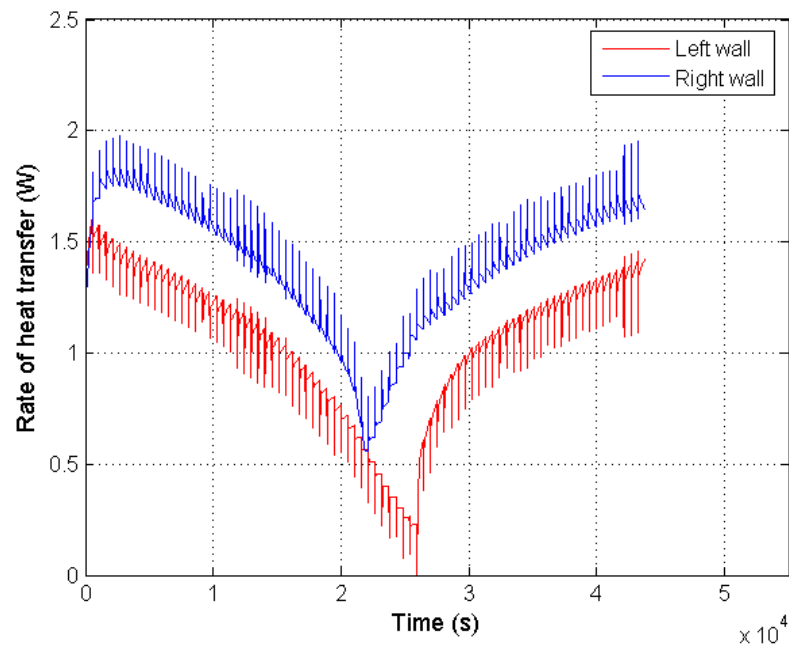


Figure 5.2-16 Rate of heat leaving and entering a rectangular enclosure of water with dimensions of 0.12 m x 0.06 m x 0.06 m as it is cooled from 8°C to 0°C. (Nu_H ranges from 20.8 to 2.8 and Nu_C ranges from 24.3 to 8.3.)

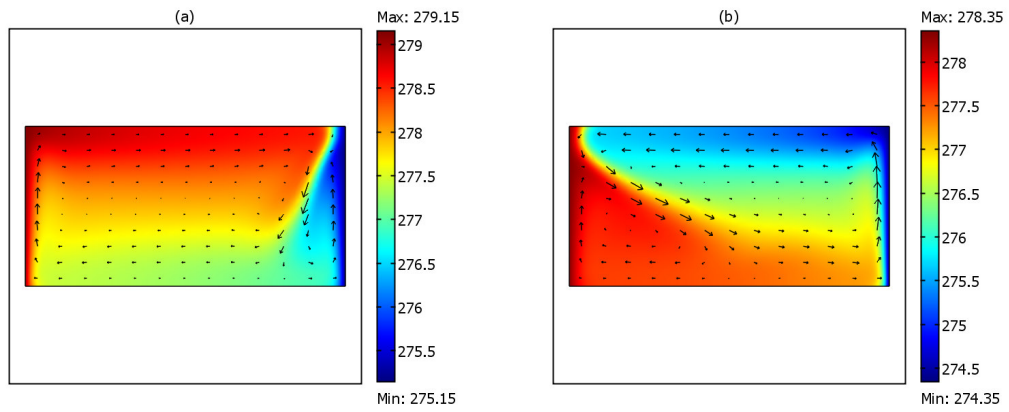


Figure 5.2-17 (a) The velocity (arrow plot) and temperature (surface plot) field when the rate of heat flowing out of the cavity is a minimum. (b) The velocity (arrow plot) and temperature (surface plot) field when the rate of heat flowing into the cavity is a minimum. (note: the temperature scales change in each of the surface plots).

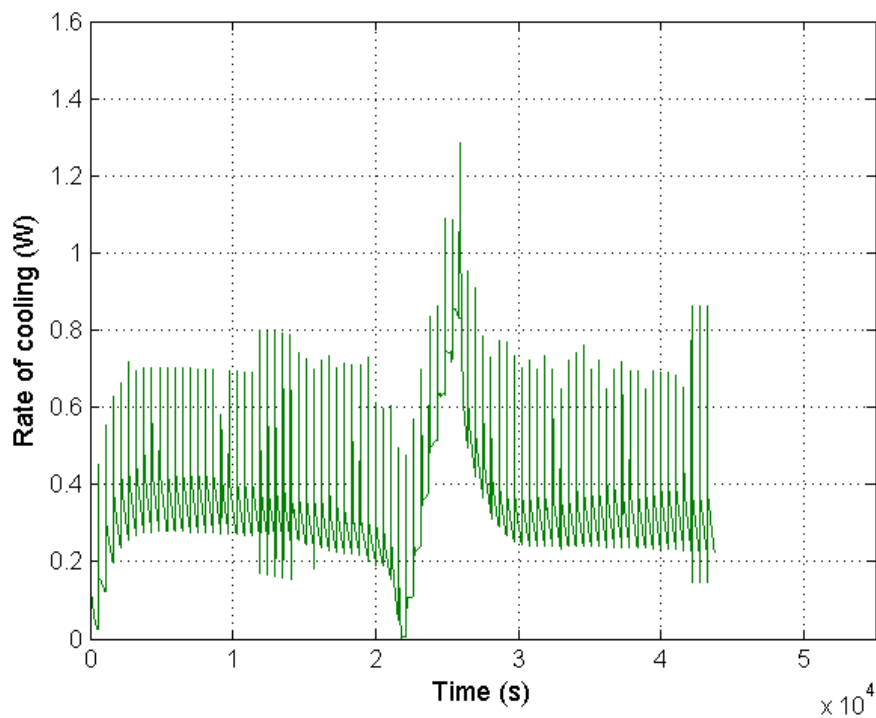


Figure 5.2-18 Rate of cooling of a rectangular enclosure of water with dimensions of $0.12\text{ m} \times 0.06\text{ m} \times 0.06\text{ m}$.

The difference between the rate of heat flowing into and out of the chamber is plotted in Figure 5.2-18. This difference is the rate of cooling of the sample and the area underneath the curve represents the amount of energy that must be extracted from the sample of water in order to cool it from a mean temperature of 8°C to 0°C. The area underneath the curve yields a value of 14,300 ±720J and this compares favourably to the value of 14,238J obtained from equation (3.3-1).

The rate of cooling of the sample begins to decrease when the cold cell forms at the cold wall. When the sample of water enters the vicinity of its density maximum the rate of cooling reaches a minimum, this minimum occurs when the cold cell straddles the cold wall as shown in part (a) of Figure 5.2-17. When this occurs, the cold cell prevents the hot cell from making any direct contact with the cold wall and this greatly reduces the rate of cooling of the hot cell; thus, the rate of cooling of the entire liquid reaches a minimum. The rate of cooling increases as the cold cell grows across the container cooling the liquid as it does so. The rate of cooling reaches a maximum when the cold cell reaches the hot wall as shown in part (b) of Figure 5.2-17. The rate of cooling decreases as the hot cell begins to shrink. Eventually, the rate of cooling returns to its previous state. This occurs when the hot cell ceases to exist.

Figure 5.2-19 shows the temperature profiles, the boundary temperatures and the monitoring temperatures for water as it is cooled in a quasi-steady state manner from 8°C to 0°C and it is warmed immediately back to 8°C in the same manner. An anomaly feature occurs in the temperature profiles centred on 4°C during the cooling and the warming. This anomaly feature has been explained in section 5.2.2 and it is due to the formation of the double convective cell. In both cooling and warming a single convection cell exists in the liquid before and after the anomaly feature. During cooling a second convection cell develops at the cold wall and grows across the container until the previous cell ceases to exist; during warming a second convection cell develops at the hot wall and grows across the container until the previous cell no longer exists.

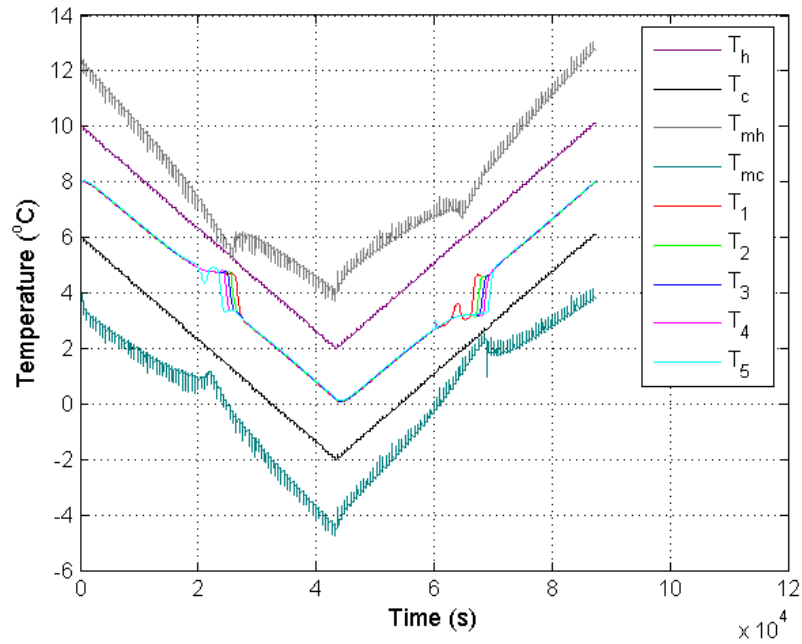


Figure 5.2-19 An enclosure of water is cooled from 8°C to 0°C and immediately warmed back from 0°C to 8°C . The temperature difference between T_h and $T_{m,h}$, and between T_c and $T_{m,c}$, indicate the behaviour of the rate of heat flow into and out of the enclosure, respectively.

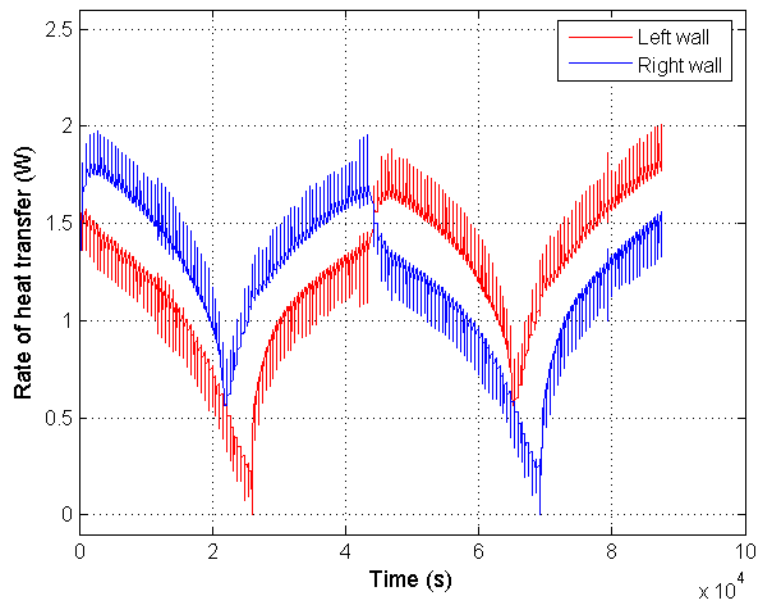


Figure 5.2-20 Rate of heat leaving and entering a rectangular enclosure of water with dimensions of $0.12\text{ m} \times 0.06\text{ m} \times 0.06\text{ m}$ as it is cooled from 8°C to 0°C (first 43,740 seconds) and immediately warmed back from 0°C to 8°C (last 43,740 seconds).

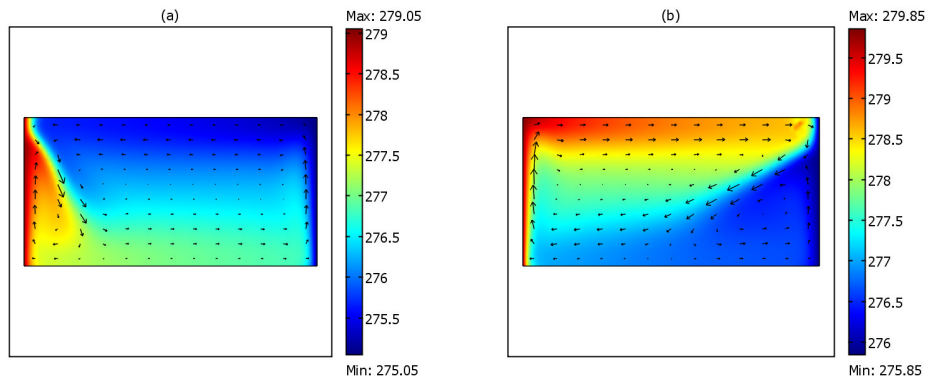


Figure 5.2-21 (a) The velocity (quiver plot) and temperature (surface plot) field when the rate of heat flowing into the cavity is a minimum during warming. (b) The velocity (quiver plot) and temperature (surface plot) field when the rate of heat flowing out of the cavity is a minimum during warming. (note: the temperature scales change in each of the surface plots).

The rate of heat transfer at the hot and cold walls is indicated by the temperature difference between the wall temperatures and their corresponding monitoring temperatures in Figure 5.2-19. These temperature differences are plotted as heat transfer rates in Figure 5.2-20. The heat transfer rates show that the rate of heat flowing in is less than the rate of heat flowing out during cooling and that the rate of heat flowing in is greater than the rate of heat flowing out during warming; this agrees with the behaviour of ethanol and it is due the extraction of heat required to lower the temperature of the liquid for cooling and the injection of heat to raise the temperature during warming. The staggering of the minima during cooling is different to the staggering during warming. During cooling the minimum in the rate of heat flowing out occurs before the minimum in the rate of heat flowing in; during warming the minimum in the rate of heat flowing out occurs after the rate of heat flowing in. This difference is due to the formation of the second convective cell in the vicinity of the density maximum. During cooling the second convective cell forms at the cold wall and straddles it, thus reducing the rate of heat transfer at the cold wall first; during warming the second convective cell forms at the hot wall and straddles it, thus reducing the rate of heat transfer at the hot wall first. During warming, the minimum in the rate of heat flowing into the container occurs when the clockwise convective cell straddles the hot wall as shown in part (a) of Figure 5.2-21; the minimum in the rate of heat flowing out of the container occurs when the

clockwise cell makes contact with the cold wall as shown in part (b) of Figure 5.2-21.

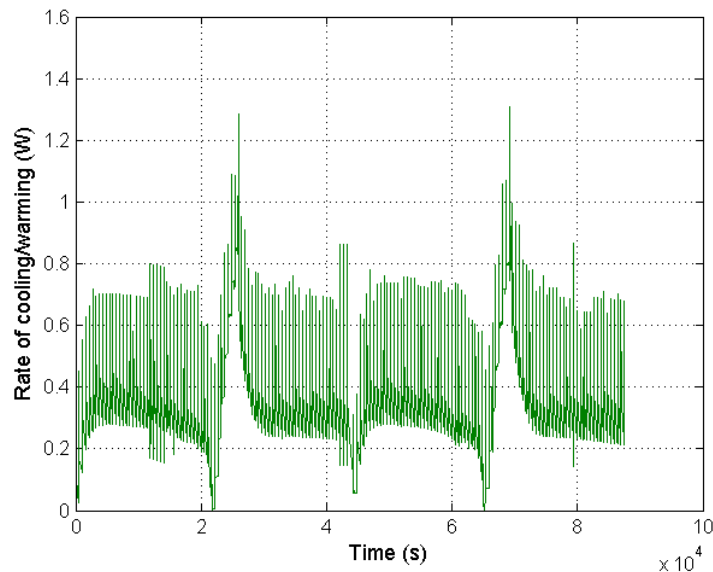


Figure 5.2-22 Rate of cooling and warming of a rectangular enclosure of water with dimensions of 0.12 m x 0.06 m x 0.06 m as it is cooled from 8°C to 0°C (first 43,740 seconds) and immediately warmed back from 0°C to 8°C (last 43,740 seconds).

The difference between the two rates of heat transfer is plotted in Figure 5.2-22. The first 43,740 seconds shows the rate of cooling of water and the last 43,740 seconds shows the rate of warming. The anomaly feature that occurs in the rate of cooling is the same as the anomaly feature in the rate of warming. Both rates reach a minimum when a second convective cell straddles one of the boundaries and they reach a maximum when the second convective cell makes contact with both walls.

5.2.5 Measurement technique for the temperature of maximum density of aqueous solutions

A chi-squared technique is described in Cawley *et al.* [61], which determines the temperature of maximum density of an aqueous solution from the temperature profiles in the liquid as it is cooled. Water is cooled from a mean temperature of 8°C to 0°C under the controlled conditions outlined in section 4.3.1 and in Mooney and Cawley [63]. An identical procedure is applied to an aqueous solution. An anomaly feature centred on the temperature of maximum density is observed in the temperature profiles of both the solution and water. The chi-squared technique compares the anomaly feature in the temperature profiles of an aqueous solution to

the anomaly feature of water to obtain the temperature of maximum density of the aqueous solution.

This measurement technique has been used in section 3.3.4 to obtain the temperature of maximum density of a variety of aqueous solutions. The technique is verified here using CFD. Water is cooled from 8°C to 0°C under the conditions described in section 4.3.1 and outlined in Cawley *et al.* [61]. The temperature of maximum density of water is 4°C. A second liquid that has identical properties to water but which has a temperature of maximum density at 3°C undergoes the exact same procedure. The temperature profiles of water are shown in Figure 5.2-23. The temperature profiles for a liquid with identical properties to water but which has a temperature of maximum density at 3°C are shown in Figure 5.2-24. The chi-squared technique is applied to both of these liquids and the result is plotted in Figure 5.2-25. The chi-squared comparison shows a minimum at 5,400 seconds and this value is inserted to equation (2.5-1) to obtain a temperature of maximum density at 3.01°C.

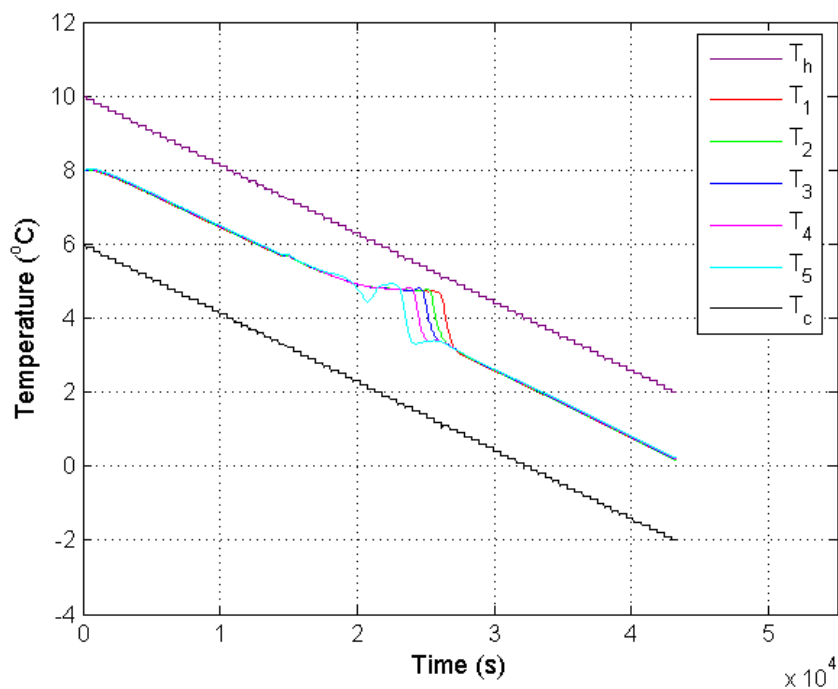


Figure 5.2-23 The temperature profiles of pure water, with a temperature of maximum density at 4°C, as it is cooled in the vicinity of its density maximum under the conditions outlined in section 4.3.1.

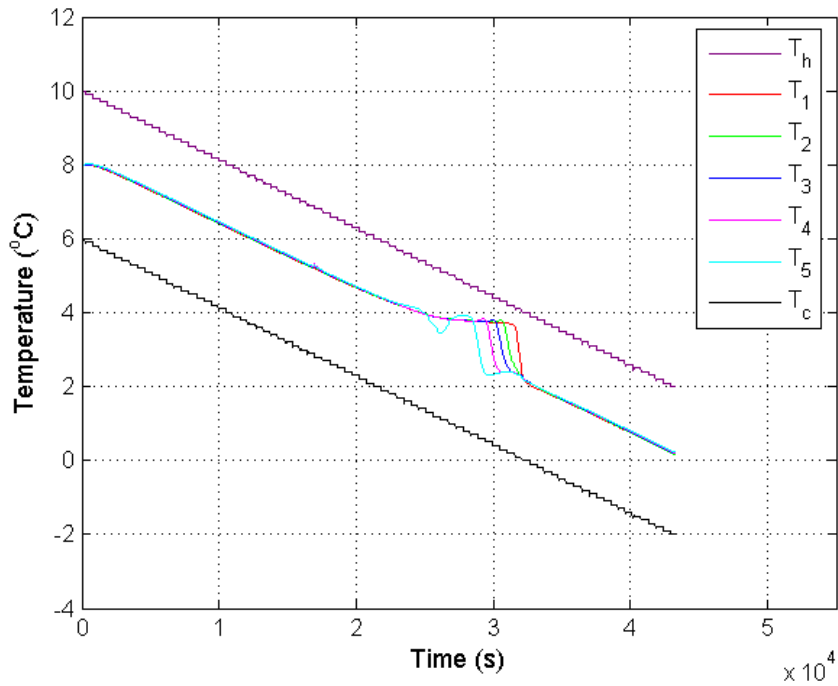


Figure 5.2-24 The temperature profiles of a liquid, with the same properties of water but which has a temperature of maximum density at 3°C, as it is cooled in the vicinity of its density maximum under the conditions outlined in section 4.3.1.

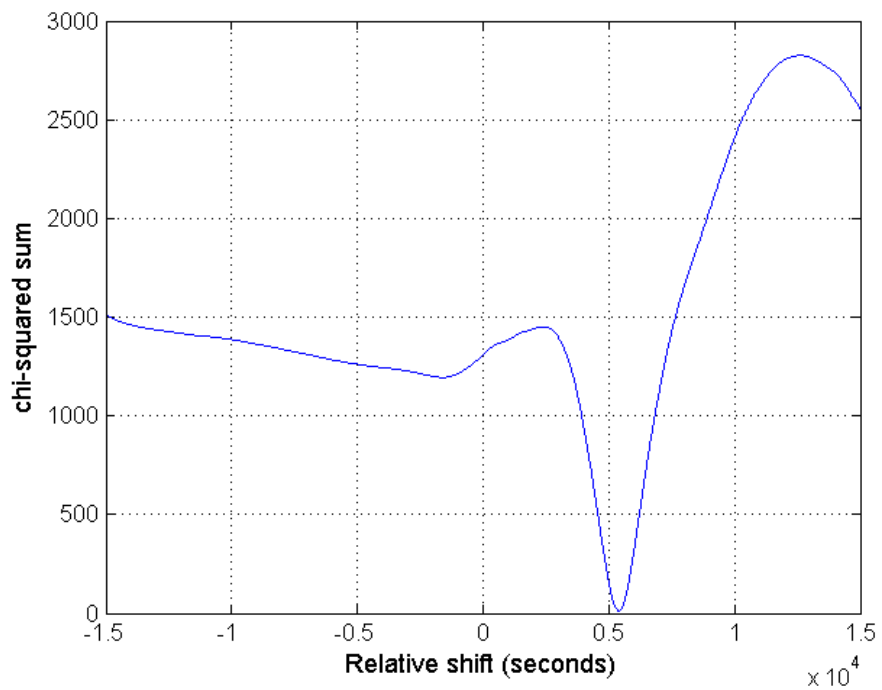


Figure 5.2-25 A chi-squared comparison between the temperature profiles in Figure 5.2-23 and the temperature profiles in Figure 5.2-24.

It has been shown in this study both experimentally in section 3.3.2 and numerically in section 5.2.2 that when a liquid is cooled in the vicinity of a density maximum, an anomaly feature is also observed in the rate of cooling of the liquid. It has been shown experimentally in section 3.3.3 that this feature in the rate of cooling of an aqueous solution can be compared with the feature in the rate of cooling of water to obtain the temperature of maximum density of the aqueous solution.

Water is cooled from 8°C to 0°C under the conditions outlined in Cawley *et al.* [61]. The temperature of maximum density of water is 4°C. A second liquid that has identical properties to water but which has a temperature of maximum density at 3°C undergoes the exact same procedure. The rate of cooling of water is shown in Figure 5.2-26 and the rate of cooling of the second liquid is shown in Figure 5.2-27. A chi-squared comparison between these two rates of cooling is shown in Figure 5.2-28. The chi-squared comparison shows a minimum at 5,400 seconds and this indicates that the temperature of maximum density of the second liquid is 3.01°C. This result validates the experimental technique used in section 3.3.3. The good agreement between the temperature of maximum density specified in the density function (3.00°C) with the chi-squared sum analysis (3.01°C) shows that the measurement technique described in section 3.3.3 is a valid technique.

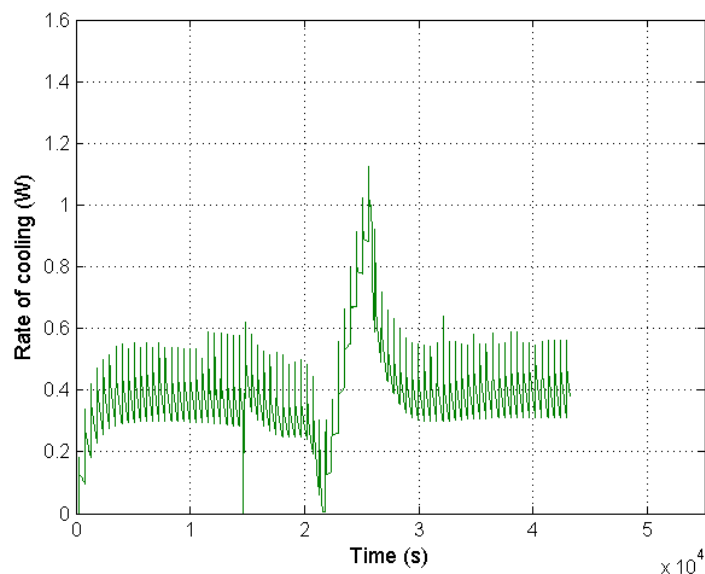


Figure 5.2-26 The rate of cooling of water with a temperature of maximum density at 4°C as it is cooled under the controlled conditions outlined in section 4.3.1.

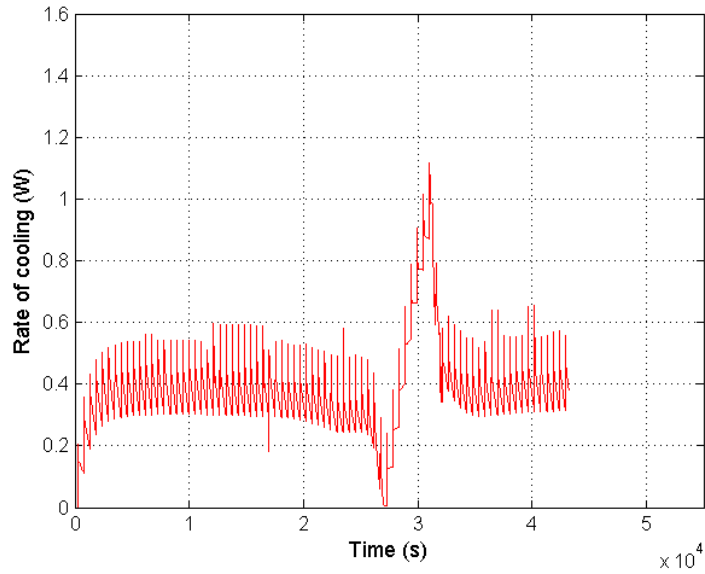


Figure 5.2-27 The rate of cooling of water with an artificial temperature of maximum density at 3°C as it is cooled under the controlled conditions outlined in section 4.3.1.

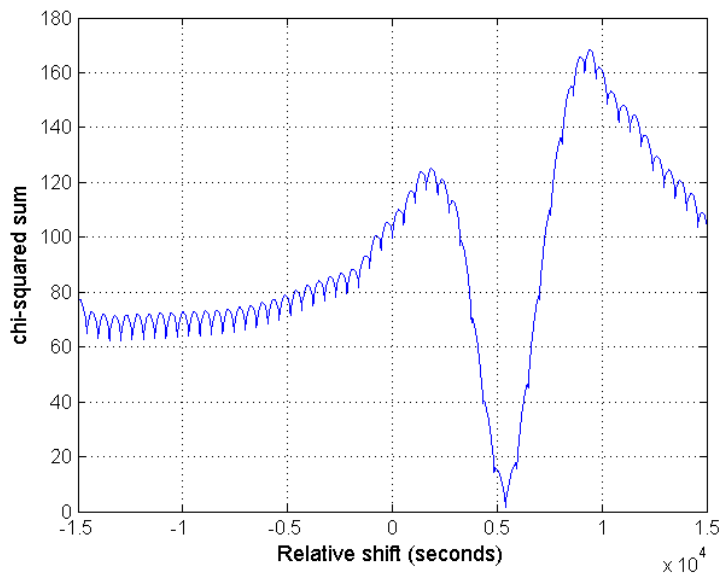


Figure 5.2-28 The chi-squared comparison between the rate of cooling shown in Figure 5.2-26 and the rate of cooling shown in Figure 5.2-27. The method shows that the temperature of maximum density of the liquid, whose rate of cooling is shown in Figure 5.2-27, is 3.01°C .

5.2.6 The shape of the anomaly feature

This section aims to investigate the influence of various parameters on the shape of the anomaly feature in the temperature profiles. It has been observed previously in section 3.3.1 that changing the dimensions of the container alters the shape of the anomaly feature. This observation prompted the investigation of the influence of the aspect ratio of the container on the shape of the anomaly feature. The results of this investigation are presented in section 5.2.6.1 and they confirm the experimental observations.

The temperature profiles used for the measurement of the temperature of maximum density of aqueous solutions presented in section 3.3.4 are obtained from five thermistors equally spaced along a vertical axis at a depth of 0.03m in a container with a height of 0.06m. The influence of the position of this vertical axis on the shape of the anomaly feature is investigated numerically and the results are presented in section 5.2.6.2. The experimental error on the position of the vertical axis is 0.001m. An offset of 0.001m on the position of the vertical axis does not noticeably alter the shape of the anomaly feature. This statement is validated by the numerical results as it will be shown that an offset as large as 0.01m does not significantly alter the shape of the anomaly feature.

The investigation of the shape of the anomaly feature concludes in section 5.2.6.3 with the analysis of the influence of the properties of the liquid on the shape of the anomaly feature. The addition of solutes to water alters the properties of water. This necessitates the study of the influence of the properties of the liquid on the shape of the anomaly feature. The study investigates the influence of the thermal diffusivity by examining the behaviour of the shape of the anomaly feature as a function of the magnitude of the thermal conductivity, specific heat capacity and density.

5.2.6.1 *The container dimensions*

In this section the shape of the anomaly feature is examined for three different container aspect ratios ($\alpha = \text{width} / \text{height}$): 0.5, 1.0, and 2.0. In these investigations, the height of the container remains constant at 0.06m while the width of the container changes. An aspect ratio of 1.0 corresponds to the aspect ratio of the experimental container used for flow visualization (Figure 3.3-3); an aspect ratio of 2.0 corresponds to the aspect ratio of the experimental container used for measuring the temperature of maximum density of aqueous solutions (Figure 3.3-2). These two results show experimentally that changing the dimensions of the container alters the shape of the anomaly feature. This is confirmed by the numerical plots in Figure 5.2-29.

It is evident from the numerical plots that the temperature range spanned by the anomaly feature does not change significantly. However, the time range spanned by the anomaly feature does change. The time span of the feature for an aspect ratio of 0.5 is almost twice that for an aspect ratio of 2.0. The anomaly feature for an aspect ratio of 0.5 is shown in Figure 5.2-29(a). The point closest to the cold wall is the first to show the usual rapid cooling, and the point closest to the hot wall is the last to exhibit this behaviour. In comparison to the feature for an aspect ratio of 2.0 (the typical anomaly feature throughout this study), the point closest to the cold wall cools early. During the anomaly feature in Figure 5.2-29(a), the temperature of the three points in the centre of the container decrease, before increasing and decreasing again. These behaviours are due to the restricted space in the container for the development of the second convection cell.

During the anomaly region, a small counter-clockwise cell develops at the cold wall. As it grows, it engulfs the four points closest to the cold wall, thus the temperatures of the four points decrease. When this cell has developed to a certain size, it begins to stretch along the cold wall and rise to the top of the container. As it does so, it leaves behind the three points in the centre of the container and so their temperatures increase. When the cell reaches the top of the container it starts to grow across the container and cools each of the four remaining points in turn. This behaviour occurs in each of the aspect ratios. However, for high aspect ratios, the points move further

away from the cold wall (where the counter-rotating convection cell develops) while the size of the counter-clockwise cell in the early stages of development does not increase significantly. Thus, the temperature profiles do not sense the early stages of development for high aspect ratios.

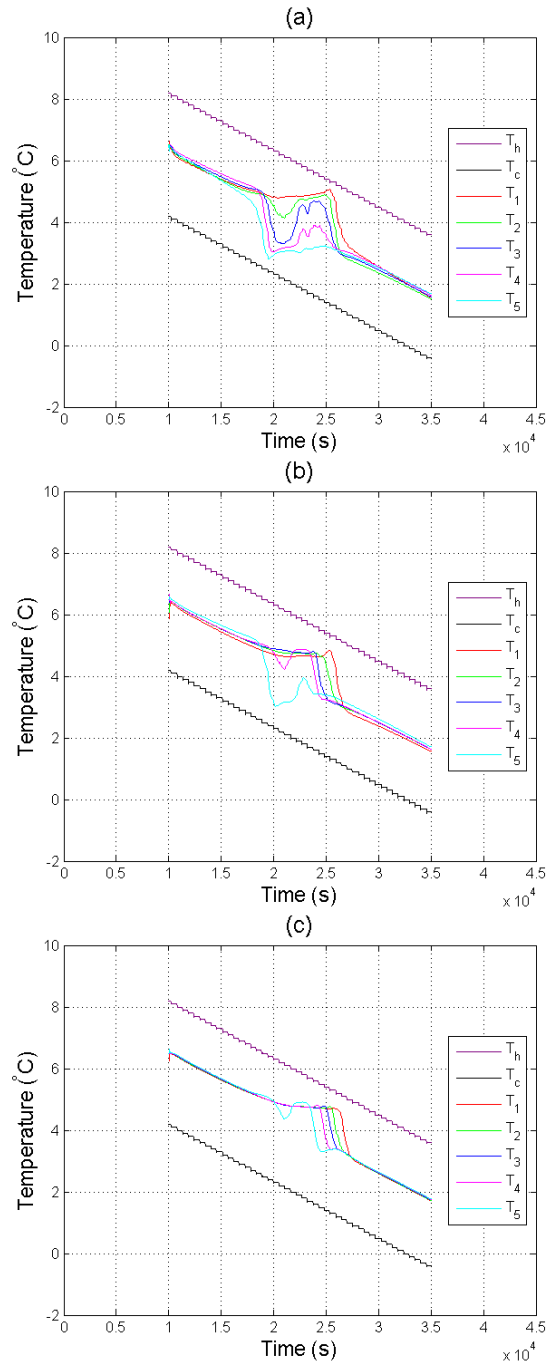


Figure 5.2-29 The density anomaly feature as a function of aspect ratio (α). The height and length for a container with an aspect ratio of 1.0 is 0.10m x 0.10m. The aspect ratio for the plots (a)-(c) are: (a) $\alpha = 0.5$, (b) $\alpha = 1.0$, and (c) $\alpha = 2.0$.

5.2.6.2 The vertical position of the temperature points

The influence of the vertical position of the temperature points on the shape of the anomaly feature is investigated by examining the shape of the anomaly feature for the set of temperature points along different vertical lines through the test chamber as shown in Figure 5.2-30. The shape of the anomaly feature typically observed in this study is that shown in part (c) of Figure 5.2-31, in this graph the temperature points are equally spaced along a vertical line 3cm from the bottom of the chamber (0.06m x 0.12m – height x length) and graphs (a), (b), (d), and (e) have their set of points located along a vertical line 1cm, 2cm, 4cm, and 5cm from the bottom of the cavity, respectively as shown in Figure 5.2-30. It is shown in Figure 5.2-31 that as the vertical height of the set increases, the temperature at the point closest to the cold wall behaves more similar to the other points at regions of the graph outside the anomaly feature, the anomaly feature spans a greater temperature, i.e. the height of the signature increases and the parallelogram shape of the feature tends towards a rectangular shape. These trends can be understood by examining the graphs in Figure 5.2-32 and Figure 5.2-33. The graphs in Figure 5.2-32 show the velocity field (quiver plot) and the temperature field (surface plot) of the liquid at 18000 seconds, 20000 seconds, 22000 seconds, 24000 seconds, 26000 seconds, and 28000 seconds. The graphs in Figure 5.2-33 shows the velocity field and the density of the liquid at the same times as those shown in Figure 5.2-32.

When the set of points is located near the bottom of the chamber, the temperature at the point located closest to the cold wall decreases for a while and then increases to the same temperature as the other points before the five points form the anomalous shape. This behaviour becomes less noticeable and eventually disappears from the graph as the set moves further away from the bottom of the chamber. This behaviour can be understood by observing the temperature and velocity fields of the liquid as it enters the vicinity of the density maximum. A small cold counter-clockwise cell is observed in the liquid at 18,000 seconds, 2,000 seconds later this cell has grown in size. During this time points closest to the cold wall (that belong to the sets close to the bottom wall), are located in the cold cell while the other points lie in a warm cell. Therefore, the temperature of the points in the cold cell behaves differently to the other four points in their set.

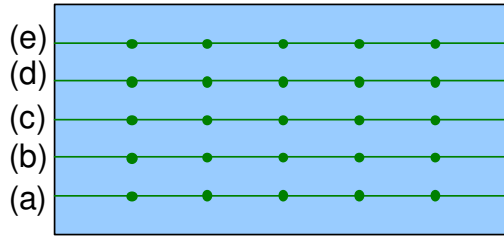


Figure 5.2-30 The position of the array of temperature probes that are plotted in parts (a-e) of Figure 5.2-31.

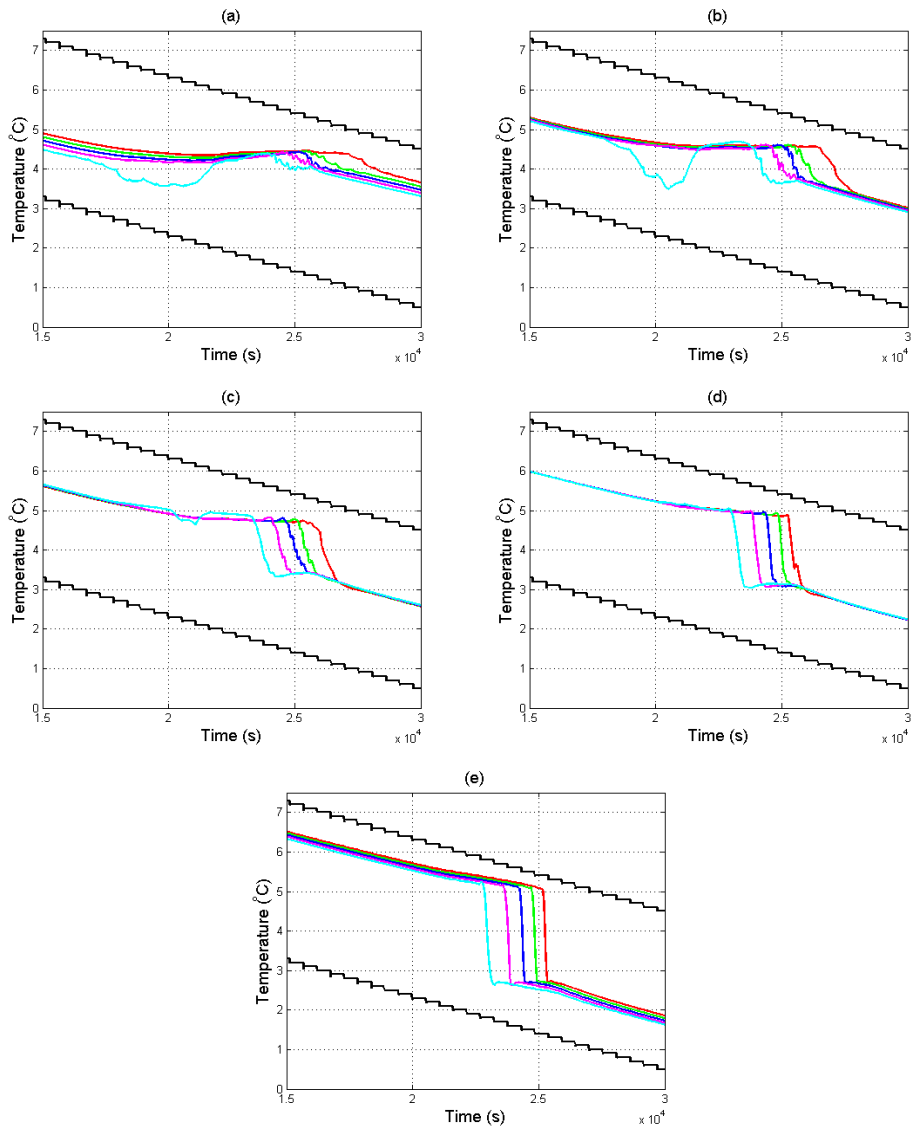


Figure 5.2-31 The influence of the vertical position of the temperature points on the shape of the anomaly feature. In the first graph the five temperature points are located along a horizontal line 0.01m from the bottom of the geometry, the second, third, fourth, and fifth graphs have the five points located along a horizontal line 0.02m, 0.03m, 0.04m, and 0.05m from the bottom of the geometry, respectively.

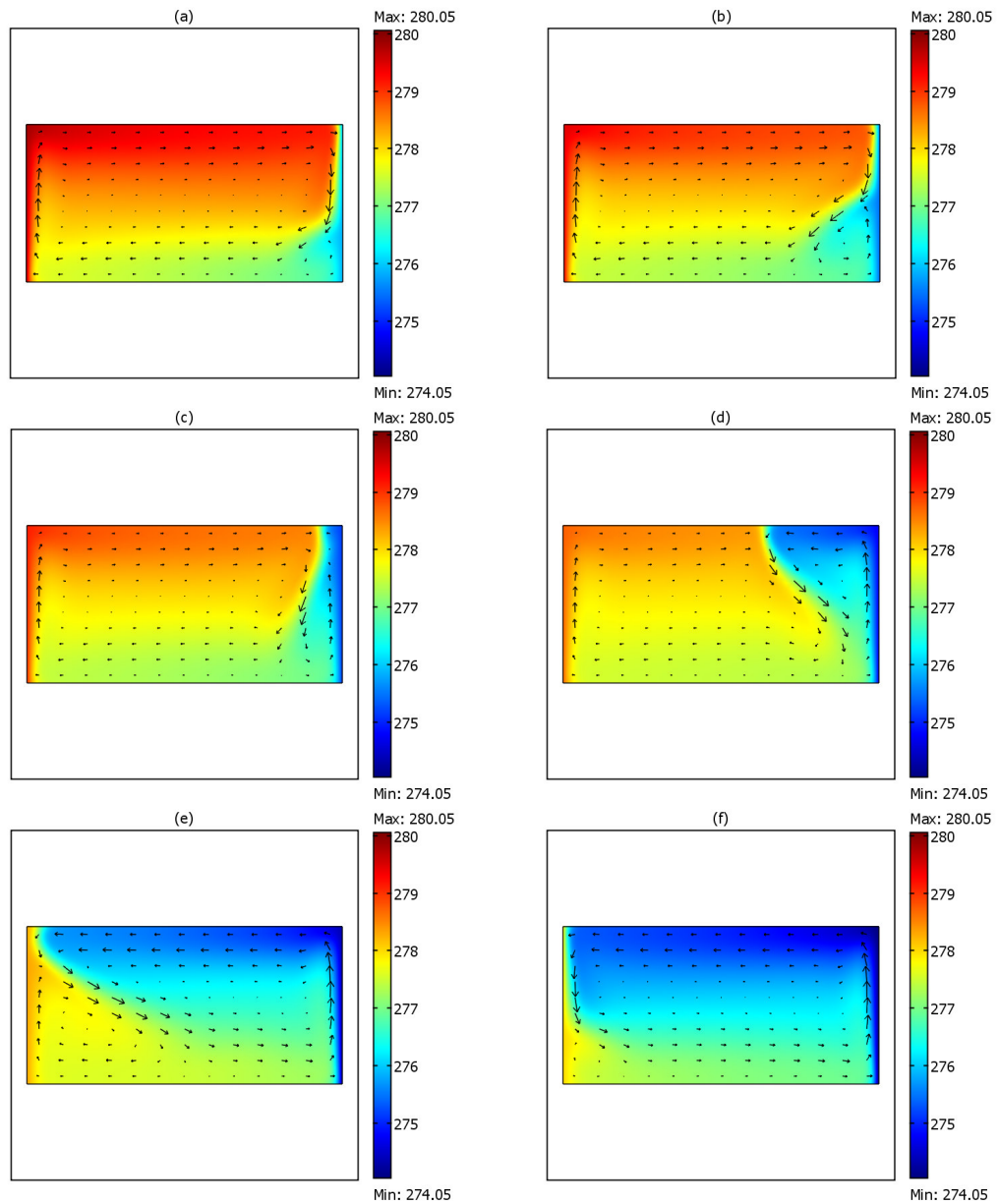


Figure 5.2-32 These graphs, from left to right moving down the graphs, show the behaviour of the velocity field (quiver plots) and the temperature field (surface plot) at the following times (a) 18000 seconds, (b) 20000 seconds, (c) 22000 seconds, (d) 24000 seconds, (e) 26000 seconds, and (f) 28000 seconds. (note: the temperature scales do not change in each of the surface plots).

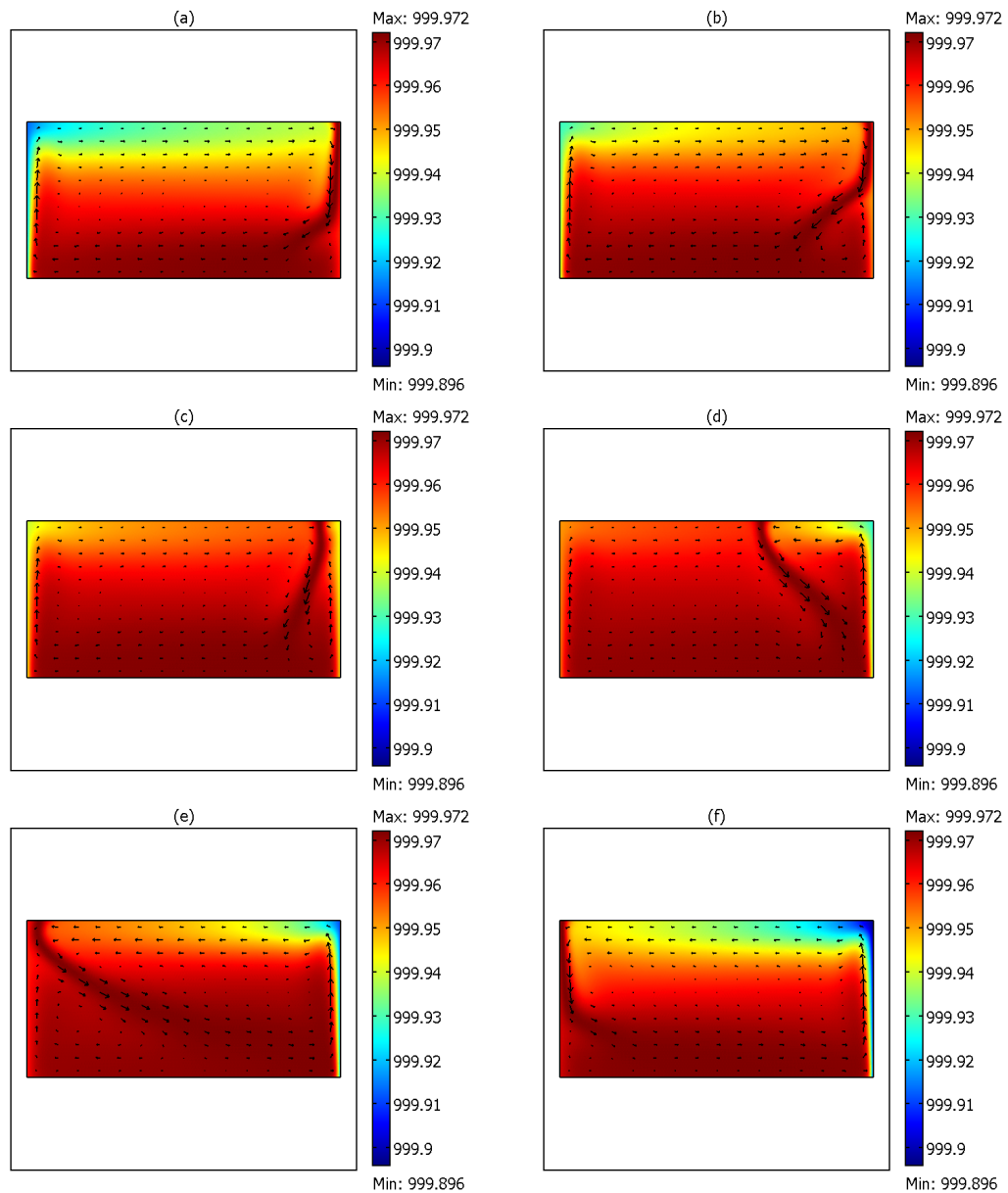


Figure 5.2-33 These graphs, from left to right moving down the graphs, show the behaviour of the velocity field (quiver plots) and the density (surface plot) at the following times (a) 18000 seconds, (b) 20000 seconds, (c) 22000 seconds, (d) 24000 seconds, (e) 26000 seconds, and (f) 28000 seconds. (note: the density scales do not change in each of the surface plots and the density is in units of kg.m^{-3}).

The cold cell lies at the bottom of the chamber since this liquid is the densest. As the temperature of the walls continues to decrease the temperature of the two cells decreases also, consequently, the cold cell becomes less dense and the density of the hot cell increases. As the cold cell becomes less dense, it begins to rise along the

cold wall to the top of the chamber, during this time the size of the cell reduces. The temperature of the point located close to the cold wall begins to increase when this happens as the hot cell moves into the area previously occupied by the cold cell. When the point closest to the cold wall once again lies in the same cell as the other four points, the five points exhibit similar temperatures. The anomalous shape begins when the cold cell starts growing at the top of the chamber. All points in the sets located far away from the bottom of the chamber remain in the same cell before the anomaly shape begins but each set of points at the bottom of the chamber have at least one point in a different cell. Therefore, the points close to the top do not exhibit this behaviour.

It is shown in Figure 5.2-31 that as the vertical position of the set of temperature points increases, the anomaly feature spans a greater temperature range, i.e. the height of the anomaly feature increases. In these investigations of free convection, the densest liquid is at the bottom of the chamber and the least dense liquid is at the top of the chamber. When the wall temperatures change from 8°C and 4°C to 4°C and 0°C (the density anomaly feature occurs in this temperature range) the temperature of the least dense liquid changes from 8°C to 0°C while the temperature of the densest liquid is relatively undisturbed, it remains in the vicinity of 4°C . This suggests that the temperature at the bottom of the chamber does not change dramatically as the liquid is cooled through its density maximum, while the temperature at the top of the chamber changes dramatically. This can be seen in the temperature plots in Figure 5.2-32.

Figure 5.2-31 shows that as the vertical position of the set of points increases the shape of the anomaly feature changes from a parallelogram to a rectangle. The anomaly feature occurs due to the growth of the counter clockwise cell across the container. The counter clockwise cell grows more rapidly across the top of the container than the bottom. Consequently, as the cell grows it changes the temperature at the top of the container more rapidly than at the bottom so that the slope of the temperature profiles decreases as the vertical height of the set of temperature points increases.

It is also observed that, in the region outside of the anomaly shape, the temperature points exhibit similar values in the centre of the chamber, but there is a noticeable difference between the temperature points when they are located a considerable distance from the centre. This difference in temperature occurs because the points are located in moving liquid that is transporting heat from the hot wall to the cold wall. The points in the centre of the chamber are located in stationary liquid where heat is transported by conduction in a direction that is almost vertical.

5.2.6.3 *The properties of water*

The density anomaly feature in the temperature profiles is primarily due to the growth of the of the counter-clockwise cell across the container. The rate of growth of the counter-clockwise cell across the container is due to the thermal diffusion. The thermal diffusivity of a substance is defined as

$$\alpha = \frac{k}{\rho C_p} \quad (5.2-1)$$

where k is the thermal conductivity in $\text{W.m}^{-1}.\text{K}^{-1}$, C_p is the specific heat capacity in $\text{J.kg}^{-1}.\text{K}^{-1}$ and ρ is the density in kg.m^{-3} . The influence of these three properties on the anomaly feature is investigated by varying them according to the combinations presented in Table 5.2-1.

Figure 5.2-34 shows the influence of the thermal conductivity on the anomaly feature. The temperature span of the density maximum feature does not change considerably as a function of thermal conductivity, however it is noticeable that the time span decreases as the thermal conductivity increases. The time span is measured by obtaining the time at which T_5 reaches 4°C and the time at which T_1 reaches 4°C . The time difference between these two times is considered to be the time span. The time span for the typical anomaly feature discussed throughout this study is 2,417 seconds and the feature is shown in part (b) of Figure 5.2-34. The time spans for the thermal conductivities of $0.5k$ and $2.0k$ are 2576 seconds and 1,786 seconds, respectively. The rate of diffusion of heat throughout the liquid increases with increasing thermal conductivity, therefore the time taken for the liquid to undergo the changes induced by the density maximum decreases as the thermal

conductivity increases. This behaviour is as expected since the thermal diffusivity is directly proportional to the thermal conductivity.

The influence of the specific heat capacity on the density anomaly feature is shown in Figure 5.2-35. As noticed for the thermal conductivity, the temperature span does not change but the time span does. The time span for a specific heat capacity of $0.5C_p$ is 1,784 seconds and for $1.25C_p$ is 2,997 seconds, respectively. The time span of the feature increases as the specific heat capacity increases as shown in Figure 5.2-35. The rate of diffusion of heat throughout the liquid decreases with increasing specific heat capacity, therefore it takes longer for the liquid to undergo the changes induced by the density maximum as the specific heat capacity increases. This behaviour is also as expected since the thermal diffusivity is inversely proportional to the specific heat capacity.

A similar effect on the shape of the density maximum feature occurs for the density of the liquid. The temperature span does not change but the time span changes from 2,482 seconds to 2,966 seconds when the density changes from 0.5ρ to 1.5ρ , respectively. Figure 5.2-36 shows that the time span of the density anomaly feature increases as the density of the liquid increases. The rate of diffusion of heat throughout the liquid decreases with increasing density, therefore it takes longer for the liquid to undergo the thermal changes induced by the density maximum as the density increases. This behaviour is as expected since the thermal diffusivity is inversely proportional to the density.

It is interesting to note that in Table 5.2-1 configuration (iii) and configuration (iv) have the same effect on the thermal diffusivity; as expected from this trend, the anomaly feature in Figure 5.2-34(iii) and the anomaly feature in Figure 5.2-35(iv) are similar in shape and they have the same time span. Similarly, configuration (iv) and configuration (vi) have the same effect on the thermal diffusivity, but the corresponding anomaly features are not the same. This is not unexpected since unlike the other two properties the density appears elsewhere in the Navier-Stokes equations. These investigations confirm that the shape of the density anomaly is dependent on the properties of the liquid and that the shape of the anomaly feature

for aqueous solutions would be different if the addition of solutes to water significantly changes the properties.

Plot number in the following three figures	Thermal conductivity [$W.m^{-1}.K^{-1}$]	Specific heat capacity [$J.kg^{-1}.K^{-1}$]	Density [$kg.m^{-3}$]
(i)	$0.5 \times k_{water}$	$C_{p, water}$	ρ_{water}
(ii)	k_{water}	$C_{p, water}$	ρ_{water}
(iii)	$2.0 \times k_{water}$	$C_{p, water}$	ρ_{water}
(iv)	k_{water}	$0.5 \times C_{p, water}$	ρ_{water}
(v)	k_{water}	$1.25 \times C_{p, water}$	ρ_{water}
(vi)	k_{water}	$C_{p, water}$	$0.5 \times \rho_{water}$
(vii)	k_{water}	$C_{p, water}$	$1.5 \times \rho_{water}$

Table 5.2-1 The influence of the properties of water on the shape of the anomaly feature is investigated using the combinations of the values of the three properties shown in this table.

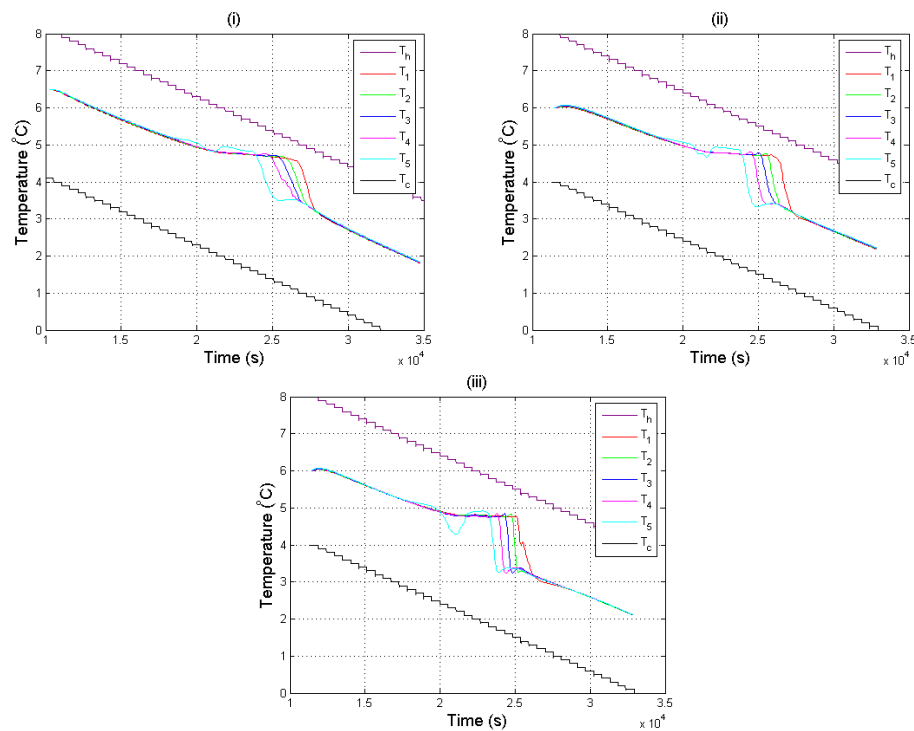


Figure 5.2-34 The influence of the thermal conductivity on the shape of the anomaly feature. The thermal conductivity in (i) is $0.5 \times k_c$, (ii) is k_c , and (iii) is $2 \times k_c$. The symbol k_c is the thermal conductivity of water.

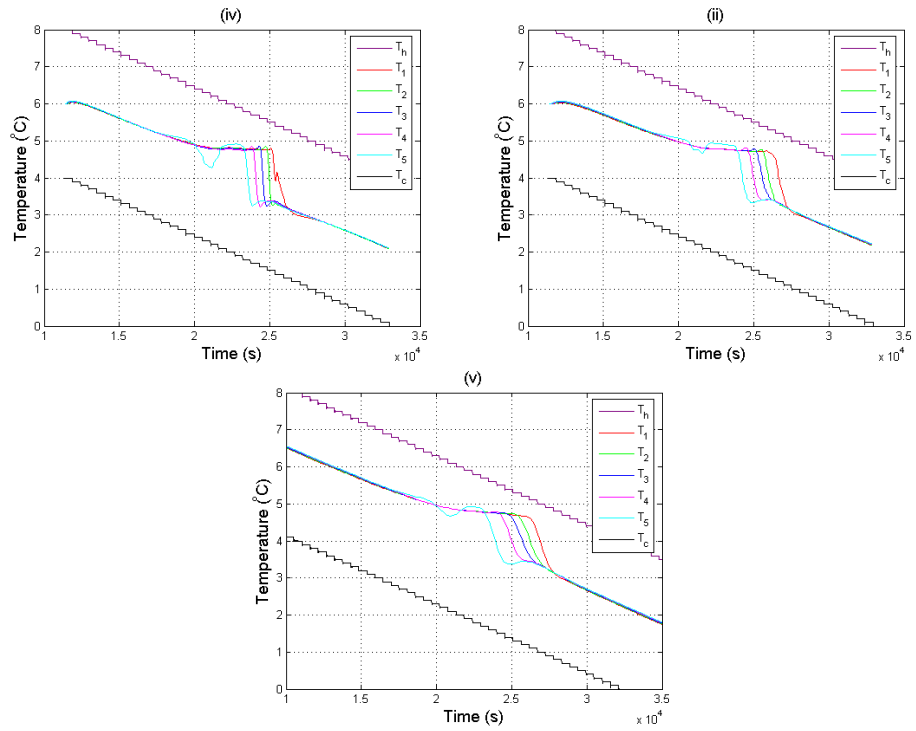


Figure 5.2-35 The influence of the specific heat capacity on the shape of the anomaly feature. The specific heat capacity in (iv) is $0.5 \times C_{p, \text{water}}$, (ii) is $C_{p, \text{water}}$, and (v) is $1.25 \times C_{p, \text{water}}$. $C_{p, \text{water}}$ is the specific heat capacity of water.

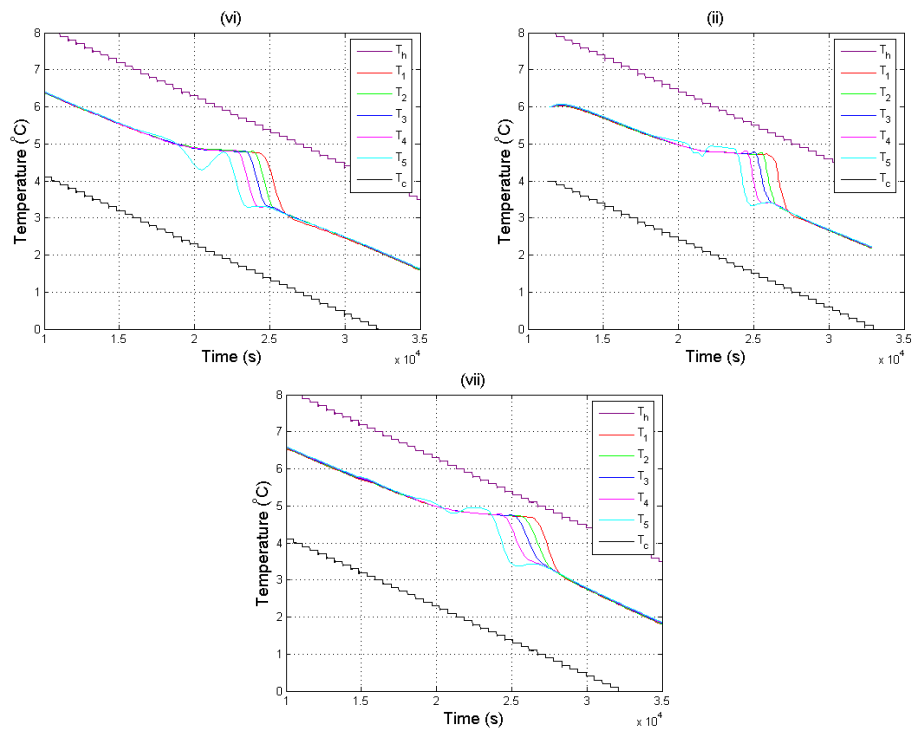


Figure 5.2-36 The influence of the density on the shape of the anomaly feature. The density in (vi) is $0.5 \times \rho_{\text{water}}$, (ii) is ρ_{water} , and (vii) is $1.5 \times \rho_{\text{water}}$. The symbol ρ_{water} is the density of water.

5.3 Asymmetrical heat transfer

Experimentally, asymmetrical heat transfer has been observed in a composite system of water and a saline solution (water-saline diode) and in a composite system of water and Perspex (water-Perspex diode). This section aims to confirm the experimental results, to aid understanding of the experimental results, and to explore the possibility of obtaining a greater percentage rectification for the water-saline diode and the water-Perspex diode. The conditions of the experimental results of the water-saline diode presented in Mooney and Cawley [37] and in section 3.4.2 are reproduced using computational fluid dynamics and the results are presented in section 5.3.1. The CFD results confirm the experimental results and the explanation given for them in section 3.4.2. This numerical model is used to explore the influence of the bounding temperatures, the size of the diode, and the number of liquid compartments on the percentage rectification of the water-saline diode. The results of these investigations are presented in section 5.3.2.

In the CFD studies, asymmetrical heat transfer is investigated in a composite system of water and Perspex. The numerical model simulates the conditions of the experimental investigation presented in Cawley *et al.* [36] and in section 3.4.3, and the results are presented in section 5.3.3. It is suggested in section 3.4.3 that the offset in the boundary temperatures in the experiment of 0.2°C causes the temperature profiles in the experiment to bunch together. This postulation is examined in section 5.3.3. Similarly to the water-saline diode, the numerical model investigates the optimal conditions for the water-Perspex diode. The influence of the bounding temperatures and the length of the Perspex slab on the percentage rectification was investigated and the results are presented in section 5.3.4.

Asymmetrical heat transfer is also investigated in two composite systems involving a phase change material (phase change diodes). The first composition consists of a liquid and a Phase Change Material (PCM) and the second composition consists of a solid and a phase change material. The basis of the phase change diode is that when heat flows in a given direction the PCM is in its solid state, so heat flows through the PCM via conduction in this direction; when the direction is reversed the PCM is in its liquid state and heat flows via convection. This change in the mechanism of heat

transfer alters the rate of heat flow. The results of this phase change diode are analysed in section 5.3.5. This chapter concludes in section 5.3.6 with a discussion on the electrical analogy of asymmetrical heat transfer. The electrical analogy provides an alternative approach to the illustration of the mechanism by which asymmetrical heat transfer arises.

5.3.1 Water-saline diode

The water-saline diode is the main focus of this study and it consists of a square enclosure of a saline solution adjacent to a square enclosure of water as shown in Figure 5.3-1 and described in Mooney and Cawley [37]. The basis of this thermal diode is that heat transfer is reduced in the vicinity of the density maximum. This section aims to confirm the experimental results presented in section 3.4.2 and to aid understanding of them. The experimental procedure for investigating asymmetrical heat transfer holds a constant temperature gradient across the composition for a set time. When this time has elapsed, the gradient is reversed by swapping the wall temperatures. The walls are then held at these temperatures for the same period of time as before. This experimental procedure is simulated numerically as described in section 4.4.1 and the results are presented in Figure 5.3-2.

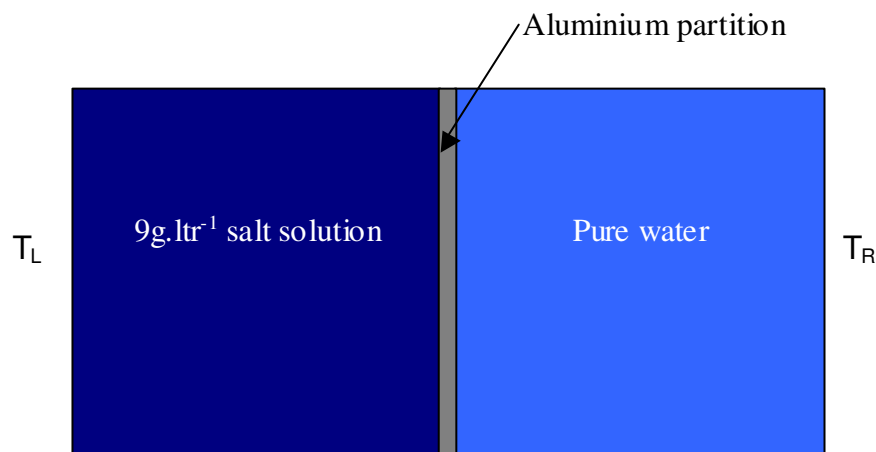


Figure 5.3-1 The water-saline diode consists of a square enclosure of a saline solution adjacent to a square enclosure of water. The square enclosures have dimensions of $0.06\text{m} \times 0.06\text{m} \times 0.06\text{m}$. The saline solution has a density maximum at 2°C and pure water has a density maximum at 4°C .

The results presented in Figure 5.3-2 show the boundary temperatures, the monitoring temperatures and the temperatures at select points inside each compartment. In the first 30,000 seconds of this graph, the temperature of the left wall (T_L) is 1°C and the temperature of the right wall (T_R) is 5°C. During this time, heat flows from the water compartment to the saline compartment. In the latter 30,000 seconds, heat flows in the opposite direction. As described in Cawley *et al.* [36], the temperature differences between the monitoring temperatures and the boundary temperatures are directly proportional to the rate of heat transfer. It is evident from Figure 5.3-2 that the rate of heat transfer in the first 30,000 seconds is less than the rate of heat transfer in the latter 30,000 seconds. Thus, the rate of heat transfer changes when the direction of heat flow is reversed. A plot of the rate of heat transfer is shown in Figure 5.3-3 (blue line). This plot shows that the rate of heat transfer changes from 0.18W to 0.52W when the direction of heat flow is reversed. This yields a percentage rectification of 65.4% for the water-saline diode.

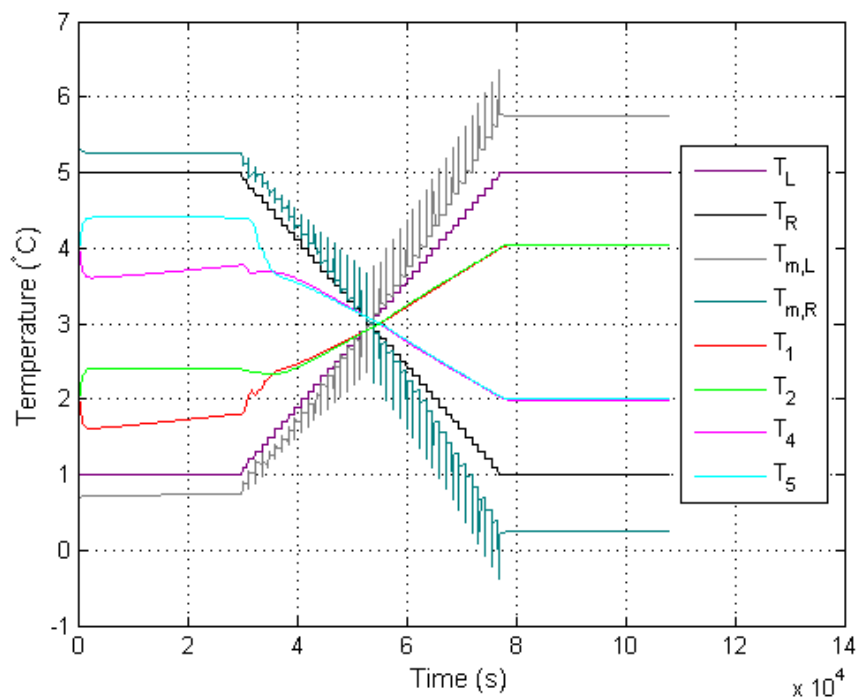


Figure 5.3-2 The behaviour of the temperature field when the thermal diode effect is observed in the water-saline diode. ($Ra \approx 9.3 \times 10^3$ in the first 30,000 seconds and $Ra \approx 9.2 \times 10^5$ in the last 30,000 seconds).

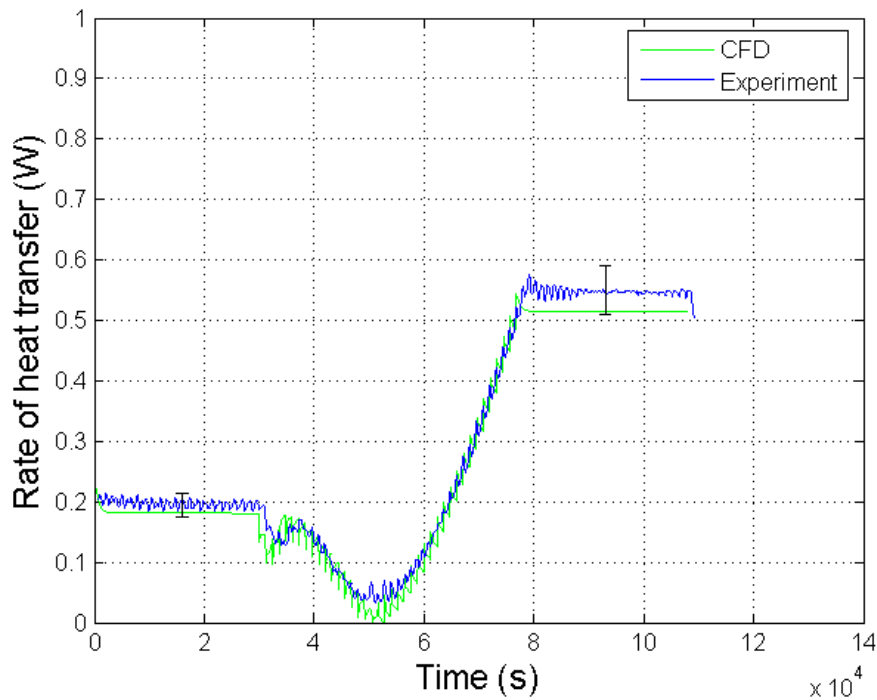


Figure 5.3-3 The average rate of heat flow through the water-saline diode when heat flows from right to left (the first 30,000 seconds) and from left to right (the last 30,000 seconds). It is evident that the rate of heat flow changes when the direction is reversed. ($Nu \approx 1.2$ in the first 30,000s and $Nu \approx 3.6$ in the last 30,000s).

Figure 5.3-3 shows the rate of heat transfer for both the experimental investigation (green line) and the numerical investigation (blue line) that correspond to the temperature against time plots in Figure 3.4-5 (experimental) and in Figure 5.3-2 (numerical). It is evident from this graph that the results from both investigations are in good agreement with each other; each line shows the same trends and the numerical results are within the margin of error on the experimental results. Discrepancies between the experimental results and the numerical results can be ascribed to the approximations in the CFD calculations, the departure from the ideal conditions in the experiment, and the assumption that the two-dimensional geometry represents a two-dimensional slice of a three dimensional chamber.

In section 3.4.2, it is inferred from the dispersal of the temperature profiles in the liquids and the density range spanned by the temperature gradient, that when heat flows from right to left, the convective flow pattern in each compartment consists of

two counter-rotating convective cells. This analysis is supported numerically by the plot of the velocity field (quiver plot) and the temperature field (surface plot) shown in part (a) of Figure 5.3-4. Similarly, when heat flows from left to right, it is inferred from the bunching together of the two thermistors in each compartment and the density range of the liquids spanned by the temperature gradient, that a single convective cell exists in each compartment. This analysis is supported by the velocity field (quiver plot) and the temperature field (surface plot) shown in part (b) of Figure 5.3-4.

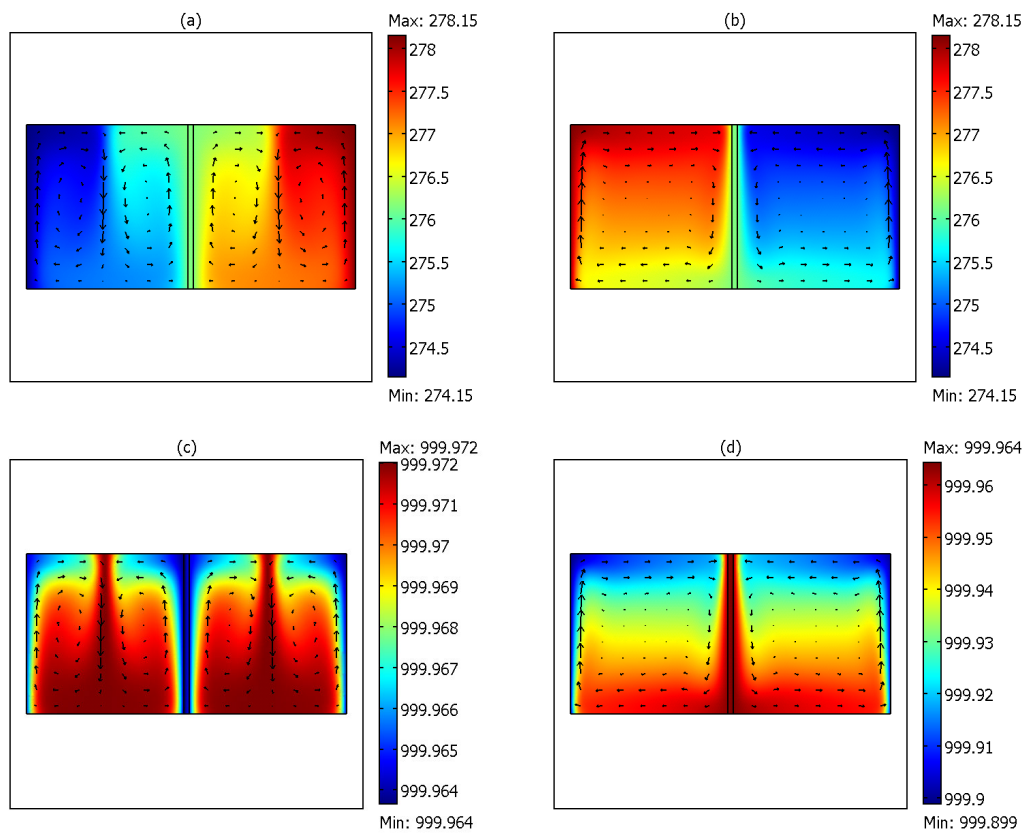


Figure 5.3-4 Numerical results for the flow patterns (quiver plot) in the two conductance modes of the water-saline diode (saline solution on the left and pure water on the right). (a) The temperature field (surface plot; degrees Kelvin) for low conductance mode: $T_L=1^\circ\text{C}$ and $T_R=5^\circ\text{C}$. (b) The temperature field (surface plot; degrees Kelvin) for high conductance mode: $T_L=5^\circ\text{C}$ and $T_R=1^\circ\text{C}$. (c) The density (surface plot; $\text{kg}\cdot\text{m}^{-3}$) for low conductance mode: $T_L=1^\circ\text{C}$ and $T_R=5^\circ\text{C}$. (d) The density (surface plot; $\text{kg}\cdot\text{m}^{-3}$) for high conductance mode: $T_L=5^\circ\text{C}$ and $T_R=1^\circ\text{C}$.

The transient region of Figure 5.3-2 (30,000 seconds to 78,000 seconds) shows that the temperature profiles in each compartment converge before the temperature gradient ceases to encompass each liquid's temperature of maximum density. This behaviour is also observed in the experimental results. It is suggested in section 3.4.2, that this occurs when two convection cells of unequal size exist in both compartments, so that both temperature points lie in the same convection cell and thus they exhibit similar temperatures. This analysis is supported by the plot of the velocity field (quiver plot) and the temperature field (surface plot) shown in Figure 5.3-5.

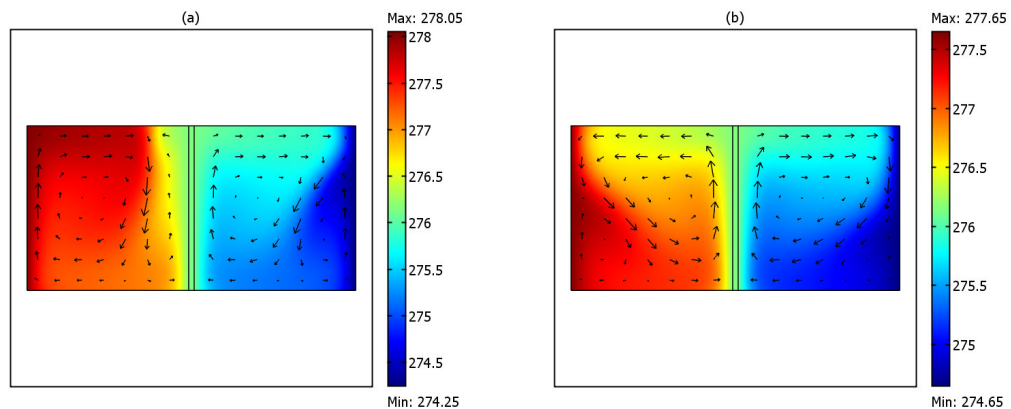


Figure 5.3-5 Numerical results for the flow patterns (quiver plot) and the temperature fields (surface plots; degrees Kelvin) during the transient region of Figure 5.3-2 when (a) $T_L=4.9^\circ\text{C}$ and $T_R=1.1^\circ\text{C}$ and (b) $T_L=4.5^\circ\text{C}$ and $T_R=1.5^\circ\text{C}$. (Note: the temperature scales change in each of the surface plots).

Figure 5.3-3 shows the rate of heat transfer from the experimental investigations (green line) and the numerical investigations (blue line). Both investigations show that as the temperature difference decreases the rate of heat transfer decreases, but between 35,000 seconds and 40,000 seconds the rate of heat transfer increases before decreasing again. As explained in section 3.4.2 two convection cells exist in each compartment prior to the interchanging region and when the temperature difference begins to decrease the size of one cell in each compartment decreases while the size of the other cell increases. As the rate of heat transfer initially decreases, one of the convection cells shrinks and the other convection cell grows as shown in part (a) of Figure 5.3-5. When the latter convection cell is large enough to make direct contact with the isothermal wall and the partition wall, as shown in part (b) of Figure 5.3-5,

the rate of heat transfer increases. However, the temperature difference continues to decrease and so the rate of heat transfer decreases again.

5.3.2 Optimization of the water-saline diode

Experimental results presented in section 3.4.2 and in Mooney and Cawley [37], have shown that a composite system of water and an aqueous solution exhibits asymmetrical heat transfer. CFD analysis of the water-saline diode has confirmed that the results obtained experimentally are accurate and that the density maximum phenomenon of water is directly responsible for decreasing the rate of heat transfer through the test geometry when the two liquids have a temperature difference that encompasses their temperatures of maximum density. Due to the accuracy of the CFD results acquired, it was decided that the model would be extended to include a study on the optimisation of the water-saline diode. There are five explorations for the optimal conditions of the water-saline diode; the first exploration changes the boundary temperatures while keeping the gradient constant, the second exploration applies the previous exploration to various gradients, the third exploration increases the length while keeping the temperature difference constant, the fourth exploration keeps the aspect ratio of the diode constant but varies the scale and the final exploration keeps the gradient constant while increasing the number of partitions.

As described in Cawley *et al.* [36], the influence of the bounding temperatures on the percentage rectification was investigated by selecting a constant temperature difference of 4°C and changing the mean temperature of the boundary temperatures from 0°C to 6°C in steps of 0.01°C. This procedure was applied to a selection of temperature differences ranging from 1°C to 8°C.

The influence of the length of the cavity on the percentage rectification was investigated using the scripting feature in Comsol Multiphysics. The temperature difference across the cavity was chosen to be 4°C and the boundary temperatures were chosen to be 5°C and 1°C. The length of the cavity was varied from 0.02 m to 0.22 m in steps of 0.002 m. In contrast, the influence of the scale of the diode was investigated by varying the size of the diode but keeping the aspect ratio constant.

The influence of the number of compartments in the cavity was investigated by keeping the temperature gradient constant at $16.667^{\circ}\text{C}\cdot\text{m}^{-1}$ (1°C temperature difference across a compartment of length 0.06 m) while changing the length of the cavity. The addition of a compartment increased the temperature difference across the composite by 1°C . Each compartment contained water with a different temperature of maximum density. The compartment on the extreme left had a temperature of maximum density at 4°C and the temperature of maximum density of each consecutive compartment was 1°C less than its left hand neighbour.

5.3.2.1 Significance of the boundary temperatures

The first optimization study applies a temperature difference of 4°C across the water-saline diode. The boundary temperatures are initially chosen so that they are centred on 0°C , e.g. for a temperature difference of 4°C the boundary temperatures are 2°C and -2°C . These temperatures are incremented by 0.01°C and the percentage rectification for each set of boundary temperatures is obtained. The percentage rectification of the water-saline diode as a function of the mean temperature of the boundary temperatures is plotted in Figure 5.3-6. Three peaks are observed in Figure 5.3-6, each peak has two local maxima and one local minimum. The maximum percentage rectification of 65.4% occurs in the middle peak when the central temperature is 3°C . The boundary temperatures that correspond to this central temperature are the same as those used in the experimental investigations in section 3.4.2. An experimental value of 65.4% is obtained in section 3.4.2 for the percentage rectification of the water-saline diode with these exact conditions. When heat flows in a certain direction under these boundary conditions the velocity field in each compartment has two counter rotating convection cells, i.e. each compartment has its minimum thermal conductivity. When the direction of heat flow is reversed, each compartment has just one convection cell, this dramatic change in the velocity field results in a very dramatic difference in the rate of heat flow for each direction. The behaviour of the thermal and velocity fields in both directions of heat flow is shown in Figure 5.3-7.

A local secondary maximum occurs at 2.97°C and a local minimum occurs at 2.99°C . It is important to note that the difference in the percentage rectification of these three extremum points is less than the change in the percentage rectification obtained when

the currently used mesh density changes to a higher mesh density. Therefore, it is possible that there is only one extremum point in this peak, however the occurrence of three extremum points is observed in all peaks shown in Figure 5.3-6 (and in each of the peaks in all eight plots shown later in Figure 5.3-10). It is difficult therefore to conclude that these features are due to any dependency of the results on the mesh density.

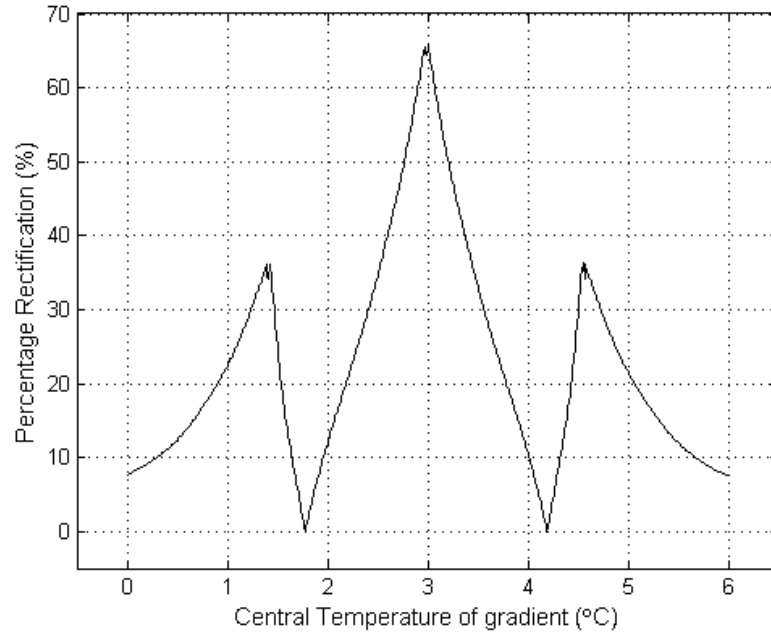


Figure 5.3-6 The percentage rectification of the water-saline diode with a temperature difference of 4°C . The percentage rectification changes as the central temperature of the temperature gradient changes.

Two secondary maxima are observed in the percentage rectification shown in Figure 5.3-6. The first of these two maxima occurs when the mean temperature of the boundary temperatures is 1.38°C . As described in Cawley *et al.* [36], this maximum occurs when there is a single convection cell in both compartments for a given direction of heat flow and when this direction is reversed there are two convection cells in the compartment containing water at 2°C and a single convection cell in the compartment containing water at 4°C , as shown in parts (a) and (b) of Figure 5.3-8. The second of these two maxima occurs when the mean temperature of the boundary temperatures is 4.56°C . A similar argument is presented for the occurrence of the maximum at this temperature. A single convection cell exists in each compartment

when heat flows in a given direction and when this direction is reversed two counter-rotating convection cells exist in the compartment containing water with a density maximum at 4°C and a single convection cell is observed in the other compartment, as shown in parts (c) and (d) of Figure 5.3-8.

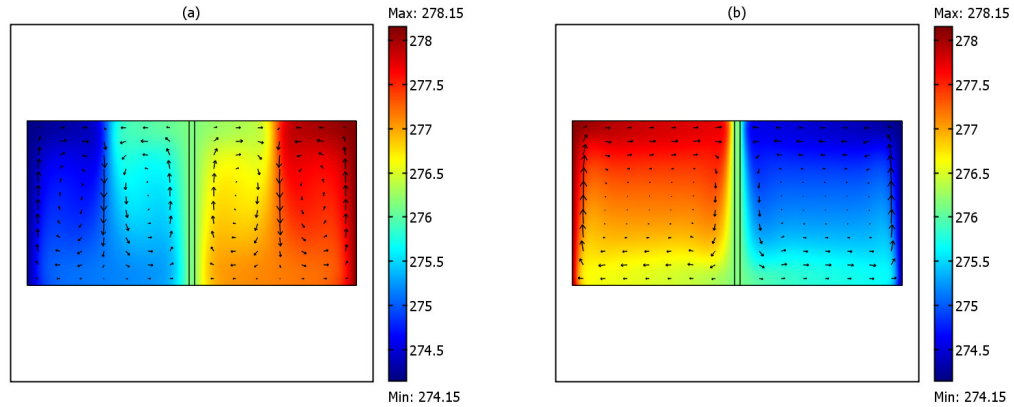


Figure 5.3-7 The temperature and velocity field of the water-saline diode containing water with a density maximum at 2°C in the first compartment and water with a temperature of maximum density at 4°C in the second compartment; the boundary conditions are 5°C (278.15 K) and 1°C (274.15 K). (Note: the temperature scales do not change in each of the surface plots).

The percentage rectification is zero if the rate of heat flow does not change when the direction of heat flow is reversed. In Figure 5.3-6 the percentage rectification is zero when the mean temperature of the temperature difference is 1.78°C and 4.19°C. When the central temperature is 1.78°C and heat flows from the compartment of water with a temperature of maximum density at 4°C to the other compartment, a single convection cell is observed in each compartment as shown in part (a) of Figure 5.3-9. When the rate of heat flow is reversed two convection cells of unequal size is observed in the saline compartment and just one convection cell is observed in the water compartment as shown in Figure 5.3-9. The effective thermal conductance (which is the ratio of the rate of heat transfer to the temperature difference across the compartment, it is not the same as the thermal conductivity of the liquid) of the saline compartment decreases due to the changes in the velocity field; this change is counteracted by an increase in the second compartment so that the overall effective thermal conductance is the same for both directions of heat flow. The increase in the effective thermal conductance of the water compartment is due to the moving away

of the temperature difference, that spans the water compartment, from the liquids temperature of maximum density. A similar effect is observed when the central temperature is 4.19°C . In this case, convection in each compartment occurs via a single cell when heat flows from the compartment with a density maximum at 4°C as shown in part (c) of Figure 5.3-9. When the direction of heat flow is reversed, two convection cells exist in the water compartment and one convection cell exists in the saline compartment as shown in part (d) of Figure 5.3-9. Again, the overall effective thermal conductance does not change when the direction of heat flow changes despite the change in the effective thermal conductance of the individual compartments. The effective thermal conductance of the water compartment decreases and this decrease is counteracted by an increase in the effective thermal conductance of the saline compartment.

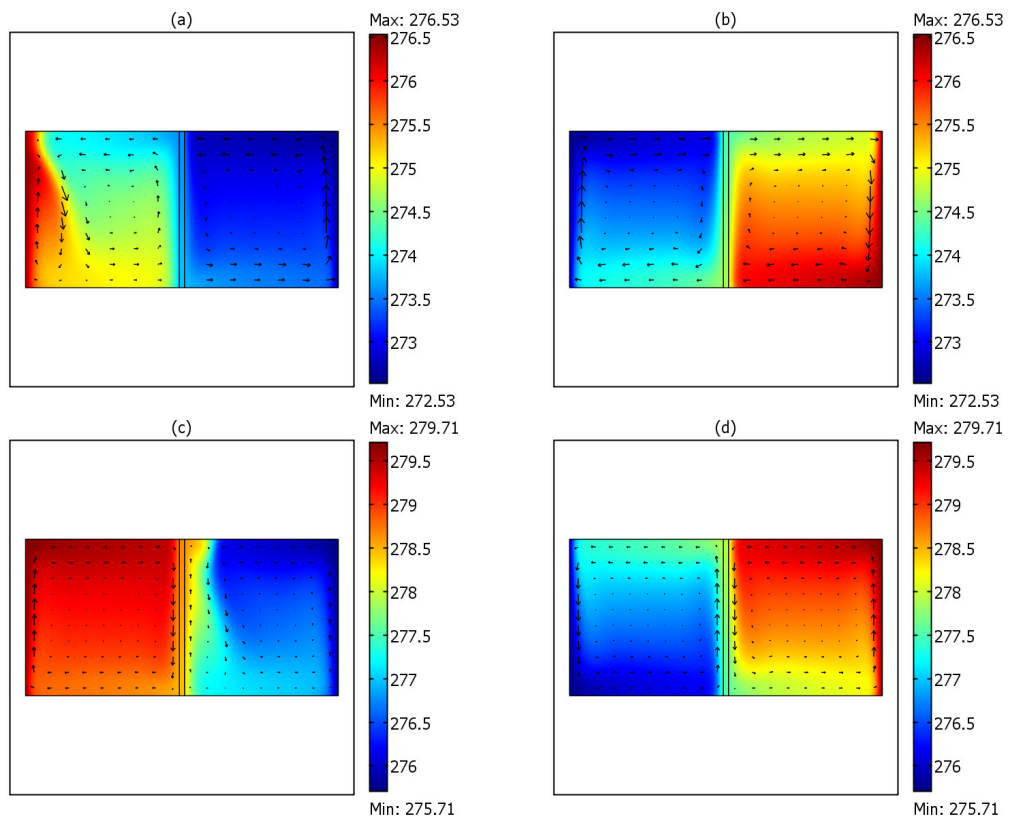


Figure 5.3-8 The temperature and velocity field of the water-saline diode containing water with a density maximum at 2°C in the first compartment and water with a temperature of maximum density at 4°C in the second compartment. The boundary conditions in the plots (a) to (d) are: (a) $T_L=3.38^{\circ}\text{C}$ and $T_R=-0.62^{\circ}\text{C}$, (b) $T_L=-0.62^{\circ}\text{C}$ and $T_R=3.38^{\circ}\text{C}$, (c) $T_L=6.56^{\circ}\text{C}$ and $T_R=2.56^{\circ}\text{C}$, and (d) $T_L=2.56^{\circ}\text{C}$ and $T_R=6.56^{\circ}\text{C}$. (Note: the temperature scales change in the surface plots).

Figure 5.3-6 shows that as the value of the mean temperature decreases from 1.38°C to 0°C, the percentage rectification drops considerably and tends towards 0%. The occurrence of this behaviour is due to the migration of the boundary temperatures away from the density maxima. A similar behaviour is seen when the mean temperature of the boundary temperatures increases from 4.56°C to 6°C. Likewise, this behaviour is due to the migration of the boundary temperatures away from the density maxima.

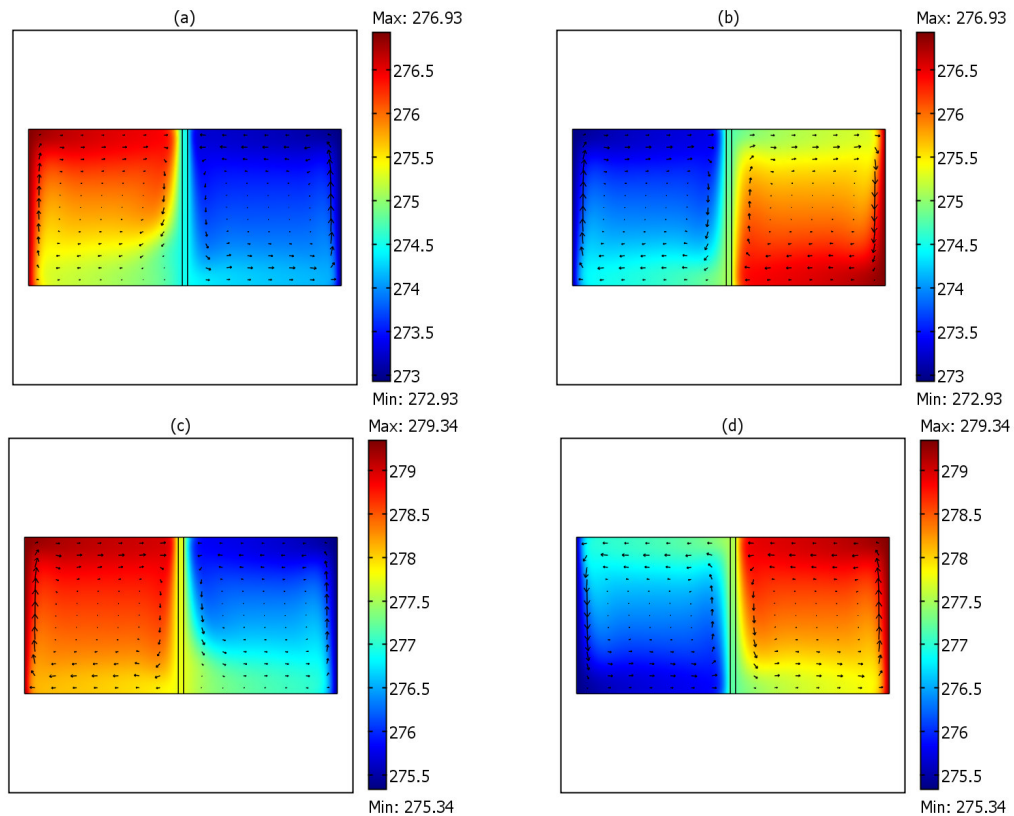


Figure 5.3-9 The temperature and velocity field of the water-saline diode containing water with a density maximum at 2°C in the first compartment and water with a temperature of maximum density at 4°C in the second compartment. The boundary temperatures in the plots (a)-(d) are: (a) 3.78°C and -0.22, (b) -0.22°C and 3.78°C, (c) 6.19°C and -2.19°C, (d) 6.19°C and 2.19°C. (Note: the temperature scales change in the surface plots).

5.3.2.2 Significance of the size of the temperature difference

Since the effective thermal conductance of the compartments is dependent on the temperature difference across the compartments, it was necessary to investigate the

effect of the temperature difference on the percentage rectification. The results of this investigation are shown in Figure 5.3-10. The temperature difference changes from 1°C to 8°C in steps of 1°C. For each temperature difference, the mean temperature of the boundary temperature changes from 0°C to 6°C in steps of 0.01°C. It is found that the maximum percentage rectification is achieved when the temperature difference is 4°C and the boundary temperatures are 5°C and 1°C (these conditions are identical to those of the experimental investigation). The main result of this investigation is summarized in Figure 5.3-11.

Figure 5.3-11 shows the maximum percentage rectification value obtained for each temperature difference investigated. The temperature differences that are less than or equal to 2°C are not large enough to encompass both temperatures of maximum density simultaneously and they are not large enough to achieve two symmetric convection cells in any compartment at any temperature, therefore these temperature differences never achieve the minimum effective thermal conductance in any compartment at any time. Consequently, the overall change in the effective thermal conductance when the direction of heat flow changes is much smaller than the change in the effective thermal conductance when both compartments exhibit the two counter rotating convection cells. Hence the maximum percentage rectification for $\Delta T < 3^\circ\text{C}$ is less than the maximum percentage rectification for $\Delta T = 4^\circ\text{C}$.

A temperature difference of 3°C is large enough to encompass both temperatures of maximum density simultaneously, however it is not large enough to achieve two symmetric convection cells in both compartments simultaneously. Consequently, the maximum percentage rectification for this temperature difference is greater than the maximum percentage rectification obtained by the temperatures of 1°C and 2°C, but is less than that obtained for a temperature difference of 4°C. A temperature difference of 4°C is the only temperature difference that can achieve two symmetric convection cells in both compartments simultaneously. Temperature differences larger than 4°C are too large to achieve two symmetric cells in each compartment simultaneously, and therefore these temperature differences do not obtain a percentage rectification greater than the percentage rectification achieved by a temperature difference of 4°C.

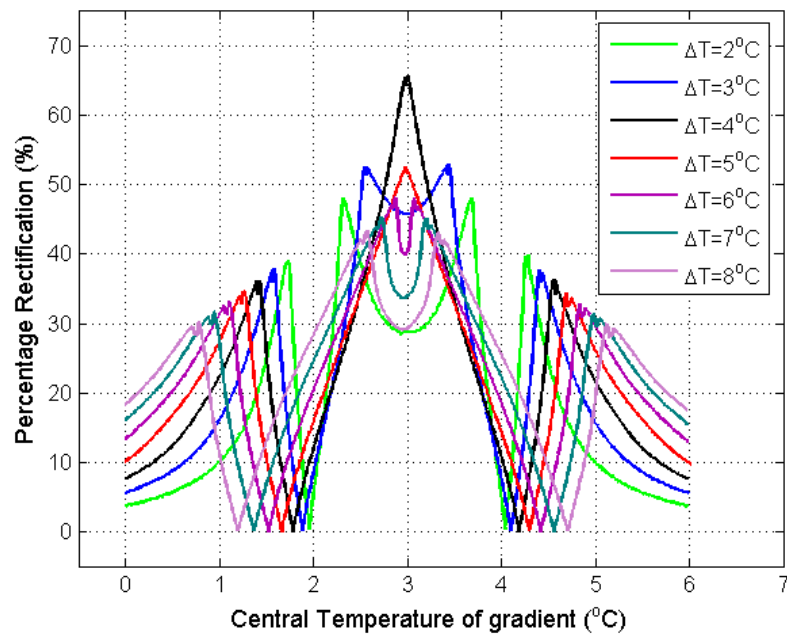


Figure 5.3-10 Multiple plots of the behaviour of the percentage rectification of the water-saline diode as a function of the centre temperature of the temperature gradient. The maximum percentage rectification occurs when the temperature difference is 4°C and the central temperature of the gradient is 3°C.

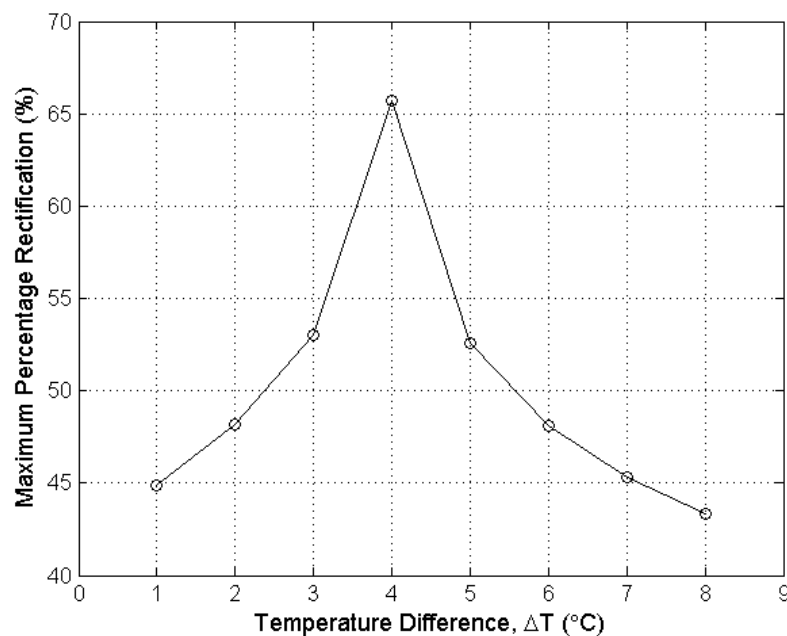


Figure 5.3-11 CFD optimization study of the water-saline diode; the maximum percentage rectification obtained for each temperature gradient over a temperature span of 0°C to 6°C (the gradient is varied from 1°C to 8°C across 0.12m).

5.3.2.3 Significance of the aspect ratio and scale of the container

The influence of the temperature difference on the percentage rectification of the water-saline diode has shown that a temperature difference of 4°C centred on 3°C achieves the maximum percentage rectification. The influence of the length of the diode and the scale of the diode on the percentage rectification under these conditions is shown in Figure 5.3-12 and Table 5.3-1.

The percentage rectification is very low for small cavities, but as the length of the cavity increases, the percentage rectification increases and reaches a maximum percentage rectification when the length of the cavity is 0.06m (the length of each compartment is 0.029m). The maximum percentage rectification is 67%; this value decreases as the length of the cavity increases until the length of the cavity is approximately 0.08m. The percentage rectification is approximately constant as the length of the cavity increases above this length. The percentage rectification is approximately 65% for all lengths greater than 0.08m.

The low rectification factor for rectifiers with a length less than 0.06m is due to the mechanism of heat transfer in both the low and high-conductance mode. In the low-conductance mode the convection pattern is the typical double cell structure; this structure results in the transfer of heat via conduction between the two convection cells, hence a low heat transfer rate. In the high-conductance mode, a single convection cell exists in each compartment. Typically, the single cell pattern efficiently transports heat from one wall to the other, but as shown in section 5.2.1 heat is transferred primarily by conduction for geometries with small lengths. This results in a low rate of heat transfer in the high-conductance mode. Thus, the rectification factor in Figure 5.3-12 is low for small diode lengths. In the high-conductance mode, the vigour of the convection increases as the length of the diode increases, and convection becomes the dominant mechanism of heat transfer. Consequently, the rate of heat transfer increases in the high-conductance mode as the length increases while the rate of heat transfer in the low-conductance mode remains relatively unchanged; thus, the rectification factor increases as the length increases to 0.06m.

A similar trend is observed in the investigation of the influence of the scale of the rectifier on the rectification factor. In this investigation, the aspect ratio (length/height) of the diode is constant and it has a value of 2. The dimensions of the diode increment from the micrometer scale to the meter scale. The results of this investigation are shown in Table 5.3-1. As the scale increases, the rectification factor increases and it remains relatively unchanged when the scale changes from centimetres to meters. The same argument as above applies here. For small lengths, heat is transferred primarily by conduction in the high-conductance mode. As the size increases, the vigour of the convection increases and becomes the dominant mechanism of heat transfer; while the mechanism of heat transfer in the low-conductance mode is always dominated by conduction between the two counter-rotating cells. Thus, the rectification factor increases to the point where convection is the primary mechanism of heat transfer.

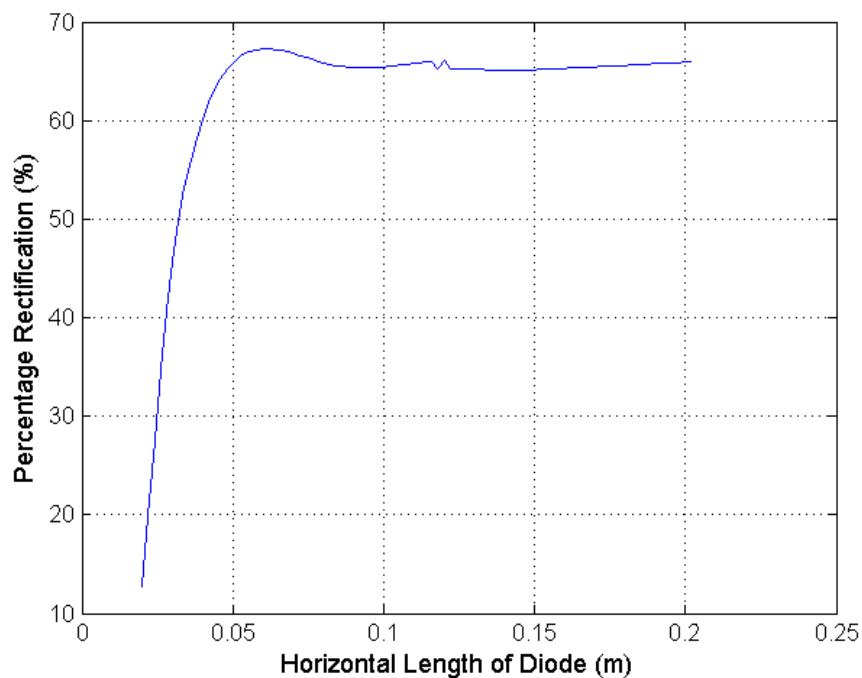


Figure 5.3-12 Percentage rectification of the water-saline diode as a function of the horizontal length of the cavity. The temperature difference is 4°C and the central temperature of the gradient is 3°C .

Length of the diode (m)	Percentage rectification (%)
0.0012	0
0.0120	3.3
0.1200	65.4
1.2000	64.1

Table 5.3-1 The percentage rectification of the water-saline diode, with a constant aspect ratio (length/height) of 2, as a function of the horizontal length of the rectifier. The temperature difference is 4°C and the central temperature of the gradient is 3°C.

5.3.2.4 Significance of the number of liquid compartments

The influence of the number of compartments in the diode is investigated by adding compartments to the rectifier as shown in Figure 5.3-13. Adding compartments to the cavity increases the size of the cavity, so that the thermal diode of length 0.12m increases to a length of 0.18m when the number of compartments is three. Since the length of the container increases by approximately 0.06m when the number of compartments is increased, the temperature difference is increased by 1°C so that the temperature gradient remains unchanged.

The results in Figure 5.3-14 show that the percentage rectification behaves differently for odd and even numbered compartments. The boundary temperatures of the multiple compartment diodes with an even number of compartments are chosen so that when the direction of heat flow changes the convection pattern inside each compartment changes from a single convection cell to two counter rotating cells. This arrangement is not obtainable for an odd number of compartments since the compartment in the centre has two counter rotating cells for both directions of heat flow. Consequently, the percentage rectification for the even numbers is greater than the percentage rectification of the odd numbers.

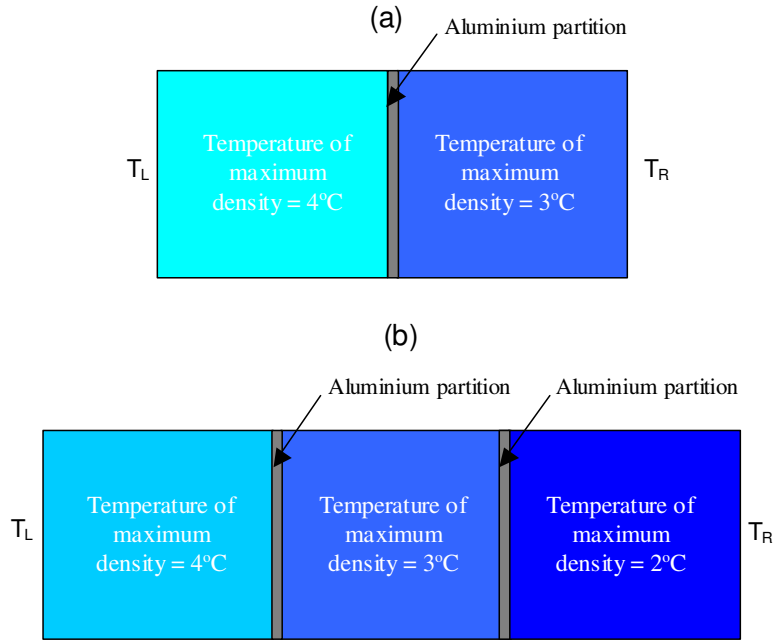


Figure 5.3-13 The influence of the number of liquid compartments in the diode on the percentage rectification is investigated by adding compartments to the rectifier. (a) The typical construction of the water-saline diode. (b) The addition of one compartment to the water-saline diode shown in (a).

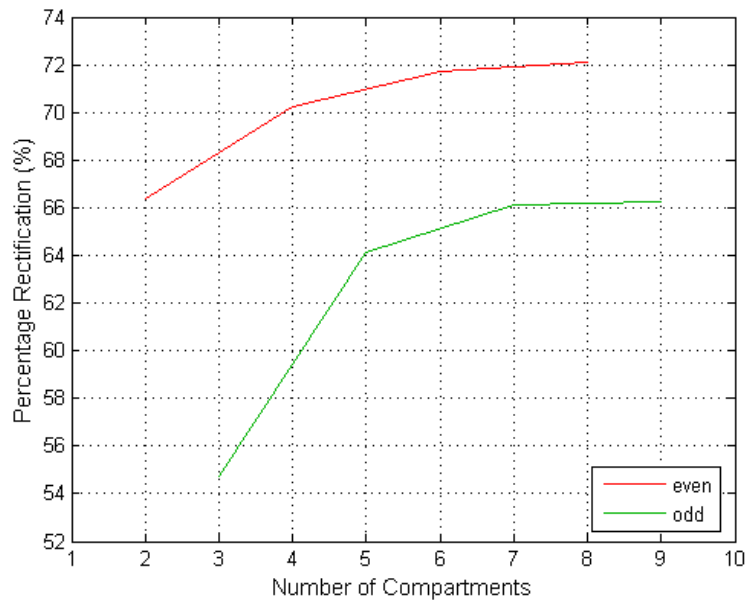


Figure 5.3-14 The influence of the number of liquid compartments in the water-saline diode on the percentage rectification. Adding a compartment to the cavity increases the cavity size. Each compartment has dimensions of 0.06 m by 0.059m.

The percentage rectification increases as the number of compartments increases and the maximum percentage rectification is obtained for eight compartments as shown in Figure 5.3-14. The maximum percentage rectification obtained is 72%. For a diode with any number of compartments the effective thermal conductance is the same inside all compartments when two counter rotating cells exist in all compartments. However, when one convection cell exists in all of the compartments (with the exception of the centre compartment for odd numbers) the effective thermal conductance increases as the number of compartments increases.

Since the temperature difference across each individual compartment is centred on a different temperature than the others, the density difference in each compartment is different; hence, the effective thermal conductance of each compartment is different. As the number of compartments increases, the centre of the temperature difference moves further away from the maximum in the density curve and the density differences increase, hence the effective thermal conductance increases. Since the effective thermal conductance in the direction of lowest heat transfer is unaffected by the addition of compartments while the effective thermal conductance in the direction of maximum heat flow increases the percentage rectification increases as the number of compartments increases.

5.3.3 Water-Perspex diode

The water-Perspex diode consists of a rectangular enclosure of water adjacent to a slab of Perspex as described in Cawley *et al.* [36] and as shown in Figure 5.3-15. The basis of this thermal diode is that heat transfer is reduced in the vicinity of the density maximum. This section aims to confirm the experimental results presented in section 3.4.3 and to aid understanding of them. The experimental procedure for investigating asymmetrical heat transfer holds a constant temperature gradient across the composition for a set time. When this time has elapsed, the gradient is reversed by swapping the wall temperatures. The walls are then held at these temperatures for the same period of time as before. This experimental procedure is simulated numerically as described in section 4.4.1 and the results are presented in Figure 5.3-16.

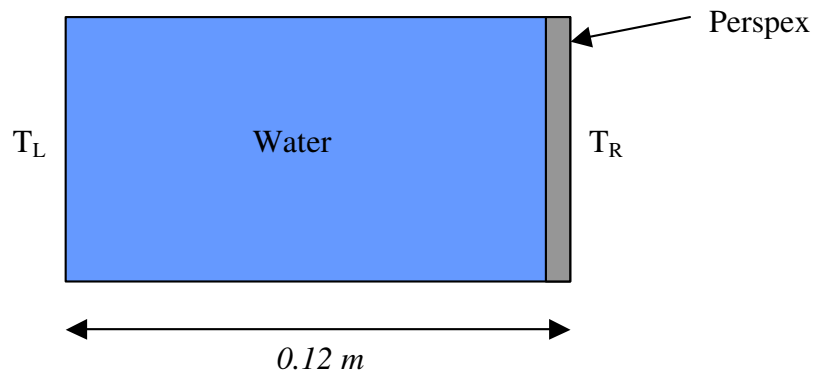


Figure 5.3-15 The water Perspex diode consists of a rectangular enclosure of water (dimensions of $0.06\text{m} \times 0.06\text{m} \times 0.118\text{m}$) adjacent to a slab of Perspex (dimensions of $0.06\text{m} \times 0.06\text{m} \times 0.002\text{m}$).

The results presented in Figure 5.3-16 and Figure 5.3-17 show the boundary temperatures, the monitoring temperatures, and the temperatures at select points inside the water compartment. In the first 30,000 seconds of this graph, the temperature of the left wall (T_L) is 2.5°C and the temperature of the right wall (T_R) is 6.5°C . During this time, heat flows from the Perspex slab to the water compartment and the convection pattern inside the water compartment is that of a single convection cell as shown in part (a) of Figure 5.3-18. In the latter 30,000 seconds, heat flows in the opposite direction and two unequal convection cells exist in the water compartment as shown in part (b) of Figure 5.3-18. The temperature differences between the monitoring temperatures and the boundary temperatures are directly proportional to the rate of heat transfer. It is evident from Figure 5.3-2 that the rate of heat transfer in the first 30,000 seconds is greater than the rate of heat transfer in the latter 30,000 seconds. Thus, the rate of heat transfer changes when the direction of heat flow is reversed. A plot of the rate of heat transfer is shown in Figure 5.3-17. This plot shows that the rate of heat transfer changes from 0.58W to 0.36W when the direction of heat flow is reversed. This yields a percentage rectification of 38% for the water-Perspex diode.

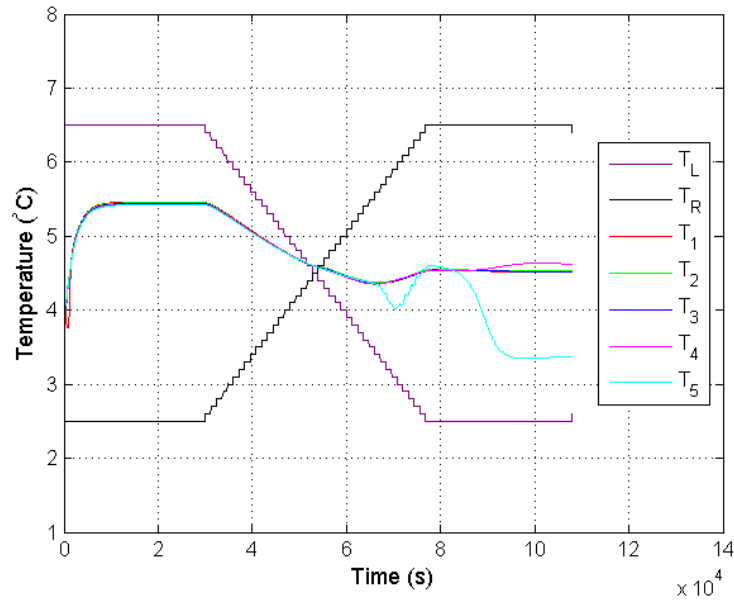


Figure 5.3-16 The behaviour of the temperature field when the thermal diode effect is observed in the water-Perspex diode. These results can be directly compared to the experimental results in Figure 3.4-9. ($Ra \approx 5.0 \times 10^6$ in the first 30,000 seconds and $Ra \approx 8.8 \times 10^5$ in the last 30,000 seconds).

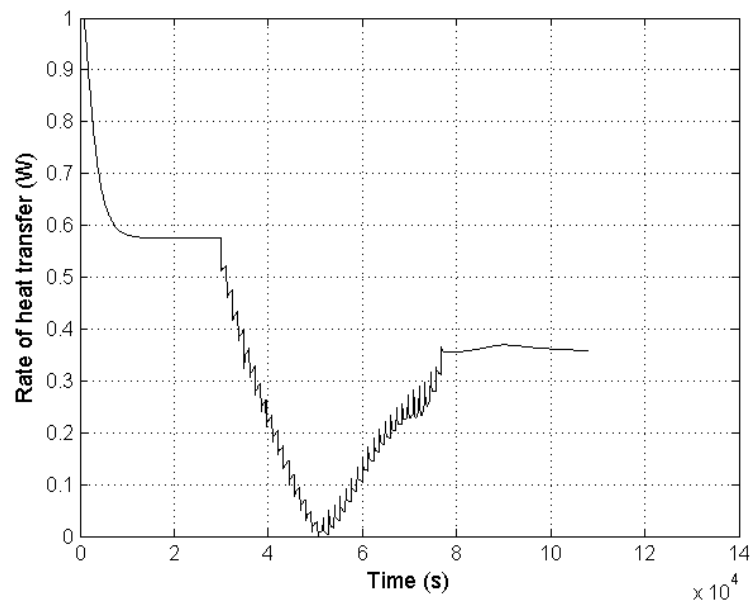


Figure 5.3-17 The average rate of heat flow through the water-Perspex diode when heat flows from right to left (the first 30,000 seconds) and from left to right (the last 30,000 seconds). It is evident that the rate of heat flow changes when the direction is changed. ($Nu \approx 7.9$ in the first 30,000 seconds and $Nu \approx 4.9$ in the last 30,000 seconds.)

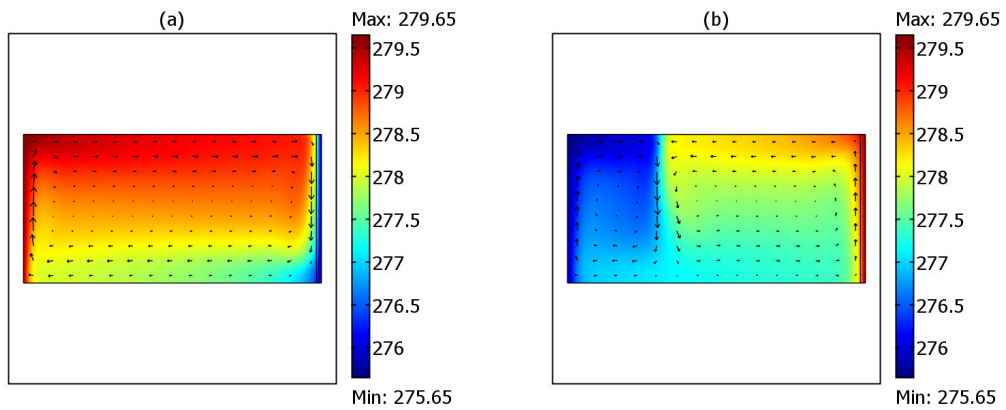


Figure 5.3-18 Numerical results for the flow patterns (arrow plot) and the temperature fields (surface plots; degrees Kelvin) in the two conductance modes of the water-Perspex diode (water on the left and Perspex on the right). (a) High conductance mode: $T_L=6.5^\circ\text{C}$ and $T_R=2.5^\circ\text{C}$. (b) Low conductance mode: $T_L=2.5^\circ\text{C}$ and $T_R=6.5^\circ\text{C}$. (Note: the temperature scales do not change in each of the surface plots).

Parts (a) and (b) of Figure 5.3-19 show the experimental results for the water-Perspex diode and parts (c) and (d) show the corresponding numerical results. It is evident from these plots that the rate of heat transfer is high for the first direction of heat transfer and low for the second direction in both sets of results. In region (i) of the experimental results, the temperature profiles are within 0.2°C of each other. During the interchanging region, the temperature profiles show the typical anomaly feature observed during the cooling of water in the vicinity of the density maximum. Afterwards in region (ii), the temperature profiles converge and remain within 0.2°C of each other again. This compares to the numerical results in Figure 5.3-19(c). In region (i) the temperature profiles are within 0.2°C of each other; this agrees with the experiment. During the interchanging region, one temperature profile diverges from the other momentarily; this does not agree with the experimental results. In region (ii) of the numerical results, one of the temperature profiles exhibits a lower temperature than the others which are at 4.5°C ; this also disagrees with the experimental results. The corresponding heat transfer plots do not show good quantitative agreement. It is observable in the experimental results in Figure 5.3-19(a) that the boundary temperatures in region (ii) are actually 6.3°C and 2.5°C . This offset in the boundary temperatures may account for some of the discrepancies.

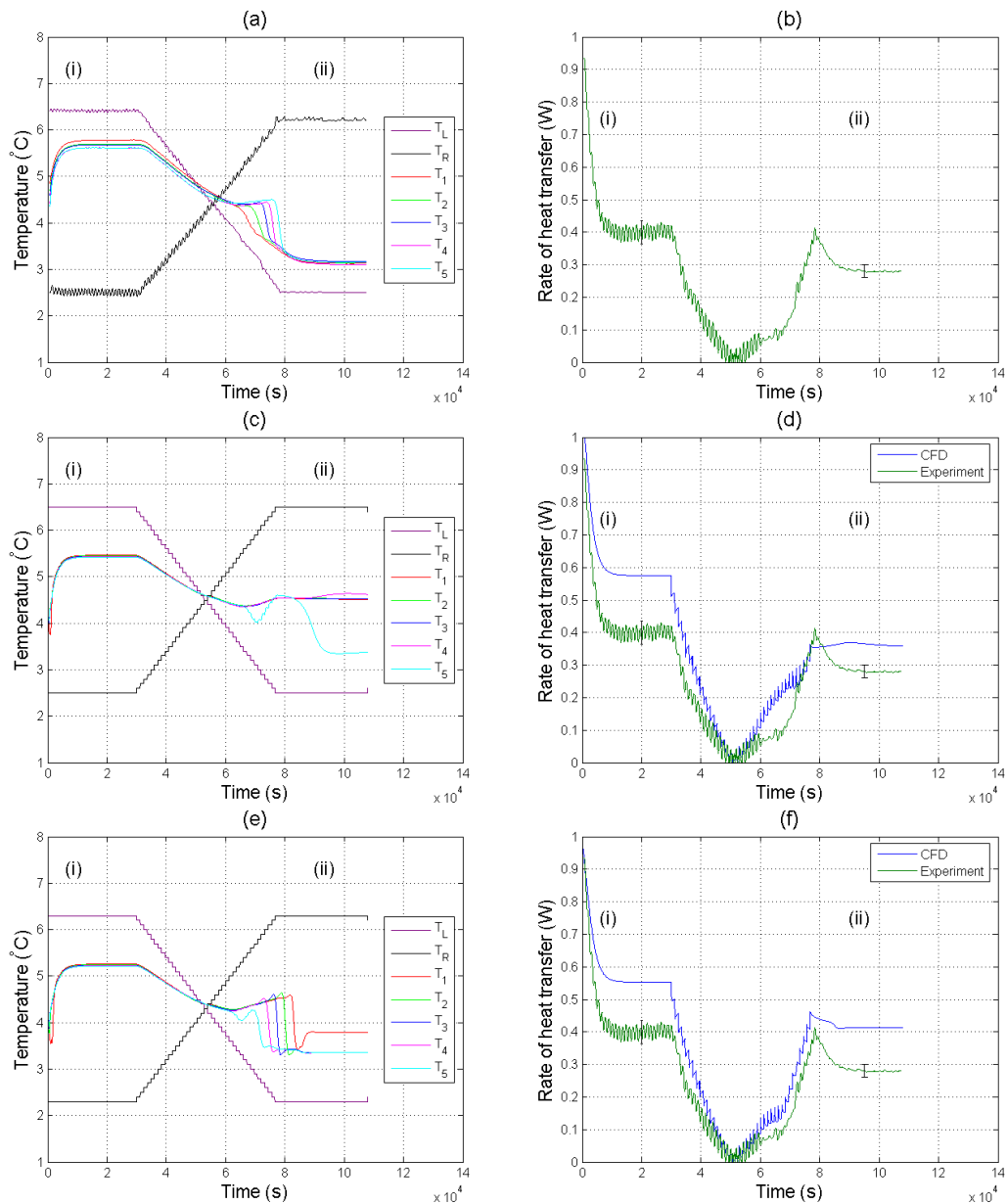


Figure 5.3-19 Temperature against time for the water-Perspex diode (a) and (b) the experimental results with boundary temperatures of 6.5°C and 2.5°C (c) and (d) the CFD results with boundary temperatures of 6.5°C and 2.5°C , and (e) and (f) the CFD results with boundary temperatures of 6.3°C and 2.3°C . In each plot region (i) corresponds to the diode in its high conductance mode and region (ii) corresponds to the low conductance mode.

The numerical results for the water-Perspex diode with boundary temperatures of 6.3°C and 2.3°C are shown in parts (e) and (f) of Figure 5.3-19. In region (i) of the temperature profiles plot, the profiles are within 0.2°C of each other; this agrees with

the experimental results. During the interchanging region, the temperature profiles show the typical anomaly feature observed during the cooling of water in the vicinity of the density maximum; this agrees with the experimental results. Afterwards in region (ii), one of the temperature profiles diverges from the others which remain within 0.2°C of each other at 3.3°C; the divergence of one profile does not agree with the experimental results, but the bunching together of the other four temperature profiles at 4.3°C does agree with the experimental results.

The heat transfer results for both the experimental investigation and the numerical investigation (with boundary temperatures of 6.3°C and 2.3°C) are shown in Figure 5.3-19(f). The numerical results are not within the margin of error on the experimental results but the two plots do show good qualitative agreement. Each plot shows that the rate of heat transfer is high in region (i) and low in region (ii), decreases as the temperature difference decreases (in the interchanging region) and reaches 0W at approximately 50,000 seconds, increases as the temperature difference increases. Both plots show that the rate of this increase slows down between 60,000 seconds and 70,000 seconds before increasing rapidly. The rapid increase between 70,000 seconds and 80,000 seconds results in an overshoot of the rate of heat transfer in region (ii).

It is postulated in section 3.4.3 that this rapid increase and overshoot is due to the rapid cooling of the water sample induced by the density inversion (due to the rapid growth of a second convection cell across the enclosure). Figure 5.3-20 (a-d) shows a selection of plots of the velocity and temperature fields for the water-Perspex diode with boundary temperatures of 6.3°C and 2.3°C. These plots show that in region (i) a single convection cell transfers heat from the hot wall to the cold wall. As the wall temperatures are being reversed, a small counter-rotating cell develops at the left wall, grows across the compartment, and dominates the flow. However, the boundary temperatures stop changing before the other cell ceases to exist, and so the convection pattern in region (ii) contains a small counter-rotating cell at the left wall. The small clockwise convection cell develops and grows up along the left wall between 60,000 seconds and 70,000 seconds, thus the slow rate of increase between 60,000 seconds and 70,000 seconds. The growth of this cell across the compartment

occurs between 70,000 seconds and 80,000 seconds, thus the rapid increase in the rate of heat transfer between 70,000 seconds and 80,000 seconds.

It is also postulated in section 3.4.3, that the bunching together of the experimental temperature profiles in region (ii) is due to the offset of the boundary temperature from 6.5°C to 6.3°C. This analysis is supported by the numerical plots in parts (c) and (e) of Figure 5.3-19 and the velocity and temperature field plots in Figure 5.3-18(b) and Figure 5.3-20(f). In Figure 5.3-19(c), the boundary temperatures are 6.5°C and 2.5°C; this results in a divergence of two of the temperature profiles while the others are at 4.5°C. An offset of 0.2°C is shown in Figure 5.3-19(e), four of the temperature profiles are bunched together at 2.3°C (compared to 2.2°C for the experiment). The offset of 0.2°C reduces the size of the smallest convection cell, thus four of the temperature profiles are in the same convection cell.

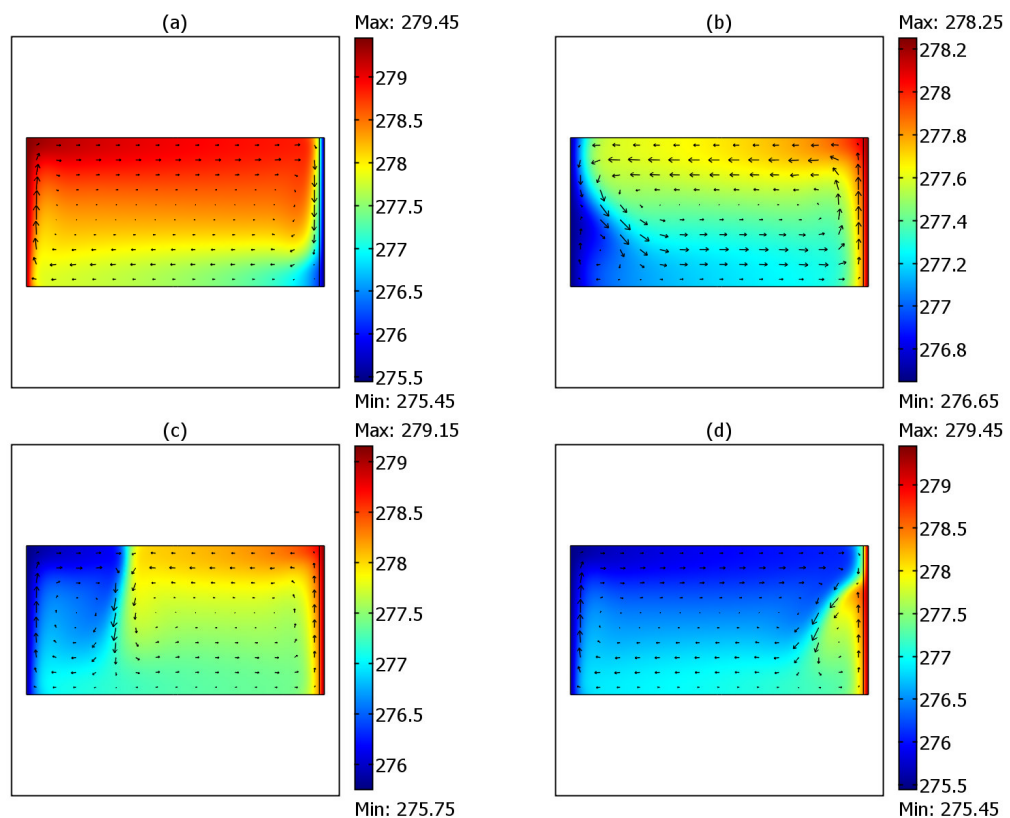


Figure 5.3-20 Numerical results for the flow patterns (quiver plot) and the temperature fields (surface plots; degrees Kelvin) for the water-Perspex diode. (a) High conductance mode: $T_L=6.3^\circ\text{C}$ and $T_R=2.3^\circ\text{C}$. (b) $T_L=3.55^\circ\text{C}$ and $T_R=5.5^\circ\text{C}$, (c) $T_L=2.6^\circ\text{C}$ and $T_R=6^\circ\text{C}$, (d) Low conductance mode: $T_L=2.3^\circ\text{C}$ and $T_R=6.3^\circ\text{C}$. (Note: the temperature scales change in the surface plots).

5.3.4 Optimization of the water-Perspex diode

Experimental results presented in section 3.4.2 have shown that a composite system of water and Perspex exhibits asymmetrical heat transfer. CFD analysis of the water-Perspex diode has confirmed that the results obtained experimentally are qualitatively accurate and that the density maximum phenomenon of water is directly responsible for decreasing the rate of heat transfer through the water-Perspex diode when the water compartment is placed in the region of the temperature gradient that encompasses the temperature of maximum density. Before commencing the experimental investigations, it was decided that the optimal boundary temperatures for the water-Perspex diode (with a water compartment of length 0.118m and a Perspex slab of length 0.002m) should be investigated numerically. The optimal temperatures obtain in this investigation were used as the boundary temperatures in the experimental investigations. Due to the accuracy of the CFD results acquired, it was decided that the model would be extended to include a study on the influence of the ratio of the length of the water compartment to the length of the Perspex slab.

As previously mentioned, the purpose of the first investigation was to obtain the optimal boundary temperatures for the water-Perspex diode, with a Perspex length of 0.002m that would be used in the experimental investigations. Using the scripting feature in Comsol Multiphysics, the optimal boundary temperatures were investigated by selecting a constant temperature difference of 4°C and changing the mean temperature of the boundary temperatures from 2°C to 6°C in steps of 0.01°C. The results of this investigation are presented in section 5.3.4.1.

The influence of the ratio of the length of the water compartment to the length of the Perspex slab was also investigated using the scripting feature in Comsol Multiphysics. The temperature difference across the composite system was chosen to be 4°C and the above procedure was applied to eight different ratios. The total length of the system remained unchanged at 0.12m and the height of the system was 0.06m. The Perspex thickness ranged from 1mm, 2mm, 3mm, 4mm, 5mm, 6mm, 7mm and 8 mm and the corresponding values for the length of the compartment of water are 119mm, 118mm, 117mm, 116mm, 115mm, 114mm, 113mm and 112mm. The results of this investigation are presented in section 5.3.4.2.

5.3.4.1 Significance of the boundary temperatures

The first optimization study applies a temperature difference of 4°C across the water-Perspex diode. The boundary temperatures are initially chosen so that they are centred on 2°C, e.g. for a temperature difference of 4°C the boundary temperatures are 4°C and 0°C. These temperatures are incremented by 0.01°C and the percentage rectification for each set of boundary temperatures is obtained. The percentage rectification of the water-Perspex diode as a function of the mean temperature of the boundary temperatures is plotted in Figure 5.3-21. As discussed in Cawley *et al.* [36], two peaks are observed in Figure 5.3-21, each peak has two local maxima and two local minima. The maximum percentage rectification of 40% occurs in the latter peak when the central temperature is 4.51°C. When heat flows in a certain direction under these boundary conditions the velocity field in the water compartment has two counter rotating convection cells, i.e. the compartment has its minimum thermal conductivity. When the direction of heat flow is reversed, the water compartment has just one convection cell, this dramatic change in the velocity field results in a very dramatic difference in the rate of heat flow for each direction. The behaviour of the thermal and velocity fields in both directions of heat flow is shown in Figure 5.3-22.

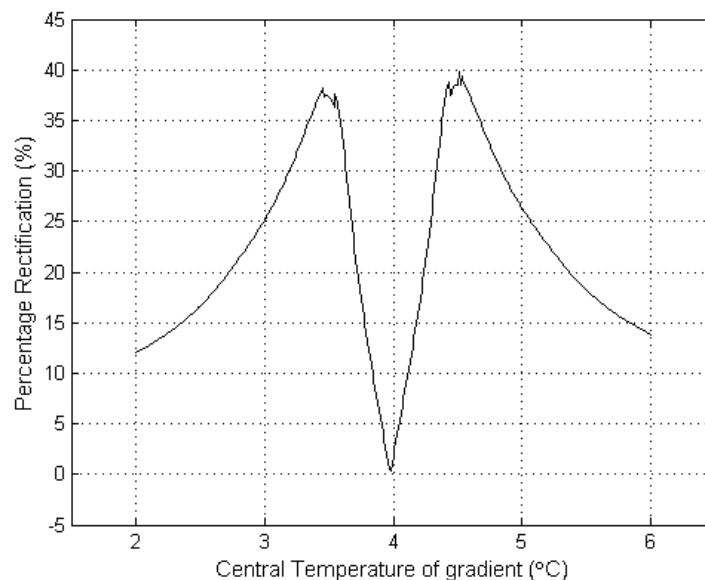


Figure 5.3-21 The percentage rectification of the thermal diode with a temperature difference of 4°C. The percentage rectification changes as the centre temperature of the temperature gradient changes.

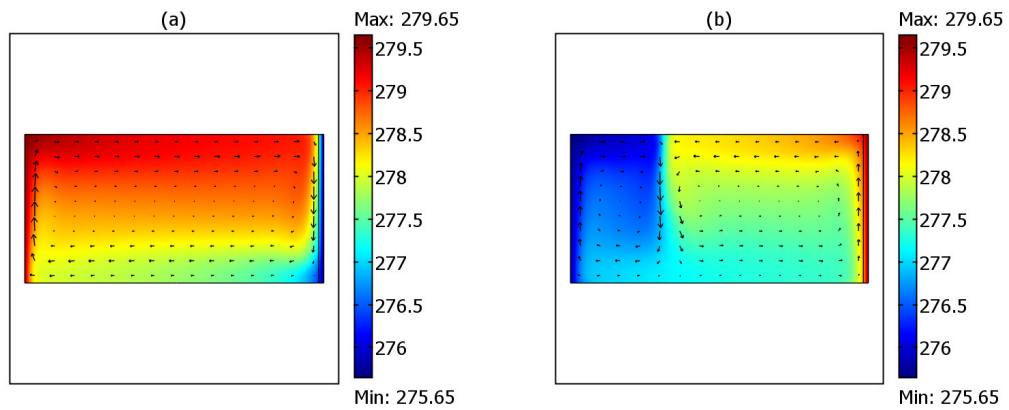


Figure 5.3-22 The temperature and velocity field of the water-Perspex diode containing water with a density maximum at 4°C adjacent to a slab of Perspex of length 0.002m under the conditions that correspond to the second peak in Figure 5.3-21. The boundary temperatures are (a) $T_L=6.5^\circ\text{C}$ (279.65 K) and $T_R=2.5^\circ\text{C}$ (275.65 K), (b) $T_L=2.5^\circ\text{C}$ (275.65 K) and $T_R=6.5^\circ\text{C}$ (279.65 K). (Note: the temperature scales do not change in each of the surface plots).

A second primary maximum is found in the percentage rectification shown in Figure 5.3-21 that occurs when the mean temperature of the boundary temperatures is 3.46°C. This maximum occurs when there is a single convection cell in the water compartment for a given direction of heat flow and when this direction is reversed there are two unequal convection cells in the compartment containing water as shown in parts (a) and (b) of Figure 5.3-23.

Each peak contains two local maxima and two local minima. It is important to note that the difference in the percentage rectification of these four extremum points is less than the change in the percentage rectification obtained when the currently used mesh density changes to a higher mesh density. Therefore, it is possible that there is only one extremum point in this peak, however the occurrence of four extremum points is observed in both peaks shown in Figure 5.3-21 (and in each of the peaks in all eight plots shown later in Figure 5.3-25). It is difficult therefore to conclude that these features are due to any dependency of the results on the mesh density.

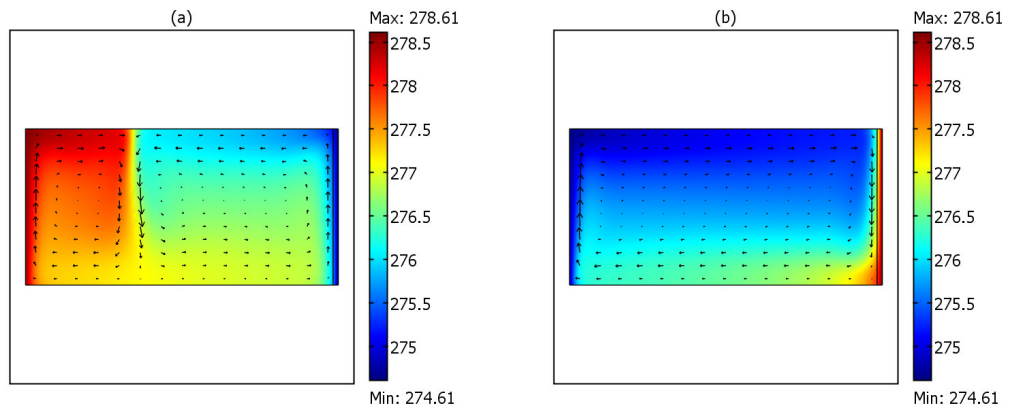


Figure 5.3-23 The temperature and velocity field of the water-Perspex diode containing water with a density maximum at 4°C adjacent to a slab of Perspex of length 0.002m under the conditions that correspond to the second peak in Figure 5.3-21. The boundary temperatures are (a) $T_L=5.46^{\circ}\text{C}$ and $T_R=1.46^{\circ}\text{C}$, (b) $T_L=1.46^{\circ}\text{C}$ and $T_R=5.46^{\circ}\text{C}$. (Note: the temperature scales do not change in each of the surface plots).

The percentage rectification is zero if the rate of heat flow does not change when the direction of heat flow is reversed. In Figure 5.3-21, the percentage rectification is zero when the mean temperature of the temperature difference is 3.98°C . When the central temperature is 3.98°C and heat flows from left to right, a small counter clockwise convection cell exists at the wall adjacent to the Perspex slab as shown in part (a) of Figure 5.3-24. When the direction of heat flow is reversed, the same convection pattern occurs again in the water compartment as shown in part (b) of Figure 5.3-24. Consequently, the effective thermal conductance of the liquid is the same in both directions of heat flow, thus there is no change in the rate of heat flow and the percentage rectification is zero.

Figure 5.3-21 shows that as the value of the mean temperature decreases from 3.46°C to 2°C , the percentage rectification drops considerably and tends towards 0% . The occurrence of this behaviour is due to the migration of the boundary temperatures away from the density maximum. A similar behaviour is seen when the mean temperature of the boundary temperatures increases from 4.51°C to 6°C . Likewise, this behaviour is due to the migration of the boundary temperatures away from the density maximum.

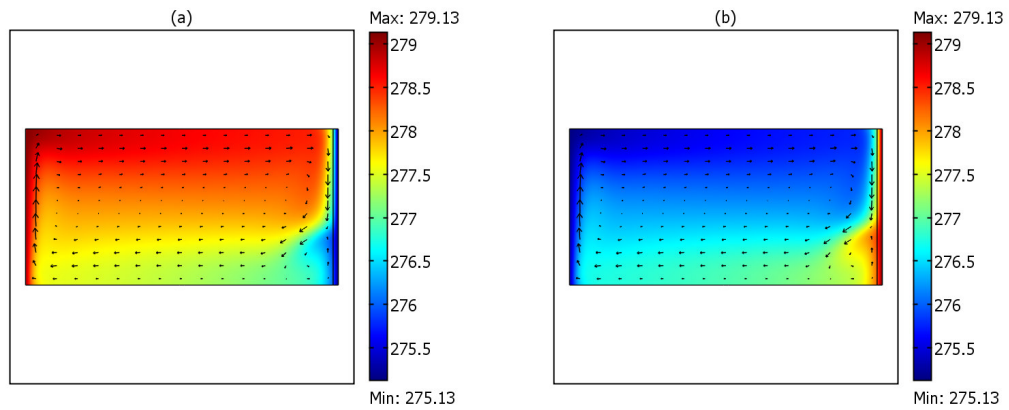


Figure 5.3-24 The temperature and velocity field of the water-Perspex diode containing water with a density maximum at 4°C adjacent to a slab of Perspex of length 0.002m under the conditions that correspond to the trough in Figure 5.3-21. The boundary temperatures are (a) $T_L=5.98^\circ\text{C}$ and $T_R=1.98^\circ\text{C}$, (b) $T_L=1.98^\circ\text{C}$ and $T_R=5.98^\circ\text{C}$. (Note: the temperature scales do not change in each of the surface plots).

5.3.4.2 Significance of the width of the Perspex slab

The basis of the water-Perspex diode is that the temperature difference across the water compartment changes when the direction of heat flow changes. The effective thermal conductivity of the Perspex slab is constant for a constant length regardless of the temperature difference across it. In contrast, the effective thermal conductivity of the water compartment changes when either the size of the temperature difference across the compartment or the mean temperature of the temperature difference across the compartment changes. It is the changing effective conductivity of the water compartment that causes the system to exhibit asymmetrical heat transfer. The purpose of the Perspex slab is to change the bounding temperatures across the water compartment when the direction of heat flow is reversed. Since the effective thermal conductivity of the water compartment depends on the temperature difference across the compartment, it was decided to investigate the influence of the length of the Perspex slab on the rectification factor. The results of this investigation are shown in Figure 5.3-25. The length of the Perspex slab changes from 0.001m to 0.008m in steps of 0.001m. For each Perspex length, the mean temperature of the temperature difference changes from 2°C to 6°C in steps of 0.01°C. As discussed in Cawley *et al.* [36], it is found that the maximum percentage rectification is achieved when the

length of the Perspex slab is 0.002m and the boundary temperatures are 6.51°C and 2.51°C (these conditions were used in the experimental investigation). It is evident from Figure 5.3-25 that as the length of the Perspex slab increases from 0.002m to 0.008m, the maximum percentage rectification decreases and the mean temperatures at which the two peaks occurs move away from the temperature of maximum density.

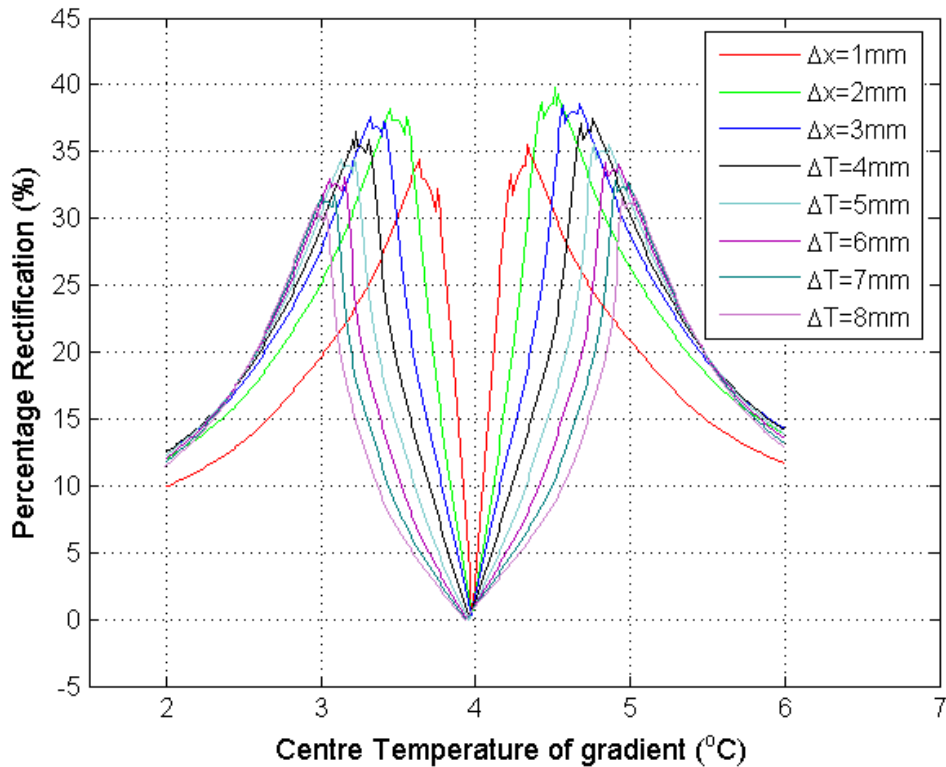


Figure 5.3-25 Multiple plots of the behaviour of the percentage rectification of the water-Perspex diode as a function of the centre temperature of the temperature gradient. The maximum percentage rectification occurs when the temperature difference is 4°C and the width of the Perspex slab is 2mm.

Figure 5.3-26 shows the maximum percentage rectification as a function of the ratio of the length of the Perspex slab to the length of the water compartment. The effective thermal conductivity of the Perspex slab decreases as the length increases. Consequently, the temperature difference across the water compartment decreases. In the high-conductance mode, the effective thermal conductivity of the compartment depends on the density difference encompassed by the gradient and hence the temperature difference across it. Thus, as the length of the Perspex slab increases,

the effective thermal conductivity of the water compartment in the high conductance mode decreases. In the low-conductance mode, the effective thermal conductivity of the water compartment depends on the convection pattern more so than the density difference, thus the effective thermal conductivity remains relatively unchanged as the length of the Perspex slab increases. In summary, as the length of the Perspex slab increases, the effective thermal conductivity of the water-Perspex diode in the high conductance mode decreases, and it remains relatively unchanged in the low-conductance mode. Thus, the rectification factor decreases as the length of the Perspex slab increases.

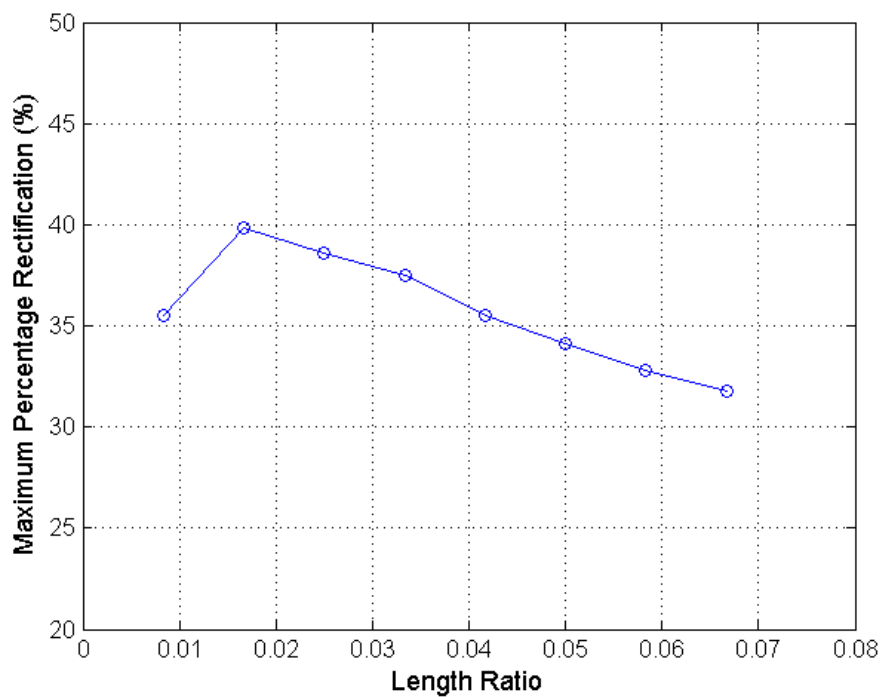


Figure 5.3-26 CFD optimization study of the water-Perspex diode: percentage rectification as a function of the ratio of the width of the Perspex slab to the width of the water compartment (with the total length fixed at 12cm). The Perspex width is varied from 0.1cm to 0.8cm.

It is evident from Figure 5.3-25 that as the length of the Perspex slab increases the mean temperature of the boundary temperatures for the maximum percentage rectification moves away from 4°C. This trend can be understood by noting that the maximum percentage rectification occurs when the mean temperature of the temperature difference across the water compartment is close to 4°C. As the length

of the Perspex slab increases the temperature difference across the water compartment decreases. Consequently, the central temperature of the gradient across the entire composition moves away from 4°C for the maximum percentage rectification as the length of the Perspex slab increases.

5.3.5 Phase change diode

This section investigates asymmetrical heat transfers in two composite systems involving a phase change material (phase change diodes). The first composition consists of a liquid and a Phase Change Material (PCM) and the second composition consists of a solid and a phase change material. The basis of the phase change diode is that when heat flows in a given direction the PCM is in its solid state, so heat flows through the PCM via conduction in this direction; when the direction is reversed the PCM is in its liquid state and heat flows via convection. This change in the mechanism of heat transfer alters the rate of heat flow. In both of these configurations the first compartment consist of water with a freezing point at 0°C and the second compartment contains water with an artificial freezing point at -3°C. Using the same substance in each compartment ensures that changes in the rate of heat flow are entirely due to the phase change.

Figure 5.3-27 shows the results for the first configuration, whereby one compartment contains water in its liquid state for two opposing directions of heat flow while the other compartment undergoes a phase change when the direction of heat flow is reversed. The boundary temperatures for this configuration are 2°C and -2°C. In part (a) of Figure 5.3-27 heat flows via convection in each compartment and the rate of heat transfer is 0.61W. In part (b) of Figure 5.3-27, heat flows via convection in the first compartment and via conduction in the second compartment (the phase change material changes from a liquid to a solid). This change in the mechanism of heat transfer reduces the rate of heat flow to 0.30W. This results in a rectification factor of 50%.

Figure 5.3-28 shows the results for the second configuration whereby the first compartment is in its solid state for both directions of heat flow and the second compartment undergoes a phase change when the direction of heat flow is reversed. The boundary temperatures for this configuration are -1°C and -5°C. In part (a) of

Figure 5.3-28 heat is transferred via conduction in both compartments and the resulting rate of heat transfer is 0.24W. In part (b) of Figure 5.3-28, heat is transferred by conduction in the first compartment and via convection in the second compartment. This change in the mechanism of heat transfer in the second compartment increases the rate of heat transfer to 0.30W. This results in a rectification factor of 20% for this configuration.

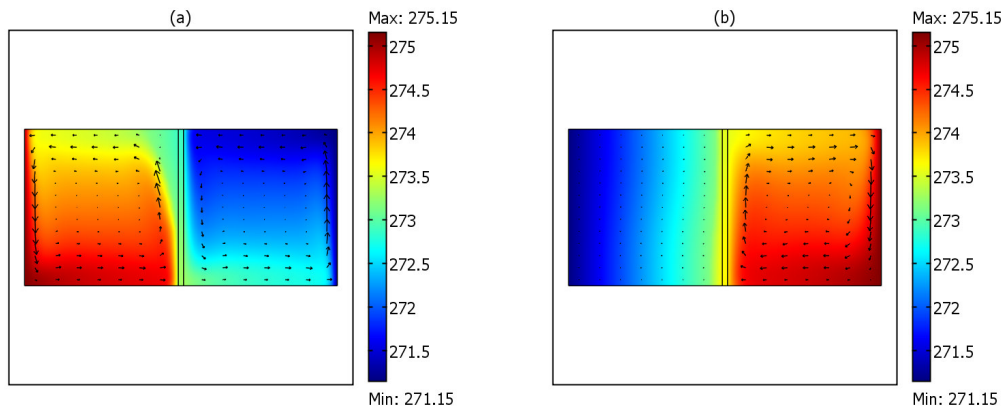


Figure 5.3-27 The phase change diode contains a PCM in the left chamber and water with an artificial freezing point at -3°C in the second cavity. The PCM is water with a freezing point at 0°C . (a) Heat flows from left to right and the PCM is in its liquid state, (b) heat flows from right to left and the PCM is in its solid state.

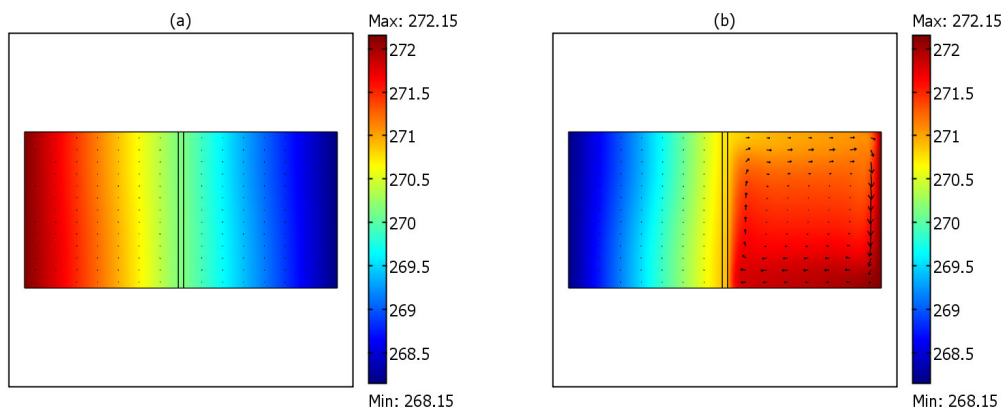


Figure 5.3-28 This diode contains a PCM in the right chamber and water with freezing point at 0°C in the second cavity. The PCM is water with an artificial freezing point at -3°C . (a) Heat flows from left to right and the PCM is in its solid state, (b) heat flows from right to left and the PCM is in its liquid state.

5.3.6 Thermal analogy of Ohm's law for the water-saline diode

In thermal engineering, there exists an analogy to Ohm's Law and it is as follows:

$$\Delta V = IR \dots \text{Ohm's Law}$$

$$\Delta T = \frac{dQ}{dt} R_{th} \dots \text{Thermal analogy}$$

where ΔV is the voltage difference across the resistor R and I is the current flowing through it. In the thermal analogy, ΔT is the temperature difference across the system with a thermal resistance of R_{th} and $\frac{dQ}{dt}$ is the rate of heat flowing through it.

A Matlab script has been developed using Ohm's Law that simulates the electrical conditions that represent the water-saline diode. In electrical engineering, a diode effect is observed when the current through the diode is different for two opposing directions. The analogous circuit of the water-saline diode is represented by placing a 4V difference across two resistors in series as shown in Figure 5.3-29. The two resistors represent the two compartments of the water-saline diode. The first resistor (R_s) represents the saline compartment and its resistance is plotted in part (a) of Figure 5.3-30; the second resistor (R_w) represents the water compartment and its resistance is plotted in part (b) of Figure 5.3-30. The asymmetrical flow of current through the circuit is investigated by swapping the values of the voltages V_1 and V_2 . An optimisation study of this electrical diode is conducted that simulates the optimisation study of the water-saline diode presented in section 5.3.2.1 for the purpose of verifying the analogy.

A software routine was developed that simulated the current through the electrical diode for the mean voltage of V_1 and V_2 that ranges from $-2V$ to $8V$ in increments of $0.01V$. Gaussian profiles are used to determine the degree of change of the resistances as the voltages across them approach their maximum resistances. The width of the Gaussian function was optimised to give a percentage rectification that closely matches the experimental and numerical conditions. The routine operates as follows: the values of V_1 and V_2 are chosen and the appropriate value for each resistor is determined using the gaussian profiles. The total resistance of the circuit is now determined and from this the current flowing through the circuit is obtained; the current in the electrical diode is analogous to the rate of heat flow in the thermal

diode. The values of V_1 and V_2 are then swapped so that current now flows from V_2 to V_1 and the above procedure is repeated to obtain the current for this direction. The percentage rectification is obtained for this set of voltages and the entire process above is repeated until the mean voltage of V_1 and V_2 has changed from -2V to 8V. A flow diagram of the software routine is shown in Figure 5.3-31.

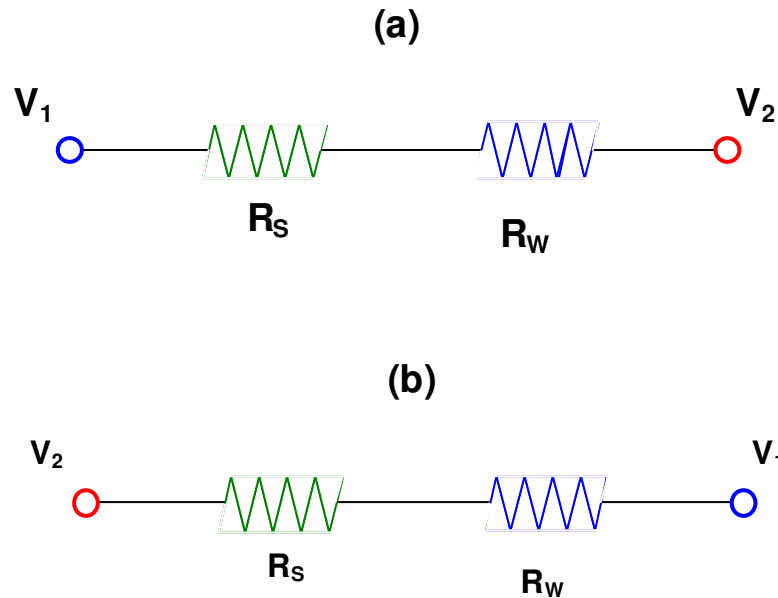


Figure 5.3-29 Circuits that describe the electrical analogy of the water-saline diode. (a) Electrical representation of the low conductance mode of the water-saline diode. (b) Electrical representation of the high conductance mode of the water-saline diode. R_W and R_S are the thermal resistance of the saline solution and water, respectively.

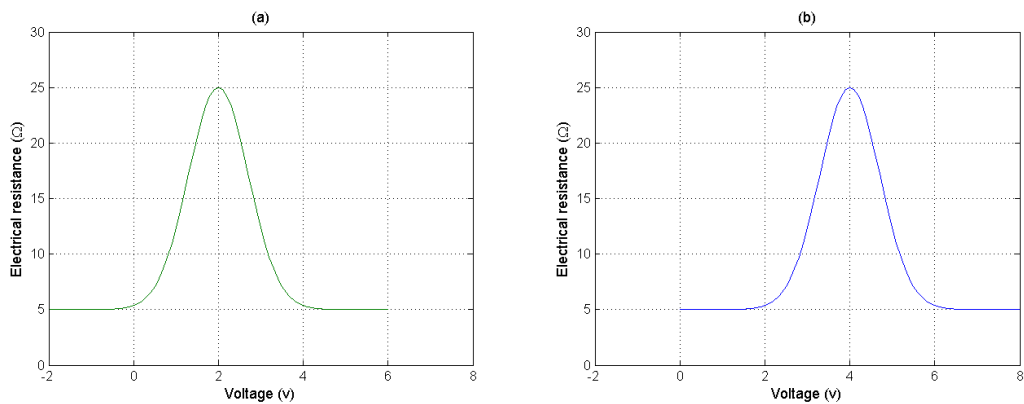


Figure 5.3-30 (a) The electrical resistance of the saline resistor as a function of voltage. (b) The electrical resistance of the water resistor as a function of voltage.

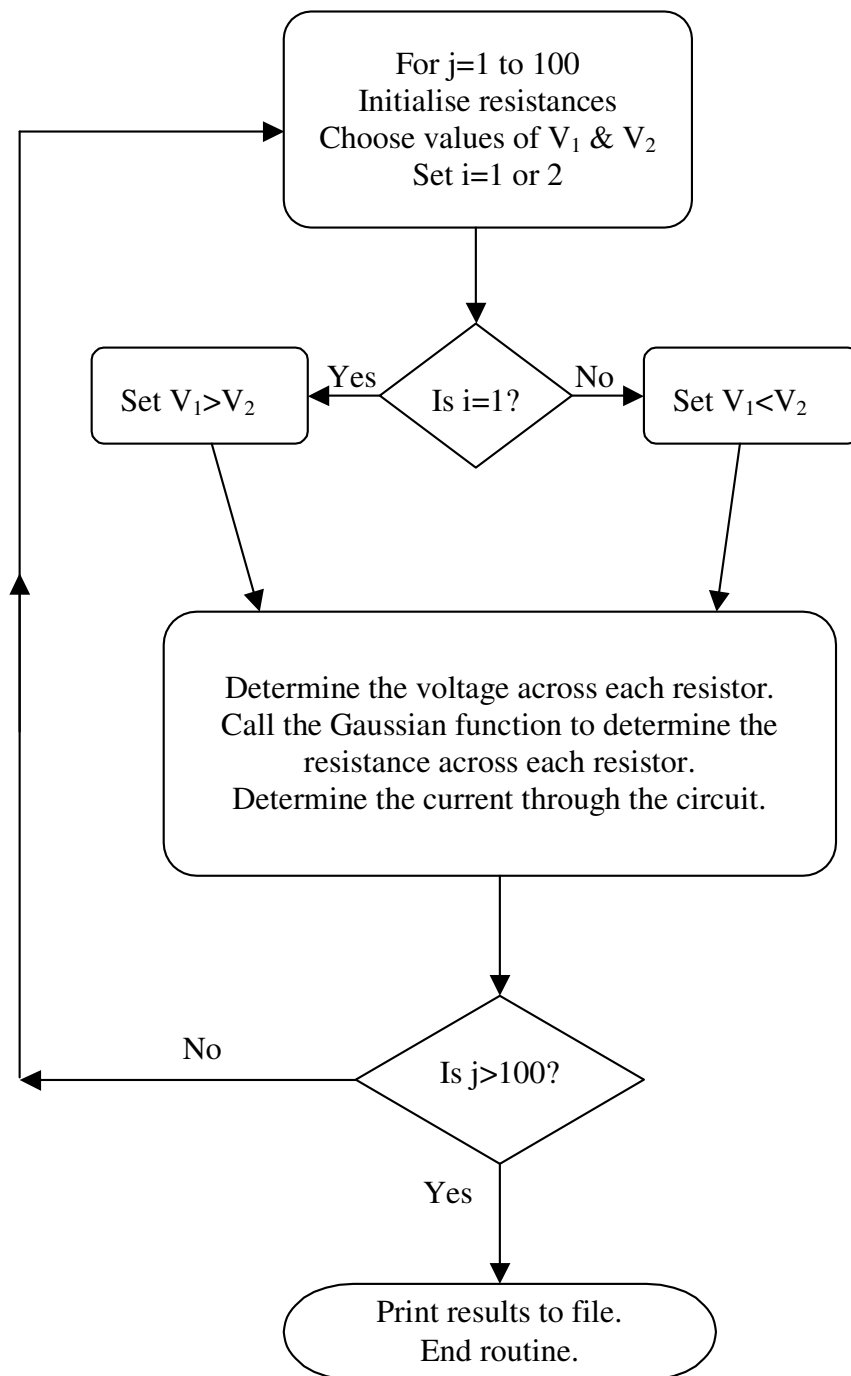


Figure 5.3-31 Flow diagram of the software routine that simulates the Ohm's Law representation of the water-saline diode.

Figure 5.3-32 shows a plot of the successive values of the percentage rectification between the current flowing through circuits (a) and (b) in Figure 5.3-29 as a function of the mean voltage. Figure 5.3-32 is the Ohm's Law analogy to the numerical plot shown in Figure 5.3-6. Despite the two different approaches taken, a good agreement is obtained between the two plots. Both plots show three peaks and two troughs. The highest peak occurs at a mean temperature of 3°C in Figure 5.3-6 with a percentage rectification of 65%; the highest peak in Figure 5.3-32 occurs at a mean voltage of 3V with a percentage rectification of 64%. In Figure 5.3-6 two minima with a percentage rectification of 0% occur at mean temperatures of 1.78°C and 4.19°C ; this compares to the 0% rectification values that occur at mean voltages of 1.63V and 4.37V in Figure 5.3-32. The two secondary maxima in Figure 5.3-32 occur at voltages of 0.60V and 5.40V with rectification values of 40%; this compares to Figure 5.3-6 where the two secondary maxima occur at 1.38°C and 4.19°C , each with a rectification value of 35%.

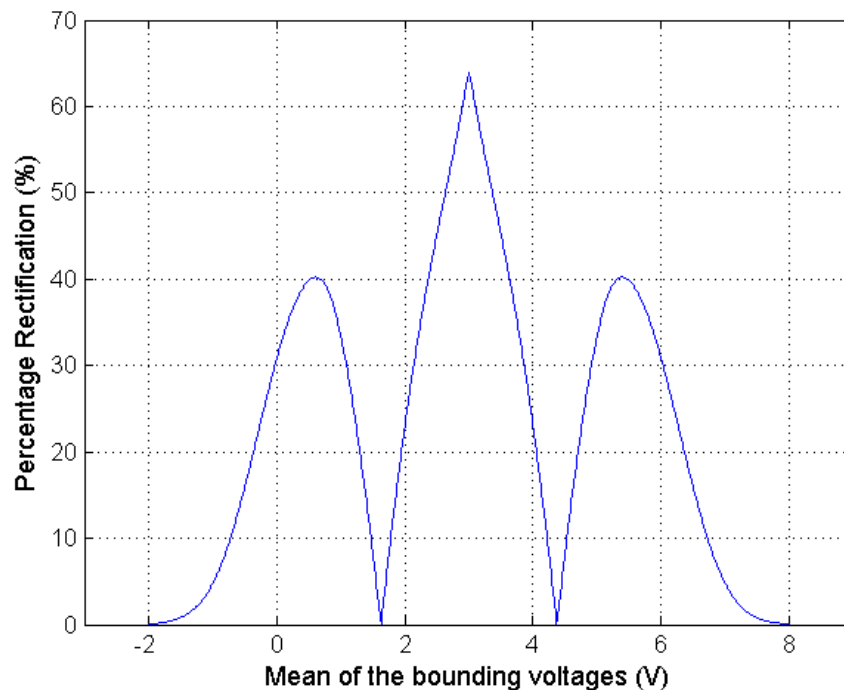


Figure 5.3-32 *Electrical analogy to the water-saline diode that investigates the influence of the absolute bounding voltages on the rectification factor. This plot compares to the optimization plot in Figure 5.3-6.*

These five extrema are the most significant features of the optimization studies and the good agreement between the two alternate approaches presents the Ohm's Law analogy as an alternative approach to estimating the peak values in the percentage rectification and their corresponding boundary temperatures. This approach is useful for both experimental and numerical investigations as it performs the investigation more quickly than the numerical and experimental approaches. For example, Figure 5.3-32 was acquired within 10 minutes, while the Comsol simulation of Figure 5.3-6 required several days. The simplicity of this approach allows the simulation to perform more quickly than the Comsol approach and it also offers an alternative means of illustrating the basis of asymmetrical heat flow through the water-saline diode.

Chapter 6

Conclusions

6.1 Conclusions

The main body of work in this thesis is concerned with asymmetrical heat transfer through composites of water and aqueous solutions in the presence of the density maximum. The study of asymmetrical heat transfer in the presence of the density maximum required the construction of an experimental apparatus, knowledge of the behaviour of the temperature of maximum density of aqueous solutions, and numerical models to confirm experimental results. The experimental apparatus used in this study is a modified version of the system described by McBride [57]. A major modification to the system was the introduction of a technique for measuring heat transfer. The results from the technique used in this study were compared to results from studies conducted by Lin and Nansteel [29] and Tong [30]. The results are in good agreement with the work of these researchers. The viability of the technique is further confirmed by the good agreement with the results from the numerical studies in this thesis.

The requirement of the knowledge of the behaviour of the temperature of maximum density of aqueous solutions was fulfilled by devising a technique for measuring the temperature of maximum density of aqueous solutions. The technique relies on changes in the convective flow pattern induced by the density maximum. When a liquid is cooled through its density maximum in a quasi-steady state manner, an anomalous feature is observed in the temperature profiles at five equally spaced points along the central horizontal axis. This feature is centred on the liquid's temperature of maximum density. The temperature of maximum density of water is well known and a chi-squared comparison between the anomaly feature of water and the aqueous solution yields the temperature of maximum density. Results from this technique were compared to results obtained by other researchers using different techniques (such as dilatometers) and the results are in good agreement. The viability of this technique is further confirmed by the good agreement between the experimental and numerical results.

The ability to measure heat transfer provided an alternative approach to this technique. An anomalous feature is observed in the rate of cooling of the liquid when it is cooled under the same conditions as above. Instead of comparing the

temperature profiles of the aqueous solution to the temperature profiles of water, a chi-squared comparison between the rates of cooling of each liquid is carried out. The flexibility of the experimental system is such that both of these approaches (temperature profiles approach and the rate of cooling approach) can be conducted simultaneously. Simultaneous measurements were compared and it was found that the results from the two techniques were in good agreement. Furthermore it was found that measurements from the technique based on the rate of cooling compared favourably with measurements conducted with the previous technique that were obtained prior to the inclusion of the heat transfer device into the experimental system. A numerical investigation of this technique further validates the approach.

Both techniques are accurate and simple to implement. Sources of uncertainty in the procedures described in this study can all be reduced if required. As with the zero-crossing approach advocated by Caldwell [20], the method described here does not rely on direct detection of an extremum in the density state function (in contrast to the more standard dilatometry techniques). The inherent accuracy of the approach arises from the detection of the sharp temperature transitions introduced by the migration of the boundary between the double convective cells from right to left of the sample chamber as the solution cools through the density anomaly. Although the two approaches are viable means of measuring the temperature of maximum density of aqueous solutions, only the technique based on the temperature profiles was used in this study to investigate the behaviour of the temperature of maximum density of some aqueous solutions. The reason for this is that the latter technique was not developed until after the study of the temperature of maximum density of aqueous solutions had been completed for this body of work.

It is evident both from historical measurements of the temperature of maximum density of aqueous solutions and from the data presented in this thesis that the shift in the temperature of the maximum density as a function of solute nature and concentration does not follow any simple pattern. In particular, the non-linear dependence of the temperature of maximum density on concentration for the monohydric alcohols would seem to eliminate any simple relationship such as the colligative model where the shift of the temperature of maximum density would be independent of the nature of the species. This in turn draws a clear distinction

between the behaviour of the temperature of maximum density and the depression of the temperature of freezing. To the author's knowledge there is as yet no model of the density maximum phenomenon of water which permits prediction of the temperature of the density maximum given information on the nature of the solute and the concentration.

The study of the temperature of maximum density of aqueous solutions shows that a 9g.ltr^{-1} solution of sodium chloride has a density maximum at 2°C . This solution is used in the experimental study of asymmetrical heat transfer through a composite of water and a sodium chloride solution (the water-saline diode). The experimental investigation showed that heat transfer through this composite system in the presence of the density maximum is different for opposing temperature gradients. Experimental results showed that the water-saline diode rectifies the flow of heat by 65%. The numerical investigations confirm this result and further the study of asymmetrical heat transfer. An extensive study of the optimal conditions for the water-saline diode showed that the maximum performance of the rectifier occurred when the boundary temperatures were 5°C and 1°C , and the dimensions of the rectifier were $0.06\text{m} \times 0.12\text{m}$ (height \times length).

Asymmetrical heat transfer was also investigated for other composites. Experimental studies of a composite system of water and Perspex showed a rectification of 30%. The numerical study showed a percentage rectification of 39%. Discrepancies between the two techniques were investigated numerically and it was found that the discrepancies were partially due to the offset in the boundary temperature of the experimental results. The performance of the water-Perspex diode was studied extensively using the numerical technique. It was found that the optimal conditions for the water-Perspex diode occurred when the boundary temperatures were 6.5°C and 1.5°C , and the dimensions of the water compartment and the Perspex slab were $0.06\text{m} \times 0.118\text{m}$ and $0.06\text{m} \times 0.002\text{m}$, respectively.

It is conceivable that the phenomenon described in this study could occur in natural situations. For example, the water-saline asymmetry could occur in environments with melting ice in seawater that can give rise to pockets of cold water and seawater adjacent to each other. It is also evident from the study of the water-Perspex diode

that asymmetrical heat transfer should occur in natural situations where bodies of cold water are adjacent to solid regions, e.g. rock fractures. There is a possibility that such asymmetry could occur in biological processes. Psychrophiles are types of extremophiles that have evolved to thrive under extremely cold conditions [69]. These organisms exploit the supercooling nature of water and the depression of the freezing point by the addition of solutes to survive at temperatures below the freezing point of water. It is therefore conceivable that these extremophiles might also exploit the phenomenon described in this study to survive in such conditions. Asymmetrical heat transfer can also be of importance for industrial applications. However, the device described in this study requires further investigation if it is to be implemented in practical situations. The present rectification factor needs to be improved and the range of temperatures of operation needs to be expanded. The possibility of overcoming these difficulties will be discussed in the next section.

6.2 Future work

The experimental apparatus described in this study is a relatively inexpensive and elegant system with capabilities beyond those that are utilised in this study (e.g. solenoid valves are available for use but not required for this study). While the system is more than adequate for the purpose of this study, the system may be improved with a few minor changes. In the heat transfer system described in this thesis a warm reservoir is contained in each refrigerator. In certain cases, these reservoirs reach temperatures of 16°C with the aid of heaters. The author suggests that these reservoirs could be placed outside the refrigerators in the room ambient, which would place a lesser strain on the refrigerators and eliminate the heaters from the system. The same system currently uses four reservoirs, a hot and cold reservoir for each side chamber. Sharing a hot and cold reservoir between the two side chambers could reduce this number to two. This eliminates the need for two refrigerator units.

Currently the heat transfer measurements were obtained with an uncertainty of 7%. This uncertainty could be reduced by calibrating the device in a similar manner to the calibration of the thermistors. The thermistors record a voltage drop that corresponds to a certain temperature and they are calibrated by noting the voltage drop for known temperatures. A similar approach may be applied to the heat transfer device. The

heat transfer device records a temperature drop across a Perspex slab that corresponds to a certain rate of heat flow. They could be calibrated by noting the temperature drop for known rates of heat flow. A thermometer of high resolution is used to determine the temperature when calibrating the thermistors. In the case of the heat transfer device, a known temperature difference across a solid could be used to provide and determine the rate of heat flow. The main source of uncertainty in the heat transfer device is the error of 0.14°C on the temperature difference. Thus, a large temperature difference across the solid would reduce the uncertainty in the heat transfer measurements. Alternatively, the uncertainty in the heat transfer measurements could be improved by changing the reference material (currently Perspex with $k=0.19\text{W}\cdot\text{m}^{-1}\cdot\text{K}^{-1}$ and width 0.00125m) so that a larger temperature drop is measured across the reference material for the same rates of heat flow. Although there are improvements that could be made to the experimental system, it is more than adequate for this study and it was successfully used to measure asymmetrical heat transfer and the temperature of maximum density of aqueous solutions.

The observed variations of the temperature of maximum density for the investigated solutes in this study do not conform to any simple predictive model. The behaviour of the temperature of maximum density of other solutes might provide insightful information regarding the occurrence of the density maximum in water and a predictive model for the temperature of maximum density of aqueous solutions. It has been observed in this study that the temperature of maximum density as a function of concentration for the monohydric alcohols behaves non-linearly. It has also been shown that the two isomers of propanol alter the temperature of maximum density in different ways. This clearly suggests that the behaviour of the temperature of maximum density depends on the molecular arrangement of the atoms. The study described in this thesis could be extended to include other monohydric alcohols such as butanol and pentanol. Butanol has four isomers: butan-1-ol, butan-2-ol, 2-methylpropan-1-ol and 2-methylpropan-2-ol. Butan-1-ol has an OH group attached to the end of the carbon chain in a similar manner to propan-1-ol. On the basis of structure, it might be expected that Butan-1-ol would not elevate the temperature of maximum density but butan-2-ol might; butan-2-ol has a similar structure as propan-2-ol. It is also worth noting that as the size of the alkyl group

increases so too did the elevation of the temperature of maximum density; thus, it might be expected that butan-2-ol will elevate the temperature of maximum density to higher temperatures than propan-2-ol. The structure of the remaining two isomers is different to that of all the other alcohol molecules, thus it is difficult to speculate about the influence of these solutes on the temperature of maximum density. The behaviour of the isomers of butanol and other larger alcohol molecules could provide important information for determining the molecular occurrence of the density maximum. However, it is important to note that alkyl group of the alcohol molecules is hydrophobic and as a result, the solubility of the molecule decreases as its size increases. For example, the solubility of butanol in water is 90g.ltr^{-1} , which gives a large range of solution concentrations for which the temperature of maximum density could be obtained. Pentanol, which is the next largest molecule, has a solubility of just 27g.ltr^{-1} . Although this line of enquiry is limited, it is undoubtedly an important one. The behaviour of the temperature of maximum density of aqueous solutions of acids and bases might also present important information for explaining the occurrence of the temperature of maximum density on a molecular level. The development of the measurement technique based on the rate of cooling described in this thesis permits the study of such corrosive solutions. Other possible lines of enquiry into the behaviour of the temperature of maximum density could include a study on binary systems or a study on the emulsion of two immiscible liquids.

During the investigation of the temperature of maximum density of aqueous solutions, it was observed for sodium carbonate solutions that the anomaly feature was distorted. Experimental evidence is provided in this body of work for the occurrence of such behaviour, but it is impossible to draw conclusions on the reason for such behaviour. Further work is required in this field. One possible line of enquiry for this behaviour is stratification. If the solute is not fully dissolved in the solution, it could set up a concentration gradient within the liquid. The density of a solution varies as a function of temperature and concentration. Thus, the introduction of a concentration gradient into the liquid will affect the convective flow pattern and hence the temperature profiles in the liquid. This line of enquiry would require an extensive study on the behaviour of free convection in the vicinity of the density maximum in an enclosure subjected to temperature and concentration gradients.

A study of the temperature of maximum density of aqueous solutions could potentially provide a solution that elevates the temperature of maximum density to a temperature that is more useful for the implementation into practical situations of the heat rectifier described in this study. The heat rectifier described in this study is limited by the narrow band of temperatures over which it operates and the confinement of this band to cold temperatures. The latter problem could be overcome if there existed a solute that would elevate the temperature of maximum density to warmer temperatures. The former problem may be overcome by cascading together several cubic enclosures of solutions with different temperatures of maximum density. An investigation described in this study on the influence of the bounding temperatures on the water-saline diode showed that, while the maximum rectification occurred when the two compartments contained the symmetrical double cell flow pattern in one direction of heat flow, rectification values of almost 40% were obtained when either compartment contained this type of flow. A study on the influence of the bounding temperatures on a rectifier with multiple compartments could present a solution to the narrow temperature range of operation with the current water-saline diode.

Analogies may be drawn between heat flow and electrical current. The current rectifier (junction diode) is a passive device of fundamental importance in electrical and electronic engineering – it is to be expected that a heat rectifier would find many applications in thermal engineering. Unfortunately, heat diodes with high levels of rectification have proved elusive. The main device discussed here – the water-saline diode – is still well removed from what might constitute a useful heat diode: its 65% rectification does not compare favourably with rectification levels in excess of 99.99% for current rectifiers (a typical 1 Ampere PN junction diode has a maximum reverse bias current of the order of 50 μ A). In electrical and electronic engineering, the discovery of the transistor revolutionised that field and the abilities of electronics. A discovery of a thermal transistor may also have profound implications for thermal engineering. This study has shown that the anomalous behaviour of the density of water gives rise to a heat rectifier; future work on free convection in the vicinity of the density maximum may lead to the discovery of a thermal transistor.

Appendix A

Comsol m-script for the Water-Saline Diode


```

%This ends the third loop and hence the first iteration of the second loop.
%The purpose of the second loop is to slide the T gradient up in steps of x.
%E.G. for the first iteration i=1 and x=i*0.25 this increases the temperature of
%273.15 by 0.25oC with every iteration in the second for loop.

%When the second loop ends the script enters the first loop.
%The first loop sets the temperature difference deltaT.
%For example j=1 means that deltaT=1. This means that t1 and t2 must change by 0.5oC
%each, this splits the gradient equal between t1 and t2, so if t1>t2 then t1=273.15+y and
%t2=273.15-y. where y=j/2. In the instance where j=1, y=0.5 and so t1=273.65
%and t2=272.65.

```

```

%open, clear and close file for writing
attempt=0;
datetime=datestr(now,'yyyy-mm-dd');

```

```

while attempt<9
    attempt=attempt+1;
    filename=sprintf('cfd%s_%d.dat',datetime,attempt);
    fid=fopen(filename,'r');
    if(fid==-1)
        break;
    fclose(fid);
end
end
fid=fopen(filename,'w+');
fclose(fid);

```

```

%Initialize the variables
q1sa=0;
q1sb=0;
t1s=0;
tcentre=273.15;
for j=1:1
    %this loop sets the gradient
    y=j/2;

```

```

for i=0:0.01:10
    %this loop shifts the gradient up or down
    x=i;
    q1sa=0;
    q1sb=0;

```

```

for flip=1:2
    %this loop is responsible for flipping the direction of the gradient

```

```

    %set temperature values on the boundaries
    if flip==1
        t1=tcentre+x+y;
        t2=tcentre+x-y;

        t01=t1-(j/4);
        t02=t1-2*(j/4);

```

```

    t03=t1-3*(j/4);
end
if flip==2
    t1=tcentre+x-y;
    t2=tcentre+x+y;

    t01=t1+(j/4);
    t02=t1+2*(j/4);
    t03=t1+3*(j/4);
end

%clear workspace and command window
clc
clear fem s1 a1 a2 t len

%create geometry
s1=rect2(0.059,0.06,'base','corner','Pos',[0.0 0.0]);
s2=rect2(0.002,0.06,'base','corner','Pos',[0.059 0.0]);
s3=rect2(0.059,0.06,'base','corner','Pos',[0.061 0.0]);
fem.geom=s1+s2+s3;
%geomplot(fem.geom,'edgelabels','on','sublabels','on');

%define constants
fem.const={'t0','281.15','t1','283.15','t2','279.15' ...
'rho0','999.971','mu','0.001','cp','4120', ...
'kc','0.6','g0','9.8','c0','999.845', ...
'c1','0.064','c2','-0.008','beta0','2e-4'};
fem.expr={'th','273.15-round(t/5400+0.05)*0.1', ...
'tc','273.15-round(t/5400+0.05)*0.1', ...
'bouss1','-9.81*(999.9+0.05*(T-273.15)-0.00625*(T-273.15)*(T-273.15))' ...
'bouss2','-9.81*(999.975+0.025*(T-273.15)-0.00625*(T-273.15)*(T-273.15))'};
fem.functions{1}.type='interp';
fem.functions{1}.name='crc_cp';
fem.functions{1}.method='linear';
fem.functions{1}.extmethod='const';
fem.functions{1}.x={'273.15' '283.15' '293.15' '303.15' '313.15' '323.15' '333.15'
'343.15' '353.15' '363.15' '373.15'};
fem.functions{1}.data={'4217.6' '4192.1' '4181.8' '4178.4' '4178.5' '4180.6' '4184.3'
'4189.5' '4196.3' '4205.0' '4215.9'};

fem.functions{2}.type='interp';
fem.functions{2}.name='crc_mu';
fem.functions{2}.method='cubic';
fem.functions{2}.extmethod='const';
fem.functions{2}.x={'273.15' '283.15' '293.15' '303.15' '313.15' '323.15' '333.15'
'343.15' '353.15' '363.15' '373.15'};
fem.functions{2}.data={'0.001793' '0.001307' '0.001002' '0.0007977' '0.0006532'
'0.000547' '0.0004665' '0.000404' '0.0003544' '0.0003145' '0.0002818'};

fem.functions{3}.type='interp';
fem.functions{3}.name='crc_kc';
fem.functions{3}.method='linear';
fem.functions{3}.extmethod='const';
fem.functions{3}.x={'273.15' '283.15' '293.15' '303.15' '313.15' '323.15' '333.15'
'343.15' '353.15' '363.15' '373.15'};
fem.functions{3}.data={'0.561' '0.580' '0.5984' '0.6154' '0.6305' '0.6435' '0.6543'
'0.6631' '0.67' '0.6753' '0.6791'};

fem.functions{4}.type='interp';

```

```

fem.functions{4}.name='crc_rho';
fem.functions{4}.method='cubic';
fem.functions{4}.extmethod='const';
fem.functions{4}.x={'273.15' '273.25' '273.35' '273.45' '273.55' '273.65' '273.75'
'273.85' '273.95' '274.05' '274.15' '274.25' '274.35' '274.45' '274.55' '274.65' '274.75' '274.85'
'274.95' '275.05' '275.15' '275.25' '275.35' '275.45' '275.55' '275.65' '275.75' '275.85' '275.95'
'276.05' '276.15' '276.25' '276.35' '276.45' '276.55' '276.65' '276.75' '276.85' '276.95' '277.05'
'277.15' '277.25' '277.35' '277.45' '277.55' '277.65' '277.75' '277.85' '277.95' '278.05' '278.15'
'278.25' '278.35' '278.45' '278.55' '278.65' '278.75' '278.85' '278.95' '279.05' '279.15' '279.25'
'279.35' '279.45' '279.55' '279.65' '279.75' '279.85' '279.95' '280.05' '280.15' '280.25' '280.35'
'280.45' '280.55' '280.65' '280.75' '280.85' '280.95' '281.05' '281.15' '281.25' '281.35' '281.45'
'281.55' '281.65' '281.75' '281.85' '281.95' '282.05'};
fem.functions{4}.data={'999.8426' '999.8493' '999.8558' '999.8622' '999.8683'
'999.8743' '999.8801' '999.8857' '999.8912' '999.8964' '999.9015' '999.9065' '999.9112'
'999.9158' '999.9202' '999.9244' '999.9284' '999.9323' '999.9360' '999.9395' '999.9429'
'999.9461' '999.9491' '999.9519' '999.9546' '999.9571' '999.9595' '999.9616' '999.9636'
'999.9655' '999.9672' '999.9687' '999.9700' '999.9712' '999.9722' '999.9731' '999.9738'
'999.9743' '999.9747' '999.9749' '999.9750' '999.9748' '999.9746' '999.9742' '999.9736'
'999.9728' '999.9719' '999.9709' '999.9696' '999.9683' '999.9668' '999.9651' '999.9632'
'999.9612' '999.9591' '999.9568' '999.9544' '999.9518' '999.9490' '999.9461' '999.9430'
'999.9398' '999.9365' '999.9330' '999.9293' '999.9255' '999.9216' '999.9175' '999.9132'
'999.9088' '999.9043' '999.8996' '999.8948' '999.8898' '999.8847' '999.8794' '999.8740'
'999.8684' '999.8627' '999.8569' '999.8509' '999.8448' '999.8385' '999.8321' '999.8256'
'999.8189' '999.8121' '999.8051' '999.7980' '999.7908'};

```

%-----specify application modes-----

%*****begin heat transfer mode*****

```

a1.mode.class='FIConvCond';
a1.mode.type='cartesian';

```

```

%assign mode properties
a1.prop.weakconstr.value='off';
a1.prop.weakconstr.dim={'lm3'};
a1.assignsuffix = '_cc';

```

%specify boundary conditions

```

%q0 is thermal insulation
%T is temperature condition
a1.bnd.type={'q0' 'cont' 'T' 'T'};
%boundaries now have three groups
%first group is thermal insulation
%other two groups are temperature(isothermal conditions)
a1.bnd.T0={'0' t2 t1 t2};
%above line sets the temperature of group 2 to t1
%and the temperature of group 3 to t2
%group 1 has T=0 but this is ignored since we choose q0
a1.bnd.ind=[3 1 1 2 1 1 2 1 1 4];
%the above line sets boundary 1 to group 3 (isothermal – t1)
%boundaries 2,3,5,6,8 & 9 to group 1 (insulation)
%boundaries 4 & 7 to group 2 (continuity)
%boundary 10 to group 4 (isothermal – t2)

```

```

%specify subdomain conditions

a1.equ.init={t01 t02 t03};
% the above sets the initially temperatures
a1.equ.rho = {'crc_rho(T)' [2710] 'crc_rho(T)'};
a1.equ.C = {'crc_cp(T)' [900] 'crc_cp(T)'};
a1.equ.k = {'crc_kc(T)' [200] 'crc_kc(T)'};
a1.equ.u = {'u' [0] 'u'};
a1.equ.v = {'v' [0] 'v'};
a1.equ.ind=[1 2 3];

%-----end of heat transfer mode-----

%*****begin fluid dynamics mode*****

%assign fluid dynamics mode

a2.mode.class='FINavierStokes';
a2.mode.type = 'cartesian';

%specify point settings
a2.pnt.pnton={ [0] [1] };
a2.pnt.ind=[1 1 2 1 2 1 1 1];

%specify boundary conditions

%no slip boundary conditions
a2.bnd.type={'noslip'};
a2.bnd.ind=[1 1 1 1 1 1 1 1 1];
%boundaries now have one group
%first group is no slip conditions
%the second line sets boundaries 1-10 to group 1

%specify subdomain settings

%set the initial values to 0
a2.equ.init='0';

%assign values on the subdomain
a2.equ.rho = 'crc_rho(T)';
a2.equ.eta = 'crc_mu(T)';
a2.equ.F_y = {'bouss1' 'bouss1' 'bouss2'};
a2.equ.usage = {[1] [0] [1]};
a2.equ.ind = [1 2 3];

%-----end of fluid dynamics mode-----

%--put both modes together into Comsol to use the predefined equations
fem.appl={a2 a1};
fem=multiphysics(fem);

```

```

%----initialize mesh

fem.mesh=meshmap(fem,'edgelem',[1 4 7 10] 40 [2 3 8 9] [0:0.001:0.01
0.012:0.002:0.048 0.049:0.001:0.059] [5 6] 2));

%refine mesh
%fem.mesh=meshrefine(fem);
%meshplot(fem)

%--extend the mesh (required by COMSOL for solving)
fem.xmesh=mesnextend(fem);

%--Use Comsol solver to solve the model
fem.sol=femtime(fem,'Tlist',[0:1:100000],'tsteps','strict');

%save solution to file
centemp=(t1+t2)/2;
q2sa=abs(q1sa);
q1sa=abs(postint(fem,'ntflux_T_cc','edim',1,'DI',1,'solnum',length(fem.sol.tlist)));
q2sb=abs(q1sb);
q1sb=abs(postint(fem,'ntflux_T_cc','edim',1,'DI',10,'solnum',length(fem.sol.tlist)));
t2s=t1s;
t1s=(postint(fem,'T','edim',2,'DI',2,'solnum',length(fem.sol.tlist)))/(0.06*0.002);

end

%save solutions to file
fid=fopen(filename,'a');
fprintf(fid,'%6.2f, %6.2f, %6.2f, %6.2f, %6.2f, %6.2f, %6.2f, %6.2f\n',j, centemp, q1sa,
q2sa, q1sb, q2sb, t1s, t2s);
fclose(fid);

end
end

```

Appendix B

Thermal Analogy code

```

%the name of this matlab program is rsingle.m
%electrical analogy of  $dT=R*(dQ/dt)$ 
%routine which calculates V and I for circuit
%with non-linear voltage-dependent resistances
%
%circuit computed by this script is
%*****
%V1 o---^^^---[ $^{4}V^{}$ ]---[ $^{2}V^{}$ ]---^^^---o V2
%   r1   r2   r3   r4
%*****
%deltaV = V1 - V2
%r1=1ohm
%r2=function of voltage with a maximum at 4V
%r3=function of voltage with a maximum at 2v
%r4=1ohm

fid=fopen('rsingle_out.dat','w');

y=2;
num2a=0.1/y;

for num2=1:1000
    % this for loop computes the rectification as V1 moves up
    % from 0.1V to 10V in steps of 0.1V
    % note that  $dV = V1 - V2$ 
    x=num2*num2a*0.1;
    n=10000;
    np=0;
    xp=zeros(n,1);
    yp1=zeros(n,1);
    yp2=zeros(n,1);
    yp3=zeros(n,1);

    gauss_sig=0.4;
    v1=6.0;
    v2=0.0;
    r1=1.0;
    r4=1.0;
    r2=5;
    r3=5;

    for j=1:100
        %this for loop sinusoidally interchanges
        %the voltages of v1 and v2
        %changing y by 0.5 changes the values
        %of V1 and V2 by 0.5V and hence dV by 1V
        theta=2*pi*(j*0.03);
        v1=y*(sin(theta)-1.0+x);
        v2=y*(sin(theta+pi)-1.0+x);

        for i=1:100
            %this for loop computes the current
            np=np+1;
            xp(np)=np;
            yp1(np)=v1;
            yp2(np)=v2;
            rtot=r1+r2+r3+r4;
            itot=(v1-v2)/rtot;
        end
    end
end

```

```

delvr1=itot*r1;
valpha=v1-delvr1;
delvr2=itot*r4;
vbeta=v2+delvr2;

i1=(valpha-vbeta)/(r2+r3);
vx=valpha-i1*r2;
yp3(np)=i1;
r2=gauss_pro(4,gauss_sig,valpha,vx);
r3=gauss_pro(2,gauss_sig,vx,vbeta);
end
end

[a,b]=max(yp1);
[c,d]=min(yp1);
hotleft(1,num2)=a;
hotright(1,num2)=c;

%assign absolute values
mynum1=abs(yp3(b));
mynum2=abs(yp3(d));

%calculate rectification value
if(mynum2>mynum1)
    rectify(1,num2)=((mynum2-mynum1)/mynum2)*100;
else
    rectify(1,num2)=((mynum1-mynum2)/mynum1)*100;
end

fprintf(fid,'%8.2f, %8.2f, %8.2f \n',hotleft(1,num2),hotright(1,num2),rectify(1,num2));

end
fclose(fid);

%-----
%-----function below is called by the above program-----
%-----

function r = gauss_pro(vrmax,gauss_sig,v1,v2)
% This function is called by rsingle to obtain the resistance of r2 and r3

n=50;
r0=5.0;

raccum=0;
vmin=min(v1,v2);
vmax=max(v1,v2);
delv=vmax-vmin;

for i=1:n+1
    vinc=vmin+(i-1)*(delv/n);
    arg1=((vinc-vrmax)/(2*gauss_sig))^2;
    rinc=r0+4*r0*exp(-arg1);
    raccum=raccum+rinc;
end
r=raccum/(n+1);

```

Bibliography

- [1] Handbook of Chemistry and Physics, 65th ed., CRC Press (Boca Raton, Florida) (1984).
- [2] Handbook of Chemistry and Physics, 83rd ed., CRC Press (Boca Raton, Florida) (2002).
- [3] P. Ball, H₂O – A biography of water, Phoenix, London (2001).
- [4] P. Chappuis. Dilatation de l'eau, Travaux et Mémoires du Bureau International des Poids et Mesures, 13 (1907) D1-D40.
- [5] G. S. Kell, Density, Thermal expansivity and compressibility of liquid water from 0°C to 150°C: Correlations and tables for atmospheric pressure and saturation reviewed and expressed on 1968 temperature scale, Journal of chemical and engineering data, 20 (1) (1975) 97-105.
- [6] M. Thiesen, K. Scheel, H. Diesselhorst, Untersuchungen über die thermische Ausdehnung von festen und tropfbar flüssigen Körpern – Bestimmung der Ausdehnung des Wassers für die zwischen 0 ° und 40 ° liegenden Temperaturen, Wiss. Abhandlungen der Physik.-Techn. Reichsanst., 3 (1900) 1-70.
- [7] M. Thiesen, Untersuchungen über die thermische Ausdehnung von festen und tropfbar flüssigen Körpern – Bestimmung der Ausdehnung des Wassers für die zwischen 0 ° und 40 ° liegenden Temperaturen, Wiss. Abhandlungen der Physik.-Techn. Reichsanst., 4 (1918) 1-32
- [8] C. -T. Chen, F. J. Millero, The equation of seawater determined from sound speeds, Journal of Marine Research, 36, (1978) 657-691.
- [9] R. Feistel, A new extended Gibbs thermodynamic potential of seawater, Progress in Oceanography, 58 (2003) 43-114.

- [10] N.P. Fofonoff, Physical properties of seawater: a new salinity scale and equation of state for seawater, *Journal of Geophysical Research*, 90 (1985) 3332-3342.
- [11] International Critical Tables of Numerical Data, Physics, Chemistry and Technology, National Research Council, 1928 (Electronic Edition: Knovel, 2003), Vol. III, 107-111.
- [12] <http://brunelleschi.imss.fi.it/cimento/>, Court Scientists – The Art of Experimentation in the Galilean Accademia del Cimento (1657-1667), Institute and Museum of the History of Science, Florence, 2001.
- [13] T.C. Hope, Experiments and observations upon the contraction of water by heat at low temperatures, *Trans. Royal Soc. Edinburgh* 5 (1805) 379-405.
- [14] M. Depretz, Recherches sur le maximum de densite des dissolutions aqueuses, *Annales de Chimie et de Physique*, 70 (1839) 49-81.
- [15] M. Depretz, Le maximum de densite des liquides, *Annals de Chimie et de Physique*, 73 (1840) 296-310.
- [16] M.F. Rossetti, Sur le maximum de densite et la dilatation de l'eau distille, *Annals de Chimie et de Physique*, 10 (1867) 461-473.
- [17] M.F. Rosetti, Sur le maximum de densite et la dilatation de l'eau distillee, de l'eau de l'adriatique et de queldque solutions salines, *annals de Chimie et de Physique*, 17 (1869) 370-384.
- [18] R. Wright, The effect of some simple electrolytes on the temperature of maximum density of water, *J. Chemical Soc.*, 115 (1919) 119-126.
- [19] A.G. Mitchell, W.F.K. Wynne-Jones, Thermodynamic and other properties of solutions involving hydrogen bonding, *Discuss. Faraday Soc.* 15 (1953) 161-168.

- [20] D. R. Caldwell, The maximum density points of pure and saline water, *Deep-Sea Research*, 25 (1978) 175-181.
- [21] C.H. Cho, S. Singh, G.W. Robinson, An explanation of the density maximum in water, *Phys. Rev. Lett.*, 76 (10) (1996) 1651-1654.
- [22] H. Tanaka, Simple physical explanation of the unusual thermodynamic behaviour of liquid water, *Phys. Rev. Lett.*, 80 (26) (1998) 5750-5753.
- [23] P. Jedlovszky, M. Mezei, R. Vallauri, A molecular level explanation of the density maximum of liquid water from computer simulations with a polarizable potential model, *Chem. Phys. Lett.*, 318 (2000) 155-160.
- [24] C.H. Cho, S. Singh, G.W. Robinson, Understanding all of water's anomalies with a nonlocal potential, *J. Chem. Phys.* 107 (19) (1997) 7979-7988.
- [25] H.I.M. Veiga, L.P.N. Rebelo, M. Nunes de Ponte, J. Szydlowski, Water and Gallium at absolute negative pressures. Loci of maximum density and of melting. Fourteenth Symposium on Thermophysical Properties, June 25-30 (2000) Boulder, Colorado, U.S.A.
- [26] G.K. Batchelor, Heat transfer by free convection across a closed cavity between vertical boundaries at different temperatures', *Quart. J. Mech. Appl. Math.*, 121 (1954) 209233.
- [27] P.H. Oosthuizen, The development of convective motion in a bottom heated square enclosure containing ice and water, *Int. J. Therm. Sci.* 40 (2001) 145-151.
- [28] C.D. Seybert, J.W. Evans, PIV measurements of velocity of water in the presence of ice and comparison with calculated values, *Int. J. Heat Mass Transfer*, 48 (2005) 67-73.

- [29] D.S. Lin, M.W. Nansteel, Natural convection heat transfer in a square enclosure containing water near its density maximum, *Int. J. Heat Mass Transfer*, 30 (11) (1987) 2319-2329
- [30] W. Tong, Aspect ratio effect on natural convection in water near its density maximum temperature, *Int. J. Heat Mass Transfer*, 30 (11) (1987) 2319-2329.
- [31] W. Tong, J.N. Koster, Density inversion effect on transient natural convection in a rectangular enclosure, 37 (6) (1994) 927-938.
- [32] A. Watson, The effect of the inversion temperature on the convection of water in an enclosed rectangular cavity, *Quart. Journ. Mech. and Applied. Math.*, 25 (4) (1972) 423-446.
- [33] S.L. Braga, R. Viskanta, Transient natural convection of water near its density extremum in a rectangular cavity, *Int. J. Heat Mass Transfer*, 35 (4) (1992) 861-875.
- [34] M.W. McDonagh, A. Faghri, Experimental and numerical analyses of the natural convection of water through its density maximum in a rectangular enclosure, *Int. J. Heat Mass Transfer*, 37 (5) (1994) 783-801.
- [35] N. Seki, S. Fukusako, H. Inaba, Free convective heat transfer with density inversion in a confined rectangular vessel, *Wärme-und Stoffübertragung Thermo and Fluid Dynamics*, 11, (1978) 145-156.
- [36] M.F. Cawley, P.A. Mooney, P. O'Connor, Asymmetrical heat flow through composites of water and aqueous solutions in the presence of the density maximum, in press, *Int. J. Heat Mass Transfer*, (2007), doi: 10.1016/j.ijheatmasstransfer.2007.04.008 (<http://dx.doi.org>).
- [37] P.A. Mooney, M.F. Cawley, Thermal diode effect due to the influence of the density maximum in water and aqueous solutions on natural convection,

Conference proceedings, COMSOL Users Conference 2006, Hyatt Regency Cambridge, Boston, (October 22-24 2006).

- [38] A.D. Ochoa, J.W. Baughn, A.R. Byerley, A new technique for dynamic heat transfer measurements and flow visualization using liquid crystal thermography, *Int. J. Heat Fluid Flow*, 26, (2005) 264-275.
- [39] J.E. Mayhew, J.W. Baughn, A.R. Byerley, The effect of freestream turbulence on film cooling adiabatic effectiveness, *Int. J. Heat Fluid Flow*, 24, (2003) 669-679.
- [40] J.W. Baughn, Liquid crystal methods for studying turbulent heat transfer, *Int. J. Heat Fluid Flow*, 16, (1995) 365-375.
- [41] T.V. Jones, Heat transfer, skin friction, total temperature and concentration measurement. In: B.E. Richards. (Ed.), *Measurements of unsteady fluid dynamic phenomena*. McGraw Hill, Berlin, (1977) 63-102.
- [42] W.H. Leong, K.G.T. Holland, A.P. Brunger, On a physically-realizable benchmark problem in internal natural convection, *Int. J. Heat Mass Transfer*, 41, (1998) 3817-3828.
- [43] H. Suehrcke, D. Daldehog, J.A. Harris, R.W. Lowe, Heat transfer across corrugated sheets and honeycomb transparent insulation, *Solar Energy*, 76 (2004) 351-358.
- [44] Standard Test Method for Thermal Conductivity of Solids by means of the Guarded-Comparative-Longitudinal Heat Flow Technique, E 1225-87, *Annual Book of ASTM Standards*, 14.02, ASTM (1994).
- [45] V.A.F. Costa, M.S.A. Oliveira, A.C.M. Sousa, Laminar natural convection in a vertical stack of parallelogrammic partial enclosures with variable geometry, *Int. J. Heat. Mass Transfer*, 48 (2005) 779-792.

- [46] C. Starr, 'The Copper Oxide Rectifier', *Physics*, 7 (1936) 15-19.
- [47] J.S. Moon, R.N. Keeler, A theoretical consideration of directional effects in heat flow at the interface of dissimilar metals, *Int. J. Heat Mass Transfer*, 5 (1962) 697-971.
- [48] A. Jones, P.W. O'Callaghan, S.D. Probert, Differential expansion thermal rectifier, *J. Phys. E: Scientific Instruments*, 4 (1971) 438-440.
- [49] C.W. Chang, D.Okawa, A. Majumdar, A. Zettl, Solid state thermal rectifier, *Science*, 314 (2006) 1121-1124.
- [50] M. Terraneo, M. Peyrard, G. Casati, Controlling the energy flow in nonlinear lattices: a model for a thermal rectifier, *Phys. Rev. Lett.* 88 (2002) 094302: 1-4.
- [51] B. Li, L. Wang, G. Casati, Thermal diode: Rectification of heat flux, *Physical Review Letters*, 92, 254301 (2004).
- [52] D. Segal, A. Nitzan, Heat rectification in molecular junctions, *J. Chem. Phys.* 122 (2005) 194704: 1-12.
- [53] D. Segal, A. Nitzan, Spin-boson thermal rectifier, *Phys. Rev. Lett.* 94 (2005) 034301: 1-4.
- [54] S.B. Riffat, X. Ma, R. Wilson, Performance simulation and experimental testing of a novel thermoelectric heat pump system, *Applied Thermal Engineering*, 26 (2006) 494-501.
- [55] M. Sprackling, *Thermal physics*, MacMillan Physical Science Series, UK, (1991).
- [56] D.G. Cahill, R.O. Pohl, Thermal conductivity of amorphous solids above the plateau, *Phys. Rev. B*, 35 (1987) 4067-4073.

- [57] P. McBride, A study of convection in water in the vicinity of the density maximum, PhD Thesis (2004) NUI Maynooth.
- [58] <http://www.rubini.it/pxc/>
- [59] <http://sourceforge.net/projects/matlabpiv/>
- [60] <http://www.comedi.org/>
- [61] M.F. Cawley, D. McGlynn, P.A. Mooney, Measurement of the temperature of density maximum of water solutions using a convective flow technique, *Int. J. Heat Mass Transfer* 49 (2006) 1763-1772.
- [62] P. O'Connor, The influence of the density maximum in water on the rate of heat transfer, MSc Thesis (2006) NUI Maynooth.
- [63] P.A. Mooney, M.F. Cawley, Free convection in water in the vicinity of the density maximum, Conference Proceedings, 8th Australasian heat and mass Transfer Conference, Curtin University, Perth, (July 26–29 2005)
- [64] M.F. Cawley, P. McBride, Flow visualization of free convection in a vertical cylinder of water in the vicinity of the density maximum, *Int. J. heat Mass Transfer* 47 (2004) 11175-1186.
- [65] <ftp://ftp.lrz-muenchen.de/pub/science/fluidynamics/cfd/NaSt2D>
- [66] M. Griebel, T. Dornseifer, T. Neunhoffer, Numerical simulation in fluid dynamics – A practical introduction, Society for Industrial and Applied Mathematics (SIAM), Philadelphia, 1998.
- [67] D. McGlynn, A study of the change in the temperature of the density maximum of water as a function of solute nature and concentration, MSc Thesis (2005) NUI Maynooth.

- [68] Comsol Multiphysics, Comsol Ltd., London, (www.Comsol.com).
- [69] J.W. Deming, Psychrophiles and polar regions, *Curr. Opin. Microbiol.* 5 (3) (2002), pp. 301–309.